# Investigating the effect of amyotrophic lateral sclerosis-associated mutant vesicle-associated membrane protein B on axonal transport

Morotz, Gabor Miklos

*Awarding institution:*
King's College London

**Title:** Investigating the effect of amyotrophic lateral sclerosis-associated mutant vesicle-associated membrane protein B on axonal transport

**Author:** Gabor Miklos Morotz

# INVESTIGATING THE EFFECT OF AMYOTROPHIC LATERAL SCLEROSIS-ASSOCIATED MUTANT VESICLE-ASSOCIATED MEMBRANE PROTEIN-ASSOCIATED PROTEIN B ON AXONAL TRANSPORT

**Gábor Miklós Mórotz BSc (Hons) MSc (Hons)**

Thesis submitted in fulfilment of the degree of Doctor of Philosophy,
King's College London, Institute of Psychiatry (University of London)

**London**

**July 2012**

# ABSTRACT

Amyotrophic lateral sclerosis (ALS) is a fatal neurodegenerative disease characterised by selective degeneration and death of motor neurons. The architecture of neurons makes them dependent upon the proper transport of protein and organelle cargoes, especially through axons (axonal transport). Indeed, disruption to axonal transport is a very early, pathological event in ALS. A proline to serine substitution at position 56 in the vesicle-associated membrane protein-associated protein B (VAPB; VAPBP56S) causes some dominantly inherited familial forms of motor neuron disease including ALS type-8. How VAPBP56S causes ALS is not properly understood. In this thesis, I investigated the effect of VAPBP56S on axonal transport of mitochondria in primary rat cortical neurons and primary mouse motor neurons. Using time-lapse microscopy, I showed that expression of VAPBP56S but not wild-type VAPB in neurons selectively disrupts anterograde axonal transport of mitochondria. Anterograde axonal transport of mitochondria is mediated by the microtubule-based molecular motor kinesin-1. Attachment of kinesin-1 to mitochondria involves the outer mitochondrial membrane protein Rho GTPase-1 (Miro1) which acts as a sensor for cytosolic calcium levels ($[Ca^{2+}]c$); elevated $[Ca^{2+}]c$ disrupts mitochondrial transport via an effect on Miro1. To gain insight into the mechanisms underlying the VAPBP56S effect on mitochondrial transport, I monitored $[Ca^{2+}]c$ levels in VAPBP56S expressing primary rat cortical neurons. Expression of VAPBP56S but not VAPB increased resting $[Ca^{2+}]c$ in these cells. Moreover, the amounts of tubulin but not kinesin-1 that were associated with Miro1 were reduced in VAPBP56S compared to VAPB transfected HEK293 cells. Also, expression of a $Ca^{2+}$ insensitive mutant of Miro1 rescued defective mitochondrial axonal transport and restored the amounts of tubulin associated with the Miro1/kinesin-1 complex to normal in VAPBP56S expressing HEK293 cells. Thus VAPBP56S may

perturb axonal transport of mitochondria by disrupting $Ca^{2+}$ homeostasis and affecting the interaction of Miro1/kinesin-1 with tubulin.

## Publications in refereed journals arising from the thesis

Mórotz GM, De Vos KJ, Vagnoni A, Ackerley S, Shaw CE, Miller CC. Amyotrophic lateral sclerosis-associated mutant VAPBP56S perturbs calcium homeostasis to disrupt axonal transport of mitochondria. *Hum. Mol. Genet.* (2012) 21:1979-1988.

De Vos KJ, Mórotz GM, Stoica R, Tudor EL, Lau KF, Ackerley S, Warley A, Shaw CE, Miller CC. VAPB interacts with the mitochondrial protein PTPIP51 to regulate calcium homeostasis. *Hum. Mol. Genet.* (2012) 21:1299-1311.

# ACKNOWLEDGEMENTS

First of all I would like to thank my parents and my family for their continuous help and support during my work. I would also like to thank my supervisors Dr Kurt De Vos and Prof Chris Miller for their help, encouragement and guidance through all the difficulties of this project. I would like to thank Prof Pontus Aspenström (Ludwig Institute for Cancer Research, Uppsala University, Uppsala, Sweden) for the Miro and TRAK constructs, Dr Kwok-Fai Lau (KCL, UK) for the VAPB constructs, Prof Frederic Saudou (Institute Curie, Orsay, France) for the mCherry-α-tubulin constructs, Dr Alessio Vagnoni (KCL, UK) for the kinesin-1 construct and Prof Ron Vale (University of California, San Francisco (UCSF), USA) for the kinesin-1 antibody. I would also like to acknowledge help and assistance from Dr Elizabeth Tudor (KCL, UK) for providing and genotyping transgenic mice and Dr Kurt De Vos for major help with motor neuron cultures. A big thank you goes to everyone in the Miller group for their friendship. Last but not least I would like to thank the blooming Mimi, the great Luca and the fantastic Éva for everything.

This work was funded by a studentship from the UK Motor Neurone Disease Association (MNDA) and also supported by grants from the Medical Research Council (MRC), the Wellcome Trust and the European Union 7$^{th}$ Framework Programme for RTD.

# TABLE OF CONTENTS

# LIST OF FIGURES

# LIST OF TABLES

# ABBREVIATIONS

**Units**

| | |
|---|---|
| °C | degree Celsius |
| Da | dalton |
| g | gram |
| h | hour |
| l | litre |
| M | molar |
| m | metre |
| $m^2$ | square metre |
| $m^3$ | cubic metre |
| min | minute |
| s | second |
| V | volt |

**Metric prefixes**

| | |
|---|---|
| M | mega |
| k | kilo |
| c | centi |
| m | milli |
| µ | micro |
| n | nano |
| p | pico |

**Other abbreviations**

| | |
|---|---|
| A | adenine |
| AD | autosomal dominant |
| ADP | adenosine diphosphate |
| ALS | amyotrophic lateral sclerosis |
| ALS-FTD | ALS accompanied by Parkinsonism or frontotemporal dementia |
| AM | acetoxymethyl ester |
| AMPA | alpha-amino-3-hydroxy-5-methylisoxazole-4-propionic acid |
| ANOVA | analysis of variance |
| AR | autosomal recessive |
| ASK1 | apoptosis signal-regulating kinase 1 |
| ATF | activating transcription factor |
| ATP | adenosine triphosphate |
| Bcl-2 | B-cell lymphoma-2 |
| bp | base pair |
| BSA | bovine serum albumin |
| C | cytosine |
| *C. elegans* | *Caenorhabditis elegans* |
| *C9ORF72* | *chromosome 9 open reading frame* 72 gene |
| $Ca^{2+}$ | calcium |
| $[Ca^{2+}]c$ | cytosolic calcium levels |
| caspase | cysteinyl aspartate-specific protease |
| CERT | ceramide transfer protein |
| CHOP | CCAAT/enhancer binding protein homologous protein |

| | |
|---|---|
| CLR-1 Lar | caterpillar-like receptor-1 leukocyte common antigene-related-like receptors |
| COP | coat protein |
| COXIV | cytochrome c oxidase IV |
| C-terminal | carboxyl terminal |
| CTRL | control |
| DABCO | 1,4-diazobicyclo[2.2.2]octane |
| Derlin-1 | ER-like protein 1 |
| DNase | desoxyribonuclease |
| DMEM | Dulbecco's modified Eagle's medium |
| DMSO | dimethyl sulphoxide |
| DNA | deoxyribonucleic acid |
| dNTP | deoxyribonucleotide triphosphate |
| DPBS | Dulbecco's phosphate buffered saline without $Ca^{2+}$ and $Mg^{2+}$ |
| DRG | dorsal root ganglia |
| DsRed | *Discosoma sp.* red fluorescent protein |
| DsRed-Mito | mitochondrial targeted *Discosoma sp.* red fluorescent protein |
| DTT | dithiothreitol |
| DVAP-33 | *Drosophila* homolog of VAPB |
| E | embryonic day |
| *E. coli* | *Escherichia coli* |
| EAAT | excitatory amino acid transporter |
| ECL | enhanced chemiluminescence |
| EDTA | ethylenediaminetetraacetic acid |
| EF-hand | E-helix-loop-F-helix |

| | |
|---|---|
| EGFP | enhanced green fluorescent protein |
| EGFP-VAPB | EGFP-tagged VAPB |
| EGFP-VAPBP56S | EGFP-tagged VAPBP56S |
| EGTA | ethylene glycol-bis (β-aminoethylether) N,N,N',N'-tetraacetic acid |
| EMD | Emerin |
| EphR | ephrin receptor |
| ER | endoplasmic reticulum |
| ERAD | ER-associated degradation |
| ERGIC | ER-Golgi intermediate compartment |
| EV | empty vector |
| FALS | familial ALS |
| FEZ1 | fasciculation and elongation protein zeta-1 |
| FFAT | two phenylalanines (FF) in acidic tract |
| Fura2 | 1-[2-(5-carboxyoxazol-2-yl)-6-aminobenzofuran-5-oxy]-2-(2'-amino-5'-methylphenoxy)-ethane-N,N,N',N'-tetraacetic acid |
| FUS | fused in sarcoma |
| G | guanine |
| GABAA | γ-aminobutyric acid A |
| GAPDH | glyceraldehyde 3-phosphate dehydrogenase |
| GluR2 | glutamate receptor 2 |
| GRIP1 | glutamate receptor interacting protein 1 |
| GRP78/BiP | glucose-regulated protein 78/immunoglobulin heavy-chain binding protein |
| GTP | guanosine triphosphate |
| HA-TRAK1 | haemagglutinin-tagged TRAK1 |

| | |
|---|---|
| HBSS(-/-) | $Ca^{2+}$, $Mg^{2+}$-free Hank's buffered salt solution |
| HBSS(+/+) | Hank's buffered salt solution with $Ca^{2+}$ and $Mg^{2+}$ |
| HEK293 | human embryonic kidney 293 |
| HEPES | 4-(2-hydroxyethyl)piperazine-1-ethanesulfonic acid |
| HSP | hereditary spastic paraplegia |
| IB | immunoblot |
| IF | immunofluorescence |
| IgG | immunoglobulin G |
| IP3R | inositol-1,4,5-triphosphate receptor |
| IP | immunoprecipitation |
| IPTG | isopropyl-1-thio-β-D-galactopyranoside |
| IRE1 | inositol requiring enzyme 1 |
| IU | international unit |
| KCL | King's College London |
| K-HEPES | HEPES buffered with KOH |
| KIF | kinesin superfamily protein |
| KLC | kinesin light chain |
| KLP6 | kinesin-like protein 6 |
| L-15 | Leibovitz's-15 |
| laminin | laminin from Engelbreth-Holm-Swarm murine sarcoma basement membrane |
| LB | Luria Bertani |
| Lys | lysine |
| MAM | mitochondria-associated ER membranes |
| MAPs | microtubule-associated proteins |

| | |
|---|---|
| mCherry-α-tubulin | mCherry-tagged α-tubulin |
| Miro | mitochondrial Rho GTPase |
| MND | Motor Neuron Disease |
| mRNA | messenger RNA |
| MSP | major sperm protein |
| MW | molecular weight |
| myc-kinesin-1 | myc-tagged kinesin-1 |
| myc-Miro1 | myc-tagged Miro1 |
| myc-VAPB | myc-tagged VAPB |
| myc-VAPBP56S | myc-tagged VAPBP56S |
| N | number |
| NAD(P)H | nicotinamide adenine dinucleotide phosphate |
| Na-HEPES | HEPES buffered with NaOH |
| Nir | N-terminal domain-interacting receptor |
| NMDA | N-methyl-D-aspartate |
| ns | not significant |
| N-terminal | amino terminal |
| Ntg | non-transgenic |
| Nups | nucleoporins |
| OD | optical density |
| OIP | β-O-linked N-acetylglucosamine transferase-interacting protein |
| Opi1 | overproducer of inositol 1 |
| ornithine | poly-DL-ornithine hydrobromide |
| OSBP | oxysterol binding protein |
| p | protein |

| | |
|---|---|
| PBS | phosphate-buffered saline |
| PCR | polymerase chain reaction |
| PDI | protein disulphide isomerase |
| pH | power of hydrogen |
| PINK1 | phosphatase and tensin homologue (PTEN)-induced putative kinase protein 1 |
| PTPIP51 | protein tyrosine phosphatase-interacting protein 51 |
| Rac1 | Ras-related C3 botulinum toxin substrate 1 |
| RanBP2 | Ras-related nuclear protein-binding protein 2 |
| Ras | rat sarcoma |
| Rho | Ras homolog |
| RIPA | radioimmunoprecipitation assay |
| RNA | ribonucleic acid |
| RNase | ribonuclease |
| ROS | reactive oxygen species |
| rpm | revolutions per minute |
| SALS | sporadic ALS |
| SAX-3 Robo | sensory axon guidance 3 Roundabout |
| Scs2 | suppressor of choline sensitivity |
| SD | standard deviation |
| SDS | sodium dodecyl sulphate |
| SDS-PAGE | sodium dodecyl sulphate-polyacrylamide gel electrophoresis |
| SEM | standard error of mean |
| Sig-1R | Sigma-1 receptor |
| SMA | spinal muscular atrophy |

| | |
|---|---|
| SNARE | soluble N-ethylmaleimide-sensitive factor-attached protein receptor |
| SOD1 | Cu/Zn superoxide dismutase 1 |
| T | thymine |
| TAE | Tris-acetate-EDTA |
| *TARDBP* | *trans-activation response DNA binding protein* gene |
| TBS | Tris-buffered saline |
| TDP-43 | trans-activation response DNA binding protein 43 |
| TE | Tris-EDTA |
| TEMED | N,N,N',N'-tetramethylethylenediamine |
| TRAK | trafficking kinesin |
| Tris | tris(hydroxymethyl)aminomethane |
| UCSF | University of California, San Francisco |
| UK | United Kingdom |
| UPR | unfolded protein response |
| USA | United States of America |
| v/v | volume/volume |
| VAPB | vesicle-associated membrane protein-associated protein B |
| VAPBP56S | proline to serine substitution at position 56 in VAPB |
| VAPBT46I | threonine to isoleucine substitution at position 46 in VAPB |
| VCP | valosin-containing protein |
| VDAC1 | voltage-dependent anion channel 1 |
| w/v | weight/volume |
| XBP1 | X-box-binding protein 1 |
| X-gal | 5-bromo-4-chloro-3-indoyl-β-D-galactopyranoside |

# 1 INTRODUCTION

## 1.1 Motor Neuron Disease

"Motor Neuron Disease" (MND) is the collective name of a group of progressive neurodegenerative disorders that involve selective loss of upper and/or lower motor neurons. Clinically, MND is characterised by progressive weakness and wasting of muscles, leading to increasing loss of mobility in the limbs and difficulties with speech, swallowing and breathing (D'Amico et al., 2011; Finsterer, 2010; Strong and Gordon, 2005). The most prevalent MND is ALS.

There are nine subtypes of MND that are categorised according to the motor neurons (upper or lower) affected and the clinical phenotype that results (Table 1.1). ALS and progressive bulbar palsy (PBP) are characterised by loss of upper and lower motor neurons in the spinal cord, motor cortex and brain stem. In contrast, primary lateral sclerosis (PLS) and hereditary spastic paraplegia (HSP) only affect cortical upper motor neurons, and in spinal muscular atrophy (SMA), spinobulbar muscular atrophy (SBMA; also known as Kennedy's disease), progressive muscular atrophy (PMA), monomelic amyotrophy (also known as Hirayama disease) and brachial amyotrophic diplegia (BAD) only lower motor neurons in the lower bulbar region and spinal cord are selectively damaged (Strong and Rosenfeld, 2003; Strong and Gordon, 2005).

***Table 1.1. Classification of motor neuron disease***

| Affected neurons | Disease type |
|---|---|
| Upper and lower motor neuron involvement | Amyotrophic lateral sclerosis (ALS)<br>Progressive bulbar palsy (PBP) |
| Pure upper motor neuron involvement | Primary lateral sclerosis (PLS)<br>Hereditary spastic paraplegia (HSP) |
| Pure lower motor neuron involvement | Spinal muscular atrophy (SMA)<br>Spinobulbar muscular atrophy (SBMA)<br>Progressive muscular atrophy (PMA)<br>Monomelic amyotrophy<br>Brachial amyotrophic diplegia (BAD) |

### *1.1.1 Clinical features and pathology of amyotrophic lateral sclerosis (ALS)*

ALS is the most common adult onset motor neuron disorder. The prevalence of ALS is between 2.7 and 7.4 per 100,000 persons and its incidence is between 1.9 and 2.4 per 100,000 persons per year in European and North American countries (Logroscino et al., 2010; Turabelidze et al., 2008; Wolfson et al., 2009; Worms, 2001). ALS is characterised by upper and lower motor neuron degeneration which leads to progressive muscle atrophy and ultimately paralysis and death. Additionally, some cases are accompanied by Parkinsonism or frontotemporal dementia (ALS-FTD) (Kiernan et al., 2011).

The majority of ALS cases are sporadic (SALS) with no known genetic linkage and familial history, but approximately 5% of ALS cases are inherited and are known as familial ALS (FALS) (Byrne et al., 2011). The clinical symptoms are similar in both sporadic and familial forms suggesting the possibility of common disease mechanisms. Following progressive degeneration of upper and lower motor neurons, death due to respiratory failure usually occurs within 2 to 5 years from onset in the majority of the

cases (Kiernan et al., 2011). In addition to this 'classical' form of ALS, there are rare juvenile forms with an age of onset varying from 1 to 25 years of age and very slow progression (Andersen and Al-Chalabi, 2011).

ALS symptoms usually start with muscle weakness in the upper or lower limbs or dysarthria of speech. The degeneration and loss of motor neurons in the primary motor cortex, brainstem and spinal cord are accompanied by astrocytic gliosis and the presence of intraneuronal inclusions (Kiernan et al., 2011; Wood et al., 2003). There are three main types of intraneuronal inclusions in ALS, namely Bunina bodies, hyaline conglomerate inclusions and ubiquitinated inclusions (Wood et al., 2003).

Bunina bodies are eosinophilic, cytoplasmic inclusions which stain positive for cystatin C, peripherin and transferrin (Bunina, 1962; Mizuno et al., 2006b; Mizuno et al., 2011; Okamoto et al., 1993). Bunina bodies are present in the majority of ALS cases but are less common in other neurological conditions. They possibly originate from smooth endoplasmic reticulum (ER) or from the Golgi apparatus (Okamoto et al., 1993; Okamoto et al., 2008; Piao et al., 2003).

Hyaline conglomerate inclusions are large accumulations of phosphorylated and non-phosphorylated neurofilaments (Hirano et al., 1984a; Hirano et al., 1984b; Itoh et al., 1992; Munoz et al., 1988). Neurofilaments are synthesised in the cell body and transported into the axon and disruption of their transport is observed in ALS mouse models (Collard et al., 1995; Williamson and Cleveland, 1999; Zhang et al., 1997). Neurofilament transport is inhibited by phosphorylation of neurofilament side arms (Ackerley et al., 2004; Ackerley et al., 2003; Shea et al., 2004), and phosphorylated neurofilament deposits have been observed in ALS patients and mutant Cu/Zn superoxide dismutase 1 (SOD1) expressing transgenic mice (Ackerley et al., 2004; Itoh et al., 1992; Munoz et al., 1988; Nguyen et al., 2001; Sobue et al., 1990; Tu et al.,

1996). Thus, their perturbed axonal transport may cause their pathological accumulation. Hyaline conglomerate inclusions have also been reported in other neurodegenerative diseases in addition to ALS and in control samples and therefore they are less specific for ALS than Bunina bodies and ubiquitinated inclusions (Kusaka and Hirano, 1985; Sobue et al., 1990).

Ubiquitinated inclusions are present in most ALS cases and are often positive for trans-activation response deoxyribonucleic acid (DNA) binding protein 43 (TDP-43) (Arai et al., 2006; Neumann et al., 2006; Piao et al., 2003). Indeed, ubiquitinated cytoplasmic accumulations of TDP-43 are present in most ALS cases and are now considered as a hallmark pathology of ALS. However, in SALS and FALS cases with mutations in SOD1 and fused in sarcoma (FUS; also known as translocated in liposarcoma (TLS)) the ubiquitinated inclusions are generally believed to be TDP-43 negative (Mackenzie et al., 2007; Vance et al., 2009). Another commonly found protein in ubiquitinated inclusions is protein 62 (p62; also known as sequestosome 1), a cytosolic protein linked to ubiquitin and protein degradation (Arai et al., 2003; Mizuno et al., 2006a; Moscat et al., 2007; Nakano et al., 2004; Seibenhener et al., 2007). p62 immunoreactivity has been observed in a number of neurodegenerative diseases in addition to ALS suggesting that p62 may be involved in the pathogenesis of a spectrum of disorders (Arai et al., 2003; Kuusisto et al., 2001; Nakano et al., 2004). Ubiquitinated inclusions can be divided into two groups according to their morphology: skein-like inclusions are filamentous whereas Lewy body-like inclusions are spherical (Kato et al., 1989; Leigh et al., 1988; Lowe et al., 1988).

### *1.1.2 Genetics of ALS*

Mutations in a number of genes have been shown to cause FALS (Table 1.2) and genetic risk factors for SALS have also been described (Table 1.3). A full list of ALS-associated genes is also available on the following websites: ALSoD (http://alsod.iop.kcl.ac.uk) and ALSGene (http://www.alsgene.org) (Abel et al., 2012; Lill et al., 2011).

FALS inheritance is mainly autosomal dominant but autosomal recessive and X-chromosome linked forms have also been reported (Table 1.2) (Andersen and Al-Chalabi, 2011). The majority of FALS is adult onset but 5 loci have been described that lead to juvenile onset disease (ALS2, ALS4, ALS5, ALS15, and ALS16) (Table 1.2) (Andersen and Al-Chalabi, 2011). Some of the most common familial forms of ALS involve mutations in the *chromosome 9 open reading frame 72* (*C9ORF72*), *SOD1*, *TARDBP* and *FUS* genes. In addition, mutations in the *VAPB* gene cause ALS type-8 (Chen et al., 2010a; Nishimura et al., 2004) as VAPB is the topic of this thesis VAPB is discussed in section 1.2.

Expansion of the GGGGCC hexanucleotide repeat in intron 1 of the *C9ORF72* gene is currently the most common genetic defect in FALS (Cooper-Knock et al., 2012; Majounie et al., 2012; Sabatelli et al., 2012). In a Finnish population, repeat expansions in *C9ORF72* underlie 46% of FALS and in a North American cohort *C9ORF72* expansions accounted for 23.5% of FALS (DeJesus-Hernandez et al., 2011; Renton et al., 2011). The *C9ORF72* gene is expressed in most tissues and encodes an uncharacterised protein. Expansion of the hexanucleotide repeat in *C9ORF72* is also seen in some patients with fronto-temporal dementia (Byrne et al., 2012; DeJesus-Hernandez et al., 2011; Renton et al., 2011).

Mutations in the *SOD1* gene on chromosome 21 account for approximately 20% of FALS (Millecamps et al., 2010; Rosen et al., 1993). More than 150 disease-associated mutations have been identified in *SOD1*. SOD1 is a widely expressed mainly cytosolic protein that functions to catalyse the dismutation of superoxide by converting it to oxygen and hydrogen peroxide (Perry et al., 2010). Mutant SOD1 is misfolded and it aggregates in insoluble complexes and forms ubiquitinated, cytosolic inclusion bodies in SOD1 transgenic mice and ALS patients (Bruijn et al., 1997; Bruijn et al., 1998; Deng et al., 1993; Johnston et al., 2000; Shibata et al., 1994; Shibata et al., 1996).

Mutations in the *TARDBP* gene (encoding TDP-43) on chromosome 1 cause adult onset, autosomal dominant FALS with or without FTD and FTD linked to TDP-43 pathology (FTLD-TDP) (Benajiba et al., 2009; Gitcho et al., 2008; Kabashi et al., 2008; Kovacs et al., 2009; Sreedharan et al., 2008; Van Deerlin et al., 2008; Yokoseki et al., 2008). Mutations in the *FUS* gene on chromosome 16 cause adult onset, autosomal dominant FALS, ALS with FTD and FTD without ALS (Kwiatkowski et al., 2009; Vance et al., 2009). Mutations in the *TARDBP* and *FUS* genes account for approximately 4.1% and 4.4% of FALS, respectively (Millecamps et al., 2010). Both TDP-43 and FUS are nuclear proteins involved in ribonucleic acid (RNA) metabolism. Mutant TDP-43 and FUS show abnormal cytoplasmic localisation and form inclusions (Arai et al., 2006; Kwiatkowski et al., 2009; Neumann et al., 2006; Vance et al., 2009).

***Table 1.2 Familial amyotrophic lateral sclerosis-associated genes.***

| FALS type | Onset | Inheritance | Locus | Gene | References |
|---|---|---|---|---|---|
| ALS1 | Adult | AD/AR | 21q22.1/21q22.11 | *SOD1* | (Rosen et al., 1993) |
| ALS2 | Juvenile | AR | 2q33.1 | *ALS2* | (Hadano et al., 2001; Yang et al., 2001) |
| ALS3 | Adult | AD | 18q21 | unknown | (Hand et al., 2002) |
| ALS4 | Juvenile | AD | 9q34.13 | *SETX* | (Chen et al., 2004a) |
| ALS5 | Juvenile | AR | 15q21.1 | *SPG11* | (Orlacchio et al., 2010) |
| ALS6 | Adult | AD/AR | 16p11.2 | *FUS* | (Kwiatkowski et al., 2009; Vance et al., 2009) |
| ALS7 | Adult | AD | 20p13 | unknown | (Sapp et al., 2003) |
| ALS8 | Adult | AD | 20q13.33 | *VAPB* | (Nishimura et al., 2004) |
| ALS9 | Adult | AD | 14q11.2 | *ANG* | (Greenway et al., 2006; van Es et al., 2009a) |
| ALS10 | Adult | AD/AR | 1p36.22 | *TARDBP* | (Gitcho et al., 2008; Kabashi et al., 2008; Sreedharan et al., 2008; Van Deerlin et al., 2008; Yokoseki et al., 2008) |
| ALS11 | Adult | AD | 6q21 | *FIG4* | (Chow et al., 2009) |
| ALS12 | Adult | AD/AR | 10p13 | *OPTN* | (Maruyama et al., 2010) |
| ALS13 | Adult | AD | 12q24.12 | *ATXN2* | (Elden et al., 2010; Van Damme et al., 2011) |
| ALS14 | Adult | AD | 9p13.3 | *VCP* | (Johnson et al., 2010) |
| ALS15 | Adult/ Juvenile | XD | Xp11.21 | *UBQLN2* | (Deng et al., 2011) |
| ALS16 | Adult/ Juvenile | AD/ AR | 9p13.3 | *SIGMAR1* | (Al-Saif et al., 2011; Luty et al., 2010) |
| ALS18 | Adult | AD | 17p13.3 | *PFN1* | (Wu et al., 2012) |

Continued from page 27.

| FALS type | Onset | Inheritance | Locus | Gene | References |
|---|---|---|---|---|---|
| ALS-FTD1 | Adult | AD | 9q21-22 | unknown | (Hosler et al., 2000) |
| ALS-FTD2 | Adult | AD | 9p21 | *C9ORF72* | (DeJesus-Hernandez et al., 2011; Renton et al., 2011) |
| uncategorised | Adult | AD | 2p13.1 | *DCTN1* | (Münch et al., 2004) |
| uncategorised | Adult | AD | 12q24.11 | *DAO* | (Mitchell et al., 2010) |

AD=autosomal dominant; ALS=amyotrophic lateral sclerosis; ALS-FTD=amyotrophic lateral sclerosis with frontotemporal dementia; AR=autosomal recessive; FALS=familial amyotrophic lateral sclerosis; XD=X-chromosome-linked dominant
Data were obtained from (Andersen and Al-Chalabi, 2011) and the ALSoD website (http://alsod.iop.kcl.ac.uk).

The majority of ALS cases are sporadic and probably originate as the result of a complex interplay between genetic and/or environmental factors. Genetic screens and genome-wide association studies have revealed several susceptibility genes and genetic variants contributing to ALS pathogenesis (Table 1.3). However, most of the susceptibility genes and genetic variants await confirmation in additional studies and no single gene has been shown to be consistently associated with ALS risk. Some of the ALS susceptibility genes that are involved in cytoskeleton, axonal transport and $Ca^{2+}$ homeostasis (i.e. relevant to this thesis) are discussed below.

Variants of the *neurofilament heavy chain* gene (*NEFH*) have been observed in several ALS cases (Al-Chalabi et al., 1999; Figlewicz et al., 1994). Moreover, mutations in the gene encoding the intermediate filament peripherin (PRPH) (Gros-Louis et al., 2004; Leung et al., 2004) have also been found in ALS patients. Interestingly, a genetic variant of *kinesin-associated protein 3* (*KIFAP3*) is associated with increased survival in ALS patients (Landers et al., 2009). Since accumulation of neurofilaments and damaged axonal transport is seen in ALS cases (Ackerley et al., 2004; Carpenter, 1968; Hirano et al., 1984a; Ince et al., 1998; Sasaki and Iwata, 2007) (also see section 1.1.3.1 and 1.1.3.7) mutations in *NEFH*, *PRPH*, and *KIFAP3* strengthen the role of transport defect in ALS pathogenesis.

Further ALS susceptibility gene variants have been identified in the *1,4,5-triphosphate receptor 2* (*IP3R2*) and *uncoordinated 13 homolog A* (*UNC13A*) genes (van Es et al., 2007; van Es et al., 2009b). IP3R2 is an ER resident $Ca^{2+}$ channel which is responsible for intracellular $Ca^{2+}$ homeostasis (Mikoshiba, 2006). UNC13A regulates transmitter release from glutamatergic and GABAergic neurons (Varoqueaux et al., 2002). Aberrant mRNA processing of *SLC1A2*, encoding excitatory amino acid transporter 2 is also found in ALS (Aoki et al., 1998; Lin et al., 1998). Since perturbed

$Ca^{2+}$ homeostasis and elevated glutamate levels have been detected in ALS patients (Rothstein et al., 1992; Rothstein et al., 1990; Siklós et al., 1996) (also see section 1.1.3.3), *ITPR2*, *UNC13A* and *SLC1A2* may be important susceptibility genes for ALS.

In addition to the genetic risk factors, environmental risk factors for ALS have been described. These risk factors include smoking (Armon, 2003; Armon, 2009), intensive sport (Beghi et al., 2010; Chio et al., 2005), active military service (Horner et al., 2003; Kasarskis et al., 2009; Schulte et al., 1996), exposure to chemicals (Fang et al., 2009), lead (Kamel et al., 2002) and neurotoxins (Cox and Sacks, 2002). However, how different environmental factors influence ALS is not known and requires further investigation.

***Table 1.3 Susceptibility genes for ALS.***

| Gene | Locus | References |
|---|---|---|
| *ALAD* | 9q33.1 | (Kamel et al., 2003) |
| *APEX1* | 14q11.2 | (Hayward et al., 1999; Olkowski, 1998) |
| *APOE* | 19q13.2 | (al-Chalabi et al., 1996; Moulard et al., 1996) |
| *CHMP2B* | 3p11.2 | (Parkinson et al., 2006) |
| *CNTF* | 11q12.1 | (Giess et al., 2002) |
| *CYP2D6* | 22q13.1 | (Siddons et al., 1996) |
| *DPP6* | 7q36.2 | (van Es et al., 2008) |
| *ELP3* | 8p21.1 | (Simpson et al., 2009) |
| *EPHA4* | 2q36.1 | (Van Hoecke et al., 2012) |
| *FGGY* | 1p32.1 | (Dunckley et al., 2007) |
| *HFE* | 6p21.3 | (Wang et al., 2004) |
| *IP3R2* | 12p11 | (van Es et al., 2007) |
| *KIFAP3* | 1q24.2 | (Landers et al., 2009) |
| *LIF* | 22q12.2 | (Giess et al., 2000) |
| *MAOB* | Xp11.23 | (Orru et al., 1999) |
| *MAPT* | 17q21.1 | (Poorkaj et al., 2001) |
| *NEFH* | 22q12.2 | (Skvortsova et al., 2004) |
| *OGG1* | 3p26.2 | (Coppede et al., 2007) |
| *PGRN* | 17q21.32 | (Sleegers et al., 2008) |
| *PON1; PON2; PON3* | 7q21.3 | (Saeed et al., 2006; Slowik et al., 2006) |
| *PSEN1* | 14q24.3 | (Panas et al., 2000) |
| *PRPH* | 12q12-q13 | (Gros-Louis et al., 2004; Leung et al., 2004) |
| *SLC1A2* | 11p13-p12 | (Aoki et al., 1998; Lin et al., 1998) |
| *SMN1; SMN2* | 5q13.2 | (Corcia et al., 2002; Veldink et al., 2001) |
| *SOD2* | 6q25.3 | (Van Landeghem et al., 1999) |
| *SQSTM1* | 5q35 | (Fecto et al., 2011) |
| *TAF15* | 17q12 | (Ticozzi et al., 2011) |
| *UNC13A* | 19p13.11 | (van Es et al., 2009b) |
| *VEGFA* | 6p12 | (Lambrechts et al., 2003) |
| *ZNF512B* | 20q13.33 | (Iida et al., 2011) |

Data were obtained from the ALSoD website (http://alsod.iop.kcl.ac.uk).

## *1.1.3 Mechanisms of neurodegeneration in ALS*

The mechanisms by which motor neurons die in ALS are not properly understood. However, the principal mechanisms are pathological protein aggregation, ER stress, glutamatergic excitotoxicity, mitochondrial dysfunction, oxidative stress, damage to RNA processing and damage to axonal transport (for review see (Ferraiuolo et al., 2011)). None of these mechanisms are mutually exclusive and it is possible/probable that all contribute to the disease process. In addition, it has become clear that ALS is not just a disease of motor neurons, but that other cell types such as microglia and astrocytes contribute significantly to the pathogenic process (for review see (Ferraiuolo et al., 2011). The evidence supporting these different mechanisms is discussed below.

### 1.1.3.1 Pathological protein aggregation

The strongest evidence that abnormal protein aggregation is a component of the ALS disease process comes from the pathology of ALS. Indeed, the presence of ubiquitinated inclusions within motor neurons is a hallmark pathology of ALS (Ince et al., 2011; Strong et al., 2005). In particular, ubiquitinated TDP-43 inclusions are a common feature in ALS (Arai et al., 2006; Neumann et al., 2006). TDP-43 is principally a nuclear protein but in ALS it is proteolytically processed and redistributes to the cytoplasm where it becomes abnormally phosphorylated and ubiquitinated (Neumann et al., 2006). Phosphorylation of TDP-43 on serines 409/410 occurs in these inclusions (Arai et al., 2010; Hasegawa et al., 2008). Since mutations in TDP-43 are linked to familial and sporadic forms of ALS (Gitcho et al., 2008; Kabashi et al., 2008; Sreedharan et al., 2008; Van Deerlin et al., 2008; Yokoseki et al., 2008), it seems likely

that aberrant aggregation of TDP-43 contributes in at least some capacity to the disease process.

Pathological accumulations of other proteins also occur in ALS. Thus, neurofilaments are present in hyaline conglomerate inclusions and abnormal hyperphosphorylated neurofilaments are seen in cell bodies; neurofilaments are normally hyperphosphorlated in axons and not in cell bodies (Ackerley et al., 2004; Carpenter, 1968; Hirano et al., 1984a; Ince et al., 1998). Also inclusions containing abnormally misfolded SOD1 are seen in some FALS patients and especially those caused by mutant SOD1 (Shibata et al., 1994). More recently, antibodies have been created that selectively detect misfolded mutant but not normal SOD1 and these antibodies label the ALS SOD1 inclusions (Rakhit et al., 2007). Finally, in FALS patients linked to mutant FUS, cytoplasmic inclusions of mutant FUS are detected; FUS is normally found mainly in the nucleus (Kwiatkowski et al., 2009; Vance et al., 2009).

Some genetic evidence also supports a role for abnormal protein aggregation in ALS. Thus mutations in *valosin-containing protein* (*VCP*) on chromosome 9 have been found in 4 patients with FALS (Johnson et al., 2010). VCP (also known as p97) is an abundantly expressed adenosine triphosphate (ATP)ase associated with various activities that is involved in several cellular processes including mitochondrial and ER protein degradation, endolysosomal sorting, the ubiquitin proteasome system, ER and Golgi reassembly, nuclear envelope formation and the cell cycle (Acharya et al., 1995; Cao et al., 2003; Dai and Li, 2001; Fu et al., 2003; Hetzer et al., 2001; Latterich et al., 1995; Rabouille et al., 1995; Ritz et al., 2011; Xu et al., 2011a; Ye et al., 2001; Ye et al., 2004). ALS-associated mutation in VCP has been shown to cause impaired clearance of aggregated proteins, perturbs endolysosomal sorting and induces autophagosome accumulation (Ju et al., 2009; Ju et al., 2008; Ritz et al., 2011; Watts et al., 2004).

Interestingly, VCP plays a central role in ER-associated degradation (ERAD) by escorting ubiquitinated proteins to the proteasome for degradation by binding to Degradation in the ER-like protein 1 (Derlin-1) (Ye et al., 2005; Ye et al., 2004). Thus VCP may also be involved in mutant SOD1 induced ER stress pathways (see section 1.1.3.2).

Mutations in *ubiquilin 2* (*UBQLN2*) cause X-chromosome linked dominantly inherited ALS with or without FTD (ALS15) (Deng et al., 2011). The ubiquitin-like protein ubiquilin 2 is involved in protein degradation and binds to poly-ubiquitin chains and 19S proteasome subunits (Seok Ko et al., 2004). Mutant ubiquilin 2 perturbs the ubiquitin proteasome system suggesting a mechanism linked to impaired protein clearance in ALS (Deng et al., 2011).

### 1.1.3.2 ER stress

Cell survival is inseparably tied to protein quality control, which is achieved by protein homeostasis or proteostasis. Proteostasis entails a complex regulatory network that balances protein biosynthesis, folding, translocation, assembly/disassembly, and clearance (degradation). Eukaryotic cells have two major degradation systems, the proteasome and the lysosome (Wong and Cuervo, 2010). The proteasome selectively recognizes ubiquitinated substrates, which are mostly short-lived proteins. Autophagy denotes the delivery of cytosolic components and organelles (dubbed mitophagy in case of mitochondria) to the lysosome for degradation. Cells use stress sensors and inducible pathways to respond to a loss of proteostatic control. One of these pathways is the unfolded protein response (UPR), an adaptive response to the accumulation of misfolded proteins in the lumen of the ER (i.e. ER stress) (for reviews see (Bernales et

al., 2006; Lin et al., 2008)). The UPR tries to restore proteostasis by (i) attenuation of translation, (ii) induction of chaperones to aid protein folding, and (iii) upregulation of degradation pathways such as ERAD and autophagy to remove misfolded proteins. However, if ER stress persists the UPR initiates apoptosis (Nakagawa et al., 2000; Nishitoh et al., 2002).

A number of lines of evidence suggest that ER stress occurs in ALS. Firstly, mutations in the gene encoding VAPB cause ALS type-8 and there is evidence that VAPB functions in mediating the UPR in response to ER stress. Since this thesis involves work with VAPB, this aspect is covered in more detail in section 1.2.1.5.

Secondly, ER stress and activation of the UPR has been described in spinal cord of presymptomatic transgenic mice that express ALS mutant SOD1 and which develop ALS, and in cell lines that express mutant SOD1 (Atkin et al., 2006; Kikuchi et al., 2006; Nishitoh et al., 2008; Tobisawa et al., 2003). Interestingly, in mutant SOD1 expressing mice the upregulation of the ER resident misfolded protein sensor glucose-regulated protein 78/immunoglobulin heavy-chain binding protein (GRP78/BiP), which is indicative of ER stress and UPR, appears to be specific for the fast-fatigable motor neurons, which are most susceptible to disease in ALS and was observed as early as postnatal day 5 (Saxena et al., 2009). How mutant SOD1 induces ER stress is not clear as SOD1 is cytosolic but it has been shown that mutant SOD1 aggregates accumulate in the ER lumen and on the cytosolic surface of the ER where they interact with GRP78/BiP and Derlin-1, respectively (Kikuchi et al., 2006; Nishitoh et al., 2008). Binding of mutant SOD1 to Derlin-1 inhibits ERAD and increases ER stress and UPR (Nishitoh et al., 2008). The aberrant interaction between mutant SOD1 and GRP78/BiP may also lead to an uncontrolled and prolonged UPR by preventing GRP78/BiP interaction with ER stress sensors (Kikuchi et al., 2006). Sustained ER stress and UPR

activates apoptosis via cysteinyl aspartate-specific protease-12 (caspase-12) and apoptosis signal-regulating kinase 1 (ASK1) (Nakagawa et al., 2000; Nishitoh et al., 2002). Caspase-12 and ASK1 are activated in ALS mutant SOD1 expressing transgenic mice suggesting that UPR dependent apoptosis may contribute to neurodegeneration in ALS (Atkin et al., 2006; Holasek et al., 2005; Kikuchi et al., 2006; Nishitoh et al., 2008; Wengenack et al., 2004; Wootz et al., 2004).

Finally, TDP-43 is cleaved to generate carboxyl (C)-terminal 25 kDa fragments, which are ubiquitinated and hyperphosphorylated in ALS; these are the main species found in cytoplasmic TDP-43 aggregates (Igaz et al., 2009; Igaz et al., 2008; Neumann et al., 2006; Zhang et al., 2009). Interestingly, chemical induction of ER stress has been shown to cause cleavage of TDP-43 (Suzuki et al., 2011).

### 1.1.3.3 Glutamatergic excitotoxicity

Glutamate is the major excitatory neurotransmitter in the central nervous system. Glutamate released from the presynaptic neuron exerts its effects by binding to a number of postsynaptic ionotropic and metabotropic receptors (Nicoletti et al., 2011; Traynelis et al., 2010). Under physiological conditions, the excitatory glutamate signal is terminated by rapid removal of glutamate from the synaptic cleft by glial and neuronal glutamate reuptake transporters (Kanai and Hediger, 2004). The most abundant glutamate reuptake transporter is the astroglial excitatory amino acid transporter 2 (EAAT2; also known as glutamate transporter 1 (GLT1)) (Danbolt, 2001). It is well established that excessive stimulation of glutamate receptors causes injury to neurons in a process called excitotoxicity (Foran and Trotti, 2009). Excitotoxicity may be caused by increased levels of glutamate at the synapse or by sensitization of the

postsynaptic neuron to glutamate because of alterations in glutamate receptor expression and/or changes in $Ca^{2+}$ and energy homeostasis. Several lines of evidence suggest that glutamate excitotoxicity is implicated in ALS and causes motor neuron damage.

Firstly, elevated levels of glutamate in the cerebrospinal fluid of ALS patients have been described (Shaw et al., 1995a). Also levels of EAAT2 are reduced in ALS spinal cord (Rothstein et al., 1992; Rothstein et al., 1995). Together, these observations suggest that glutamate metabolism is disrupted in ALS.

Secondly, motor neurons are particularly sensitive to alpha-amino-3-hydroxy-5-methylisoxazole-4-propionic acid (AMPA) receptor mediated excitotoxicity (Carriedo et al., 1996; Van Damme et al., 2005; Van Den Bosch et al., 2000) and this is most likely due to several intrinsic motor neuron properties. Thus, motor neurons express only low levels of $Ca^{2+}$ buffering proteins such as parvalbumin and calbindin-D28K (Ince et al., 1993) and consequently rely strongly on mitochondria to maintain $Ca^{2+}$ homeostasis (Alexianu et al., 1994; Andressen et al., 1993). Repeated stimulation of motor neurons leads to saturation of mitochondrial $Ca^{2+}$ buffering and permanently increases $[Ca^{2+}]c$ (Grosskreutz et al., 2007). Furthermore, excessive $Ca^{2+}$ entry into motor neurons can induce $Ca^{2+}$ overload in mitochondria, which leads to depolarization and production of reactive oxygen species (ROS) (Carriedo et al., 2000). A considerable amount of evidence suggests that mitochondrial function, including $Ca^{2+}$ buffering, is compromised in ALS (see section 1.1.3.4), which could further increase the vulnerability of motor neurons to excitotoxicity. Also, motor neurons have a high number of $Ca^{2+}$-permeable AMPA receptors because they are relatively deficient in the glutamate receptor 2 (GluR2) AMPA receptor subunit (Heath et al., 2002; Kawahara et al., 2003); AMPA receptors that include the GluR2 subunit are $Ca^{2+}$ impermeable. Additionally, the Q/R editing of GluR2 mRNA is reduced in ALS patients (Kawahara et

al., 2004; Takuma et al., 1999), and lack of Q/R editing of GluR2 increases the $Ca^{2+}$ permeability of GluR2 (Burnashev et al., 1992).

Thirdly, mutations in alsin, a guanine nucleotide exchange factor (GEF) for the small guanosine triphosphate (GTP)ases rat sarcoma (Ras)-related GTP-binding protein 5 (Rab5) and Ras-related C3 botulinum toxin substrate 1 (Rac1), cause autosomal recessive juvenile onset FALS type-2 (ALS2), infantile-onset HSP, and juvenile PLS (Eymard-Pierre et al., 2002; Gros-Louis et al., 2003; Hadano et al., 2001; Hentati et al., 1994; Otomo et al., 2003; Topp et al., 2004; Yang et al., 2001) and alsin has been linked to glutamate signalling. In particular, alsin has been shown to interact with glutamate receptor interacting protein 1 (GRIP1), a regulator of synaptic targeting of GluR2 (Lai et al., 2006). Alsin deficiency alters the subcellular distribution of GRIP1 and reduces the amount of GluR2 at the synapse leading to increased susceptibility to glutamate excitotoxicity (Lai et al., 2006).

However, perhaps the strongest evidence that excitotoxicity has a role in ALS is that riluzole, the only drug proven to slow the disease process in humans, has anti-excitotoxic properties (Bensimon et al., 1994; Lacomblez et al., 1996). Riluzole inhibits pre-synaptic glutamate release, but may also influence post-synaptic events by non-competitive inhibition of *N*-methyl-D-aspartate (NMDA) and AMPA receptors (Albo et al., 2004; Debono et al., 1993) and by affecting the γ-aminobutyric acid A (GABAA) receptor (He et al., 2002). However, other anti-glutamate drugs have failed in clinical trials (Cudkowicz et al., 2003; Miller et al., 2001), suggesting that riluzole may also act on other pathways. One such pathway may be axonal transport (Stevenson et al., 2009) (see section 1.1.3.7).

### 1.1.3.4 Mitochondrial dysfunction

Disease-associated abnormalities in mitochondrial morphology, such as mitochondrial swelling and vacuolisation have been observed in both FALS and SALS patients (Sasaki and Iwata, 1996; Sasaki and Iwata, 2007). Moreover, these morphological changes correlate with functional alterations such as defects in ATP production and the electron transport chain, and $Ca^{2+}$ buffering (Borthwick et al., 1999; Carrì et al., 1997; Fujita et al., 1996; Siklós et al., 1996; Siklós et al., 1998; Wiedemann et al., 2002). Hence it has been proposed that mitochondrial dysfunction may be a key pathogenic event in ALS.

Mitochondrial abnormalities and functional deficits have been consistently reported in ALS mutant SOD1 transgenic mouse models and mutant SOD1 expressing cell lines (Dal Canto and Gurney, 1995; Kong and Xu, 1998; Liu et al., 2004; Menzies et al., 2002; Pasinelli et al., 2004; Raimondi et al., 2006; Sotelo-Silveira et al., 2009; Vande Velde et al., 2011; Wong et al., 1995). A proportion of mutant SOD1 is localised to mitochondria and is present in the mitochondrial matrix and intermembrane space, and on the outer mitochondrial membrane, suggesting that mutant SOD1 may directly damage mitochondria (Higgins et al., 2002; Kawamata and Manfredi, 2008; Liu et al., 2004; Mattiazzi et al., 2002; Vande Velde et al., 2008; Vijayvergiya et al., 2005). This abnormal localisation of mutant SOD1 to mitochondria is specific for spinal cord mitochondria and not found in brain or liver, indicating its direct relevance for disease (Pasinelli et al., 2004; Vande Velde et al., 2008).

More recently, a molecular target in mitochondria for mutant SOD1 has been identified. Mutant SOD1 directly binds to the voltage-dependent anion channel 1 (VDAC1) in the outer mitochondrial membrane (Israelson et al., 2010). VDAC1

regulates the ion and metabolite flux between mitochondria and cytosol and is also the gatekeeper of apoptosis as part of the membrane permeability transition pore (McCommis and Baines, 2011). Interaction of mutant SOD1 with VDAC1 decreases adenosine diphosphate (ADP) transport across the outer mitochondrial membrane which can lead to reduced ATP production (Israelson et al., 2010) and thus may explain the perturbation of ATP synthesis that has been observed in mutant SOD1 models (Carrì et al., 1997; Damiano et al., 2006; Igoudjil et al., 2011). The targeting of VDAC1 by mutant SOD1 may also underlie the aberrant $Ca^{2+}$ handling and impaired $Ca^{2+}$ buffering by mitochondria observed in mutant SOD1 models (Grosskreutz et al., 2007; Jaiswal et al., 2009; Manfredi and Xu, 2005). Indeed, VDAC1 is involved in $Ca^{2+}$ exchange between ER and mitochondria via interaction with inositol-1,4,5-triphosphate receptors (IP3R) (Rapizzi et al., 2002; Szabadkai et al., 2006). Aberrant mitochondrial $Ca^{2+}$ handling has also been described in VAPB-related ALS (De Vos et al., 2012) (see section 1.2.2) and ALS patients (Siklós et al., 1996) but it is not clear if this involves VDAC1. Nevertheless, impaired mitochondrial $Ca^{2+}$ handling and increased $[Ca^{2+}]c$ have emerged as a common observation in ALS that could be a primary pathogenic event or act indirectly by inducing defects in axonal transport (Chang et al., 2006; MacAskill et al., 2009b; Rintoul et al., 2003; Saotome et al., 2008; Wang and Schwarz, 2009), or by rendering motor neurons vulnerable to excitotoxicity (see section 1.1.3.3).

In addition to VDAC1, mutant SOD1 binds and aggregates with the anti-apoptotic protein B-cell lymphoma-2 (Bcl-2) in spinal cord mitochondria (Pasinelli et al., 2004). Such sequestering of Bcl-2 may be the underlying cause of cytochrome c release and caspase activation in mutant SOD1 models (Kirkinezos et al., 2005; Takeuchi et al., 2002).

### 1.1.3.5 Oxidative stress

The main free radicals in cells are reactive oxygen species (ROS) and reactive nitric species (e.g. nitric oxide). ROS are natural by-products of aerobic metabolism that are produced mainly by the mitochondrial electron transfer chain and nicotinamide adenine dinucleotide phosphate (NAD(P)H) oxidase.

Several lines of research suggest that oxidative stress is involved in the pathology of ALS. Firstly, markers for oxidative stress have been observed in the spinal cord, the motor cortex as well as in serum of ALS patients (Abe et al., 1997; Beal et al., 1997; Ferrante et al., 1997; Shaw et al., 1995b; Simpson et al., 2004). Secondly, mutant SOD1 mice display impairment of electron transport and altered mitochondrial $Ca^{2+}$ levels which are accompanied by oxidative stress, and the generation of reactive oxygen species (Kruman et al., 1999). Finally, overexpression of ALS mutant TDP-43 has been shown to cause oxidative injury to motor neuronal cell lines (Duan et al., 2010).

The source of oxidative stress in ALS is not well defined but most likely involves mitochondria (see section 1.1.3.4) and activation of microglial superoxide production. Activated microglia increase NAD(P)H oxidase-mediated superoxide production as a defence against pathogens (Bedard and Krause, 2007). NAD(P)H oxidase activity is upregulated in ALS patients and mutant SOD1 mouse models (Marden et al., 2007; Wu et al., 2006). Mechanistically, mutant SOD1 expressed in microglia increases NAD(P)H oxidase-mediated superoxide production by binding to Rac1 and locking NAD(P)H oxidase in the activated state (Harraz et al., 2008). In addition to this direct effect of mutant SOD1 on NAD(P)H oxidase, there is also an indirect mechanism in which mutant SOD1 is aberrantly secreted by neurons and astrocytes via interactions with chromogranin-A and B to activate microglia (Urushitani et al., 2006; Zhao et al., 2010).

Indeed, extracellular wild-type and mutant SOD1 have been observed in the cerebrospinal fluid of ALS patients and SOD1 transgenic animals (Jacobsson et al., 2001; Turner et al., 2005; Urushitani et al., 2006).

### 1.1.3.6 Damage to RNA processing

Some of the first evidence that damage to RNA processing contributes to the disease process in ALS came from studies of ALS patient material (Lin et al., 1998). In particular, defective splicing of mRNA for the glial glutamate transporter EAAT2 was seen in ALS patients and this provided a link to excitoxicity in ALS (Lin et al., 1998). More recently, genetic and other studies have provided further support that defective mRNA metabolism occurs in ALS. Thus, mutations in TDP-43, FUS and senataxin have been shown to cause some familial forms of ALS and these proteins are all believed to function in mRNA metabolism (Chen et al., 2004b; Kwiatkowski et al., 2009; Sreedharan et al., 2008; Vance et al., 2009).

TDP-43 is a DNA and mRNA binding protein that regulates mRNA expression, splicing, translation and gene transcription (Cohen et al., 2011). Expression of mutant TDP-43 in cells leads to a predominantly cytoplasmic localization of the protein, particularly in cytoplasmic stress granules (Arai et al., 2006; Liu-Yesucevitz et al., 2010; Neumann et al., 2006). Stress granules are cytoplasmic aggregates of mRNA and proteins that occur within cells under certain conditions of stress. Stress granules function to sequester mRNA not needed for protection against the stress and can modulate the signalling balance between apoptosis and survival (Thomas et al., 2011).

Some of the mRNA targets for TDP-43 have now been identified and these include several that are linked to ALS including FUS, EAAT1, progranulin and TDP-43 itself (Polymenidou et al., 2011; Sephton et al., 2011; Tollervey et al., 2011).

Like TDP-43, ALS mutant FUS shows abnormal cytoplasmic localisation and can induce the formation FUS containing cytoplasmic stress granules (Dormann et al., 2010; Ito et al., 2011). FUS is also believed to function in transport of mRNAs to synapses for local translation (Kanai et al., 2004).

Lastly, expansion of a GGGGCC hexanucleotide repeat in *C9ORF72* is currently the most common genetic defect in FALS and SALS (and also in FTD) (Cooper-Knock et al., 2012; DeJesus-Hernandez et al., 2011; Majounie et al., 2012; Renton et al., 2011; Sabatelli et al., 2012). The *C9ORF72* gene encodes an uncharacterised protein but it is possible that the expanded hexanucleotide repeat acts to sequester mRNA binding proteins in foci such that mRNA metabolism is disrupted (DeJesus-Hernandez et al., 2011). In this scenario, it is mutant C9ORF72 mRNA, not the protein, that is toxic. There are precedents for toxic mRNAs causing disease in some myotonic dystrophies and ataxias (Todd and Paulson, 2010).

### 1.1.3.7 Damage to axonal transport

The correct transport of protein and organelle cargoes is a fundamental requirement for virtually every mammalian cell type. Thus ablation of genes encoding molecular motors that drive transport often results in a lethal phenotype (Hirokawa and Noda, 2008). Neurons are especially dependent upon transport processes since they are polarised with axons and dendrites, and also because some of the distances involved in transport (especially through axons) can be exceptionally long. Since most neuronal

proteins are synthesised within the cell body and then transported to their final destination, neurons require transport of proteins, organelles and other nutrients to distal regions of axons and dendrites to permit proper functioning and survival of synapses. Likewise, transport of trophic factors from synapses to the cell body is also important. Transport through axons is called “axonal transport”. Cargo transport from the cell body towards the synapse is termed anterograde axonal transport whereas transport from the synapse to the cell body is termed retrograde axonal transport. Most long-range transport of cargoes through axons is mediated by kinesin and cytoplasmic dynein-1 molecular motors that move along microtubules. Microtubules are almost uniformly orientated within axons with their plus ends (the ends to which tubulin subunits are added) positioned towards the synapse. Since most kinesins move toward the plus end of microtubules and cytoplasmic dynein-1 moves towards the minus end of microtubules, kinesins drive most anterograde and cytoplasmic dynein-1 most retrograde axonal transport of cargoes (Hirokawa and Noda, 2008).

A number of lines of evidence suggest that defective axonal transport contributes to ALS (for review see (De Vos et al., 2008)). Firstly, mutations in dynactin, a component of the cytoplasmic dynein-1 molecular motor, are linked to ALS (Münch et al., 2004; Puls et al., 2003). Mutant dynactin has now been shown to disrupt dynactin/dynein function (Levy et al., 2006).

Secondly, the pathology of ALS is consistent with damage to axonal transport. Thus, accumulations of neurofilaments are seen in cell bodies indicating that they are not being properly transported into axons (Ackerley et al., 2004; Carpenter, 1968; Hirano et al., 1984a; Ince et al., 1998). Likewise, mitochondria accumulate in proximal regions of motor neuron axons in ALS suggesting that their transport to more distal regions and synapses is perturbed (Sasaki and Iwata, 2007).

Thirdly, damage to axonal transport is seen in transgenic mouse and other models of ALS. Defective axonal transport of cytoskeleton components such as neurofilaments is seen in presymptomatic mutant SOD1 transgenic mice that develop ALS (Williamson and Cleveland, 1999; Zhang et al., 1997). Moreover, overexpression of neurofilaments including peripherin can model ALS (Beaulieu et al., 1999; Cote et al., 1993; Lee et al., 1994; Xu et al., 1993). Additionally, damage to axonal transport is also observed in these models (Collard et al., 1995; Millecamps et al., 2006). Further evidence that axonal transport defects contribute to ALS pathogenesis comes from experiments using riluzole, the only drug proven to slow the disease process in humans. Riluzole protects against glutamate-induced disruption of axonal transport of neurofilaments in rat cortical neurons (Stevenson et al., 2009).

Besides neurofilament transport, mutant SOD1 also affects axonal transport of other cargoes such as vesicles and mitochondria (Bilsland et al., 2010; De Vos et al., 2007; Kieran et al., 2005; Magrané et al., 2012; Marinković et al., 2012). In particular, mutant SOD1 has been shown to inhibit axonal transport of tetanus toxin fragment labelled endocytic carriers and mitochondria in motor but not sensory neurons *in vivo* in transgenic mice (Bilsland et al., 2010). Moreover, these transport deficits were detected in presymptomatic animals (Bilsland et al., 2010). Such elegant *in vivo* studies which demonstrate that impairment of axonal transport is one of the earliest pathological features argue strongly that defective transport contributes to the pathogenic process in ALS (Bilsland et al., 2010).

Fourthly, disruption to molecular motor function can model ALS in transgenic mice. The first evidence support this came frome analyses of the *Legs at odd angles* (*Loa*) and *Cramping1* (*Cra1*) mutant mice (Hafezparast et al., 2003). These animals carry point mutations in the gene encoding dynein heavy chain and develop a

neurological defects and ALS-type symptoms (Hafezparast et al., 2003). Moreover, retrograde axonal transport is defective in these animals (Hafezparast et al., 2003). Interestingly, crossing of *Loa* mice with mutant SOD1 mice produces a surprising phenotype involving rescue of axonal transport defects and extension of life span (Chen et al., 2007; Kieran et al., 2005). The precise mechanism for this effect is unknown but one hypothesis is that reduced retrograde transport caused by the *Loa* mutation counterbalances mutant SOD1 triggered anterograde transport defects to restore an overall balance of transport (De Vos et al., 2007; Kieran et al., 2005).

Finally, mice overexpressing p50/dynamitin develop motor neuron disease (LaMonte et al., 2002). p50/dynamitin is a component of the dynactin complex that is associated with dynein and overexpression of p50/dynamitin disrupts dynein function and axonal transport (LaMonte et al., 2002).

Although most evidence points towards an involvement of axonal transport defects in ALS, there is some evidence suggesting that damage to axonal transport is not involved in ALS. Syntaphilin is a protein that anchors mitochondria to halt their movement through axons; syntaphilin knockout mice have increased mitochondrial movement (Kang et al., 2008). Crossing of ALS mutant SOD1 transgenic mice with syntaphilin knockout mice increases mitochondrial axonal transport but this increase does not slow disease progression in the mutant SOD1/syntaphilin knockout mice (Zhu and Sheng, 2011). However, damage to transport of a number of cargoes, not just mitochondria, is seen in mutant SOD1 forms of ALS (Bilsland et al., 2010; De Vos et al., 2007; Kieran et al., 2005; Williamson and Cleveland, 1999; Zhang et al., 1997) and loss of syntaphilin only stimulates transport of mitochondria. Also, there is evidence that mutant SOD1 damage to mitochondrial transport is directional (De Vos et al., 2007) but loss of syntaphilin increases both anterograde and retrograde movement (Zhu and

Sheng, 2011). Having the correct balance of anterograde and retrograde transport is likely to be important and indeed, correction of this balance is a suggested mechanism for how the *Loa* mutation is protective in mutant SOD1 transgenic mice (Kieran et al., 2005).

More recently, analyses of different mutant SOD1 transgenic mice have also queried the role of defective axonal transport in ALS (Marinković et al., 2012). In particular, defective transport of mitochondria was not observed in mutant SOD1-G85R transgenic mice that develop disease whereas wild-type SOD1 overexpressing transgenic mice did develop a mitochondrial transport defect (Marinković et al., 2012). However, other groups have obtained differing results. In particular, SOD1-G85R transgenic mice and neurons transfected to express SOD-G85R have both been shown to have defective axonal transport whereas, no transport defects were detected in wild-type SOD1 expressing neurons (De Vos et al., 2007; Williamson and Cleveland, 1999). Also, the onset of the transport defect is remarkably late in wild-type SOD1 overexpressing mice compared to SOD1-G93A mice (postnatal day 60 vs. postnatal day 10) (Marinković et al., 2012). It has been reported that some wild-type SOD1 overexpressing mice exhibit signs of premature aging (Avraham et al., 1988; Avraham et al., 1991; Ceballos-Picot et al., 1991) and as such this late transport defect may be linked to ageing.

Thus, on balance most evidence supports a role for defective axonal transport as part of the pathogenic process in ALS. Demontrating that further mutant proteins linked to ALS also damage axonal transport would increase support for this notion. One of the aims of this thesis was to pursue such an approach.

## 1.2 Vesicle-associated membrane protein-associated protein B (VAPB)

VAPs are integral ER proteins that are expressed in mammals, insects, molluscs, plants, and fungi (Kagiwada et al., 1998; Laurent et al., 2000; Nishimura et al., 1999; Pennetta et al., 2002; Skehel et al., 2000; Skehel et al., 1995; Weir et al., 1998). In mammals, there are two VAP isoforms named VAPA and VAPB that are encoded by different genes. VAPA and VAPB share approximately 63% sequence identity and are expressed in most tissues and cell types including the nervous system (Amarilio et al., 2005; Gkogkas et al., 2008; Kim et al., 2010; Nishimura et al., 1999; Skehel et al., 2000; Teuling et al., 2007). VAPs consist of an N-terminal major sperm protein (MSP) domain, named for its similarity to the nematode MSP, a central coiled-coil domain and a carboxyl (C)-terminal transmembrane domain, which anchors them in the ER membrane (Figure 1.1) (Nishimura et al., 1999; Skehel et al., 2000; Soussan et al., 1999). A splice variant of VAPB that lacks both the coiled-coil and transmembrane domains termed VAPC has been described (Nishimura et al., 1999).

VAPB has been implicated in a variety of cellular processes, including bouton formation at the neuromuscular junction (Pennetta et al., 2002), ER to Golgi transport (Amarilio et al., 2005), microtubule organisation (Pennetta et al., 2002), lipid transport and metabolism (Peretti et al., 2008), $Ca^{2+}$ homeostasis (De Vos et al., 2012), and the UPR in response to ER stress (Gkogkas et al., 2008; Kanekura et al., 2006; Langou et al., 2010; Suzuki et al., 2009). Furthermore, a cleaved and secreted VAPB fragment acts as a ligand for ephrin receptors (Han et al., 2012; Tsuda et al., 2008). To carry out these functions, VAPB interacts with several proteins including soluble N-ethylmaleimide-

sensitive factor-attached protein receptor (SNARE) proteins (Skehel et al., 1995), two phenylalanines (FF) in acidic tract (FFAT) motif-containing proteins (Amarilio et al., 2005), microtubules (Pennetta et al., 2002; Skehel et al., 2000), protein tyrosine phosphatase-interacting protein 51 (PTPIP51) (De Vos et al., 2012), activating transcription factor 6 (ATF6) (Gkogkas et al., 2008) and some viral proteins (Hamamoto et al., 2005).

A missense mutation in exon 2 of the *VAPB* gene on chromosome 20 that results in the substitution of a conserved proline for a serine at codon 56 in VAPB (VAPBP56S) causes heterogeneous MND, including slowly progressing adult onset autosomal dominant FALS type-8 (ALS8), ALS with rapid progression, and late-onset SMA (Nishimura et al., 2004). Although this mutation was initially believed to be limited to eight Brazilian families with a common founder (Nishimura et al., 2005), VAPBP56S was subsequently found in families of European and Japanese lineage (Funke et al., 2010; Millecamps et al., 2010). An additional mutation also within the MSP domain (VAPBT46I) in a British ALS patient has been reported, although this mutation has not conclusively been linked to FALS (Chen et al., 2010a).

VAPBP56S aggregates and induces the formation of abnormal ER-derived inclusions (Fasana et al., 2010; Langou et al., 2010; Nishimura et al., 2004; Teuling et al., 2007; Tudor et al., 2010). The biological consequences of these inclusions and the mechanism by which VAPBP56S causes disease remain unclear. VAPBP56S may inhibit VAPB function by sequestering wild-type VAPB to the inclusions and preventing its interaction with other proteins (Kanekura et al., 2006; Mitne-Neto et al., 2007; Ratnaparkhi et al., 2008; Suzuki et al., 2009; Teuling et al., 2007). Alternatively, VAPBP56S could be a toxic gain-of-function mutant because VAPBP56S

overexpression has been shown to induce the UPR (Gkogkas et al., 2008; Tsuda et al., 2008).

Below I summarise our current knowledge of the cellular functions of VAPB and the proposed mechanisms underlying VAPBP56S-related ALS.

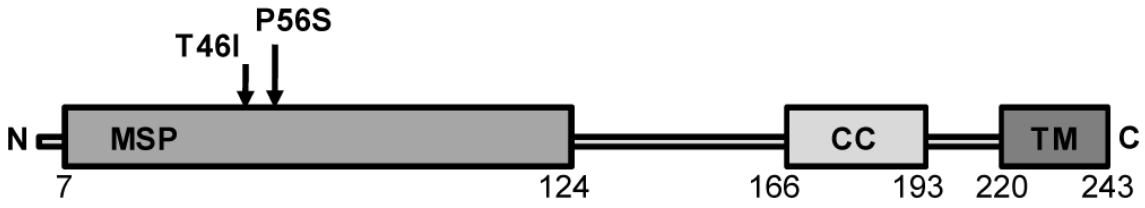


***Figure 1.1. Domain organisation of VAPB.***

VAPB consists of an amino (N)-terminal major sperm protein domain (MSP), a central coiled-coil domain (CC) and a carboxyl (C)-terminal transmembrane domain (TM). The T46I and P56S mutations involved in ALS are indicated.

## *1.2.1 Cellular functions of VAPB*

### 1.2.1.1 Role of VAPB in membrane fusion and vesicle trafficking

Budding of vesicles, their transport between different organelles and the plasma membrane, and their fusion with an appropriate acceptor is controlled by several proteins (Spang, 2008; Verhage and Sørensen, 2008). SNARE proteins facilitate membrane fusion by coordinated co-operation with Rab GTPases and tethering complexes and are essential for vesicle docking and fusion of membrane layers (Söllner et al., 1993; Wickner, 2010). VAPB was identified as an interacting partner of the synaptic vesicle SNARE protein vesicle-associated membrane protein

(VAMP)/synaptobrevin in a yeast two-hybrid screen of *Aplysia californica* and was shown to be required for synaptic transmission in *Aplysia* sensory/motor neuron co-cultures (Skehel et al., 1995). Human VAPB also interacts with VAMP *in vitro* suggesting that human VAPB might also play a role in vesicle dynamics and synaptic transmission (Weir et al., 1998).

Several lines of evidence indicate that VAPB is involved in transport of vesicles between ER and Golgi and in intra-Golgi transport. Transport through the Golgi apparatus and from the Golgi to ER is mediated by coat protein I (COPI)-coated vesicles (Letourneur et al., 1994; Orci et al., 1997) whereas transport from ER to Golgi is mediated by coat protein II (COPII)-coated vesicles via the ER-Golgi intermediate compartment (ERGIC) (Barlowe et al., 1994; Campbell and Schekman, 1997). VAPB has been shown to colocalise with COPI vesicles, ERGIC-53 and the COPII vesicle marker secretion-defective 23 (Sec23) (Moumen et al., 2011; Tran et al., 2012). Administration of anti-VAPB antibodies in *in vitro* transport assays inhibited retrograde intra-Golgi transport and caused the accumulation of COPI-coated vesicles (Soussan et al., 1999). siRNA-mediated depletion of VAPB expression caused ERGIC membrane expansion and mislocalisation of ERGIC-53, and the nuclear envelope membrane proteins nucleoporins (Nups) and Emerin (EMD) (Tran et al., 2012). VAPB also has been shown to interact with the FFAT motif-containing N-terminal domain-interacting receptor (Nir) proteins Nir2 and Nir3 (Amarilio et al., 2005; Loewen et al., 2003). Nir2 is a Golgi and ER membrane-associated protein that binds to the MSP domain of VAPB via its FFAT motif (Amarilio et al., 2005; Kaiser et al., 2005; Litvak et al., 2002). Overexpression of VAPB and Nir2 in cultured cells results in remodelling of the ER into stacked membrane arrays and attenuates protein export from the ER to the Golgi apparatus (Amarilio et al., 2005).

### 1.2.1.2 Role of VAPB in microtubule organisation

Microtubules are essential for several intracellular transport processes but also control cell shape and the localisation, shape, support, and arrangement of intracellular organelles (Brownhill et al., 2009; Kapitein and Hoogenraad, 2011; Poulain and Sobel, 2010; Vedrenne and Hauri, 2006). VAPB has been shown to interact with microtubules either directly or indirectly in light and electron microscopy studies and in *in vitro* binding assays (Amarilio et al., 2005; Pennetta et al., 2002; Skehel et al., 2000). Through its interaction with microtubules, VAPB influences the neuromuscular junction in *Drosophila melanogaster* (Pennetta et al., 2002) and ER structure in cell line (Amarilio et al., 2005). The *Drosophila* homolog of VAPB, DVAP-33, is essential for microtubule integrity and synaptic homeostasis in presynaptic terminals (Pennetta et al., 2002). DVAP-33 regulates bouton size and number at larval neuromuscular junctions in a dosage-dependent manner via association with the synaptic microtubule cytoskeleton (Pennetta et al., 2002). VAPB indirectly binds to microtubules via Nir3. Association of VAPB with Nir3 enhances microtubule stability and causes gross rearrangement of the ER and microtubule network in cultured cells (Amarilio et al., 2005).

### 1.2.1.3 Role of VAPB in lipid transport and metabolism

The unique lipid composition of organelle membranes is critical for cell function. Membrane lipids influence the physical properties of membranes and they also have a role in signalling pathways (Holthuis et al., 2003; Sprong et al., 2001). VAPB binds to the FFAT motif-containing lipid transferring, binding and sensing proteins Nir2, oxysterol binding protein (OSBP), and ceramide transfer protein (CERT) (Amarilio et al., 2005; Kawano et al., 2006; Loewen et al., 2003). The VAPB-FFAT motif

interaction is essential for lipid transfer between the ER and Golgi, and also for lipid metabolism (Loewen et al., 2003; Peretti et al., 2008). Lipids are transported by vesicular and non-vesicular mechanisms between the cellular membranes. Non-vesicular transport of lipids occurs at membrane contact sites between intracellular organelles (Lev, 2010). Although VAPB is clearly implicated in vesicular transport (see section 1.2.1.1), it has been proposed that VAPB is also a key player in the coordination of ER-Golgi membrane contact sites and non-vesicular lipid transport (Peretti et al., 2008). In this respect it is interesting to note that VAPB has also been found at ER-mitochondria contact sites (De Vos et al., 2012) (also see section 4.2.6). In mammalian cells, ceramide and phosphatidylinositol are synthesised in the ER and transported to Golgi through ER-Golgi membrane contact sites by CERT and Nir2, respectively (Hanada et al., 2003; Peretti et al., 2008). Ceramide is then converted to sphingomyelin and phosphatidylinositol to phosphatidylinositol-4-phosphate in the Golgi membrane (Balla and Balla, 2006; Yamaoka et al., 2004). VAPB recruits Nir2, OSBP and CERT to the ER-Golgi membrane contact sites where these proteins facilitate lipid transfer between the ER and Golgi membranes (Peretti et al., 2008). Depletion of VAPB results in reduced sphingomyelin and phosphatidylinositol-4-phosphate levels in Golgi, showing that VAPB regulates the lipid composition of Golgi membranes and subsequently the structure of the Golgi apparatus (Peretti et al., 2008).

VAPB also regulates lipid metabolism in yeast. The VAPB homologue in yeast is called suppressor of choline sensitivity 2 (Scs2). Scs2 binds to the FFAT motif containing protein overproducer of inositol 1 (Opi1) (Gavin et al., 2002; Loewen et al., 2003). Opi1 is a transcription regulator specific for phospholipid synthesis. Opi1 is activated when inositol levels are high and negatively regulates the expression of inositol-1-phosphate synthase. During inositol starvation Opi1 is inactivated and binds

to Scs2. Thus, it has been suggested that Scs2 regulates inositol metabolism by binding to Opi1 (Brickner and Walter, 2004; Kagiwada et al., 1998; Loewen et al., 2003; Nikawa et al., 1995).

### 1.2.1.4 Role of VAPB in $Ca^{2+}$ homeostasis

In addition to ER-Golgi apparatus contacts, membrane contact sites also have been described between ER and mitochondria (Hayashi et al., 2009). Both ER and mitochondria are $Ca^{2+}$ stores and their membrane contact sites have important roles in $Ca^{2+}$ exchange between the two organelles (Csordás et al., 2006; Csordás et al., 2010; de Brito and Scorrano, 2008; Rizzuto et al., 1998). Approximately 5 to 20% of mitochondrial membranes are in close apposition with ER membranes (Rizzuto et al., 1998). We have shown that VAPB binds to the outer mitochondrial membrane protein PTPIP51 (De Vos et al., 2012). Overexpression of PTPIP51 increases the amount of mitochondria-associated VAPB whereas decreasing the levels of PTPIP51 with small interfering RNAs reduces the amount of mitochondria-bound VAPB. Moreover, depletion of VAPB or PTPIP51 disrupts $Ca^{2+}$ homeostasis by slowing down mitochondrial $Ca^{2+}$ uptake following transient $Ca^{2+}$ release from ER stores (De Vos et al., 2012). Also overexpression of VAPBP56S increases $[Ca^{2+}]c$ in motor neurons (Langou et al., 2010).

### 1.2.1.5 The role of VAPB in the UPR

Increased trafficking of proteins through the ER or insults that affect protein folding in the ER (e.g. mutant proteins) can cause imbalances that affect the folding

capacity of the ER which leads to ER stress. To sense ER stress, eukaryotic cells have pathways termed the UPR (Bernales et al., 2006; Lin et al., 2008). The UPR senses ER stress and the accumulation of unfolded proteins in the ER and then activates pathways that include transcriptional changes which adjust the ER protein folding capacity to rectify the stress.

There are three major branches to the UPR. Each of these branches involves different ER resident proteins that sense ER stress and the presence of incorrectly folded proteins. These proteins are inositol-requiring protein 1 (IRE1), double stranded RNA activated protein kinase-like endoplasmic reticulum kinase (PERK) and ATF6. These proteins all contain domains that protrude into the ER lumen so as to sense ER stress and also have cytosolic effector domains (Bernales et al., 2006; Lin et al., 2008).

A number of lines of evidence suggest that VAPB functions in the UPR, but the precise details are unclear and there are some inconsistencies in reports from different groups. Thus, in some reports overexpression of VAPB has been shown to promote UPR whereas siRNA knockdown of VAPB blocks activation of UPR in response to chemically induced ER stress (Kanekura et al., 2006; Langou et al., 2010; Moumen et al., 2011). Moreover, this role of VAPB in the UPR has been shown to involve IRE1 and X-box binding protein-1 (XBP1) signalling (Kanekura et al., 2006; Suzuki et al., 2009). By contrast, another group has shown that VAPB binds to ATF6 and overexpression of VAPB blocks UPR via an effect on ATF6 (Gkogkas et al., 2008). VAPB overexpression has also been shown to cause an inhibitory effect on the ubiquitin proteosome system and VAPB also interacts with the 20S subunit of the proteosome but how these two features are linked is unclear (Moumen et al., 2011).

### 1.2.1.6 Role of VAPB in receptor signalling

Secreted forms of VAPB involving a cleaved region containing the MSP domain have been observed in *Drosophila*, *C. elegans* and in human serum (Han et al., 2012; Tsuda et al., 2008). This cleavage occurs between the MSP and coiled-coil domains of VAPB by an unknown mechanism (Gkogkas et al., 2011; Tsuda et al., 2008). These secreted MSP domains of *Drosophila* and *C. elegans* have been shown to function as ligands for ephrin receptors (EphRs), sensory axon guidance-3 receptor Roundabout (SAX-3 Robo) receptors and caterpillar-like receptor-1 leukocyte common antigene-related-like (CLR-1 Lar) receptors (Han et al., 2012; Tsuda et al., 2008). EphR, SAX-3 Robo and CLR-1 Lar are located in neuronal growth cones and are involved in axon guidance (Chang et al., 2004; Sun et al., 2000; Wang and Anderson, 1997). Furthermore, Han and co-workers have demonstrated that the secreted MSP domain of VAPB influences mitochondrial localisation in striated muscles via SAX-3 Robo and CLR-1 Lar receptors (Han et al., 2012). Signalling via these receptors promotes actin remodelling in an actin-related protein (ARP)2/3 dependent way and shifts the localisation of mitochondria to actin rich muscle izotrope (I)-bands (Han et al., 2012). Therefore, it is possible that MSP signalling through EphR, SAX-3 Robo and CLR-1 Lar can influence mitochondrial localisation not only in neurons but also in muscles. Interestingly, the MSP domain of VAPB is also detectable in mammalian serum (Tsuda et al., 2008). However, whether these secreted MSP domains in mammalian VAPB also function in pathways related to those described *Drosophila* and *C. elegans* is unclear.

### *1.2.2 ALS-associated mutations in VAPB*

Two different mutations in VAPB have been described that are associated with ALS. The first leads to a proline to serine substitution at position 56 (VAPBP56S); the second leads to a threonine to isoleucine substation at position 46 (VAPBT46I) (Chen et al., 2010a; Nishimura et al., 2004). Both of these mutations are thus closely located and effect conserved residues within the MSP domain. However, whilst there is strong genetic evidence that the VAPBP56S mutation is linked to ALS, the VAPBT46I mutation has been described in only one ALS patient (Chen et al., 2010a). Most studies have thus focused on VAPBP56S.

The VAPBP56S mutation leads to alterations in the secondary and tertiary structure of the MSP domain and causes destabilisation of its hydrophobic core (Nishimura et al., 2004; Shi et al., 2010). These structural changes in the MSP domain result in the exposure of hydrophobic patches to the cytoplasm and the loss of the native MSP structure (Kim et al., 2010). Expression of VAPBP56S in mammalian cells induces the formation of ubiquitinated cytoplasmic aggregates (Kanekura et al., 2006; Langou et al., 2010; Nishimura et al., 2004; Teuling et al., 2007; Tsuda et al., 2008; Tudor et al., 2010). Additionally, VAPBP56S recruits wild-type VAPB in these cytoplasmic aggregates which results in Golgi fragmentation and cell death (Kanekura et al., 2006; Langou et al., 2010; Ratnaparkhi et al., 2008; Teuling et al., 2007; Tsuda et al., 2008). The oligomerisation of wild-type VAPB and VAPBP56S is driven by the interaction of the coiled-coil and transmembrane domains (Kanekura et al., 2006; Kim et al., 2010; Teuling et al., 2007).

To date, only one transgenic VAPBP56S mouse model has been reported (Tudor et al., 2010). Even though VAPBP56S aggregates are present in the brain and spinal

cord, these mutant transgenic mice do not show neurological or motor dysfunction and have a normal life span (Tudor et al., 2010). Nevertheless, from 18 month of age onward these animals display TDP-43 and ubiquitin positive inclusions in the cytoplasm of spinal cord motor neurons suggesting that there is a link between VAPBP56S and TDP-43 pathology (Tudor et al., 2010). How VAPBP56S induces TDP-43 pathology is not clear, but VAPBP56S has been shown to enhance TDP-43 induced cell toxicity via a process that involves Bcl-2-interacting mediator of cell death (Bim) and Bcl-2-associated X protein (Bax) (Suzuki and Matsuoka, 2011).

How VAPBP56S causes motor neuron disorders is not known but both loss-of-function and toxic gain-of-function mechanisms have been proposed. In support of a loss-of-function mechanism, VAPBP56S has been shown to disturb several cellular functions of VAPB, most likely by sequestering wild-type VAPB into insoluble aggregates or by altering VAPB binding to other proteins. Thus, VAPBP56S has reduced ability to interact with FFAT motif containing proteins Nir2, OSBP related protein (ORP) 3, 6 and 9 (Teuling et al., 2007). Similarly, VAPBP56S does not interact properly with microtubules *in vitro* (Mitne-Neto et al., 2007). In addition, lower levels of VAPB mRNA are seen in spinal cords of ALS patients which also lends support for a loss-of-function hypothesis for VAPB in ALS (Anagnostou et al., 2010). Overexpression of VAPBP56S also results in nuclear envelope swelling and mislocalisation of the nuclear envelope resident proteins Nups and EMD (Tran et al., 2012). Similar Nups and EMD mislocalisation has been observed following depletion of wild-type VAPB (see section 1.2.1.1) also suggesting that VAPBP56S is a loss-of-function mutant in Nups and EMD transport (Tran et al., 2012). VAPBP56S is resistant

to proteolysis and thus its MSP domain fails to be secreted and consequently does not signal via EphR, SAX-3 Robo and CLR-1 Lar (Gkogkas et al., 2008; Han et al., 2012; Tsuda et al., 2008).

The effect of VAPBP56S on the UPR is contradictory. In some studies, it has been shown that VAPBP56S inhibits the UPR by inhibition of the IRE1/XBP1 and the ATF6 UPR pathways (Gkogkas et al., 2008; Kanekura et al., 2006). In contrast, others have found that VAPBP56S overexpression increases CCAAT/enhancer binding protein homologous protein (CHOP) and GRP78/BiP levels and IRE1 phosphorylation, suggesting that VAPBP56S induces ER-stress and the UPR, and arguing for a gain-of-function mechanism (Langou et al., 2010; Moumen et al., 2011; Tsuda et al., 2008).

Finally, VAPB has been shown to interact with the outer mitochondrial membrane protein PTPIP51 and VAPBP56S binds more strongly to PTPIP51 than wild-type VAPB (De Vos et al., 2012). The VAPB-PTPIP51 interaction impacts on cellular $Ca^{2+}$ handling by influencing mitochondrial $Ca^{2+}$ uptake following $Ca^{2+}$ release from ER stores (De Vos et al., 2012). The stronger binding of VAPBP56S to PTPIP51 thus disrupts $Ca^{2+}$ exchange between ER and mitochondria (De Vos et al., 2012). Impaired mitochondrial $Ca^{2+}$ handling and buffering is also observed in mutant SOD1 models (Grosskreutz et al., 2007; Jaiswal et al., 2009; Manfredi and Xu, 2005). Perturbed mitochondrial $Ca^{2+}$ handling and increased $[Ca^{2+}]c$ could be pathogenic in ALS by affecting axonal transport, protein folding or inducing excitotoxicity (also see section 1.1.3.3, 1.1.3.7).

There is evidence that VAPBT46I has some similar pathogenic features to VAPBP56S. Thus VAPBT46I forms ubiquitinated cytosolic protein aggregates and causes ER fragmentation and inhibits the IRE1/XBP1 UPR pathway to induce cell death (Chen et al., 2010a).

## 1.3 Axonal transport of mitochondria

Mitochondria play a key role in cellular functions such as ATP synthesis, lipid metabolism, apoptosis initiation and $Ca^{2+}$ homeostasis (Saxton and Hollenbeck, 2012). Therefore, the exact and appropriate positioning of mitochondria is essential in all cells but especially in such large, highly polarised cells such as neurons. Active transport allows mitochondria to locate to neuronal cell areas where they are most needed (e.g. the growth cone, nodes of Ranvier, pre- and postsynaptic terminals) and docking proteins anchor them at these special locations. Thus, the movement of mitochondria through neurons is regulated so that they can locate to regions in response to physiological stimuli. The mechanisms that drive and regulate mitochondrial transport are thus discussed below.

### *1.3.1 Mitochondrial molecular motors*

The major mechanism for transport of mitochondria through axons involves movement along microtubules by kinesin-1 and cytoplasmic dynein-1 molecular motors. Kinesin-1 drives anterograde and dynein retrograde transport of mitochondria through axons (for reviews see (Hirokawa et al., 2010; Saxton and Hollenbeck, 2012)).

#### 1.3.1.1 Mitochondrial kinesin and adaptor proteins

There are 45 different kinesins in the mouse kinesin superfamily and these have been classified into 15 different families (Hirokawa et al., 2009; Lawrence et al., 2004). Kinesin-1 is the main molecular motor that drives anterograde axonal transport of

mitochondria (Cai et al., 2005; Fransson et al., 2006; Glater et al., 2006; Hurd and Saxton, 1996; Pilling et al., 2006; Tanaka et al., 1998). In mammals, there are three kinesin-1 isoforms each encoded by different genes (kinesin-1A, B and C). Kinesin-1A and kinesin-1C are neuron specific whereas kinesin-1B is expressed in all cell-types (Kanai et al., 2000).

Most functional kinesin-1 comprises a heterotetramer of two kinesin-1 motor proteins and two kinesin-1 light chain (KLC) proteins. Kinesin-1 contains ATPase activity and uses the chemical energy of ATP to drive conformational changes that generate motile force. Some cargoes bind directly to kinesin-1 but most bind to KLCs; thus the KLCs act as adaptor proteins to link cargoes to kinesin-1 motors (Hirokawa et al., 2009). However, transport of mitochondria is now known to not involve KLCs. Rather mitochondria attach to kinesin-1 motors via two other sets of proteins termed mitochondrial Rho GTPase (Miro) and trafficking kinesin (TRAK) also known as Milton in *Drosophila* (for review see (Saxton and Hollenbeck, 2012)).

Miro was originally discovered in yeast as a protein affecting proteinase A secretion (Wolff et al., 1999). Later studies have revealed that Miro is an outer mitochondrial membrane protein involved in mitochondrial transport and morphology in yeast (Frederick et al., 2004), *Drosophila* (Guo et al., 2005) and mammals (Fransson et al., 2003). Miro consists of two GTPase domains, two central $Ca^{2+}$ binding E-helix-loop-F-helix (EF-hand) domains and a C-terminal transmembrane domain that anchors it in the outer mitochondrial membrane (Fransson et al., 2003; Frederick et al., 2004; Wolff et al., 1999). In *Drosophila*, one Miro orthologue has been identified (Fransson et al., 2003; Guo et al., 2005) which binds TRAK to connect mitochondria to kinesin-1 (Glater et al., 2006). Mutation of *Drosophila* Miro causes impaired mitochondrial distribution in neurons of *Drosophila* larvae indicating the essential role of Miro in

mitochondrial transport (Guo et al., 2005). In mammals, two Miro homologues Miro1 and Miro2 have been described (Fransson et al., 2003). Mammalian Miro is directly associated with TRAK (Fransson et al., 2006; MacAskill et al., 2009a) and kinesin-1 (MacAskill et al., 2009b; Wang and Schwarz, 2009). Depletion of mammalian Miro by RNA interference in a cell line and in hippocampal neurons reduces mitochondrial transport (MacAskill et al., 2009b; Saotome et al., 2008). Moreover, the first GTPase domain and the EF-hand domains of Miro seem important for normal mitochondrial distribution and transport in hippocampal neurons and cell lines (Fransson et al., 2006; MacAskill et al., 2009b; Saotome et al., 2008; Wang and Schwarz, 2009).

TRAK is a member of an evolutionary conserved coiled-coil domain protein family (Beck et al., 2002; Iyer et al., 2003). TRAK was originally described as a protein required for normal mitochondrial distribution in *Drosophila* photoreceptors (Stowers et al., 2002). TRAK binds to Miro in both *Drosophila* and mammals (Glater et al., 2006; Wang and Schwarz, 2009). In addition, TRAK is also associated with the C-terminus of kinesin-1 providing a link between the motor protein and mitochondria (Glater et al., 2006; Stowers et al., 2002; Wang and Schwarz, 2009). Null mutations in TRAK selectively alter mitochondrial distribution in *Drosophila* (Glater et al., 2006; Górska-Andrzejak et al., 2003; Stowers et al., 2002) suggesting a role for TRAK in mitochondrial transport. In mammals, two TRAK orthologues have been identified: TRAK1 (also known as β-*O*-linked *N*-acetylglucosamine transferase-interacting protein (OIP) 106) (Iyer et al., 2003) and TRAK2 (also termed OIP98 or GABAA receptor-interacting factor-1 (GRIF-1)) (Beck et al., 2002). TRAK is involved in intracellular transport of endosomes, ion channels and mitochondria (Brickley and Stephenson, 2011; Grishin et al., 2006; Kirk et al., 2006; MacAskill et al., 2009a; Webber et al., 2008). In mammals, TRAK binds to mitochondria indirectly via interaction with Miro

and for this interaction the residues 476-700 of TRAK, and the N-terminal GTPase domain of Miro are essential (Fransson et al., 2006; MacAskill et al., 2009a). Although a second mitochondrial receptor for TRAK has not been identified, it has been shown that TRAK is able to bind to mitochondria in a Miro-independent way (Koutsopoulos et al., 2010). TRAK also associates with kinesin-1 and this interaction occurs between the C-terminal cargo binding domain of kinesin-1 and the N-terminal coiled-coil domain of TRAK (Brickley et al., 2005; Pozo and Stephenson, 2006.; Smith et al., 2006). Mitochondrial transport is highly dependent on availability of TRAK. Depletion of TRAK levels by RNA interference or using dominant negative TRAK constructs, that bind to mitochondria but not to kinesin-1, decreases mitochondrial mobility in rat hippocampal neurons (Brickley and Stephenson, 2011; MacAskill et al., 2009a).

Thus, mitochondria are mainly transported anterogradely through axons via kinesin-1. Although the precise mechanism is not clear, mitochondria attach to kinesin-1 via TRAK and Miro. According to one model, Miro binds directly to kinesin-1 (MacAskill et al., 2009b). In another model, Miro binds to kinesin-1 indirectly via TRAK (Wang and Schwarz, 2009) (Figure 1.2).

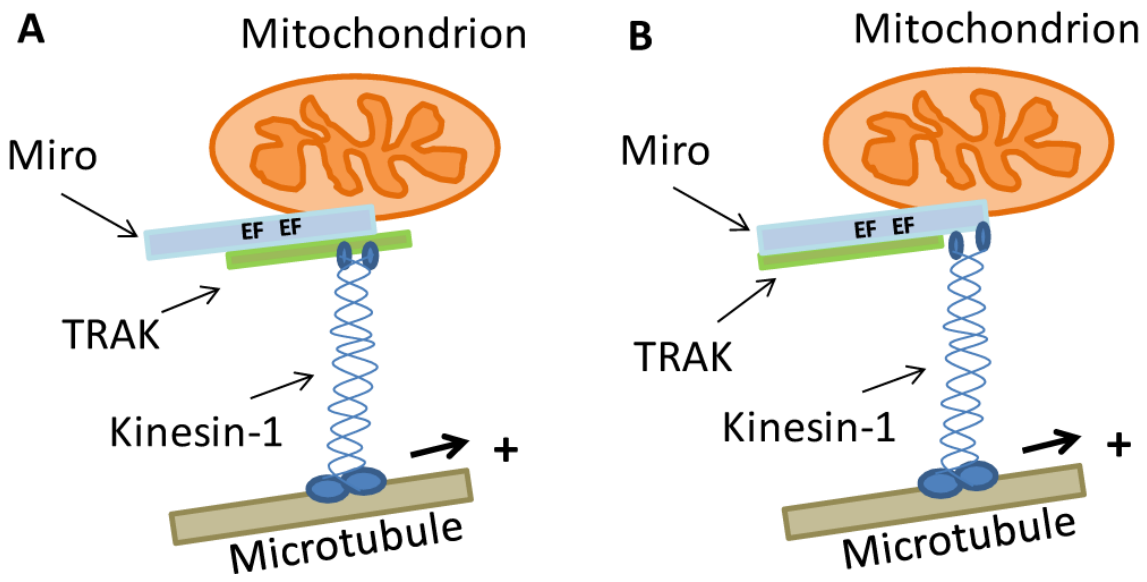


***Figure 1.2 Models of attachment of kinesin-1 to mitochondria.***

(A) Kinesin-1 is associated with TRAK which in turn binds to the outer mitochondrial membrane protein Miro. (B) Kinesin-1 binds directly to Miro independently of TRAK.

Syntabulin, fasciculation and elongation protein zeta-1 (FEZ1) and Ras-related nuclear protein-binding protein 2 (RanBP2) also have been proposed as mitochondrial kinesin-1 adaptor proteins but they are not as well studied as Miro and TRAK.

Syntabulin has been identified as an interacting partner of syntaxin-1, a key protein of the membrane fusion machinery at the presynaptic plasma membrane (Su et al., 2004). In neurons, syntabulin also binds to kinesin-1 and partially associates to mitochondria via its C-terminal (Cai et al., 2005; Su et al., 2004). Depletion of syntabulin or disruption of syntabulin-kinesin-1 interaction in neurons reduces the number of mitochondria in axons and selectively perturbs anterograde mitochondrial transport (Cai et al., 2005; Ma et al., 2009).

FEZ1 (also known as uncoordinated (UNC)-76) is a coiled-coil protein involved in neuronal development and axonal outgrowth (Maturana et al., 2010). FEZ1 binds to kinesin-1 in neurons (Fujita et al., 2007; Gindhart et al., 2003). Moreover, FEZ1 also associates to mitochondria in a cell line and its depletion by RNA interference disrupts anterograde mitochondrial transport in a cell line and hippocampal neurons (Fujita et al., 2007; Ikuta et al., 2007).

RanBP2 has been implicated in nuclear import and export (Melchior et al., 1995; Villa Braslavsky et al., 2000). RanBP2 binds to kinesin-1B and C via its kinesin-binding domain and has been shown to act as an allosteric activator of kinesin-1B (Cai et al., 2001; Cho et al., 2009). It has been demonstrated that blocking RanBP2 kinesin-1 interaction causes perinuclear mitochondrial clustering in neuron-like cell lines (Cho et al., 2007). However, the effect of RanBP2 on axonal mitochondrial transport has not been investigated.

Although kinesin-1 is the main anterograde mitochondrial motor protein, there is also evidence that the kinesin-3 family member KIF1Bα and kinesin-like protein-6

(KLP6) may also contribute to mitochondrial transport (Nangaku et al., 1994; Tanaka et al., 2011; Wozniak et al., 2005).

KIF1Bα is a monomeric mitochondrial kinesin in neurons. It is enriched in brain tissue and localises to mitochondria *in vivo* (Nangaku et al., 1994). The role of KIF1Bα in mitochondrial transport has been demonstrated in *in vitro* motility assays and cell lines (Nangaku et al., 1994; Tanaka et al., 2011; Wozniak et al., 2005). KIF1 binding protein (KBP) has been identified as interacting partner of KIF1Bα by Wozniak and co-workers (Wozniak et al., 2005). KBP is also co-localised with mitochondria but it does not mediate KIF1Bα-mitochondria interaction. At the same time KBP increases KIF1Bα motility *in vitro* and required for appropriate mitochondrial distribution (Wozniak et al., 2005).

KLP6 localises to mitochondria in *C. elegans* and in neuronal and non-neuronal cell lines, and its mutation perturbs mitochondrial transport in a neuronal cell line (Tanaka et al., 2011). To date, it is not known how KIF1Bα and KLP6 bind to mitochondria and their role in anterograde mitochondrial transport requires further investigation.

### 1.3.1.2 Mitochondrial cytoplasmic dynein motor complex

The retrograde transport of mitochondria is less well understood than their anterograde transport. Although most kinesins move towards the plus end of microtubules, a few move towards the minus end (kinesin-14B family members) (Hirokawa et al., 2009). There is no evidence for a role of a minus end-directed kinesin in mitochondrial transport. Therefore, it is generally accepted that microtubule-based retrograde mitochondrial transport is mediated by the cytoplasmic dynein-1-dynactin

complex. Interestingly, cytoplasmic dynein-1 driven retrograde mitochondrial transport requires functioning kinesin, possibly because dynein is associated with mitochondria during its transport to the cell periphery (Hirokawa et al., 1990; MacAskill et al., 2009b; Pilling et al., 2006).

Mitochondria purified from *Drosophila* brain have been shown to be associated with dynein heavy chain and dynactin subunits p50 and $p150^{Glued}$ (Pilling et al., 2006). Moreover, a mutation in dynein heavy chain inhibits dynein function and halts retrograde mitochondrial transport in cultured *Drosophila* neurons (Pilling et al., 2006). In mammals, association of cytoplasmic dynein-1 with mitochondria has been shown in ligated mouse peripheral nerves by immuno-electron microscopy (Hirokawa et al., 1990).

How cytoplasmic dynein-1 binds to mitochondria remains to be elucidated. A possible linker between dynein and mitochondria is Miro. It has been shown that overexpression or loss of Miro in *Drosophila* alters not only anterograde but also retrograde mitochondrial transport (Russo et al., 2009). However, the evidence for direct interaction between Miro and dynein is missing to date. The dynein light chain t-complex testis-specific protein 1 (Tctex1) has been identified to interact with the outer mitochondrial membrane protein VDAC in the yeast two-hybrid system suggesting another possible linkage point between mitochondria and dynein (Schwarzer et al., 2002).

### *1.3.2 Mitochondrial anchors*

When mitochondria have been delivered to the region where they are needed (e.g. growth cones, nodes of Ranvier, pre- and postsynaptic terminals) they often spend an extended period of time in those areas. Indeed, in axons, the majority of mitochondria are stationary most of the time (~60-80% of all mitochondria) (Kang et al., 2008; Morris and Hollenbeck, 1993).

Syntaphilin has been identified as a microtubule bound mitochondrial docking protein that halts mitochondrial movement (Kang et al., 2008). Syntaphilin is anchored into the outer mitochondrial membrane by its C-terminal transmembrane domain and binds to microtubules via its N-terminus. Interestingly, its interaction with microtubules is enhanced by dynein light chain LC8 which binds directly to syntaphilin (Chen et al., 2009). It has been shown that overexpression of syntaphilin immobilises almost all mitochondria whereas deletion of the *syntaphilin* gene increases the number of motile mitochondria (Kang et al., 2008). Since syntaphilin selectively localises to stationary mitochondria its main role is probably mitochondrial docking in neurons (Kang et al., 2008).

Mitochondria are also tethered to neurofilaments and intermediate-filaments (Leterrier et al., 1994; Reipert et al., 1999; Toh et al., 1980; Wagner et al., 2003; Winter et al., 2008). Neurofilament associated mitochondria are probably not transported along neurofilaments since disruption of both microtubule and actin filaments cytoskeleton eliminates mitochondrial transport in neurons (Morris and Hollenbeck, 1995). The only protein that has been shown to act as a linker between intermediate filaments and mitochondria is plectin 1b (Reipert et al., 1999; Winter et al., 2008). Interestingly, neurofilament based mitochondrial docking is highly dependent on mitochondrial

membrane potential. Mitochondria with high membrane potential bind more frequently to neurofilaments than mitochondria with low membrane potential (Wagner et al., 2003).

## *1.3.3 Regulation of mitochondrial transport in neurons*

Mitochondrial transport and docking are highly regulated mechanisms in both neuronal and non-neuronal cells. Several mechanisms for controlling mitochondrial transport have now been identified. These include alterations in $[Ca^{2+}]c$ levels, turnover of Miro, alterations in mitochondrial function and ATP/ADP levels, microtubule modifications and phosphorylation of kinesin-1.

### 1.3.3.1 Intracellular $Ca^{2+}$ and mitochondrial transport

One of the main activity dependent regulatory signals for mitochondrial transport is intracellular $Ca^{2+}$. Increased $[Ca^{2+}]c$ arrests mitochondrial motility (Chang et al., 2006; MacAskill et al., 2009b; Rintoul et al., 2003; Saotome et al., 2008; Wang and Schwarz, 2009; Yi et al., 2004). Three groups have shown independently that Miro is the molecule that mediates the effect of $Ca^{2+}$ on mitochondrial motility and in particular that it the Miro EF-hand domains (MacAskill et al., 2009b; Saotome et al., 2008; Wang and Schwarz, 2009). Two models have been described for how $Ca^{2+}$ affects Miro to halt mitochondrial transport (MacAskill et al., 2009b; Wang and Schwarz, 2009). Wang and Schwarz developed a model in which an increase in $[Ca^{2+}]c$ causes a conformational change in Miro that enables the N-terminal motor domain of TRAK-bound kinesin-1 to directly interact with Miro. Thus, the kinesin-1 motor domain is unavailable to bind to

and move along microtubules, effectively halting mitochondrial transport (Wang and Schwarz, 2009). In contrast, MacAskill *et al.* proposed that kinesin-1 directly binds to Miro independently of TRAK and that increased [$Ca^{2+}$]c disrupts this interaction, thus releasing kinesin-1 into the cytosol and inhibiting mitochondrial transport (MacAskill et al., 2009b). Whichever of these two models proves right, it is clear that the EF-hand domains of Miro mediate $Ca^{2+}$ dependent regulation of mitochondrial trafficking. Interestingly, not only cytosolic but also intra-mitochondrial $Ca^{2+}$ levels are able to influence mitochondrial motility (Chang et al., 2011). It has been shown that mitochondrial $Ca^{2+}$ levels correlate inversely with the speed but not with the direction of mitochondrial movement. Moreover, Miro regulates $Ca^{2+}$ entry into mitochondria and this is dependent on its EF-hand domains (Chang et al., 2011). However, the exact mechanism by which intra-mitochondrial $Ca^{2+}$ influences axonal mitochondrial transport remains to be elucidated.

### 1.3.3.2 Turnover of Miro and mitochondrial transport

Since Miro is required for attachment of mitochondria to kinesin-1 (see section 1.3.1.1), the mechanisms that control the levels of cellular Miro protein are likely to influence mitochondrial transport. Recently, important advances have been made in understanding how Miro levels are regulated. This regulation involves two Parkinson's disease linked proteins termed Parkin and phosphatase and tensin homologue-induced putative kinase protein-1 (PINK1). Mutations to the genes encoding Parkin and PINK1 cause some familial forms of Parkinson's disease (for review see (Thomas and Beal, 2007)).

Parkin is an E3 ubiquitin ligase involved in targeting proteins for destruction via the proteasome and PINK1 is a serine/threonine kinase that localizes to mitochondria (Thomas and Beal, 2007). Moreover, there is evidence that Parkin and PINK1 functions may be linked and in particular, linked to mitochondrial function (Thomas and Beal, 2007). A proteomic study initially identified PINK1 as being present in a multi-protein complex that included both Miro and TRAK (Weihofen et al., 2009). Recently, the implications of this finding have been comprehended more fully. PINK1 is now known to phosphorylate Miro so as to target it for destruction by the proteasome in a Parkin-dependent manner (Wang et al., 2011). Thus, phosphorylation of Miro by PINK halts mitochondrial axonal transport by reducing Miro levels and mitochondrial association with kinesin-1. These findings have clear relevance for our understanding of Parkinson's disease pathogenic mechanisms but also for other neurodegenerative diseases.

#### 1.3.3.3 Mitochondrial function, ATP/ADP levels and mitochondrial transport

Another activity dependent regulatory signal for mitochondrial trafficking is the cellular ATP/ADP ratio. Mitochondria tend to accumulate in areas with high energy consumption suggesting that ATP consumption may regulate mitochondrial transport (Mironov, 2009; Morris and Hollenbeck, 1993; Ohno et al., 2011). Indeed, mitochondrial movement correlates with local intracellular ATP and ADP levels in neurons (Mironov, 2007; Mironov and Symonchuk, 2006). Mitochondrial motility is increased in areas with high ATP concentrations whereas mitochondrial mobility is decreased in the vicinity of active synapses or regions with high ADP levels (Mironov,

2007; Mironov and Symonchuk, 2006). Mitochondrial motility also depends on the activity of mitochondria. Analysis of mitochondrial transport revealed that the majority of mitochondria with high membrane potential are transported anterogradely whereas mitochondria with low membrane potential move retrogradely (Miller and Sheetz, 2004). Reduced membrane potential leads to reduced ATP synthesis (Nicholls and Budd, 2000) therefore the selective retrograde transport of depolarised mitochondria may be linked to the reduced ATP synthesis in these mitochondria. Indeed, antimycin, a drug that reduces mitochondrial membrane potential and ATP production by blocking the mitochondrial electron transport chain, selectively increases retrograde mitochondrial transport (Hollenbeck et al., 1985; Miller and Sheetz, 2004). However, the exact mechanisms that are involved in the activity dependent regulation of mitochondrial transport and the related ATP/ADP sensors are not known.

#### 1.3.3.4 Microtubule modifications and mitochondrial transport

Microtubule dynamics are regulated by microtubule-associated proteins (MAPs). MAP1, MAP2 and tau are the three major neuronal MAPs (Conde and Caceres, 2009; Dehmelt and Halpain, 2005). Tau stabilises microtubules, increases microtubule rigidity, induces microtubule bundles, and determines the spacing between microtubules (Dehmelt and Halpain, 2005). MAPs such as tau have been shown to affect kinesin-1 based transport. Increased binding of tau to microtubules causes kinesin-1 to detach from microtubules more frequently, thus reducing the amount of anterograde transport of mitochondria (Ebneth et al., 1998; Stamer et al., 2002; Stoothoff et al., 2009). Likewise, MAP2 influences the frequency of attachment of kinesin to microtubules; increased binding of MAP2 to microtubules causes kinesin-1 to detach from

microtubules more frequently (Seitz et al., 2002). Interestingly, once kinesin is attached to microtubules, MAP2 does not affect the run length of the motor protein suggesting that MAP2 has a regulation role at the level of initial attachment at least *in vitro* (Seitz et al., 2002).

In addition to MAPs, post-translational modifications of tubulin have also been shown to influence the interaction between kinesin and microtubules. Thus, the ability of kinesin-1 to bind to microtubules and in some cases move along microtubules is enhanced by tubulin acetylation, detyrosination and glutamylation (Cai et al., 2009; Dompierre et al., 2007; Dunn et al., 2008; Hammond et al., 2010; Ikegami et al., 2007; Konishi and Setou, 2009; Larcher et al., 1996; Liao and Gundersen, 1998; Reed et al., 2006).

### 1.3.3.5 Kinesin-1 phosphorylation and mitochondrial transport

Phosphorylation of both kinesin-1 and KLC has been shown to regulate their functions (De Vos et al., 2000; Ichimura et al., 2002; Manser et al., 2011; Morfini et al., 2006; Vagnoni et al., 2011). In particular, phosphorylation of kinesin-1 by c-Jun N-terminal kinase (JNK) 3 on Ser176 has been shown to disrupt the interaction of kinesin-1 with microtubules so as to disrupt axonal transport of cargoes, possibly including mitochondria (Morfini et al., 2006; Morfini et al., 2009).

## 1.4 Hypothesis and aims of thesis

As detailed above, there is a considerable amount of evidence that damage to mitochondria and damage to axonal transport of mitochondria occur in ALS. In particular, several studies have shown that ALS mutant SOD1 damages axonal transport of mitochondria. The hypothesis that formed the basis of this thesis was that other genetic insults associated with ALS would also perturb mitochondrial transport. The aim of this thesis is to test this hypothesis further and in particular to test whether ALS mutant VAPBP56S damaged axonal transport of mitochondria, and if so, to gain insight into the underlying mechanisms of the damage.

# 2 MATERIALS AND METHODS

Unless stated otherwise, all chemicals were purchased from Sigma-Aldrich Co. All solutions and buffers were prepared using ultrapure water (resistivity ≥ 18.2 MΩ-cm) from an ELGA Purelab Ultra purification system (Veolia Water Systems Ltd., UK). When required, solutions were sterilised either by autoclaving for 20 minutes at 121 °C and 101 kPa or by filtration through a 0.2 μm pore size syringe filter (Nalgene).

In the text, some commonly used organic compounds are referred to using their non-systematic instead of systematic names, according to the guidelines of the International Union of Pure and Applied Chemistry (Panico et al., 1993). All units are written according to the guidelines of the *Bureau International des Poids et Mesures* (International Bureau of Weights and Measures) (BIPM, 2006).

## 2.1 Materials

### *2.1.1 Stock solutions*

Acrylamide-bis-acrylamide (30%, 37:5:1 stabilised solution; Geneflow, UK)

Ammonium persulphate (APS; 10% (w/v); Geneflow, UK)

Ampicillin (100 mg/ml, filter sterilised)

B27 supplement (100%; Invitrogen)

β-mercaptoethanol (14.3 M)

Bovine serum albumin (BSA; 5% (w/v))

Calcium chloride ($CaCl_2$; 1 M)

Dimethyl sulphoxide (DMSO; 100%)

Dithiothreitol (DTT; 1 M)

Ethanol (100%)

Ethidium bromide (10 mg/ml)

Ethylenediaminetetraacetic acid (EDTA; 0.5 M)

Ethylene glycol-bis (β-aminoethylether) N,N,N',N'-tetraacetic acid (EGTA; 0.25 M)

Fetal bovine serum (100%; Sera Laboratories)

Formaldehyde (37% (w/v))

Fura2 solution ((1-[2-(5-carboxyoxazol-2-yl)-6-aminobenzofuran-5-oxy]-2-(2'-amino-5'-methylphenoxy)-ethane-N,N,N',N'-tetraacetic acid); 1 mM in DMSO; Calbiochem)

Glacial acetic acid (100%)

Glycerol (80% (v/v), autoclaved)

Hydrogen chloride (HCl; 1 M)

Kanamycin (100 mg/ml, filter sterilised)

K-HEPES ((4-(2-hydroxyethyl)piperazine-1-ethanesulfonic acid); 1 M; buffered with KOH to pH 7.4)

Laminin from Engelbreth-Holm-Swarm murine sarcoma basement membrane (laminin; 1 mg/ml)

L-glutamine (200 mM; Invitrogen)

Magnesium chloride ($MgCl_2$; 1 M)

Methanol (100%)

MitoTracker Red CMXRos (1 mM in DMSO; Invitrogen)

Na-HEPES buffered with NaOH to pH 7.4

Penicillin (10,000 IU/ml) and streptomycin (10 mg/ml; PAA Laboratories)

Percoll (100%)

Phosphate-buffered saline (PBS; 137 mM NaCl; 2.7 mM KCl; 0.7 mM $KH_2PO_4$; 4 mM $Na_2HPO_4$)

Poly-DL-ornithine hydrobromide (ornithine; MW 3,000-15,000; 1.5 mg/ml)

Poly-L-lysine hydrobromide (MW 70000-150000; 0.1% (w/v))

Potassium acetate ($CH_3COOK$; 5 M)

Potassium chloride (KCl; 5 M)

Potassium hydroxide (KOH; 1M)

RNase A (10 mg/ml in Tris-EDTA)

Sodium dodecyl sulphate (SDS; 10% (w/v))

Sodium chloride (NaCl; 5 M)

Sodium deoxycholate (10% (w/v))

Sodium hydroxide (NaOH; 10 M)

Sodium hydrogencarbonate ($NaHCO_3$; 1 M)

Sodium pyruvate (100 mM)

TEMED (N,N,N',N'-tetramethylethylenediamine; 100%)

Trypsin-EDTA solution (1x; 0.05% trypsin, 0.02% EDTA in PBS; PAA Laboratories)

Tris-buffered saline (TBS; 20 mM Tris (tris(hydroxymethyl)aminomethane); 137 mM

NaCl; buffered with HCl to pH 7.6)

Citric acid (1 M)

Tris-citrate (1 M Tris; buffered with citric acid to pH 7.4)

Tris-EDTA (TE; 10 mM Tris, 1 mM EDTA; buffered with NaOH to pH 8.0)

Tris-HCl (1.5 M Tris, buffered with HCl to pH 8.8)

Tris-HCl (0.5 M, buffered with HCl to pH 6.8)

Triton X-100 (100%)

Tween-20 (100%)

## *2.1.2 General microbiology reagents*

### 2.1.2.1 Plasmids

Vectors and expression plasmids are listed in Table 2.1 and 2.2 below.

***Table 2.1 Vectors***

| Vector | Vector used | Supplier |
|---|---|---|
| pCI-neo | Mammalian expression vector | Promega |
| pcDNA3.1 | Mammalian expression vector | Invitrogen |
| pRK5 | Mammalian expression vector | BD Biosciences |

***Table 2.2 Expression plasmids***

| **Protein expressed** | **Vector backbone** | **Reference or source of plasmid** |
|---|---|---|
| EGFP | pEGFP-C1 | Clontech |
| DsRed-Mito | pDsRed | Clontech |
| EGFP-VAPB | pEGFP-C1 | Dr Kwok-Fai Lau (KCL, UK) |
| EGFP-VAPBP56S | pEGFP-C1 | Dr Kwok-Fai Lau (KCL, UK) |
| HA-TRAK1 | pRK5 | Prof Pontus Aspenström (Ludwig Institute for Cancer Research, Uppsala University, Uppsala, Sweden); (Fransson et al., 2006) |
| mCherry-α-tubulin | pcDNA3.1 | Prof Frederic Saudou (Institute Curie, Orsay, France); (Shaner et al., 2004) |
| mCherry-α-tubulin$^{K40A}$ | pcDNA3.1 | Prof Frederic Saudou (Institute Curie, Orsay, France); (Dompierre et al., 2007) |
| myc-KIF5A | pCI-neo | Dr Alessio Vagnoni (KCL, UK) |
| myc-Miro1 | pRK5 | Prof Pontus Aspenström (Ludwig Institute for Cancer Research, Uppsala University, Uppsala, Sweden) (Fransson et al., 2003) |
| myc- Miro1$^{E208K/E328K}$ | pRK5 | Gábor M Mórotz (KCL, UK) |
| myc-VAPB | pCI-neo | (De Vos et al., 2012) |
| myc-VAPBP56S | pCI-neo | (De Vos et al., 2012) |
| VAPB | pCI-neo | (De Vos et al., 2012; Tudor et al., 2010) |
| VAPBP56S | pCI-neo | (De Vos et al., 2012; Tudor et al., 2010) |

### 2.1.2.2 Media for storage and growth of *Escherichia coli* for DNA purification

Luria Bertani (LB) agar (Invitrogen), 32 g/l

LB-ampicillin (LB agar supplemented with 100 µg/ml ampicillin)

LB-kanamycin (LB agar supplemented with 100 µg/ml kanamycin)

LB broth (Invitrogen), 20 g/l

LB-ampicillin broth (LB broth supplemented with 100 µg/ml ampicillin)

LB-kanamycin broth (LB broth supplemented with 100 µg/ml kanamycin)

### 2.1.2.3 Preparation of plasmid DNA

Plasmids were isolated using a NucleoSpin® Plasmid plasmid purification kit (Macherey-Nagel GmbH & Co.KG, Düren, Germany); the following reagents are provided with the kit:

Resuspension buffer A1 supplemented with RNase A

Lysis buffer A2

Neutralisation buffer A3

Wash buffer AW

Wash buffer A4 supplemented with ethanol (80% (v/v) final ethanol concentration)

Elution buffer AE (5 mM Tris-HCl pH 8.5)

### 2.1.2.4 Agarose gel electrophoresis of plasmid DNA

*Tris-Acetate-EDTA (TAE) running buffer*

40 mM Tris

0.11% (v/v) glacial acetic acid

1 mM EDTA

buffered with NaOH to pH 8.0

*DNA loading buffer*

0.04% (w/v) Bromophenol blue (3',3",5',5"-tetrabromophenolsulfonephthalein)

6.6% (w/v) sucrose

### 2.1.2.5 Polymerase chain reaction (PCR)-based site-directed mutagenesis

Oligonucleotides:

Myc-tagged Miro1$^{E208K/E328K}$ was obtained by mutating glutamates at positions 208 and 328 to lysines with the following oligonucleotides:

5’-GGTACTCTCAATGATGCTAAACTCAACTTCTTTCAGAG-3’ and

5’-CTCTGAAAGAAGTTGAGTTTAGCATCATTGAGAGTACC-3’, and

5’-GACTGTGCTTTGTCACCTGATAAGCTTAAAGATTTATTTAAAG-3’ and

5’-CTTTAAATAAATCTTTAAGCTTATCAGGTGACAAAGCACAGTC-3’

Site-directed mutagenesis:

Site-directed mutagenesis was performed using the QuikChange® XL mutagenesis kit (Stratagene). The following materials are supplied with the kit:

10x mutagenesis buffer:

200 mM Tris-HCl (pH 8.8)

100 mM KCl

100 mM $(NH_4)_2SO_4$

20 mM $MgSO_4$

1% (v/v) Triton X-100

1 mg/ml BSA

pWhitescript™ 4.5 kb control plasmid

Oligonucleotide control primer #1:

5’-CCATGATTACGCCAAGCGCGCAATTAACCCTCAC-3’

Oligonucleotide control primer #2:

5’-GTGAGGGTTAATTGCGCGCTTGGCGTAATCATGG-3’

Deoxyribonucleotide triphosphate (dNTP) mix (the composition of the mix is proprietary)

QuickSolution

*PfuTurbo*® DNA polymerase

*Dpn* I restriction enzyme

pUC18 transformation control plasmid

XL10-Gold® ultracompetent cells

XL10-Gold® β-mercaptoethanol mix

### 2.1.2.6 Screening recombinant clones (alkaline lysis method of DNA recovery)

*Solution I*

50 mM glucose

25 mM Tris (bufferd with HCl to pH 8.0)

10 mM EDTA (buffered with NaOH to pH 8.0)

*Solution II*

0.2 M NaOH

1% (w/v) SDS

*Solution III*

3 M $CH_3COOK$

11.5% (v/v) glacial acetic acid

*Tris-EDTA*

10 mM Tris

1 mM EDTA

buffered with NaOH to pH 8.0

## *2.1.3 Mammalian cell culture and transfection media and reagents*

### 2.1.3.1 Human embryonic kidney (HEK) 293 and CV-1 cell culture media and reagents

HEK292 and CV-1 cells were grown in Dulbecco's modified Eagle's medium (DMEM) with 4.5 g/l glucose (PAA Laboratories) supplemented with:

10% (v/v) fetal bovine serum

2 mM L-glutamine

1 mM sodium pyruvate

HEK292 and CV-1 cells were washed with: $Ca^{2+}$, $Mg^{2+}$-free Hank's buffered salt solution (HBSS(-/-); PAA Laboratories)

### 2.1.3.2 Primary cortical neuron cell culture media and reagents

Rat primary cortical neurons were grown in cortical neuron cell culture media comprised of:

Neurobasal medium (Invitrogen) supplemented with:

2% (v/v) B27 supplement

2 mM L-glutamine

100 IU/ml penicillin and 100 μg/ml streptomycin

Preparation of rat primary cortical neurons involved the following solutions:

*Trypsin/HBSS solution*

0.035% (v/v) trypsin in HBSS(-/-)

*Deoxyribonuclease (DNase) solution*

10 μg/ml DNase in HBSS with $Ca^{2+}$ and $Mg^{2+}$ (HBSS(+/+); PAA Laboratories)

*Triturating solution*

1% (w/v) AlbuMAX™ I (Invitrogen)

0.5 mg/ml soybean trypsin inhibitor

10 μg/ml DNase

in HBSS(+/+)

*Poly-L-Lysine solution*

0.01% (w/v) poly-L-lysine in sterilised ultrapure water

### 2.1.3.3 Primary motor neuron cell culture media and reagents

Mouse primary motor neurons were grown in motor neuron cell culture media comprised of:

Neurobasal medium supplemented with:

2% (v/v) B27 supplement

2% (v/v) heat inactivated horse serum

0.5 mM L-glutamine

25 μM 2-mercaptoethanol

10 ng/ml ciliary neurotrophic factor (R&D Systems)

100 pg/ml glial cell-derived neurotrophic factor (R&D Systems)

1 ng/ml brain derived neurotrophic factor (R&D Systems)

100 IU/ml penicillin and 100 μg/ml streptomycin

25 μM L-glutamic acid (Invitrogen)

Preparation of mouse primary motor neurons involved the following solutions:

Leibovitz's-15 (L-15) medium (Invitrogen)

Dulbecco's phosphate buffered saline without $Ca^{2+}$ and $Mg^{2+}$ (DPBS; Invitrogen)

*Dialysed BSA*

4% (w/v) embryo tested BSA in L-15 medium

*Trypsin solution*

0.025% (w/v) trypsin in DPBS

*DNase/BSA solution I*

0.4% (w/v) dialysed BSA

0.1 mg/ml DNase

in L-15 medium

*DNase/BSA solution II*

0.4% (w/v) dialysed BSA

0.02 mg/ml DNase

in L-15 medium

*OptiPrep solution*

3.7% (v/v) OptiPrep™ (Axis-Shield)

10 mM tricine

4% (w/v) glucose

*Ornithine/laminin*

1.5 µg/ml ornithine

3 µg/ml laminin

in Neurobasal medium

### 2.1.3.4 Genotyping of VAPBP56S transgenic mice

Genotyping of VAPBP56S transgenic mice was performed using a REDExtract-N-Amp™ Tissue PCR Kit; the following materials were supplied with the kit:

Extraction solution

Tissue preparation solution

Neutralisation solution B

REDExtract-N-Amp PCR reaction mix

The genotyping primers were the following (Tudor et al., 2010):

5'-ATGGAGCAGAAACTCATCTCTGAAGAGGATCTGATGGCGAAG-3'

and

5'-GTCAAGGCCTTCTTCCTTCCCAGTTGGGC-3'

mIL3 control primers

5'-CTAGGCCACAGAATTGAAAGATCT-3' and

5'-GTAGGTGGAAATTCTAGCATCATCC-3'

### 2.1.3.5 Calcium phosphate-based transient transfection of primary neurons

Calcium phosphate-based transient transfections were performed using a ProFection® Mammalian Transfection System – calcium phosphate kit (Promega); the following reagents are provided with the kit:

Nuclease-free $H_2O$

2 M $CaCl_2$ solution

2x HEPES-buffered saline

*Kynurenic acid solution*

20 mM Na-kynurenic acid

10 mM $MgCl_2$

5 mM Na-HEPES buffered with NaOH to pH 7.4

## *2.1.4 General biochemical reagents*

### 2.1.4.1 Isolation of mitochondria, ER and mitochondria-associated ER membranes (MAM)

*Isolation-buffer*

250 mM mannitol

5 mM Na-HEPES (buffered with NaOH to pH 7.4)

0.5 mM EGTA

0.1% (w/v) BSA

EDTA-free Complete™ Protease Inhibitor Cocktail (Roche)

*30% Percoll gradient*

225 mM mannitol

25 mM HEPES (buffered with NaOH to pH 7.4)

1 mM EGTA

0.05% (w/v) BSA

30% (v/v) Percoll

*Radioimmunoprecipitation assay (RIPA)-buffer*

50 mM Tris-HCl pH 6.8

150 mM NaCl

1 mM EDTA

1 mM EGTA

0.1% (w/v) SDS

0.5% (w/v) deoxycholic acid

1% (v/v) Triton X-100

EDTA-free Complete™ Protease Inhibitor Cocktail

*5x SDS sample buffer*

250 mM Tris-HCl pH 6.8

10% (w/v) SDS

0.5% (w/v) Bromophenol blue

50% (v/v) glycerol

25% (v/v) β-mercaptoethanol

### 2.1.4.2 Immunoprecipitation

*Immunoprecipitation lysis buffer*

50 mM Tris-citrate

150 mM NaCl

1% (v/v) Triton X-100

5 mM EGTA

5 mM EDTA

EDTA-free Complete™ Protease Inhibitor Cocktail

*PBS-Triton*

0.1% (v/v) Triton X-100 in PBS

### 2.1.4.3 SDS-polyacrylamide gel electrophoresis (PAGE) and immunoblotting

#### *2.1.4.3.1 SDS-PAGE of protein samples*

*Stacking gel*

117 mM Tris-HCl pH 6.8

5.6% (v/v) acrylamide

0.1% (w/v) SDS

0.05% (w/v) APS

0.3% (v/v) TEMED

*Resolving gel*

375 mM Tris-HCl pH 8.8

8, 10 or 12% (v/v) acrylamide

0.1% (w/v) SDS

0.1% (w/v) APS

0.1% (v/v) TEMED

*Running Buffer*

25 mM Tris

192 mM glycine

0.1% (w/v) SDS

### *2.1.4.3.2 Immobilisation of proteins on nitrocellulose membranes*

*Transfer buffer*

25 mM Tris

192 mM glycine

20% (v/v) methanol

*Ponceau S solution*

5% (v/v) glacial acetic acid

0.1% (w/v) Ponceau S (3-Hydroxy-4-(2-sulfo-4-[4-sulfophenylazo]phenylazo)-2,7-naphthalenedisulfonic acid sodium salt)

### *2.1.4.3.3 Antibody probing of membrane-bound proteins*

*Blocking buffer*

0.1% (v/v) Tween-20

5% (w/v) dried skimmed milk in TBS

*TBS-Tween*

0.1% (v/v) Tween-20 in TBS

Enhanced chemiluminescence (ECL) development reagent kit (GE Healthcare); the following reagents are provided with the kit:

Detection solution A (luminol solution)

Detection solution B (peroxide solution)

***Table 2.3 Primary antibodies***

| **Antibody** | **Supplier** | **Monoclonal/Polyclonal, Species** | **Working dilution** |
|---|---|---|---|
| Acetylated tubulin (6-11B-1) | Sigma | Monoclonal, mouse | 1:20,000 (IB) |
| α-tubulin (DM1A) | Sigma | Monoclonal, mouse | 1:10,000 (IB) |
| α-tubulin | Abcam | Polyclonal, rabbit | 1:10,000 (IB) |
| COX IV (3E11) | Cell Signaling Technology | Monoclonal, rabbit | 1:2000 (IB) |
| GAPDH (14C10) | Cell Signaling Technology | Monoclonal, rabbit | 1:2000 (IB) |
| Haemagglutinin (HA)-tag | Sigma | Polyclonal, rabbit | 1:2000 (IB) |
| IgG2a,κ (UPC-10) | Sigma | Monoclonal, mouse | 1:250 (IP) |
| IP3R3 | Millipore | Polyclonal, rabbit | 1:2000 (IB) |
| Kinesin-1 (pcp42) | Prof Ron Vale (UCSF); (Niclas et al., 1994) | Polyclonal, rabbit | 1: 2000 (IB) |
| Myc-tag (9B11) | Cell Signaling Technology | Monoclonal, mouse | 1:2000 (IB)<br>1:1000 (IF)<br>1:250 (IP) |
| PDI (RL77) | Affinity BioReagents | Monoclonal, mouse | 1:2000 (IB) |
| VAPB (#3504) | In house; (Tudor et al., 2010) | Polyclonal, rabbit | 1:2000 (IB) |

IB-immunoblot, IF-immunofluorescence, IP-immunoprecipitation

***Table 2.4 Secondary antibodies***

| Antibody | Supplier | Monoclonal/Polyclonal, Species | Working dilution |
|---|---|---|---|
| anti-mouse Ig conjugated to horseradish peroxidase | Dako | Polyclonal, rabbit | 1:5000 (IB) |
| anti-rabbit Ig conjugated to horseradish peroxidase | Dako | Polyclonal, goat | 1:5000 (IB) |
| Anti-mouse IgG coupled with Alexa Fluor 488 | Invitrogen | Polyclonal, goat | 1:500 (IF) |

IB-immunoblot, IF-immunofluorescence

## *2.1.5 Microscopy*

### 2.1.5.1 Immunofluorescence

*Fixing solution*

3.7% (v/v) formaldehyde in PBS

*Quenching solution*

50 mM $NH_4Cl$ in PBS

*Permeabilising solution*

0.2% (v/v) Triton X-100 in PBS

*Blocking solution*

0.2% (v/v) gelatin from cold water fish skin in PBS

*Mowiol-DABCO mounting medium*

10% (w/v) Mowiol® 4-88 (Calbiochem)

25% (w/v) glycerol

100 mM Tris-HCl pH 8.5

2.5% (w/v) DABCO (1,4-diazobicyclo[2.2.2]octane)

### 2.1.5.2 Fura2 ratio imaging

*External solution*

145 mM NaCl

2 mM KCl

5 mM $NaHCO_3$

1 mM $MgCl_2$

2.5 mM $CaCl_2$

10 mM glucose

10 mM HEPES pH 7.0 (Invitrogen)

*External solution with 50 mM KCl*

95 mM NaCl

50 mM KCl

5 mM $NaHCO_3$

1 mM $MgCl_2$

2.5 mM $CaCl_2$

10 mM glucose

10 mM HEPES pH 7.0

*External solution with 20 mM $CaCl_2$*

145 mM NaCl

2 mM KCl

20 mM $CaCl_2$

5 mM $NaHCO_3$

1 mM $MgCl_2$

10 mM glucose

10 mM HEPES pH 7.0

*External solution with 20 mM EGTA*

145 mM NaCl

2 mM KCl

5 mM $NaHCO_3$

1 mM $MgCl_2$

20 mM EGTA

10 mM glucose

10 mM HEPES pH 7.0

## 2.2 Methods

### *2.2.1 General microbiology methods*

#### 2.2.1.1 Storage and growth of *E. coli* for DNA purification

*E. coli* containing plasmids of interest were stored at -70 °C in sterile 25% (v/v) glycerol solution in LB broth containing the appropriate antibiotic for the plasmid vector.

To grow bacteria for DNA purification, *E. coli* containing the plasmid of interest were spread out on LB agar plates (see section 2.1.2.2) containing the appropriate antibiotic for the plasmid vector and grown for 16 hours at 37 °C. Single bacterial colonies were picked and grown in 5 ml LB-ampicillin broth or LB-kanamycin broth (see section 2.1.2.2) for 12-15 hours at 37 °C while shaking at 220 rpm.

#### 2.2.1.2 Preparation of plasmid DNA

To isolate plasmid DNA a NucleoSpin® Plasmid plasmid purification kit (see section 2.1.2.3) was used according to the manufacturer's instructions. Typically 5 ml of bacterial culture yielded approximately 25 µg of pure plasmid DNA.

This kit is based on the alkaline lysis method of DNA recovery (Birnboim and Doly, 1979). In this procedure, cells (suspended in 250 µl Resuspension buffer A1 supplemented with RNase A) are lysed under alkaline conditions for 5 min using 250 µl Lysis buffer A2 which denaturates nucleic acids and proteins. RNase is used to eliminate RNA contamination from the preparation. When the lysis solution is neutralised by adding 300 µl Neutralisation buffer A3, chromosomal DNA and proteins

are unable to renaturate correctly due to their large size and form insoluble precipitates. Plasmid DNA is never fully denaturated because it is a relatively small, supercoiled, circular molecule. Therefore, plasmid DNA renaturates correctly and stays in solution following the neutralisation step effectively separating it from chromosomal DNA and proteins. Plasmid DNA is bound to silica membranes (provided with the kit) and contaminations (salts, metabolites, cellular components) are removed by washing with the appropriate buffers (500 µl Wash buffer AW and 600 µl Wash buffer A4 supplemented with ethanol). Pure plasmid DNA is eluted under low ionic strength using 50 µl slight alkaline buffer (Buffer AE).

### 2.2.1.3 Quantitation of nucleic acids

Spectrophotometric quantitation of plasmid DNA was performed using an Ultrospec 3100 pro (GE Healthcare) or NanoDrop 1000 (Thermo Scientific) spectrophotometer. The absorbance of samples at 260 nm and 280 nm was recorded. An optical density (OD) reading of 1 at a wavelength of 260 nm corresponds to a concentration of 50 µg/ml for double stranded DNA. Proteins are known to strongly absorb at a wavelength of 280 nm thus the ratio of OD readings at 260 and 280 nm ($OD_{260/280}$) gives an indication of purity of the sample. Pure DNA has an $OD_{260/280}$ value of 1.8 (Sambrook et al., 1989).

Plasmid DNA concentrations were also roughly quantified using ethidium bromide fluorescent quantitation. This method relies on the ability of ethidium bromide to bind to DNA. UV-induced fluorescence emitted by DNA-linked ethidium bromide is proportional to the total mass of DNA. The amount of DNA in a sample could then be quantified by visual comparison with the UV-induced fluorescence of a known quantity

of a DNA standard or series of standards. This technique has a detection limit of as little as 5 ng of DNA.

### 2.2.1.4 Restriction enzyme digestion of plasmid DNA

Plasmid DNA was digested using the appropriate restriction enzyme and corresponding buffer according to the manufacturer's instructions (Invitrogen). 5 units of enzyme were used per μg of DNA (1 unit is usually the amount of enzyme required to cleave 1 μg of DNA in 1 hour at 37 °C in the appropriate buffer). The volume of enzyme never exceeded 10% (v/v) of final reaction volume and the incubation time with the enzyme was 2 hours at 37 °C.

### 2.2.1.5 Agarose gel electrophoresis of plasmid DNA

Agarose (ultra pure, electrophoresis grade, Invitrogen) was dissolved in boiling TAE buffer (see section 2.1.2.4) in a final concentration of 0.6-1.5% (w/v) and cast on a gel bed with a suitable comb using a horizontal gel apparatus (Hybaid). On setting, gels were placed in an electrophoresis tank containing TAE buffer to a level just above the gel surface. DNA samples containing DNA loading buffer (see section 2.1.2.4) were loaded into the sample wells and were run at 100 V. Gels were stained with 10 μg/ml ethidium bromide to visualise DNA. Gels were then placed on a 3UV™ transilluminator emitting ultra violet light (λ=302 nm), visualised on a Sony video monitor and videographed using a Sony video graphic printer.

To determine the size of the separated DNA, nucleic acid size markers were used:

Phage λ DNA digested with *Hind* III (sizes in bp): 23,130; 9416; 6557; 4361; 2322; 2027; 564; 125.

MassRuler™ DNA ladder mix (Thermo Scientific; sizes in bp): 10,000; 8000; 6000; 5000; 4000; 3000; 2500; 2000; 1500; 1031; 900; 800; 700; 600; 500; 400; 300; 200; 100; 80.

### 2.2.1.6 PCR-based site-directed mutagenesis

Myc-tagged Miro1$^{E208K/E328K}$ was obtained by mutation of glutamate residues at positions 208 and 328 to lysine using the mutagenic primers listed in section 2.1.2.5 and a QuikChange® XL site-directed mutagenesis kit (Stratagene) (see section 2.1.2.5) according to the manufacturer's instructions.

The QuikChange® XL site-directed mutagenesis system is designed to produce mutations in double stranded plasmids using primers containing the entire mutation and the high fidelity, thermostable *PfuTurbo*® DNA polymerase in PCR. Experimental reactions and control reactions, to test mutation efficiency using pWhitescript™ control plasmid, were set up as shown below and used for PCR as shown in Table 2.5. The pWhitescript™ mutagenesis control plasmid contains a stop codon instead of a glutamine codon in the gene of *β-galactosidase* thus β-galactosidase is inactive in cells containing this plasmid. Competent cells containing this plasmid appear white on LB-ampicillin agar plates pre-spread with X-gal (5-bromo-4-chloro-3-indoyl-β-D-galactopyranoside) and IPTG (isopropyl-1-thio-β-D-galactopyranoside) because the inactive β-galactosidase enzyme is unable to cleave X-gal to galactose and an insoluble

blue product. During the mutagenesis the control primers mutate the stop codon back to glutamine in the *β-galactosidase* gene. The active β-galactosidase is able to cleave X-gal and the appearing blue products are obvious markers of the successful mutagenesis.

Reactions were performed in 0.2 ml PCR tubes (Thermo Fisher). Reactions were mixed gently by pipetting and then placed in a T3 Thermocycler (Biometra) for the PCR (cycling parameters are shown in Table 2.5). The lowest number of amplification cycles was used to minimise the possibility of errors by the DNA polymerase whilst at the same time generating enough amplified product for DNA purification. A sample of each PCR product was analysed for size, quality and quantity by restriction enzyme digestion and agarose gel electrophoresis alongside appropriate DNA markers (see section 2.2.1.4 and 2.2.1.5).

Control reaction (reagents, except $H_2O$, were supplied with the kit):

2 µl (10 ng) of pWhitescript™ control template DNA

5 µl of 10x mutagenesis buffer (see section 3.1.2.5)

1 µl of dNTP mix

1.25 µl (125 ng) of oligonucleotide control primer #1

1.25 µl (125 ng) of oligonucleotide control primer #2

3 µl QuickSolution

36.5 µl H2O to final volume of 50 µl

1 µl (2.5 U/µl) *PfuTurbo*® DNA polymerase

Experimental reaction (reagents, except DNA template, oligonucleotides and $H_2O$, were supplied with the kit):

5 µl of 10x mutagenesis buffer

10 ng DNA template

1 µl dNTP mix

125 ng of each oligonucletide

3 µl QuickSolution

$H_2O$ to a final volume of 50 µl

1 µl (2.5 U/µl) *PfuTurbo*® DNA polymerase

***Table 2.5 PCR-based site-directed mutagenesis cycling parameters.***

| **Step** | **Cycles** | **Temperature (°C)** | **Time** |
|---|---|---|---|
| 1. Initial denaturation | 1 | 95 | 1 min |
| 2. Denaturation, annealing and elongation | 18 | 95 | 50 s |
| | | 60 | 150 s |
| | | 68 | 10 min |
| 3. Extension/Elongation | 1 | 68 | 7 min |
| 4. Cooling | | 4 | unlimited |

#### *2.2.1.6.1 Digesting the PCR product*

Following PCR, the reactions were placed on ice, 1 µl (10 U/µl) of the *Dpn* I restriction enzyme (supplied with the kit) was added and the reaction was incubated at 37 °C for 1 hour. The *Dpn* I endonuclease (target sequence 5'-Gm$^6$ATC-3') is specific for methylated and hemimethylated DNA and is used to digest parental DNA and to select for mutation-containing amplified DNA.

#### *2.2.1.6.2 Transformation into XL10-Gold® ultracompetent cells*

2 µl of XL10-Gold® β-mercaptoethanol mix (provided with the kit) was added to 45 µl thawed XL10-Gold® ultracompetent cells (provided with the kit) and the reaction incubated on ice for 10 minutes. 2 µl of the *Dpn* I-treated DNA was transferred to the competent cells and the reaction incubated on ice for 30 minutes. A second control was set up to verify transformation efficiency: 0.1 ng of pUC18 transformation control plasmid (provided with the kit) was added to 45 µl XL10-Gold® ultracompetent cells and incubated on ice for 30 minutes. The cells were then heat pulsed for 30 seconds at 42 °C, and then placed on ice for 2 minutes. Following the heat pulse, 0.5 ml of super optimal broth with catabolite repression (S.O.C.) medium (Invitrogen) was added to the cells. Following incubation at 37 °C for 1 hour with shaking at 220 rpm, the samples were spread on LB-ampicillin agar plates. The transformed control pWhitescript™ and pUC18 cells were plated on LB-ampicillin agar plates pre-spread with 40 µl of X-gal (20 mg/ml in DMSO) and 20 µl of 100 mM IPTG for colour selection. The plates were incubated at 37 °C for 16 hours. The successfully mutagenised pWhitescript™ control colonies appeared as blue colonies. The number of pUC18 control colonies was greater than 100 colonies and most of them displayed the blue phenotype. The number of the colonies for the experimental reaction was about 100 colonies.

#### *2.2.1.6.3 Screening recombinant clones (alkaline lysis method of DNA recovery)*

Following overnight incubation, bacterial colonies present on the LB-ampicillin agar plate were picked with sterile inoculation loops and each used to inoculate 5 ml LB-ampicillin broth. These samples were placed for 16 hours at 37 °C while shaking at 220 rpm. Plasmid DNA from these samples was prepared by the alkaline lysis method which exploits differences in properties between plasmid and bacterial genomic DNA (Birnboim and Doly, 1979). Briefly, 1.5 ml of culture was pelleted by centrifugation at 14,000 x g for 2 minutes and the supernatant discarded. The pellet was resuspended in 100 µl ice-cold Solution I (see section 2.1.2.6) by vortexing. 200 µl freshly prepared Solution II (see section 2.1.2.6) was added and mixed by inverting the tube several times, before placing the tubes on ice for no longer than 5 minutes. 150 µl Solution III (see section 2.1.2.6) was then added and the contents of the tube mixed by inversion. The resulting mixture was left to precipitate on ice for 5 minutes before centrifugation at 14,000 x g for 10 minutes; this stage efficiently removes the precipitated genomic DNA and proteins. The plasmid DNA was precipitated by adding 2 volumes of 100% ethanol and incubation at 20 °C for 5 minutes. Since DNA is negatively charged and insoluble in organic solvents, ethanol was used to precipitate DNA from the aqueous solution. The precipitate was then pelleted by centrifugation at 14,000 x g for 10 minutes. Pellets were washed in 70% (v/v) ethanol, air-dried and then resuspended in 50 µl TE (see section 2.1.2.6) containing 20 µg/ml RNase A. To prevent DNA degradation by contaminating nucleases TE-buffer contains EDTA which chelates $Mg^{2+}$, a cofactor of nucleases. RNase is used to eliminate RNA contamination from the prep. An aliquot of the plasmid DNA was removed and used for restriction enzyme digestion and agarose gel electrophoresis (see section 2.2.1.4 and 2.2.1.5) to screen for the desired construct.

#### *2.2.1.6.4 DNA sequencing*

The isolated plasmid DNA was sent to Eurofins MWG, UK for sequencing to confirm the presence of the desired mutations.

## *2.2.2 Mammalian cell culture and transfection methods*

### 2.2.2.1 HEK293 and CV-1 cell culture

HEK293 and CV-1 cells were maintained in monolayer culture in DMEM with supplements (see section 2.1.3.1) at 37 °C under an atmosphere of 5% $CO_2$. Cells were passaged when they formed an approximately 80% confluent layer in the culture vessel. Medium was removed and cells were washed once with HBSS(-/-) (see section 2.1.3.1). To dislodge cells from the surface of the vessel, enough trypsin-EDTA solution (see section 2.1.3.1) was added to cover the monolayer (e.g. 1 ml trypsin-EDTA solution for a 25 $cm^2$ flask) and the cells were incubated at 37 °C for 2-3 min. DMEM with supplements (e.g. 4 ml for a 25 $cm^2$ flask) was then added to inactivate the trypsin, and cells were pipetted up and down to triturate them. Finally, the cell suspension was distributed into vessels for further culturing.

### 2.2.2.2 Primary cortical neuron cell culture

All work involving animals was conducted in accordance with the UK Animals (Scientific Procedures) Act 1986 and the guidelines issued by KCL. Cortical neurons were obtained from embryonic day 18 (E18) Sprague Dawley rat embryos (Charles River Laboratories).

A time-mated Sprague Dawley pregnant rat was sacrificed by asphyxiation with $CO_2$ followed by cervical dislocation. The abdominal wall was cut through and the two horns of the uterus removed. The foetuses (typically 12-14 per animal) were removed and dissected in HBSS(-/-). The foetuses were removed from amniotic sac and decapitated. The embryonic brain was removed from the skull and transferred to HBSS(-/-). The embryonic brains were then carefully cleaned from meninges to prevent contamination of the cultures with fibroblasts and the cortices were dissected. The dissected cortical tissue of all embryos were pooled, washed once with HBSS(-/-) and re-suspended in 5 ml trypsin/HBSS solution (see section 2.1.3.2). Following incubation for 15 min at 37 °C, 5 ml DNase solution was added (see section 2.1.3.2). After mixing by inversion, the solution was aspirated and the tissue was re-suspended in 1 ml of trituration solution (see section 2.1.3.2). The tissue was gently triturated with flamed-polished glass Pasteur pipettes of progressively smaller bore to obtain single cells. Cortical neuron cell culture media (see section 2.1.3.2) was added up to a final volume of 5 ml and the cell number was determined by counting a sample of the cell suspension using a Neubauer haemocytometer (Agar Scientific). To include only viable cells in the cell qantification, a sample of cell suspension was diluted tenfold with 0.4% (w/v) Trypan Blue ((3*Z*,3'*Z*)-3,3'-[(3,3'-dimethylbiphenyl-4,4'-diyl)di(1*Z*)hydrazin-2-yl-1-ylidene]bis(5-amino-4-oxo-3,4-dihydronaphthalene-2,7-disulfonic acid)) and loaded into the haemocytometer. Trypan Blue is a vital dye derived from toluidin. Trypan Blue is excluded by viable cells but it diffuses through the plasma membrane of dead cells effectively staining them. Cells stained by Trypan Blue appear dark blue in the microscope thus they can be easily excluded from the cell counting. The haemocytometer contains two identical, ruled chambers. The ruled area consists nine 1 x 1 mm squares with a depth of 0.1 mm. Thus, the volume of each square is 0.1 $mm^3$

($10^{-4}$ ml) when the haemocytometer is coverslipped. The number of viable cells was tallied in 4-4 squares in both chambers. Cells that touched the border on two sides of the square were included in the cell count and cells on the other two borders were excluded from the count. To calculate the number of cells per ml, the average number of counted cells was multiplied by 10,000 ($10^4$) and further multiplied by the dilution factor (10). Finally, 4.5 x $10^6$ cells were seeded and cultured on poly-L-lysine-coated (see section 2.1.3.2) square (22 x 22 mm; No. 1) or round (18 mm; No. 1) glass coverslips (Marienfield GmbH & Co.KG, Lauda-Königshofen, Germany) in cortical neuron cell culture media (see section 2.1.3.2) in 6 or 12 well plates (Thermo Scientific). Cells were cultured for 7 days at 37 °C under an atmosphere of 5% $CO_2$ before they were used for experiments. The purity of the cortical neuron cell cultures prepared and cultured in this way has been shown to be greater than 97% and routine staining for glia confirmed this finding in our group (Ackerley et al., 2000; Nikolic et al., 1996).

### 2.2.2.3 Primary motor neuron cell culture

VAPBP56S transgenic mice were described previously (Tudor et al., 2010). Motor neurons from VAPBP56S transgenic and control littermate mice were prepared in collaboration with Dr Elizabeth Tudor (KCL, UK) and Dr Kurt De Vos (KCL, UK). In the following procedure each embryo was kept separately to ensure the genotype of each culture. Retrospective genotyping was carried using DNA extracted from non-spinal cord tissue (see section 2.2.2.4).

Motor neurons were obtained from E13 time-mated mouse embryos. A time-mated pregnant animal was sacrificed by cervical dislocation. The abdominal wall was cut through and the two horns of the uterus removed. The foetuses (typically 8-10 per

pregnant animal) were removed and dissected in DPBS (see section 2.1.3.3). The foetuses were removed from amniotic sac and decapitated below the skull. The anterior portion of the abdomen, thorax and all the viscera were cut away and stored at -70 ºC for subsequent genotyping. The vertebral columns were carefully opened and the spinal cord removed. Spinal cords that were cleaned of meninges and dorsal root ganglia were cut into small pieces and incubated in trypsin solution (see section 2.1.3.3) for 10 min at 37 °C. Following the incubation, the tissue was mixed with 1 ml DNase/BSA solution I (see section 2.1.3.3) and agitated vigorously until tissue fragments disaggregated. The tissue fragments were triturated using a 1 ml pipette (two strokes) and were transferred into 1 ml DNase/BSA solution II (see section 2.1.3.3) and triturated an additional 6 strokes with a 1 ml pipette. The resulting cell suspension was layered onto a 4% (w/v) dialysed BSA (see section 2.1.3.3) cushion and centrifuged at 370 x g for 5 min. The pellet was re-suspended in 1 ml L-15 medium (see section 2.1.3.3) and loaded onto a 3.7% OptiPrep solution (see section 2.1.3.3) and centrifuged at 755 x g for 15 min. Motor neurons were collected at the interface between the L-15 medium and OptiPrep solution, diluted in L-15 medium and re-pelleted through 4% (w/v) dialysed BSA cushion at 370 x g for 5 min to wash out the OptiPrep solution. The cell pellet was resuspended in motor neuron cell culture media (see section 2.1.3.3) and the cell density was determined by counting a sample of the cell suspension. 2 x $10^4$ cells were seeded and cultured on ornithine/laminin-coated (see section 2.1.3.3) square glass coverslips in motor neuron cell culture media in 6 well plates. Cells were cultured for 7 days at 37 °C under an atmosphere of 5% $CO_2$ before they were used for experiments. Motor neurons were distinguished from other types of neurons and any glia in the cultures by morphological criteria as described by others (Roy et al., 1998; Tradewell et al., 2011). In particular, they have much larger cell bodies (greater than 20 μm in diameter) as

compared to other spinal neurons, noteable dendritic trees and a prominent axon. Also, they are readily distinguishable from any large sensory dorsal root ganglion (DRG) neurons remaining in the culture since DRG cells lack dendrites. The purity of motor neurons in the cultures was approximately 70%.

### 2.2.2.4 Genotyping of VAPBP56S transgenic mice

Genotypes were determined by PCR amplification of tissue DNA extracted using the REDExtract-N-Amp™ Tissue PCR Kit (see section 2.1.3.4) according to the manufacturer's instructions. In brief, each tissue sample was mixed with 100 µl extraction solution and 25 µl tissue preparation solution, and incubated for 10 minutes at 20 °C and for 3 minutes at 95 °C. Finally, 100 µl neutralisation solution B was added to the samples. An aliquot of each sample was then mixed with REDExtract-N-Amp PCR reaction mix and primers as described below and used for PCR (cycling parameters are shown in Table 2.6). PCR products were then resolved on 1.5% (w/v) agarose gels and visualised with ethidium bromide.

PCR mixture:

10 µl REDExtract-N-Amp PCR reaction mix

4 µl PCR grade $H_2O$

10 pmol of each primer (see section 2.1.3.4)

4 µl tail/tissue extract

***Table 2.6 PCR cycling parameters for genotyping VAPBP56S transgenic mice.***

| Step | Cycles | Temperature (°C) | Time (min) |
|---|---|---|---|
| 1. Initial denaturation | 1 | 94 | 3 |
| 2. Denaturation, annealing and elongation | 34 | 94 | 1 |
| | | 55 | 1 |
| | | 72 | 2 |
| 3. Extension/Elongation | 1 | 72 | 10 |
| 4. Cooling | | 4 | unlimited |

### 2.2.2.5 Transient transfection of HEK293 and CV-1 cell cultures

HEK293 and CV-1 cells were transfected using ExGen 500 (Thermo Scientific), a polyethylenimine based transfection reagent. Polyethylenimine is a cationic polymer with high proton buffer capacity ("proton sponge effect"). The mechanism of polyethylenimine based transfection was described by Boussif and Sonawane (Boussif et al., 1995; Sonawane et al., 2003). The positively charged polyethylenimine polymer interacts with negatively charged DNA and forms small particles (polyplexes). Polyplexes settle on and bind to anionic cell surface residues and are taken up by the cells via endocytosis (Boussif et al., 1995). The "proton sponge effect" of polyethylenimine neutralises the acidic pH of the endosome/lysosome and this results in a charge driven chloride influx into the endosome. The chloride influx causes osmotic swelling and disruption of the endosome and allows the escape of the polyplexes from the endosome (Sonawane et al., 2003). The DNA then dissociates from the polyplex and translocates to the nucleus.

Transfections were conducted according to the manufacturer's instructions. Cells were plated on 18 mm diameter coverslips in 12 well plates, in 25 $cm^2$ flasks or in 10 cm diameter petri dishes (Greiner Bio-One) the day before transfection so that they

reached 50-70% confluency on the day of transfection. For each transfection, the amounts of reagents were vortexed as indicated in Table 2.7 for 10 s. The transfection solution was then incubated for 10 min at 20 °C and added drop-wise to the cells. The cells were kept in an incubator at 37 °C under an atmosphere of 5% $CO_2$ and used for analysis 24 h post-transfection. The average transfection efficiency (as detected by immunostaining) was approximately 30%.

***Table 2.7 Amounts of reagents for ExGen 500 based transient transfection.***

| Plate Format | Plasmid DNA per well/dish (µg) | ExGen 500 per dish (µl) | 150 mM NaCl per dish (µl) |
|---|---|---|---|
| 12 well plate | 1 | 4.3 | 50 |
| 25 $cm^2$ dish | 6 | 25.8 | 300 |
| 10 cm petri dish | 12 | 51.6 | 600 |

### 2.2.2.6 Calcium phosphate-based transient transfection of primary cortical neurons

The calcium phosphate transfection method involves mixing DNA with $CaCl_2$ in phosphate buffer. The mixed components form fine calcium phosphate-DNA co-precipitates, which bind to the cell surface and are taken up by the cells via endocytosis. DNA is released from the endocytic vesicles due to osmotic swelling and disruption of the endocytic vesicles caused by $Ca^{2+}$ driven chloride influx. The released DNA then translocates to the nucleus (Kovtun et al., 2009).

Cortical neurons were transfected using a ProFection® Mammalian Transfection System – calcium phosphate kit (see section 2.1.3.5) after 7 days in culture as previously described (Ackerley et al., 2000; Xia et al., 1996). The conditioned cortical

neuron cell culture media were removed and kept at 37 °C while neurons were incubated with 1 ml (6 well plate) or 0.5 ml (12 well plate) kynurenic acid solution (see section 2.1.3.5) in cortical neuron cell culture media (see 2.1.3.2) for 30 min at 37 °C. Kynurenic acid solution inhibits ionotropic glutamate receptors and as such protects the cells from $Ca^{2+}$ mediated toxicity during transfection. Kynurenic acid blocks NMDA and AMPA glutamate receptors in a competitive manner via binding to the glycine and glutamate-binding sites of the receptors while $Mg^{2+}$ selectively blocks NMDA receptors through binding to a site deep within the pore forming region (Dingledine et al., 1999). For each transfection, the amounts of reagents were used as indicated in Table 2.8. The last reagent 2x HEPES-buffered saline (see section 2.1.3.5) was added drop-wise to the DNA mixture while continuously vortexing and was vortexed for a further 10 s after addition. The transfection solution was then added drop-wise to the cells and cells were incubated for 45 min at 37 °C. After incubation the cells were washed once with fresh cortical neuron cell culture media and once with conditioned cortical neuron cell culture media. Finally, a 1:1 mixture of conditioned and fresh cortical neuron cell culture media was added and the cells were transferred to an incubator and kept at 37 °C under an atmosphere of 5% $CO_2$. After 36-48 h of transfection, cells were used for time-lapse microscopy or Fura2 ratio imaging studies (see section 2.2.4.2 and 2.2.4.3). The average transfection efficiency was approximately 5%.

***Table 2.8 Amounts of reagents for calcium phosphate-based transient transfection.***

| **Plate Format** | **Plasmid DNA per well (µg)** | **Nuclease-free $H_2O$ per well (µl)** | **2 M $CaCl_2$ per well (µl)** | **2x HEPES-buffered saline per well (µl)** |
|---|---|---|---|---|
| 6 well plate | 5 | 190 | 26 | 200 |
| 12 well plate | 10 | 95 | 13 | 100 |

## *2.2.3 General biochemical methods*

### 2.2.3.1 Isolation of mitochondria, ER and MAM

Mitochondria, ER and MAM were prepared by differential centrifugation as described previously (Vance, 1990). The whole procedure was conducted at 4 °C or on ice. 24 h after transfection, HEK293 cells were harvested from 25 $cm^2$ flasks or 10 cm diameter petri dishes by trypsinisation and washed once with PBS (see section 2.1.1) and once with isolation buffer (see section 2.1.4.1) by centrifugation at 13,000 x g for 30 s. Cells were re-suspended in 500 µl ice-cold isolation-buffer and homogenised on ice using a pre-cooled glass/Teflon Potter Elvehjem dounce homogeniser (100 strokes by hand) (No19; Kimble Chase, Vineland, NJ, USA). A sample was removed as "Total" cell proteins and lysed in 5x SDS sample buffer (see section 2.1.4.1). The remaining homogenate was centrifuged twice at 600 x g for 5 minutes to pellet and remove nuclei and any large cellular debris. Mitochondria containing MAM were then pelleted from the supernatant by centrifugation at 10,300 x g for 10 minutes. The supernatant obtained after removal of the MAM-enriched mitochondrial fraction was centrifuged at 100,000 x g for 30 min to pellet the ER/microsomes. To separate MAM and mitochondria, the MAM-enriched mitochondrial pellet was resuspended in isolation buffer and layered on top of a self-forming 30% Percoll gradient (see section 2.1.4.1). After centrifugation at 95,000 x g for 30 min, a dense band containing the mitochondria was recovered at the bottom of the gradient; the MAM-containing band was retrieved above the mitochondrial band. To remove residual Percoll, the mitochondrial fraction was diluted in threefold in isolation medium and mitochondria were washed twice by centrifugation at 6,300 x g for 10 min. The MAM fraction was diluted with isolation buffer in threefold and centrifuged once at 6,300 x g for 10 min to remove contaminating

mitochondria. MAM was pelleted from the resulting supernatant by centrifugation at 100,000 x g for 1 h. All final organelle pellets were resuspended and lysed in RIPA-buffer (see section 2.1.4.1) and the protein concentrations were determined using Bradford assay (see section 2.2.3.3). Protein concentrations were adjusted to 1 µg/µl with sterile water and 5x SDS sample buffer, and protein samples were used for SDS-PAGE (see section 2.2.3.4).

### 2.2.3.2 Immunoprecipitation

Immunoprecipitations were performed at 4 °C or on ice. Cells were harvested by trypsinisation and washed once in ice-cold PBS (see section 2.1.1). 1/10 of the sample was removed ("Input") and lysed in 5x SDS sample buffer (see section 2.1.4.1). The rest of the sample was incubated in immunoprecipitation lysis buffer (see section 2.1.4.2) for 1 h after which the lysates were centrifuged at 100,000 x g for 40 minutes to pellet insoluble particles. Supernatants were transferred to fresh tubes and were precleared by incubation with 30 µl of Protein G-sepharose beads (50% (v/v) in PBS-Triton) (see section 2.1.4.2) for 30 minutes. Following centrifugation at 3,000 x g for 10 s to settle the beads supernatants were transferred to fresh tubes and total protein concentrations were quantified by Bradford assay (see section 2.2.3.3). The protein concentration was adjusted to 1 µg/µl if needed and equal amounts of protein (500 µg) for each sample were then used for immunoprecipitation. Appropriate primary antibody was added (see Table 2.3) and the samples were incubated with mild mixing on a rotary shaker for 16 hours at 4 °C. After addition of 30 µl of Protein G-sepharose beads (50% (v/v) in PBS-Triton) the samples were incubated for a further 2 hours on a rotary shaker before centrifuging at 3,000 x g for 10 s to pellet the beads. The pelleted beads were retained

and washed four times with 1 ml PBS-Triton. The bound proteins were then eluted from the beads by incubation in 50 µl of 2x SDS sample buffer and heating at 95 °C for 5 minutes and used for SDS-PAGE (see section 2.2.3.4).

### 2.2.3.3 Protein concentration determination – Bradford Assay

Protein concentrations were determined using a Bio-Rad protein assay kit according to the manufacturer's instructions (Bio-Rad). The assay is based on the colorimetric reaction described by Bradford (Bradford, 1976). Essentially, the binding of Coomassie Brilliant Blue G-250 dye to proteins shifts its absorption peak from 465 nm to 595 nm (Bradford, 1976). In brief, eight dilutions were prepared from a freshly prepared BSA standard from 50 µg/µl to 3.9 µg/µl for a standard curve and four dilutions from each protein sample with the Bradford reagent. 50 µl of each dilution was moved in a 96 well microtiter plate and absorbance readings were recorded at a wavelength of 595 nm using a VICTOR3 multilabel plate reader (Perkin Elmer). Protein concentrations of the samples were calculated using the recorded absorbance values and a standard curve drawn from the freshly prepared BSA stanard.

### 2.2.3.4 SDS-PAGE and immunoblotting

#### *2.2.3.4.1 SDS-PAGE of protein samples*

Protein samples in SDS sample buffer were heated on a heat block for 5 minutes at 95 ºC. Samples were then separated by SDS-PAGE on 8, 10 or 12% (v/v) (depending on the size of the proteins of interest) acrylamide gels (see section 2.1.4.3.1) using the

Mini-PROTEAN 3 gel electrophoresis system (Bio-Rad) with a discontinuous buffer system (see section 2.1.4.3.1).

Gels were run at 100 V until the dye front reached the bottom of the gel or proteins were separated as required. To follow the progress of protein separation and to determine protein size Precision Plus Protein™ Standards (Bio-Rad) were used. Precision Plus Protein™ Standards are broad range protein ladders consisting of 10 pre-stained proteins, sizes in kDa: 250; 150; 100; 75; 50; 37; 25; 20; 15; 10.

#### *2.2.3.4.2 Immobilisation of proteins on nitrocellulose membranes*

After SDS-PAGE, proteins were transferred from gels to a Protran nitrocellulose membrane (0.45 μm pore size; Whatman) using the following filter sandwich:

Cathode – sponge / extra thick cellulose blot paper (Whatman) / SDS-PAGE gel / nitrocellulose membrane / extra thick cellulose blot paper / sponge – Anode

This sandwich was assembled whilst totally immersed in transfer buffer (see section 2.1.4.3.2), secured in cassettes and placed in a Mini Trans-Blot electrophoretic transfer cell (Bio-Rad), and run at 100 V for 60 min or at 30 V for 16 h. Membranes containing transferred proteins were referred to as “blots”. Blots were incubated with Ponceau S solution (see section 2.1.4.3.2) for 1 to 2 min to determine the efficiency of protein transfer. Blots were then rinsed for 1 to 2 min with ultrapure water to destain.

#### *2.2.3.4.3 Antibody probing of nitrocellulose membrane-bound proteins – immunoblot*

Blots were incubated in blocking buffer (see section 2.1.4.3.3) for 1 h at 20 °C to reduce non-specific antibody binding. Blots were then incubated with an appropriate dilution of primary antibody in blocking buffer for 1 h at 20 °C or for 16 h at 4 °C. All primary antibodies that were used during the experiments are listed in Table 2.3. Blots were then washed (3 x 10 min) in TBS-Tween (see section 2.1.4.3.3) and an appropriate dilution of horseradish peroxidase-coupled secondary antibody in TBS-Tween was added for 1 h at 20 °C. Secondary antibodies were used depending on the species in which the primary antibody was raised (for details see Table 2.4). Following washing with TBS-Tween (3 x 10 min), immunoreactive species were visualised using enhanced chemiluminescence (ECL) development reagents (see section 2.1.4.3.3) and Hyperfilm-ECL (GE Healthcare), a blue light sensitive autoradiography film, according to the manufacturer's instructions. ECL protein signal visualisation is based on antibody bound horseradish peroxidase catalysed oxidation of luminol in the presence of hydrogen peroxide in alkaline conditions (Whitehead et al., 1979). Oxidised luminol is in an increased energy state and when luminol returns to ground state it emits the energy as light. In ECL detection the light output of luminol is enhanced by the presence of chemical enhancers (Whitehead et al., 1979). The light emission maximum of luminol is at 428 nm which is easily detectable by blue light sensitive autoradiography films. To visualise nitrocellulose membrane-bound proteins, detection solution A (luminol solution) and detection solution B (peroxide solution) were mixed in a 1:1 ratio in a final volume of 0.125 ml/cm$^2$ nitrocellulose membrane and incubated with the blot for 2 min at 20 ºC with continuous mixing. Following incubation, blots were placed in an X-ray film cassette and Hyperfilm-ECL was placed on top of the membrane in a dark

room, and exposed for a time varying between 5 s and 1 hour. The Hyperfilm-ECL was developed using a Konica Minolta SRX-101A developer.

#### *2.2.3.4.4 Quantification of bands from immunoblots*

Developed films were scanned using an Epson Perfection V700 Photo scanner (Seiko Epson Corp.). Signals on films were background-corrected and quantified using ImageJ developed by Wayne Rasband (NIH, Bethesda, USA; http://rsb.info.nih.gov/ij/) (Abrámoff et al., 2004). Each of the background-corrected OD signals was compared to an OD calibration curve obtained from a calibrated OD step tablet (Kodak) to ensure that signals were obtained within the linear range of the film. Only the signals within the linear OD range were used for statistical analysis. In experiments involving the association of Miro1 with kinesin-1 and α-tubulin (shown in Figures 4.5 and 4.9), OD values of empty vector, VAPB and VAPBP56S transfected samples were normalised to OD values obtained from empty vector transfected cells. This normalisation resulted in a reference value of 1.0 for empty vector transfected samples. Kinesin-1 signals were then further normalised to Miro1 signals whereas α-tubulin signals were normalised to Miro1 or kinesin-1 signals. Statistical analysis was performed using Excel (Microsoft Corporation, Redmond, WA), and Prism software (GraphPad Software Inc., San Diego, CA).

## *2.2.4 Microscopy*

### 2.2.4.1 Immunofluorescence

All steps of the procedure were performed at 20 ºC. Cells grown on glass coverslips were washed once with PBS (see section 2.1.1) to remove culture medium and incubated in fixing solution (see section 2.1.5.1) for 15 min. The cells were then washed twice with PBS and once with quenching solution (see section 2.1.5.1) to remove the fixing solution, and quenching solution was added for 15 min to quench unreacted formaldehyde and reduce autofluorescence. Following quenching the cells were washed once with PBS and permeabilised with permeabilisation solution (see section 2.1.5.1) for 3 min. Cells were then washed three times with blocking solution (see section 2.1.5.1) and incubated in blocking solution for 30 min to reduce non-specific antibody binding. After blocking, the cells were incubated with an appropriate dilution of primary antibody in blocking solution for 1 hour. All primary antibodies that were used during the experiments are listed in Table 2.3. The cells were washed three times with blocking solution and incubated with an appropriate dilution of secondary antibody in blocking solution for 45 min. Fluorescently labelled secondary antibody were chosen depending on the species in which the primary antibody was raised and the fluorophore (for details see Table 2.4). Following incubation with the secondary antibody the cells were washed three times with blocking solution and once with PBS. Finally, coverslips were mounted onto slides using Mowiol-DABCO mounting medium (see section 2.1.5.1). Images were captured at the appropriate excitation wavelengths using Leica LAS AF software on a Leica DM5000 B microscope equipped with a Leica DFC360 FX camera and 20x/0.50NA, 40x/0.75NA or 63x/1.25NA HCX-PL-FLUOTAR Leica objectives (all from Leica Microsystems CMS GmbH).

### 2.2.4.2 Time-lapse microscopy and image analysis

#### *2.2.4.2.1 Time-lapse microscopy*

Time-lapse microscopy of mitochondrial axonal transport was performed with an Axiovert S100 microscope (Zeiss) equipped with a Lambda LS Xenon-Arc light source (Sutter Instrument Company, Novato, CA), an enhanced green fluorescent protein (EGFP)/*Discosoma sp*. red fluorescent protein (DsRed) filterset (Chroma Technology Corp., Rockingham, VT), 40x EC Plan-Neofluar 1.3 N.A. objective (Zeiss), Lambda 10-3 filter wheel (Sutter Instrument Co.) and a Photometrics Cascade-II 512B High Speed EMCCD camera (Photometrics, Tuscon, AZ). 36-48 h post-transfection, neurons on coverslips were transferred to a custom observation chamber (Dr Kurt De Vos, KCL, UK) (De Vos and Sheetz, 2007) mounted on the stage of the microscope. The cells were maintained at 37 °C using an objective heater (Tempcontrol 37-2, Zeiss) and 'The Box' and 'The Cube' Microscope Temperature Control System (Life Imaging Systems, Basel, Switzerland). Mitochondrial movements were recorded for 10 minutes with 100 ms exposure time and 3 s time-lapse interval using Metamorph software (Molecular Devices).

Axons in both cortical and motor neurons were easily identified in the cultures by morphological criteria being the longest process with sparse arborisation; many others studies have used such criteria (Ackerley et al., 2000; Nikolic et al., 1996; Roy et al., 1998; Tradewell et al., 2011). In cortical neurons mitochondria were visualised by transfection with DsRed-Mito (Clontech). DsRed is a red fluorescent protein from *Discosoma sp.* (Matz et al., 1999). DsRed-Mito was created by fusion of DsRed and the mitochondrial targeting sequence from subunit VIII of human cytochrome c oxidase. In motor neurons mitochondria were visualised by labeling with MitoTracker Red

CMXRos (Invitrogen). MitoTracker Red CMXRos is a mitochondria selective red fluorescent dye derived from X-rosamine (Poot et al., 1996). It passively diffuses across the plasma membrane and accumulates in active mitochondria due to its cationic properties. MitoTracker Red CMXRos contains an alkylating chloromethyl moiety which can form a stabile covalent bond with free thiol groups in mitochondria (Poot et al., 1996). To visualise mitochondria for live cell imaging, motor neurons were incubated with 66 nM MitoTracker Red CMXRos in fresh motor neuron cell culture media for 3 min at 37 °C.

### *2.2.4.2.2 Image analysis*

Image analysis was performed using ImageJ extended with custom plug-ins developed by Dr Kurt De Vos (KCL, UK), or Metamorph. Further calculations and statistical analysis were performed using Excel and Prism software.

#### 2.2.4.2.2.1 Analysis of overall mitochondrial transport

Overall transport of mitochondria was quantified from kymographs which are representing movement obtained from time-lapse movies. On a kymograph the distance of movement is plotted along the x-axis and time along the y-axis. Kymographs were created using the Kymograph plugin of ImageJ (De Vos and Sheetz, 2007). Before converting the time-lapse movie to a kymograph, any bends in the imaged axon were straightened using the Straighten plugin of ImageJ (Kocsis et al., 1991).

The overall transport of mitochondria in Figure 3.2, 3.3 and 4.10 was quantified from kymographs using the SlopeToVelocity plugin of ImageJ described previously (De

Vos and Sheetz, 2007). Briefly, this plugin calculates the overall velocity by measuring the distance between the position of individual mitochondria at the start and end of time-lapse recordings and dividing by the time elapsed. This yields an overall velocity of transport that includes anterograde and retrograde movements and stationary periods. Mitochondria were subsequently classified as motile (velocity > 0.1 μm/s) or stationary (velocity ≤ 0.1 μm/s). This threshold was empirically determined by Dr Kurt De Vos (De Vos et al., 2003).

#### 2.2.4.2.2.2 Full quantitative characterisation of mitochondrial transport

All calculations of mitochondrial transport parameters were as described before (De Vos and Sheetz, 2007). For this analysis all positions of all mitochondria were determined at each time point in the time-lapse recordings using the Organel_Dynamics plugin of ImageJ developed by Dr Kurt De Vos (KCL, UK). From this positional information the frequency of movement, the duration of stationary periods between movements, the absolute velocity, and the persistence of unidirectional continuous movements were calculated.

Movement events were defined using an absolute velocity threshold of 0.3 μm/s. This threshold was applied to exclude non microtubule-based mitochondrial transport from the calculations. The velocity of microtubule-based mitochondrial transport is higher 0.3 μm/s whereas the velocity of actin-based mitochondrial transport is below 0.3 μm/s (Morris and Hollenbeck, 1995). Events with absolute velocity ≥ 0.3 μm/s were classified as motile and events with absolute velocity < 0.3 μm/s as stationary.

#### *2.2.4.2.2.2.1 The frequency of movement*

The frequency of mitochondrial movement events was defined as the number of movement events per minute. The total frequency of movement (anterograde and retrograde movements combined) as well as the frequency of anterograde and of retrograde movement were calculated. To do so, the number of anterograde and retrograde movement events were tallied and divided by the recording time. The frequency of movement examines the transport activities underlying overall transport.

#### *2.2.4.2.2.2.2 The duration of stationary periods between movements*

The duration of stationary periods is defined as the length time mitochondria spent without moving between either anterograde or retrograde movements. To determine the duration of stationary periods in seconds, I tallied the number of time points a given mitochondria remained stationary after a movement. The duration was converted to seconds by multiplication by the time-lapse interval. The duration of stationary periods is a measure of the activity of the motors driving transport.

#### *2.2.4.2.2.2.3 Absolute velocity of movement*

The absolute velocity of movement was determined by measurement of the distance each mitochondrion has moved relative to its position at the previous time point and dividing this distance by the time-lapse interval. Only velocities $\geq 0.3$ μm/s were included to exclude stationary periods and non-microtubule based mitochondrial transport.

In contrast to the overall velocity of movement determined from the kymographs, the absolute velocity is a parameter that describes a physical property of the molecular motor driving transport.

#### *2.2.4.2.2.2.4 The persistence of unidirectional continuous movements*

The persistence of unidirectional continuous movement is defined as the duration of a continuous movement in either anterograde or retrograde direction without pausing or reversal of direction. To calculate the persistence of anterograde and retrograde mitochondrial transport, the number of motile events that follow each other in one direction without pausing or reversals were tallied. Multiplication of this number by the time-lapse interval yielded the persistence of unidirectional movement in seconds. The persistence of movement measures the processivity of the molecular motors driving transport.

### 2.2.4.3 Fura2 ratio imaging

$[Ca^{2+}]c$ were measured using Fura2/AM (Fura2/acetoxymethyl ester; Calbiochem). Fura2/AM is a membrane-permeable form of the ratiometric $Ca^{2+}$ indicator Fura2. Upon entry into the cell endogenous esterases readily hydrolyse the acetoxymethyl ester moiety and generate membrane-impermeable Fura2. Fura2 is a polyamino carboxylic acid with properties similar to the $Ca^{2+}$ chelator EGTA and BAPTA (1,2-bis(o-aminophenoxy)ethane-N,N,N',N'-tetraacetic acid). Fura2 has excitation maxima at a wavelength of 340 and 380 nm and an emission maximum at 510 nm. Upon binding of $Ca^{2+}$ the excitation peak of Fura2 shifts from 380 to 340 nm.

The ratio of the fluorescent intensities at the two excitation wavelengths directly correlates to the intracellular $Ca^{2+}$ concentration and is independent of total dye concentration or illumination intensity (Grynkiewicz et al., 1985).

To measure $[Ca^{2+}]c$, neurons were loaded with 5 μM Fura2/AM in external solution (see section 2.1.5.2) for 20 min at 37 °C followed by washing in external solution for 20 min at 37 °C. Fura2 340 nm and 380 nm image pairs were recorded in time-lapse mode (100 ms exposure time, 1 s interval for 10 min) at 37 °C using MetaFluor software (Molecular Dynamics) on an Axiovert 200M microscope (Zeiss) equipped with a Polychrome V light source (Till Photonics), Fura2 filterset (Chroma Technology Corp.), 40x 1.3NA Fluar objective (Zeiss), Lambda 10-2 filter wheel (Sutter Instrument Co.) and a CoolSnap HQ2 camera (Photometrics, Tuscon, AZ). Neurons were kept at 37 °C on the microscope in a Ludin imaging chamber (Life Imaging Systems) using an objective heater (Tempcontrol 37, Zeiss) and 'The Box' and 'The Cube' Microscope Temperature Control System. During experiments, neurons were perfused continuously with external solution (0.5 ml/min) using an Ismatec REGLO peristaltic pump (IDEX Corporation, Glattbrugg, Switzerland). To invoke transient $Ca^{2+}$ influx, 50 mM KCl was applied in external solution (NaCl was replaced with equimolar amounts of KCl) (see section 2.1.5.2) for 2 min. The $[Ca^{2+}]c$ was calculated from the ratio of Fura2 fluorescent signals at excitation 340 and 380 nm and calibrated by sequential addition of saturating $CaCl_2$ (20 mM) and EGTA (20mM) in external solution (see section 2.1.5.2) after incubation with 10 μM A23187 ionophore and then converted to nM using the Grynkiewicz formula (Grynkiewicz et al., 1985). Resting $[Ca^{2+}]c$ was determined as the average value between 60 and 180 s of recording; statistical analysis was performed using Prism software.

# 3 VAPBP56S DISRUPTS ANTEROGRADE AXONAL TRANSPORT OF MITOCHONDRIA

## 3.1 Introduction

Previous work from our laboratory showed that ALS mutant SOD1 selectively reduced anterograde axonal transport of mitochondria in transfected cortical neurons as well as in motor neurons from SOD1-G93A transgenic mice (De Vos et al., 2007). Since then several other groups have also reported damage to axonal transport of mitochondria by ALS mutant SOD1 (Bilsland et al., 2010; Magrané et al., 2012; Marinković et al., 2012). Mitochondria play a pivotal role in many cellular events including energy metabolism, fatty-acid oxidation, cellular signalling, lipid biosynthesis, $Ca^{2+}$ handling, and apoptosis. They are therefore a critical axonal cargo because they supply the vast amount of ATP required to maintain ionic gradients for firing action potentials, mobilise vesicles for synaptic transmission and to support axonal transport itself.

To enquire whether other genetic insults associated with ALS damage axonal transport of mitochondria, I quantified mitochondrial transport in the axons of living rat cortical neurons that were transfected with control vector, wild-type VAPB or ALS mutant VAPBP56S. In addition, I quantified mitochondrial axonal transport in motor neurons derived from VAPBP56S transgenic mice or their non-transgenic littermates. The bulk of the data was obtained from transfected rat cortical neurons and this was because of breeding problems with the wild-type VAPB expressing transgenic mice (Dr Elizabeth Tudor, KCL, UK; personal communication). Indeed, these lines have since been lost.

## 3.2 Results

### *3.2.1 VAPBP56S selectively disrupts anterograde axonal transport of mitochondria in transfected cortical neurons*

To investigate any effect of VAPB and VAPBP56S on axonal transport of mitochondria, mitochondrial transport was first quantified through axons of living transfected rat cortical neurons by time-lapse microscopy using methods previously established in our laboratory (De Vos et al., 2007). EGFP-tagged VAPB (EGFP-VAPB) and EGFP-tagged VAPBP56S (EGFP-VAPBP56S) were used in this study because this allowed easy identification of transfected neurons, and also allowed an estimation of expression level of transfected proteins by monitoring the fluorescent signal intensity. The latter is important because excessive overexpression could cause artefacts.

It has been shown that axonal transport is affected by neuronal outgrowth (Morris and Hollenbeck, 1993). Therefore the neurons used in this study were kept in culture for 7 days before transfection as it has been shown that cortical neurons do not noticeably have axonal growth after 7 days in culture (Ackerley et al., 2000). Neurons were co-transfected with DsRed-Mito (to visualise mitochondria) and either EGFP control vector, EGFP-VAPB or EGFP-VAPBP56S. Several groups have successfully utilised EGFP-tagging to study VAPB/VAPBP56S metabolism (Chen et al., 2010a; Gkogkas et al., 2008; Kanekura et al., 2006; Landers et al., 2008; Nishimura et al., 2004). All constructs readily expressed in the cortical neurons (Figure 3.1). EGFP and EGFP-VAPB were observed throughout the cell body and in neurites, whereas EGFP-VAPBP56S formed intracellular aggregates that were mostly restricted to the cell body and excluded from neurites (Figure 3.1). Others have described similar VAPBP56S aggregates in neurons and cell lines (De Vos et al., 2012; Fasana et al., 2010; Kanekura et al., 2006; Langou et al., 2010; Nishimura et al., 2004; Teuling et al., 2007).

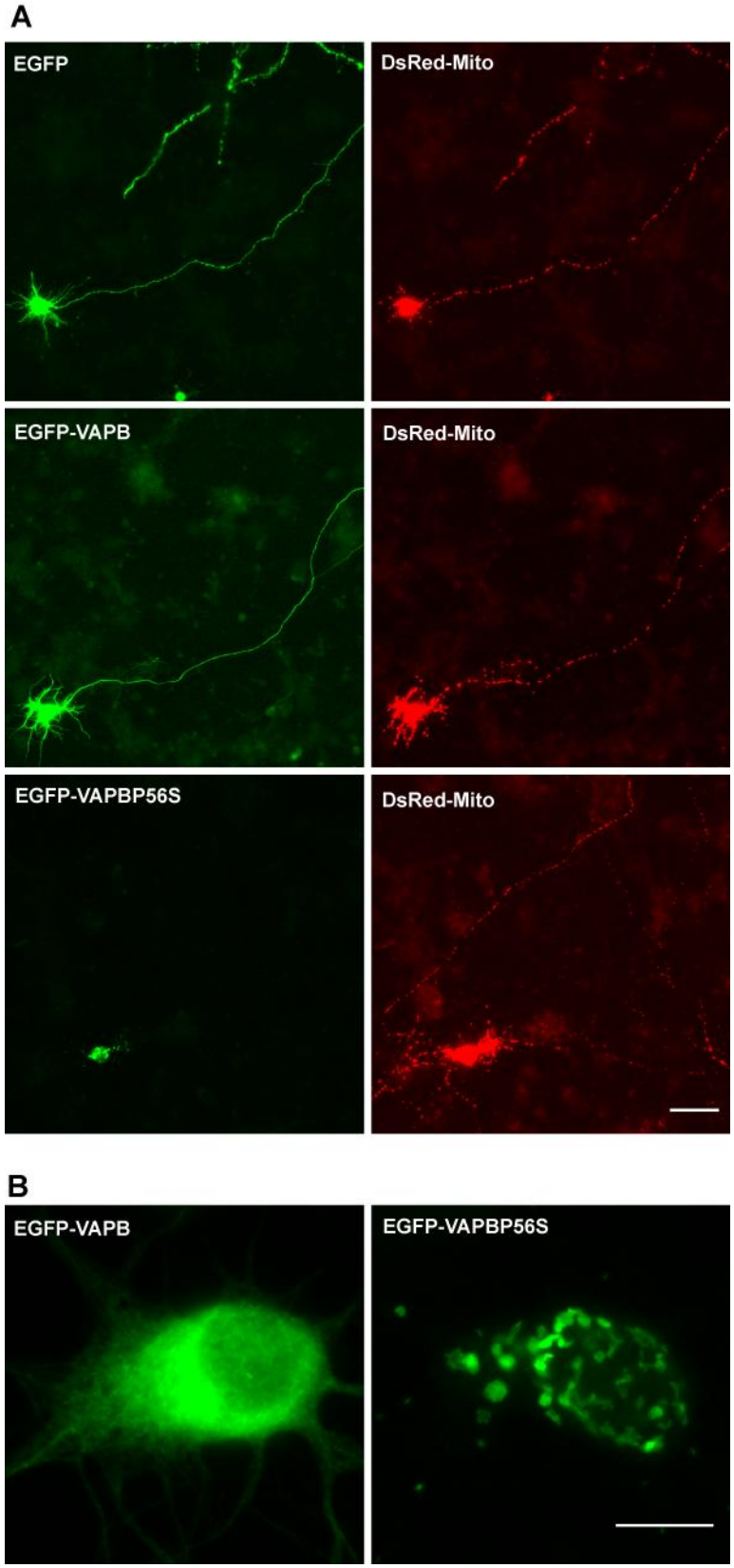


***Figure 3.1. EGFP-VAPBP56S forms aggregates in cortical neurons.***

(A) Cortical neurons were co-transfected with DsRed-Mito (red) and EGFP, EGFP-

VAPB or EGFP-VAPBP56S (green) as indicated. EGFP and EGFP-VAPB were localised in both the cell body and neurites. In contrast, EGFP-VAPBP56S formed aggregates and localised mostly in the cell body. Representative images are shown. Scale bar: 50 μm. (B) Representative high power micrographs of the cell bodies of cortical neurons transfected with EGFP-VAPB or EGFP-VAPBP56S. Scale bar: 10 μm.

36 to 48 hours after transfection the neurons were transferred to the microscope and cells expressing low levels of transfected proteins (as judged by brightness of EGFP signal) were chosen for recording to avoid any possible artefacts produced by high-level expression (Ackerley et al., 2003; Vagnoni et al., 2011). Mitochondrial transport was recorded in a 100 to 200 μm section approximately in the middle of the axon with a 3 s time-lapse interval for 10 min.

Mitochondrial transport was analysed from these recordings by creating kymographs and analysing overall transport of mitochondria. To do so, the distance between the position of individual mitochondria at the start and end of time-lapse recordings was calculated and divided by the time elapsed. This yielded an overall velocity for each mitochondrion that included both anterograde and retrograde movements and stationary periods. Mitochondria were classified as motile when their overall velocity exceeded 0.1 μm/s or as stationary when their velocity was equal to or below 0.1 μm/s.

Quantification of the overall transport of mitochondria revealed that in the axon of EGFP control neurons, approximately 38% of mitochondria were motile with approximately 24% and 14% moving in anterograde and retrograde directions, respectively (Figure 3.2). These levels of motility are in agreement with previous studies of mitochondrial transport in cortical neurons (De Vos et al., 2007). Expression of EGFP-VAPB had no significant effect on mitochondrial transport compared to the EGFP control. However, expression of EGFP-VAPBP56S induced a significant decrease in total mitochondrial motility and this was due to a selective reduction in the number of anterograde moving mitochondria (Figure 3.2).

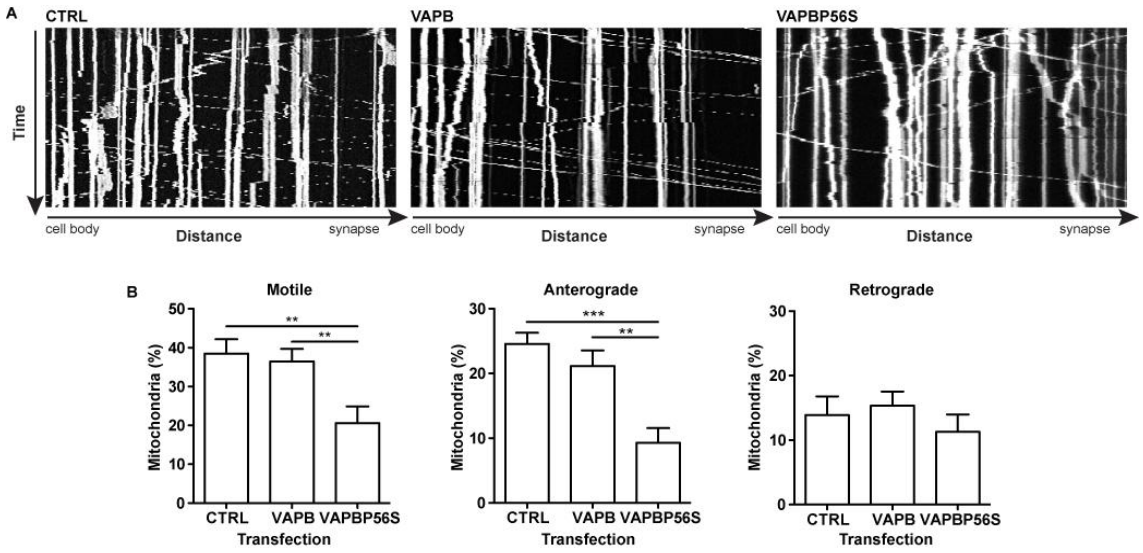


***Figure 3.2. VAPBP56S disrupts anterograde axonal transport of mitochondria in transfected rat cortical neurons.***

Mitochondrial transport was recorded in neurons co-transfected with DsRed-Mito and EGFP (control; CTRL), EGFP-VAPB (VAPB) or EGFP-VAPBP56S (VAPBP56S) as indicated. (A) Representative kymographs show axonal transport of mitochondria in EGFP, EGFP-VAPB or EGFP-VAPBP56S transfected neurons. (B) The percentage of motile, anterograde and retrograde moving mitochondria are shown. Expression of EGFP-VAPB had no effect on mitochondrial transport. By contrast, EGFP-VAPBP56S reduced mitochondrial transport and this was due to a selective inhibition of anterograde but not retrograde transport. Statistical significance was determined by one-way ANOVA followed by Tukey's post hoc test. N=11-14 cells from 3 different neuronal cell cultures for each transfection. Error bars are SEM ** $p<0.01$; *** $p<0.001$.

### *3.2.2 VAPBP56S selectively disrupts anterograde axonal transport of mitochondria in VAPBP56S transgenic motor neurons*

ALS is characterised by selective death of motor neurons. Thus to further investigate the possible relevance of the findings in transfected cortical neurons, I next quantified mitochondrial transport in embryonic motor neurons isolated from transgenic mice that express myc-tagged VAPBP56S (myc-VAPBP56S) in the central nervous system under control of the prion promoter. Myc-VAPBP56S forms aggregates in the cell body of motor neurons (Figure 3.3) that are similar to those I found in transfected cortical neurons (Figure 3.1) and those described by others (Langou et al., 2010; Tudor et al., 2010). Motor neurons isolated from non-transgenic littermates were used as controls. The VAPBP56S transgenic mice were generated in our laboratory and have been described previously (Tudor et al., 2010).

Motor neuron mitochondria were visualised using the mitochondrial dye MitoTracker Red CMXRos and mitochondrial transport was imaged by time-lapse microscopy (3 s time interval, 10 min movies) as described previously (De Vos et al., 2007). In non-transgenic motor neurons approximately 37% of mitochondria were motile and their anterograde and retrograde transport was balanced (approximately 18% anterograde and 19% retrograde) (Figure 3.4). Similar levels of mitochondrial transport have been observed in mouse motor neurons previously (De Vos et al., 2007). However, compared to the non-transgenic neurons, myc-VAPBP56S expressing motor neurons showed a significant reduction in the number of anterogradely moving mitochondria (Figure 3.4). The total number of motile mitochondria (retrograde + anterograde) did not change in VAPBP56S motor neurons because a slight, non-significant increase in retrograde transport compensated for the drop in anterograde mitochondria (Figure 3.4).

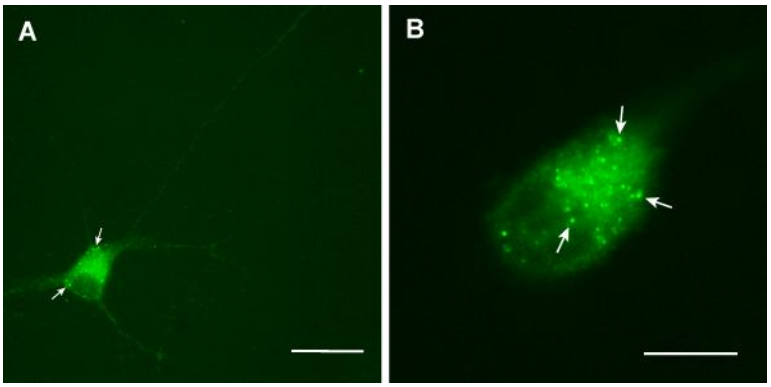


***Figure 3.3 VAPBP56S forms aggregates in motor neurons.***

(A-B) Representative images of motor neurons derived from VAPBP56S transgenic mouse embryos. VAPBP56S was stained using an antibody against the myc-tag. VAPBP56S forms punctate aggregates (arrows) in the cell body. Scale bar: 50 μm in A and 20 μm in B.

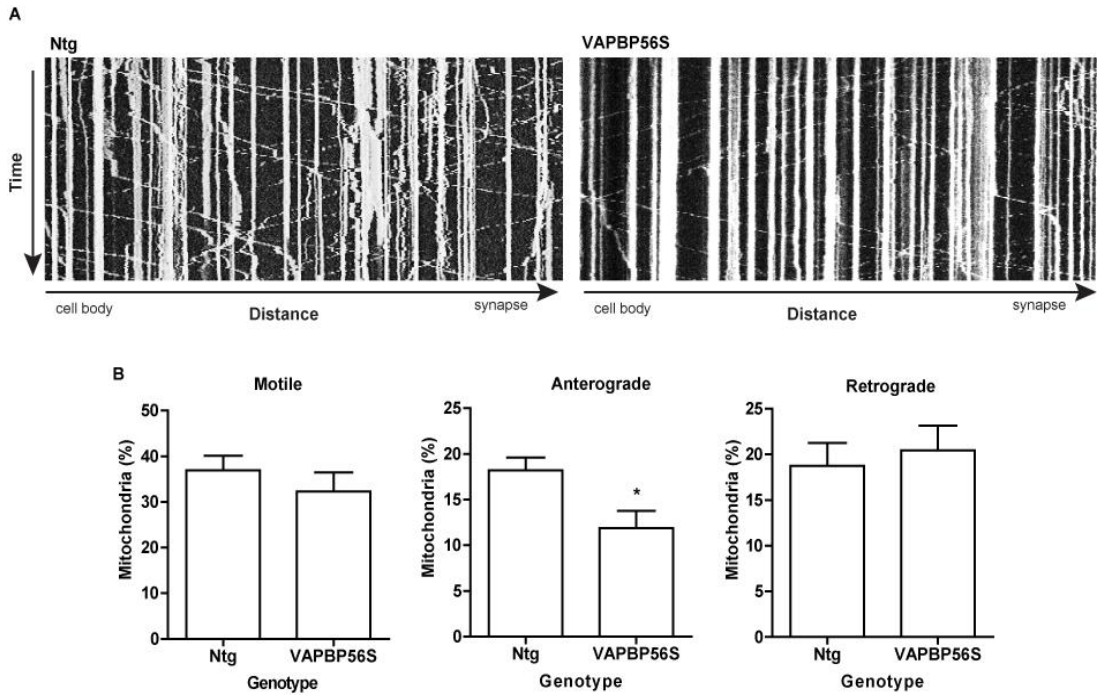


***Figure 3.4. VAPBP56S disrupts anterograde axonal transport of mitochondria in transgenic mouse motor neurons.***

Mitochondria were visualised by MitoTracker Red CMXRos and mitochondrial transport was recorded in motor neurons isolated from VAPBP56S transgenic mouse embryos (VAPBP56S) or their non-transgenic littermates (Ntg) as indicated. (A) Representative kymographs show axonal transport of mitochondria in Ntg or VAPBP56S motor neurons. (B) The percentage of motile, anterograde and retrograde moving mitochondria are shown. VAPBP56S selectively reduced anterograde mitochondrial but not retrograde transport in motor neurons. Statistical significance was determined by t-test. N=5 Ntg cells from 3 different embryos and N=10 VAPBP56S cells from 5 different embryos. Error bars are SEM * $p<0.05$.

### *3.2.3 VAPBP56S decreases the frequency, velocity and persistence of anterograde mitochondrial movement*

To analyse the features underlying the anterograde axonal transport defect in VAPBP56S-expressing neurons, the positions of all mitochondria at each time point in the time-lapse recordings were tracked and from this positional information, the frequency of anterograde and retrograde movement events, the duration of stationary periods between movements, the absolute velocities of movement and the persistence of unidirectional continuous movements were calculated. The average number of mitochondria examined per cell were not significantly different between EGFP, EGFP-VAPB and EGFP-VAPBP56S transfected cells (Figure 3.5).

The overall (anterograde and retrograde combined), anterograde and retrograde frequencies of movement events were not significantly different (approximately 4-5 events per mitochondria per minute) between control EGFP and EGFP-VAPB transfected neurons (Table 3.1 and Figure 3.5). In contrast, expression of EGFP-VAPBP56S reduced the overall frequency of mitochondrial movement by approximately 50% and this was caused by a selective inhibition to anterograde but not retrograde transport activity (Table 3.1 and Figure 3.6). This reduction in the frequency of anterograde movement events in EGFP-VAPBP56S expressing cells was accompanied by changes in the amount of time that mitochondria spent pausing. The average time mitochondria spent pausing between movements was not significantly different in control EGFP and EGFP-VAPB transfected cells (45.95±98.07 s (mean±SD) and 58.77±129.90 s, respectively). However, in EGFP-VAPBP56S transfected neurons the amount of time mitochondria spent stationary was significantly increased (79.71±121.20 s) (Table 3.2 and Figure 3.7).

To further characterise the properties of the molecular motors driving transport, the duration of unidirectional, continuous movement (the persistence of movement) and the velocity of movement were determined. This revealed that compared to EGFP and EGFP-VAPB transfected neurons, EGFP-VAPBP56S significantly reduced the persistence and velocity of anterograde mitochondrial movement but did not affect the persistence or velocity of retrograde movement (Table 3.3 and 3.4, and Figure 3.8 and 3.9).

Thus, the disruption to anterograde mitochondrial transport induced by VAPBP56S is a consequence of reductions in the frequency, velocity and persistence of anterograde mitochondrial movements.

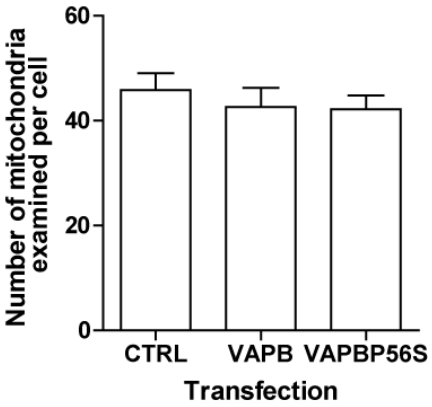


***Figure 3.5 The average number of mitochondria examined per cell are not significantly different between transfections.***

The numbers of mitochondria were quantified in DsRed-Mito plus either EGFP (CTRL), EGFP-VAPB (VAPB) or EGFP-VAPBP56S (VAPBP56S) co-transfected cortical neurons. No significant differences were detected between the transfections. Statistical significance was determined by one-way ANOVA followed by Tukey's post hoc test. N=11-14 cells from 3 different neuronal cell cultures for each transfection. Error bars are SEM.

***Table 3.1 VAPBP56S decreases the frequency of anterograde mitochondrial movement events.***

| Transfection | Motile Frequency (events/ mitochondria/min) | SD | p-value | Anterograde Frequency (events/ mitochondria/min) | SD | p-value | Retrograde Frequency (events/ mitochondria/min) | SD | p-value |
|---|---|---|---|---|---|---|---|---|---|
| Ctrl | 4.089 | 6.28 | | 2.793 | 5.42 | | 0.784 | 1.84 | |
| VAPB | 4.733 | 6.78 | ns | 3.234 | 6.11 | ns | 1.196 | 3.00 | ns |
| VAPBP56S | 2.031 | 4.40 | <0.001 | 0.726 | 2.64 | <0.001 | 0.856 | 2.48 | ns |

Frequencies of movement were quantified in DsRed-Mito plus either EGFP (Ctrl), EGFP-VAPB (VAPB) or EGFP-VAPBP56S (VAPBP56S) co-transfected cortical neurons. EGFP-VAPBP56S induced a significant decrease in the frequency of anterograde movements without affecting retrograde movement compared to control EGFP or EGFP-VAPB transfected neurons. Statistical significance was determined by one-way ANOVA (Kruskal-Wallis) followed by Dunn's Multiple Comparison Test. N=11-14 cells from 3 different neuronal cell cultures for each transfection. ns, not significant.

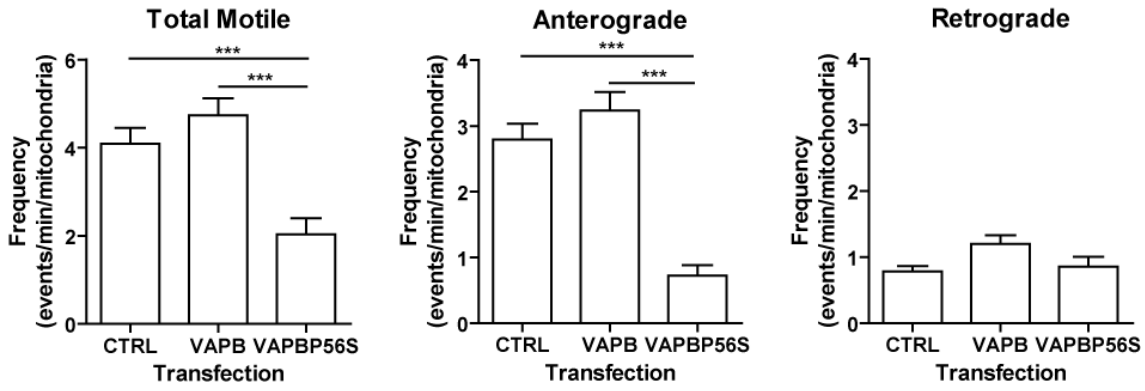


***Figure 3.6 VAPBP56S decreases the frequency of anterograde mitochondrial movement.***

Frequencies of movement were quantified in DsRed-Mito plus either EGFP (CTRL), EGFP-VAPB (VAPB) or EGFP-VAPBP56S (VAPBP56S) co-transfected cortical neurons. EGFP-VAPBP56S induced a significant decrease in the frequency of anterograde movements without affecting retrograde movement compared to control EGFP and EGFP-VAPB transfected neurons. Statistical significance was determined by one-way ANOVA (Kruskal-Wallis) followed by Dunn's Multiple Comparison Test. N=11-14 cells from 3 different neuronal cell cultures for each transfection. Error bars are SEM *** $p<0.001$.

***Table 3.2 VAPBP56S increases the duration of stationary periods between mitochondrial movements.***

| Transfection | Time (s) | SD | N (events) | p-value |
|---|---|---|---|---|
| Ctrl | 45.95 | 98.07 | 2106 | |
| VAPB | 58.77 | 129.90 | 1805 | ns |
| VAPBP56S | 79.71 | 151.20 | 753 | <0.001 |

The duration of stationary periods between movements was quantified for mitochondria in DsRed-Mito plus either EGFP (Ctrl), EGFP-VAPB (VAPB) or EGFP-VAPBP56S (VAPBP56S) co-transfected cortical neurons. The duration of stationary periods between movements was significantly increased in EGFP-VAPBP56S transfected cells compared to control EGFP or EGFP-VAPB transfected neurons. Statistical significance was determined by one-way ANOVA (Kruskal-Wallis) followed by Dunn's Multiple Comparison Test. N=11-14 cells from 3 different neuronal cell cultures for each transfection. ns, not significant.

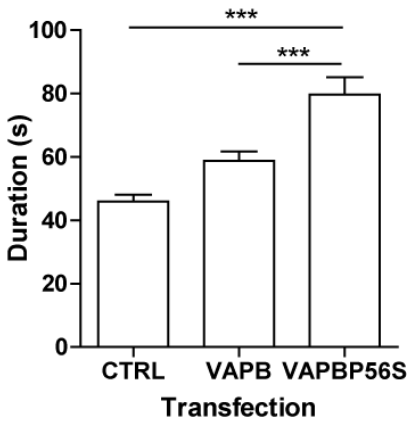


***Figure 3.7 VAPBP56S increases the duration of stationary periods between mitochondrial movements.***

The duration of stationary periods between movements was quantified for mitochondria in DsRed-Mito plus either EGFP (CTRL), EGFP-VAPB (VAPB) or EGFP-VAPBP56S (VAPBP56S) co-transfected cortical neurons. The duration of stationary periods between movements was significantly increased in EGFP-VAPBP56S compared to control EGFP or EGFP-VAPB transfected neurons. Statistical significance was determined by one-way ANOVA (Kruskal-Wallis) followed by Dunn's Multiple Comparison Test. N=11-14 cells from 3 different neuronal cell cultures for each transfection. Error bars are SEM *** $p<0.001$.

***Table 3.3 VAPBP56S decreases the velocity of anterograde mitochondrial movement.***

| | Anterograde | | | | Retrograde | | | |
|---|---|---|---|---|---|---|---|---|
| Transfection | Velocity (μm/s) | SD | N (events) | p-value | Velocity (μm/s) | SD | N (events) | p-value |
| Ctrl | 0.78 | 0.37 | 5249 | | 0.75 | 0.40 | 2592 | |
| VAPB | 0.80 | 0.39 | 4938 | ns | 0.77 | 0.41 | 2765 | ns |
| VAPBP56S | 0.68 | 0.37 | 1157 | <0.001 | 0.78 | 0.42 | 1255 | ns |

Velocities were quantified in DsRed-Mito plus either EGFP (Ctrl), EGFP-VAPB (VAPB) or EGFP-VAPBP56S (VAPBP56S) co-transfected cortical neurons. EGFP-VAPBP56S induced a significant decrease in anterograde but not retrograde velocities compared to control EGFP or EGFP-VAPB transfected neurons. Statistical significance was determined by one-way ANOVA (Kruskal-Wallis) followed by Dunn's Multiple Comparison Test. N=11-14 cells from 3 different neuronal cell cultures for each transfection. ns, not significant.

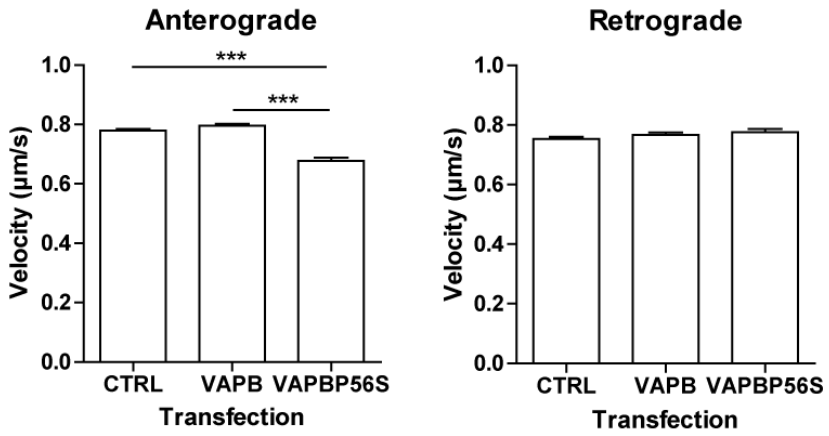


***Figure 3.8 VAPBP56S decreases the velocity of anterograde mitochondrial movement.***

Velocities were quantified in DsRed-Mito plus either EGFP (CTRL), EGFP-VAPB (VAPB) or EGFP-VAPBP56S (VAPBP56S) co-transfected cortical neurons. EGFP-VAPBP56S induced a significant decrease of anterograde but not retrograde velocity compared to control EGFP or EGFP-VAPB transfected neurons. Statistical significance was determined by one-way ANOVA (Kruskal-Wallis) followed by Dunn's Multiple Comparison Test. N=11-14 cells from 3 different neuronal cell cultures for each transfection. error bars are SEM *** $p<0.001$.

***Table 3.4 VAPBP56S decreases the persistence of anterograde mitochondrial movement.***

| | Anterograde | | | | Retrograde | | | |
|---|---|---|---|---|---|---|---|---|
| Transfection | Time (s) | SD | N (events) | p-value | Time (s) | SD | N (events) | p-value |
| Ctrl | 8.20 | 13.46 | 1928 | | 5.50 | 5.88 | 1422 | |
| VAPB | 9.18 | 15.08 | 1624 | ns | 5.75 | 6.06 | 1456 | ns |
| VAPBP56S | 5.96 | 10.04 | 563 | <0.01 | 5.74 | 6.32 | 664 | ns |

The persistence of continuous unidirectional movement was quantified in DsRed-Mito plus either EGFP (Ctrl), EGFP-VAPB (VAPB) or EGFP-VAPBP56S (VAPBP56S) co-transfected cortical neurons. EGFP-VAPBP56S induced a significant decrease in the persistence of anterograde but not retrograde compared to control EGFP or EGFP-VAPB transfected neurons. Statistical significance was determined by one-way ANOVA (Kruskal-Wallis) followed by Dunn's Multiple Comparison Test. N=11-14 cells from 3 different neuronal cell cultures for each transfectio. ns, not significant.

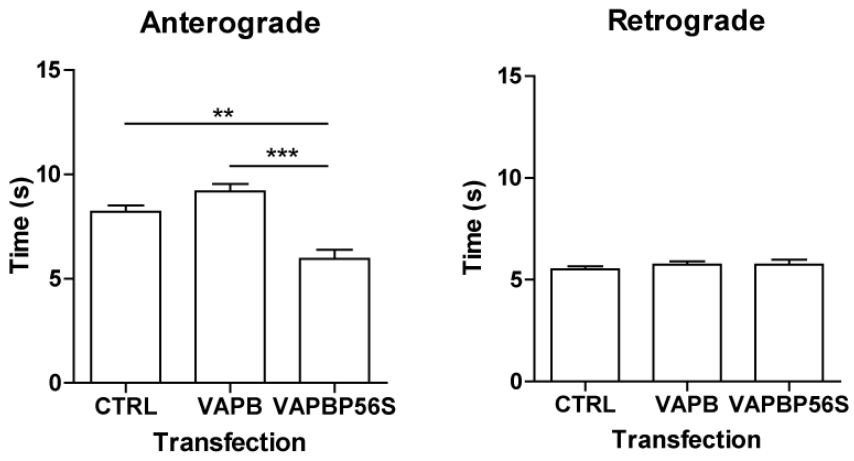


***Figure 3.9 VAPBP56S decreases the persistence of anterograde mitochondrial movement.***

The persistence of continuous unidirectional movement was quantified in DsRed-Mito plus either EGFP (CTRL), EGFP-VAPB (VAPB) or EGFP-VAPBP56S (VAPBP56S) co-transfected cortical neurons. EGFP-VAPBP56S induced a significant decrease in the persistence of anterograde but not retrograde movements compared to control EGFP or EGP-VAPB transfected neurons. Statistical significance was determined by one-way ANOVA (Kruskal-Wallis) followed by Dunn's Multiple Comparison Test. N=11-14 cells from 3 different neuronal cell cultures for each transfection. Error bars are SEM ** $p<0.01$; *** $p<0.001$.

## 3.3 Discussion

In this chapter, I investigated the effect of VAPB and ALS mutant VAPBP56S on axonal transport of mitochondria using time-lapse microscopy. I utilized two different experimental systems. The first involved cortical neurons transfected with EGFP control vector, EGFP-VAPB or EGFP-VAPBP56S. Here, mitochondria were visualized by co-transfection with DsRed-Mito. The second system involved motor neurons that were prepared from VAPBP56S transgenic mice and their non-transgenic littermates (Tudor et al., 2010). Here mitochondria were visualized by use of MitoTracker Red CMXRos. The use of motor neurons is advantageous since these are the cell-types affected in ALS. However, only a limited number of experiments could be performed with these cells as there were breeding problems with the transgenic lines; no wild-type VAPB transgenics were available. Nevertheless, similar results were obtained with both systems. VAPBP56S but not VAPB induced selective damage to anterograde but not retrograde axonal transport of mitochondria. Moreover, this damage involved perturbation to the velocity, frequency and processivity of anterograde mitochondria movements. Interestingly, this anterograde-specific damage to mitochondrial transport is similar to that described by some other groups in mutant SOD1 expressing neurons (De Vos et al., 2007).

Mitochondria are known to be a target for damage by ALS mutant SOD1 and as such it is not perhaps surprising that their axonal transport is perturbed by mutant SOD1 (Ferri et al., 2006; Higgins et al., 2002; Liu et al., 2004; Mattiazzi et al., 2002; Pasinelli et al., 2004). Indeed, there is evidence that damage to mitochondria via other agents disrupts their anterograde axonal transport (Miller and Sheetz, 2004). However, VAPB is an integral ER protein (Amarilio et al., 2005; Fasana et al., 2010; Kanekura et al.,

2006; Langou et al., 2010; Nishimura et al., 2004; Skehel et al., 2000; Soussan et al., 1999; Teuling et al., 2007) and so an effect of VAPBP56S on mitochondrial transport was less easy to predict. In the course of this study, the outer mitochondrial membrane protein PTPIP51 was identified as a binding partner for VAPB and the VAPB-PTPIP51 interaction regulates $Ca^{2+}$ homeostasis (De Vos et al., 2012). Also, a secreted fragment of VAPB has recently been linked to mitochondrial localization in *Drosophila* and *C. elegans* muscle cells (Han et al., 2012). Thus, there are now known links between VAPB and mitochondria. These links are discussed in more detail in Chapter 5 and the effect of VAPB and VAPBP56S on cellular $Ca^{2+}$ homeostasis and axonal transport of mitochondria is the focus of the next results chapter (Chapter 4).

There are now powerful methods for analyzing mitochondrial transport *in vivo* using *MitoMouse*; this transgenic mouse expresses CFP in mitochondria (Misgeld et al., 2007). Others have now exploited this mouse to analyse the effect of mutant SOD1 on mitochondrial transport *in vivo* (Bilsland et al., 2010; Marinković et al., 2012). Clearly, future studies using such approaches will be very valuable in confirming and extending the findings reported in this chapter.

To summarise, the results described here show that a further mutant protein associated with FALS damages axonal transport. As such, they reinforce the role of defective axonal transport in the pathogenesis of ALS.

# 4 UNDERSTANDING THE MECHANISM UNDERLYING VAPBP56S-INDUCED DISRUPTION OF MITOCHONDRIAL TRANSPORT

## 4.1 Introduction

In Chapter 3, I demonstrated using time-lapse microscopy that expression of VAPBP56S but not wild-type VAPB decreased anterograde, but not retrograde axonal transport of mitochondria. Mutant SOD1 has also been shown to selectively perturb anterograde axonal transport of mitochondria in cultured neurons (De Vos et al., 2007). Thus, the transport phenotype induced by VAPBP56S is similar to that induced by mutant SOD1.

The studies described in this chapter aimed to gain information on the mechanism by which VAPBP56S perturbs anterograde axonal transport of mitochondria. Since anterograde axonal transport of mitochondria involves kinesin-1 (Cai et al., 2005; Fransson et al., 2006; Glater et al., 2006; Hurd and Saxton, 1996; Pilling et al., 2006; Tanaka et al., 1998) it seems likely that VAPBP56S might somehow target kinesin-1 driven transport of mitochondria.

An established route whereby mitochondria attach to kinesin-1 involves Miro and TRAK (Brickley et al., 2005; Brickley and Stephenson, 2011; Fransson et al., 2006; Glater et al., 2006; Guo et al., 2005; MacAskill et al., 2009b; Saotome et al., 2008; Smith et al., 2006; Stowers et al., 2002; Wang and Schwarz, 2009). Elevation of $[Ca^{2+}]c$ disrupts anterograde axonal transport of mitochondria and this involves Miro which contains two EF-hand domains that bind $Ca^{2+}$ and enable it to act as a $Ca^{2+}$ sensor

(Chang et al., 2006; MacAskill et al., 2009b; Rintoul et al., 2003; Saotome et al., 2008; Wang and Schwarz, 2009; Yi et al., 2004). The precise mechanism by which increased $[Ca^{2+}]c$ halts anterograde mitochondrial transport is not clear. In one model, elevated $[Ca^{2+}]c$ induces release of Miro from kinesin-1 (MacAskill et al., 2009b); in another it enables Miro to bind to the motor domain of kinesin-1 so releasing kinesin-1 from its microtubule rails (Wang and Schwarz, 2009). Whatever the precise scenario, disruption to $Ca^{2+}$ homeostasis is seen in ALS models (Grosskreutz et al., 2010; Langou et al., 2010; Tradewell et al., 2011).

Thus, the experiments I undertook were:

1. To determine whether VAPBP56S alters the amounts of Miro1, TRAK1 or kinesin-1 that are associated with mitochondria.

2. To determine whether VAPBP56S alters the amount of tubulin or kinesin-1 associated with Miro1.

3. To determine whether VAPBP56S alters tubulin acetylation since this influences binding of kinesin-1 to microtubules.

4. To determine whether VAPBP56S affects resting $[Ca^{2+}]c$ in neurons and if so whether the transport defect can be rescued by expression of a $Ca^{2+}$-insensitive mutant of Miro1.

5. To determine whether VAPB and VAPBP56S are present in mitochondrial associated ER membranes (MAM) since these are involved in $Ca^{2+}$ homeostasis.

### *4.1.1 Results*

### *4.1.2 VAPBP56S does not affect the interaction of Miro1, TRAK1 or kinesin-1 with mitochondria*

One way in which VAPBP56S could inhibit anterograde transport of mitochondria is by disruption of the attachment of the Miro1/TRAK1/kinesin-1 complex to mitochondria. Therefore, I investigated whether expression of VAPB or VAPBP56S affected the amounts of Miro1, TRAK1 or kinesin-1 that are associated with mitochondria. To do so, HEK293 cells were co-transfected with either myc-tagged Miro1 (myc-Miro1), haemagglutinin-tagged TRAK1 (HA-TRAK1) or myc-tagged kinesin-1 (myc-kinesin-1) and either empty vector, VAPB or VAPBP56S. The Miro1/TRAK1/kinesin-1 complex is highly conserved in different organisms and cell types and others have also used HEK293 cells to dissect the mechanisms that control the association of Miro1 with kinesin-1 and tubulin (Wang and Schwarz, 2009). Mitochondria were purified and the amounts of myc-Miro1, HA-TRAK1 and myc-kinesin-1 present in the purified mitochondria then determined by immunoblotting. Neither VAPB nor VAPBP56S altered the amounts of myc-Miro1, HA-TRAK1 or kinesin-1 that co-purified with mitochondria (Figures 4.1, 4.2 and 4.3). Thus expression of VAPB or VAPBP56S does not effect the amounts of Miro1, TRAK1 or kinesin-1 associated with mitochondria.

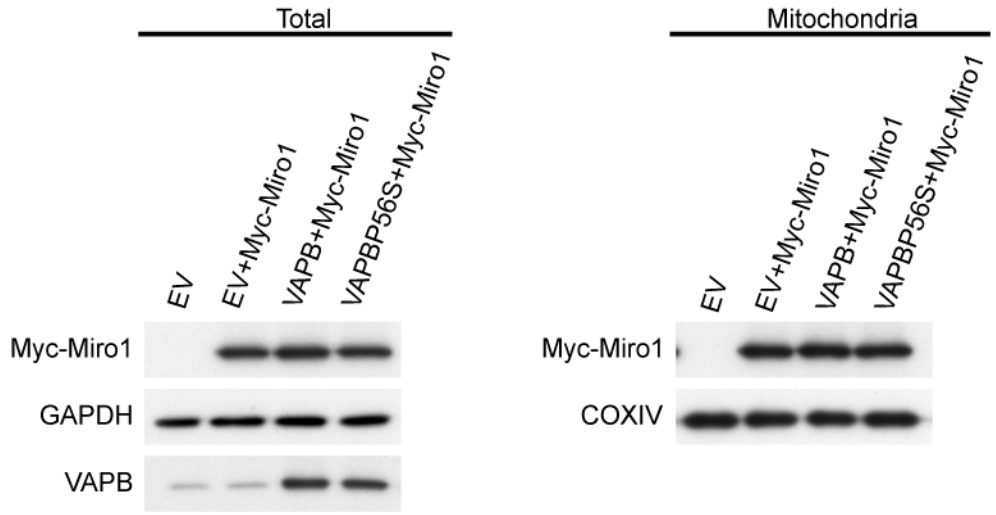


***Figure 4.1. VAPBP56S does not affect the association of Miro1 with mitochondria.***

HEK293 cells were transfected with empty vector (EV) alone or with myc-Miro1 together with empty vector, VAPB or VAPBP56S. After fractionation, equal amounts of protein (5 μg) were separated on SDS-PAGE. The amount of myc-Miro1, glyceraldehyde 3-phosphate dehydrogenase (GAPDH) and VAPB in the total cell lysate (Total), and myc-Miro1 and cytochrome c oxidase IV (COXIV) in the mitochondrial fraction (Mitochondria) were determined by immunoblotting. GAPDH and COXIV are a cytosolic and a mitochondrial marker, respectively, and were included to verify equal protein loading. The immunoblots shown are each representative of 3 independent experiments.

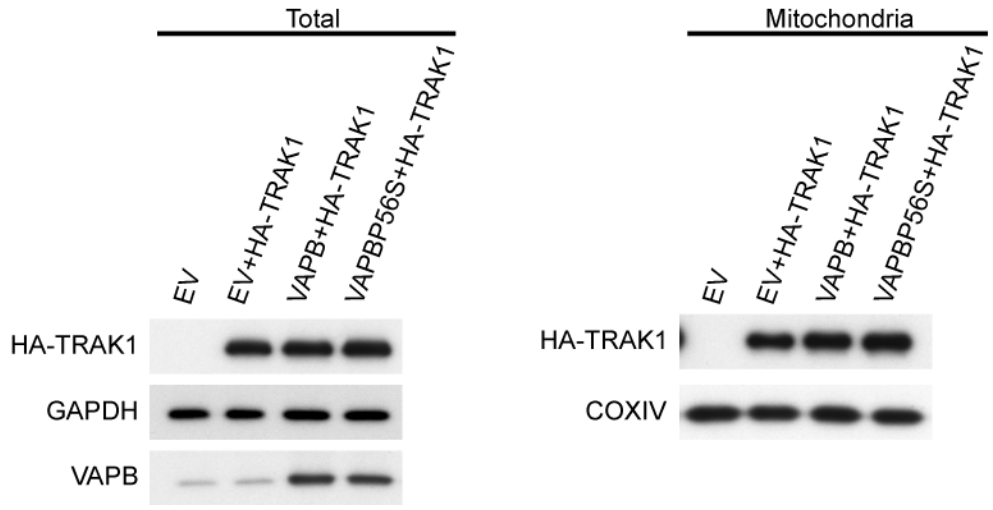


***Figure 4.2. VAPBP56S does not affect the association of TRAK1 with mitochondria.***

HEK293 cells were transfected with empty vector (EV) alone or with HA-TRAK1 together with empty vector, VAPB or VAPBP56S. After fractionation, equal amounts of protein (5 μg) were separated on SDS-PAGE. The amounts of HA-TRAK1, GAPDH and VAPB in the total cell lysate (Total), and HA-TRAK1 and COXIV in the mitochondrial fraction (Mitochondria) were determined by immunoblotting. The immunoblots shown are each representative of 3 independent experiments.

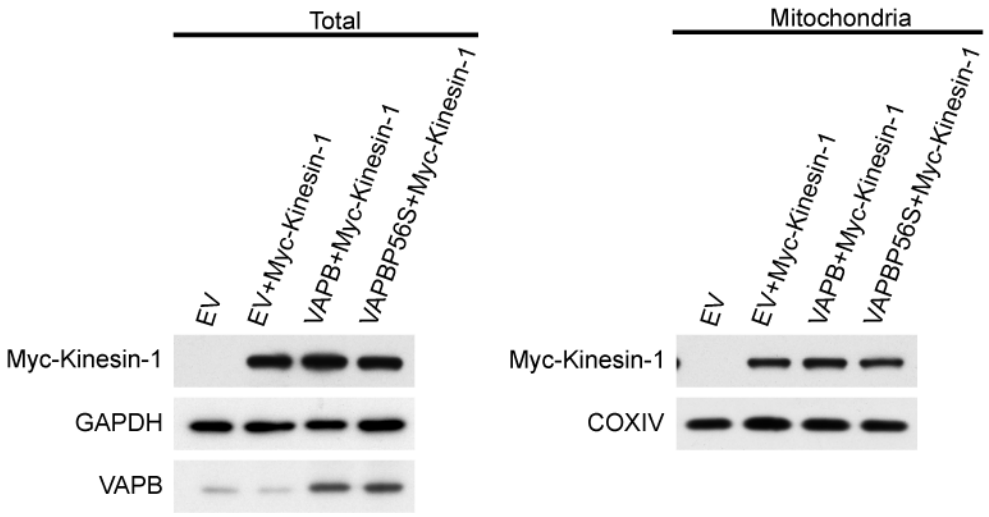


***Figure 4.3. VAPBP56S does not affect the association of kinesin-1 to mitochondria.***

HEK293 cells were transfected with empty vector (EV) alone or with myc-kinesin-1 together with empty vector, VAPB or VAPBP56S. After fractionation, equal amounts of protein (5 μg) were separated on SDS-PAGE. The amount of myc-kinesin-1, VAPB and GAPDH in the total cell lysate (Total), and myc-kinesin-1 and COXIV in the mitochondrial fraction (Mitochondria) were determined by immunoblotting. GAPDH is a cytosolic marker and COXIV is a mitochondrial marker. The immunoblots shown are each representative of 3 independent experiments.

### *4.1.3 VAPBP56S decreases the amount of tubulin but not kinesin-1 associated with Miro1*

Since VAPBP56S expression did not influence the binding of Miro1, TRAK1 and kinesin-1 to mitochondria it is possible that it instead influences the attachment of mitochondria with associated Miro1, TRAK1 and kinesin-1 with microtubules. To investigate this possibility, I monitored the effect of VAPB and VAPBP56S expression on the amounts of kinesin-1 and tubulin that were associated with Miro1 in immunoprecipitation experiments. Others have used similar immunoprecipitation assays to investigate how alterations to signalling pathways influence binding of kinesin-1 motor complexes to tubulin and axonal transport of mitochondria (Stagi et al., 2006).

Kinesin-1 binds to Miro1 directly or indirectly via TRAK (Fransson et al., 2006; Glater et al., 2006; MacAskill et al., 2009b; Wang and Schwarz, 2009). Thus before investigating VAPB and VAPBP56S, I first tested the effect of TRAK1 expression on the association of endogenous kinesin-1 to Miro1 in immunoprecipitation experiments. HEK293 cells were transfected with empty vector, empty vector plus myc-Miro1, empty vector plus HA-TRAK1 or myc-Miro1 plus HA-TRAK1. Myc-Miro1 was then immunoprecipitated from the samples using the myc-tag; non-immune IgG was used as a negative control. Endogenous kinesin-1 was detected in immunoprecipitates from myc-Miro1 transfected cells. However, a greater amount of kinesin-1 was present in immunoprecipitations from myc-Miro1 plus HA-TRAK1 transfected cells (Figure 4.4). Thus TRAK1 increases the amount of kinesin-1 associated with Miro1. I therefore monitored the effect of VAPB and VAPBP56S on the association of Miro1 with kinesin-1 and tubulin in HEK293 cells co-transfected with myc-Miro1, HA-TRAK1, and either control vector, VAPB or VAPBP56S in immunoprecipitation experiment.

HEK293 cells were co-transfected with myc-Miro1 and HA-TRAK1, and either control vector, VAPB or VAPBP56S. Myc-Miro1 was immunoprecipitated using the myc-tag and the amounts of endogenous kinesin-1 and α-tubulin in the immune pellet were determined by immunoblotting. Expression of VAPB or VAPBP56S did not alter the amounts of kinesin-1 that were associated with myc-Miro1 in these experiments (Figure 4.5) confirming my previous findings showing that expression of VAPB or VAPBP56S do not change the amount of kinesin-1 associated to mitochondria. Rather, expression of VAPBP56S but not VAPB reduced the amounts of tubulin associated with myc-Miro1 (Figure 4.5). This reduction was observed when the amounts of tubulin were normalised to the amounts of both immunoprecipitated Miro1 and co-immunoprecipitated kinesin-1. The reduction in tubulin association with Miro1 was not due to an effect of VAPBP56S on TRAK1 because the levels of TRAK1 found in Miro1 immunoprecipitates were unaffected by VAPBP56S (Figure 4.5). Thus, expression of VAPBP56S does not alter the amounts of kinesin-1 or TRAK1 that are associated with Miro1 but rather reduces the amount of tubulin that is associated with the Miro1/TRAK1/kinesin-1 complex.

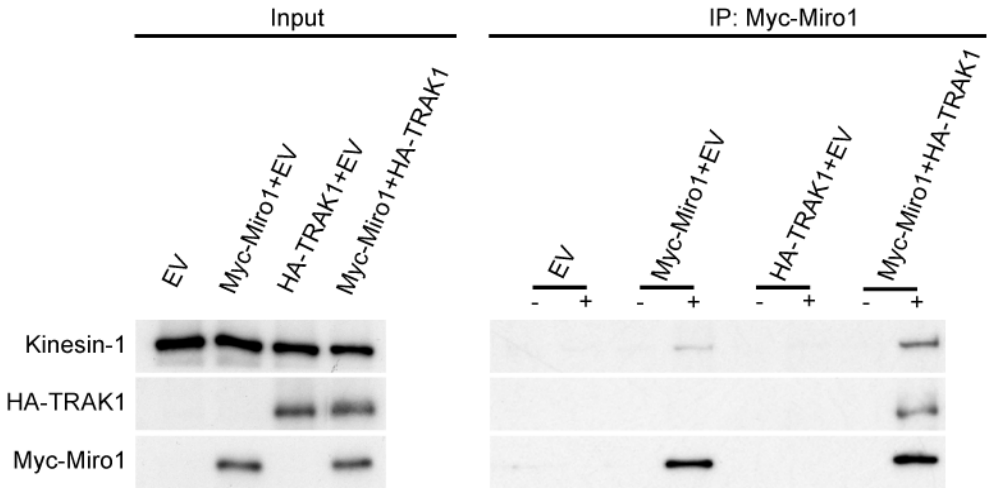


***Figure 4.4. TRAK1 modulates the amount of endogenous kinesin-1 associated with Miro1.***

HEK293 cells were transfected with either empty vector (EV), empty vector + Myc-Miro1, empty vector + HA-TRAK1 or Myc-Miro1 + HA-TRAK1 as indicated. Miro1 was immunoprecipitated using the myc-tag and the amount of bound kinesin-1 analysed on immunoblots. Samples of the input lysates (Input) and immunoprecipitates (IP: Myc-Miro1) are shown. – indicates non-immune IgG and + indicates myc antibody in the immunoprecipitations. The immunoblots shown are each representative of 3 independent experiments.

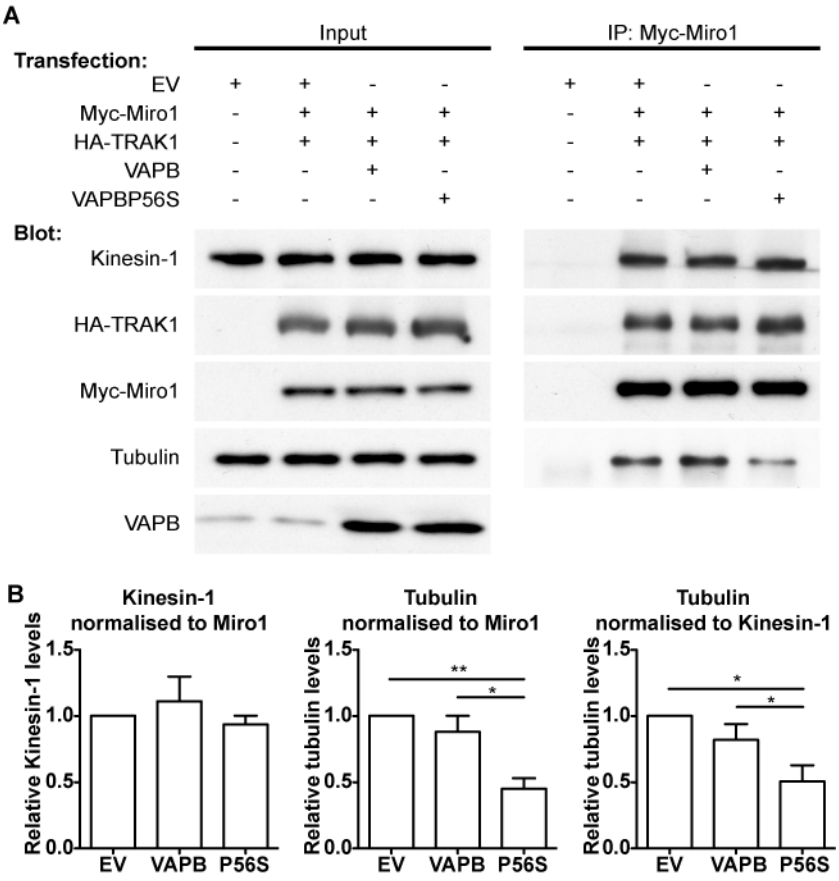


***Figure 4.5. VAPBP56S reduces the amount of endogenous tubulin but not endogenous kinesin-1 associated with Miro1.***

(A) HEK293 cells were co-transfected with either empty vector (EV), empty vector + Myc-Miro1 + HA-TRAK1, VAPB + Myc-Miro1 + HA-TRAK1, or VAPBP56S + Myc-Miro1 + HA-TRAK1 as indicated. Myc-Miro1 was immunoprecipitated using the myc-tag and the amounts of co-immunoprecipitating kinesin-1 and α-tubulin were detected by immunoblotting. Samples of the input lysates (Input) and immunoprecipitates (IP: Myc-Miro1) are shown. (B) Bar graphs show the relative levels of kinesin-1 and α-tubulin in the immunoprecipitates. Kinesin-1 signals were normalised to immunoprecipitated myc-Miro1 signal; α-tubulin signals were normalised to both immunoprecipitated myc-Miro1 and immunoprecipitated kinesin-1 signals as indicated. Values were converted so that the empty vector + Myc-Miro1 + HA-TRAK1 sample

was assigned a reference value of 1.0. The results shown are from 4 independent transfections. Statistical significance was determined by one-way ANOVA followed by Tukey's post hoc test. N=4; error bars are SEM * $p<0.05$; ** $p<0.01$.

### *4.1.4 VAPBP56S does not affect tubulin acetylation*

Posttranslational modifications have been shown to influence the interaction between microtubules and kinesin-1 (Ikegami et al., 2007; Liao and Gundersen, 1998; Reed et al., 2006). One of these modifications is the acetylation of Lys-40 in α-tubulin; Lys-40 is the major acetylation site of α-tubulin (Choudhary et al., 2009; Chu et al., 2011; LeDizet and Piperno, 1987). Acetylation of α-tubulin promotes association of kinesin-1 to microtubules and enhances mitochondrial transport (Chen et al., 2010b; Dompierre et al., 2007; Reed et al., 2006). Thus, one way for VAPBP56S to reduce the association of microtubules with the mitochondrial motor complex Miro1/TRAK1/kinesin-1 is to reduce acetylation of α-tubulin. To investigate this possibility, I monitored the levels of acetylated α-tubulin in lysates from VAPB and VAPBP56S transfected cells by immunoblotting. To ensure specific detection of tubulin acetylation in transfected cells, I co-transfected the cells with mCherry-tagged α-tubulin (mCherry-α-tubulin). Since mCherry-α-tubulin migrates differently on SDS-PAGE compared to non-tagged endogenous α-tubulin, this construct allowed me to specifically assess the acetylation status of α-tubulin in transfected cells (Shaner et al., 2004). As a control for the specificity of the anti-acetylated α-tubulin antibody a mutant mCherry-α-tubulin in which the lysine at position 40 was mutated to alanine and therefore cannot be acetylated (mCherry-α-tubulin$^{K40A}$) (Dompierre et al., 2007) was included in these experiments. Neither myc-VAPB nor myc-VAPBP56S expression affected the levels of α-tubulin acetylation (Figure 4.6). Thus, the reduction in Miro1/TRAK1/kinesin-1 motor complex-tubulin interaction in VAPBP56S-expressing cells was not caused by a reduction in α-tubulin acetylation.

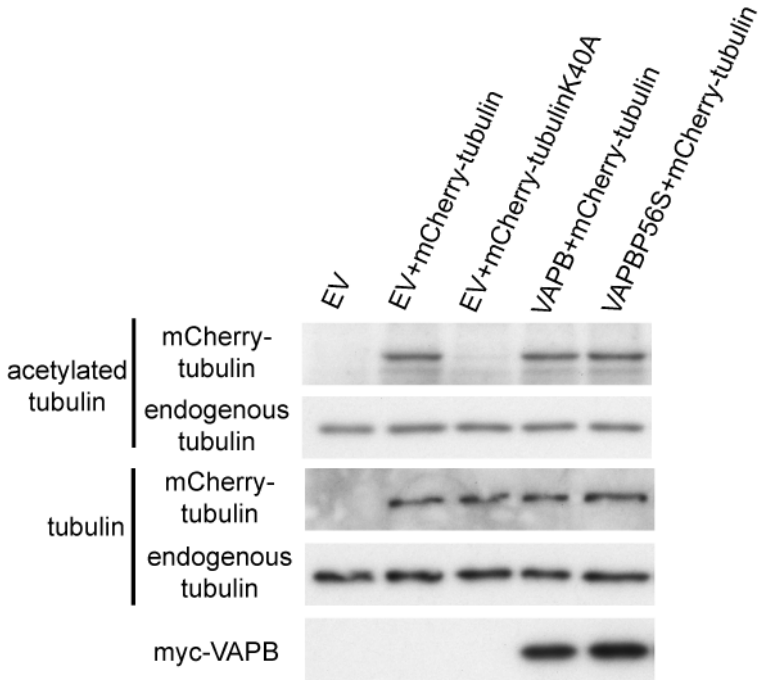


***Figure 4.6. VAPBP56S does not affect tubulin acetylation.***

HEK293 cells were transfected with either empty vector (EV), empty vector + mCherry-α-tubulin (mCherry-tubulin), empty vector + mCherry-α-tubulin$^{K40A}$ (mCherry-tubulinK40A), mCherry-α-tubulin + myc-VAPB (VAPB) or mCherry-α-tubulin + myc-VAPBP56S (VAPBP56S) as indicated. Total cell lysates of cells were probed for α-tubulin and acetylated α-tubulin as shown. No differences were detected in the amount of acetylated α-tubulin in the presence of myc-VAPB or myc-VAPBP56S compared to EV + mCherry-tubulin; mCherry-tubulinK40A shows that the anti-acetylated α-tubulin antibody is specifically recognising acetylated α-tubulin. The immunoblots shown are each representative of 3 independent experiments.

### *4.1.5 VAPBP56S increases resting [$Ca^{2+}$]c*

Elevation of [$Ca^{2+}$]c halts mitochondrial transport (Chang et al., 2006; MacAskill et al., 2009b; Rintoul et al., 2003; Saotome et al., 2008; Wang and Schwarz, 2009; Yi et al., 2004) and it has been shown that $Ca^{2+}$ mediated disruption to mitochondrial transport can involve release of Miro/TRAK/kinesin-1, and consequently mitochondria from microtubules (Wang and Schwarz, 2009). Since VAPBP56S-induced disruption to mitochondrial transport involved a reduction in the amount of tubulin associated with the Miro1/TRAK1/kinesin-1 complex but not release of kinesin-1 from Miro1 it was possible that $Ca^{2+}$ dependent release of Miro1/TRAK1/kinesin-1 from microtubules caused the defect in anterograde transport in VAPBP56S-expressing neurons. To test this hypothesis, I monitored the effect of VAPB and VAPBP56S expression on resting [$Ca^{2+}$]c by Fura2 ratio imaging in rat cortical neurons transfected with EGFP control vector, EGFP-VAPB or EGFP-VAPBP56S.

Fura2 is a ratiometric $Ca^{2+}$ indicator dye that binds free intracellular $Ca^{2+}$. Upon binding of $Ca^{2+}$ the excitation peak of Fura2 shifts from 380 nm to 340 nm, and the ratio between recordings at 340 nm and 380 nm directly correlates with the amount of intracellular $Ca^{2+}$. Furthermore, the ratio of Fura2 fluorescent signals at excitation 340 and 380 nm can be calibrated and converted to nM using the Grynkiewicz formula (Grynkiewicz et al., 1985). To ensure that only viable cells were analysed in this assay, a transient $Ca^{2+}$ influx was induced by depolarisation of the neurons with 50 mM KCl to mimic an action potential after recording resting [$Ca^{2+}$]c (Lipscombe et al., 1988). Only cells that showed a transient increase in [$Ca^{2+}$]c following the depolarisation were included in the analyses of resting [$Ca^{2+}$]c. For each individual neuron the resting [$Ca^{2+}$]c was calculated as the average value between 60 and 180 s of measurement.

Values for individual cells were averaged to yield the mean resting $[Ca^{2+}]c$.

The resting $[Ca^{2+}]c$ in EGFP-VAPB transfected neurons was 148.3±10.8 nM (mean±SEM) and this was not different significantly from resting $[Ca^{2+}]c$ in neurons transfected with control EGFP (143.7±11.3 nM) (Figure 4.7). These resting $[Ca^{2+}]c$ are well within the range observed by others in neurons (Huang et al., 2000; Sanelli et al., 2004; Tiago et al., 2011). However, expression of EGFP-VAPBP56S significantly elevated resting $[Ca^{2+}]c$ to 207.1±18.9 nM (Figure 4.7). Thus the VAPBP56S induced disruption to anterograde axonal mitochondrial transport is associated with an increase in resting $[Ca^{2+}]c$.

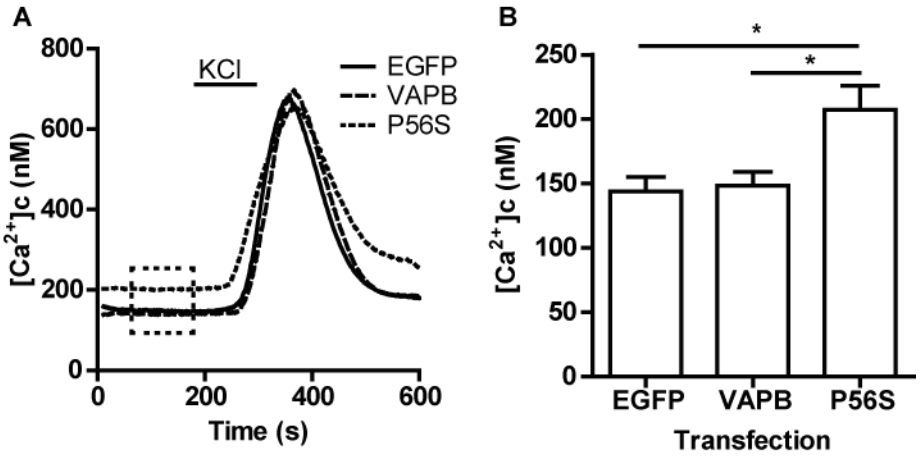


***Figure 4.7. Expression of VAPBP56S increases resting [$Ca^{2+}$]c in neurons.***

Rat cortical neurons were transfected with either control EGFP vector, EGFP-VAPB (VAPB) or EGFP-VAPBP56S (P56S) and [$Ca^{2+}$]c determined by Fura2 ratio imaging. Resting [$Ca^{2+}$]c was calculated for each individual neuron as the average resting [$Ca^{2+}$]c between 60 and 180 s of measurement (indicated with a dashed line box in A). Values for individual cells were then collated to generate the bar graph in B. To ensure that resting [$Ca^{2+}$]c was obtained from viable neurons a transient influx of $Ca^{2+}$ was induced by application of 50 mM KCl to depolarise the neurons. Only cells that showed a transient increase in [$Ca^{2+}$]c after depolarisation were included in the analysis of resting [$Ca^{2+}$]c. Statistical significance was determined by one-way ANOVA (Kruskal-Wallis) followed by Dunn's Multiple Comparison Test. N=10 (CTRL), 14 (VAPB), and 20 (VAPBP56S) cells from 3 different neuronal cell cultures for each transfection. Error bars are SEM * $p<0.05$.

### *4.1.6 Expression of a $Ca^{2+}$-insensitive mutant of Miro1 rescues the effect of VAPBP56S on the association of tubulin with Miro1 and the effect of VAPBP56S on mitochondrial transport*

VAPBP56S reduced the amount of tubulin associated with Miro1/TRAK1/kinesin-1 motor complex and increased resting $[Ca^{2+}]c$. These results are consistent with a model in which VAPBP56S elevates $[Ca^{2+}]c$ to cause release of mitochondria with associated Miro1/TRAK1/kinesin-1 from microtubules to disrupt axonal transport (Wang and Schwarz, 2009). Since elevated $[Ca^{2+}]c$ disrupts kinesin-1 based transport of mitochondria via an effect on the Miro1 EF-hand domains (MacAskill et al., 2009b; Saotome et al., 2008; Wang and Schwarz, 2009), I enquired whether expression of a mutant Miro1 in which the EF-hands were disrupted could rescue the effect of VAPBP56S on mitochondrial transport. This mutant Miro1 ($Miro1^{E208K/E328K}$) has essential glutamates in the EF-hands altered to lysine to inhibit binding of $Ca^{2+}$ (Fransson et al., 2006).

Mutant myc-tagged $Miro1^{E208K/E328K}$ (myc-$Miro1^{E208K/E328K}$) was prepared and its subcellular distribution first compared with that of wild-type myc-Miro1 in transfected cortical neurons and CV-1 cells. To do so, cells were transfected with DsRed-Mito (to visualise mitochondria) and either myc-Miro1 or myc-$Miro1^{E208K/E328K}$. Both myc-Miro1 and myc-$Miro1^{E208K/E328K}$ localised to mitochondria (Figure 4.8).

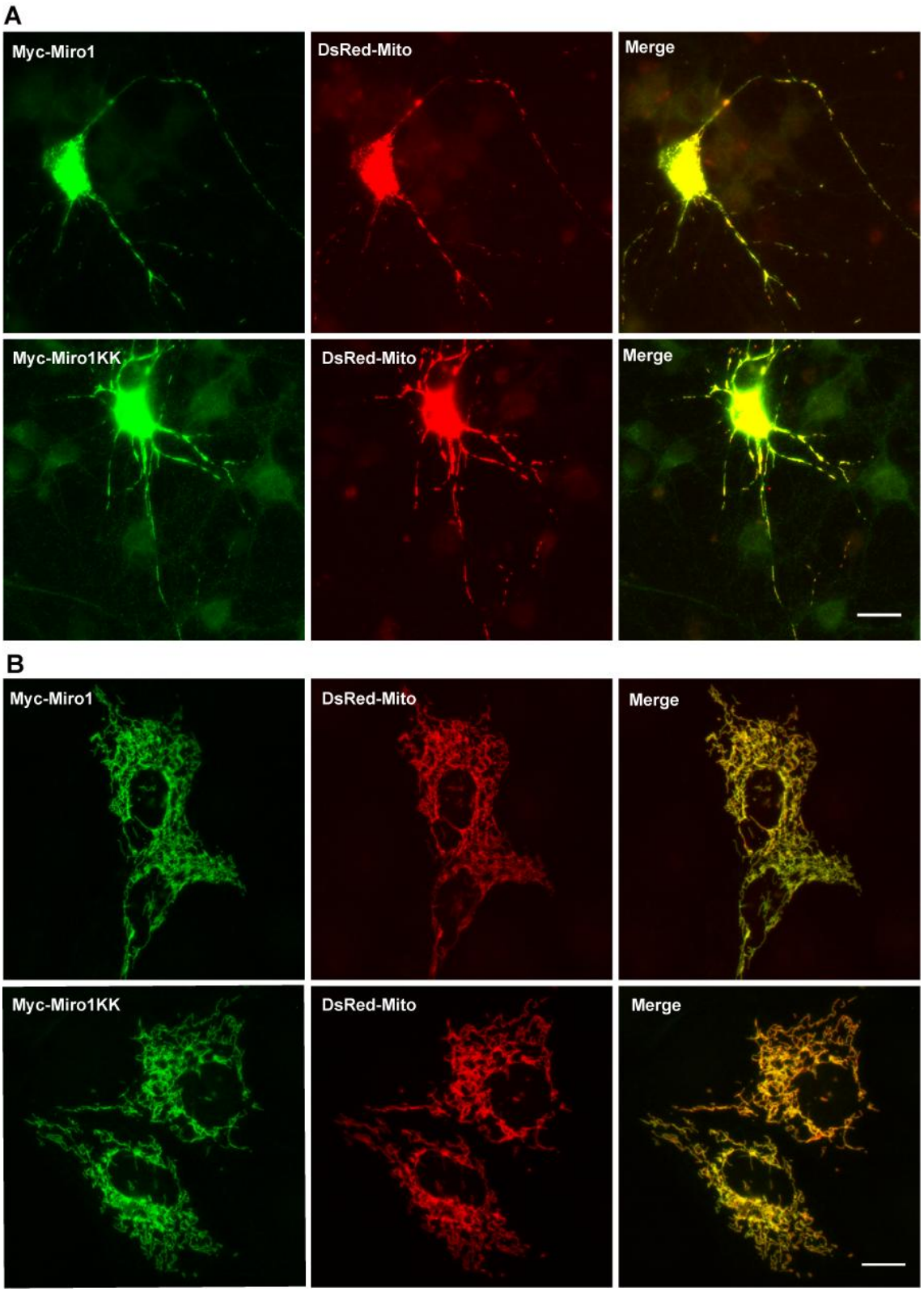


***Figure 4.8. Miro1$^{E208K/E328K}$ co-localises with mitochondria in cortical neurons and CV-1 cells.***

Cortical neurons (A) or CV-1 cells (B) were co-transfected with DsRed-Mito (to

visualise mitochondria) and either myc-Miro1 or myc-Miro1$^{E208K/E328K}$ (Myc-Miro1KK). Myc-Miro1 and myc-Miro1$^{E208K/E328K}$ were detected by immunostaining with anti-myc antibody. Both myc-Miro1 and myc-Miro1KK are co-localised with mitochondria. Representative images are shown. Scale bar 20 μm.

To test if the $Ca^{2+}$ insensitive mutant Miro1$^{E208K/E328K}$ could rescue the effect of VAPBP56S on the interaction of the Miro1/TRAK1/kinesin-1 complex with tubulin, I performed immunoprecipitation experiments. HEK293 cells were co-transfected with myc-Miro1$^{E208K/E328K}$ plus HA-TRAK1 and either control vector, VAPB or VAPBP56S, and the amounts of endogenous kinesin-1 and tubulin associated with immunoprecipitated myc-Miro1$^{E208K/E328K}$ were determined by immunoblotting. The amounts of co-immunoprecipitated HA-TRAK1, kinesin-1 and tubulin were not significantly different in any of these cells (Figure 4.9). Thus, whilst VAPBP56S reduces the amount of tubulin associated with wild-type Miro1, this effect is lost in cells expressing Miro1$^{E208K/E328K}$.

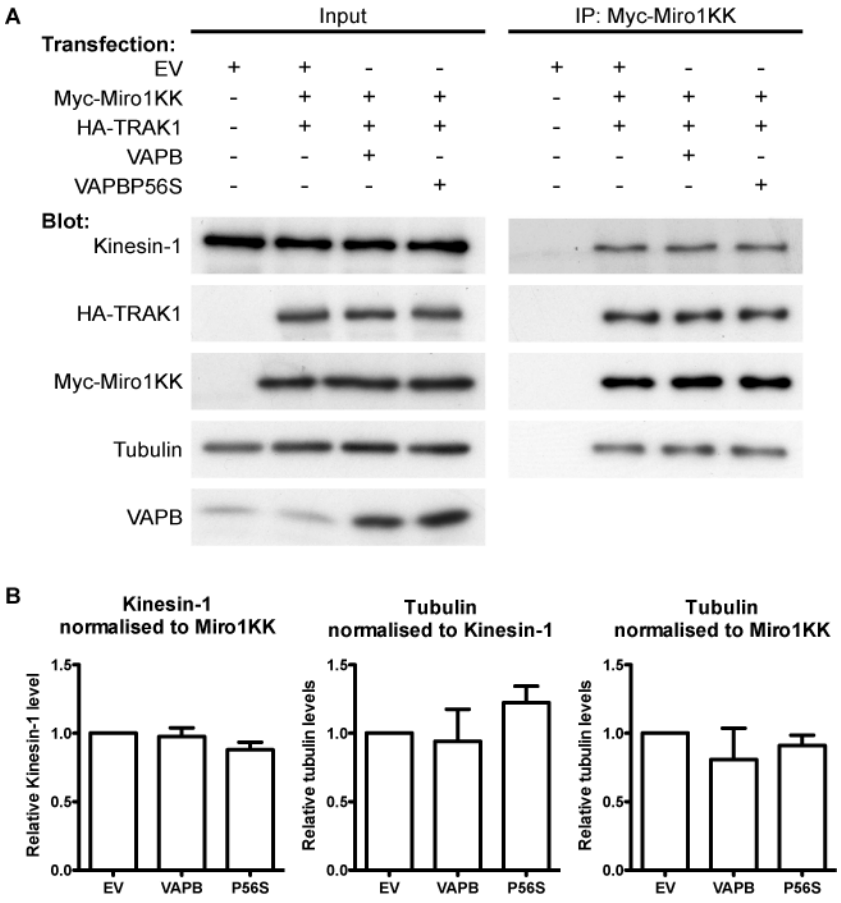


***Figure 4.9. Expression of $Ca^{2+}$-insensitive Miro1$^{E208K/E328K}$ rescues the effect of VAPBP56S on the association of tubulin with Miro1.***

(A) HEK293 cells were co-transfected with either empty vector (EV), empty vector + myc-Miro1$^{E208K/E328K}$ (Myc-Miro1KK) + HA-TRAK1, VAPB + myc-Miro1$^{E208K/E328K}$ + HA-TRAK1, or VAPBP56S + myc-Miro1$^{E208K/E328K}$ + HA-TRAK1 as indicated. Myc-Miro1$^{E208K/E328K}$ was immunoprecipitated using the myc-tag and the amounts of co-immunoprecipitating kinesin-1 and α-tubulin detected by immunoblotting. Samples of the input lysates (Input) and immunoprecipitates (IP: Myc-Miro1KK) are shown. (B) Bar graphs show relative levels of kinesin-1 and α-tubulin in the immunoprecipitates. Kinesin-1 signals were normalized to immunoprecipitated myc-Miro1$^{E208K/E328K}$ signal; α-tubulin signals were normalized to both immunoprecipitated myc-Miro1$^{E208K/E328K}$

and immunoprecipitated kinesin-1 signals as indicated. Values were converted to so that empty vector + myc-Miro1$^{E208K/E328K}$ + HA-TRAK1 transfection was assigned a reference value of 1.0. Statistical significance was determined by one-way ANOVA followed by Tukey's post hoc test. N=3 independent experiments. Error bars are SEM.

To determine whether Miro1$^{E208K/E328K}$ could also rescue the effect of VAPBP56S on defective anterograde axonal transport of mitochondria, I co-transfected rat cortical neurons with DsRed-Mito and either EGFP-VAPB plus control vector, EGFP-VAPBP56S plus control vector, EGFP-VAPBP56S plus Miro1 or EGFP-VAPBP56S plus Miro1$^{E208K/E328K}$, and recorded axonal transport of mitochondria by time-lapse microscopy as previously described. Compared to EGFP-VAPB expressing neurons, EGFP-VAPBP56S again reduced anterograde mitochondrial transport and this was unaffected by expression of Miro1. However, co-expression of Miro1$^{E208K/E328K}$ significantly increased anterograde mitochondrial transport in the EGFP-VAPBP56S expressing cells (Figure 4.10). Thus, Miro1$^{E208K/E328K}$ rescues defective axonal transport of mitochondria in EGFP-VAPBP56S expressing neurons.

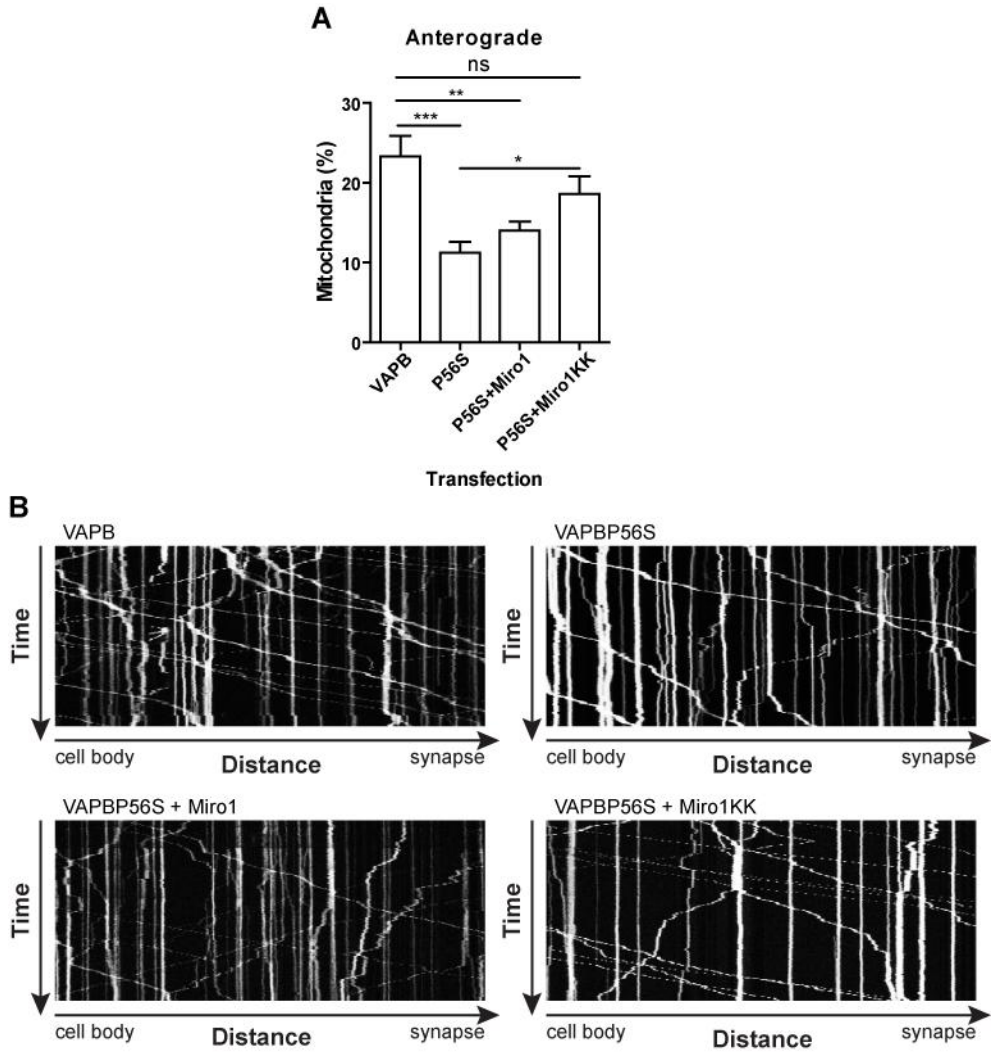


***Figure 4.10. VAPBP56S-induced defective anterograde mitochondrial transport is rescued by expression of $Ca^{2+}$-insensitive Miro1$^{E208K/E328K}$.***

Neurons were co-transfected with DsRed-Mito and either EGFP-VAPB, EGFP-VAPBP56S, EGFP-VAPBP56S + Miro1 or EGFP-VAPBP56S + Miro1$^{E208K/E328K}$. Transfections were balanced with empty vector so that all treatments received the same total amounts of DNA. (A) shows the proportion of anterograde moving mitochondria. Expression of EGFP-VAPBP56S (P56S) reduced anterograde mitochondrial transport and this was rescued by expression of Miro1$^{E208K/E328K}$ (Miro1KK) but not wild-type Miro1. Statistical significance was determined by one-way ANOVA followed by

Tukey's post hoc test. N=15-17 cells from 3 different neuronal cell cultures for each transfection. Error bars are SEM; * $p<0.05$, ** $p<0.01$; *** $p<0.001$; ns not significant. (B) shows representative kymographs of mitochondrial movement in neurons co-transfected with EGFP-VAPB (VAPB), EGFP-VAPBP56S (VAPBP56S), EGFP-VAPBP56S + Miro1 (VAPBP56S+Miro1) or EGFP-VAPBP56S + Miro1$^{E208K/E328K}$ (VAPBP56S+Miro1KK) as indicated.

### *4.1.7 VAPBP56S accumulates in mitochondria-associated ER membranes (MAM)*

Approximately 5-20% of the mitochondrial outer membrane is closely associated to ER (Rizzuto et al., 1998). These ER microdomains are termed MAM. MAM play an important role in $Ca^{2+}$ homeostasis by facilitating $Ca^{2+}$ exchange between ER and mitochondria (Csordás et al., 2006; Csordás et al., 2010; de Brito and Scorrano, 2008; Rusinol et al., 1994). VAPB is an ER protein and VAPBP56S disrupts ER (Fasana et al., 2010; Langou et al., 2010; Nishimura et al., 2004; Teuling et al., 2007; Tudor et al., 2010). Therefore, one possibility is that the disruption to $Ca^{2+}$ homeostasis induced by VAPBP56S is linked to ER-mitochondrial $Ca^{2+}$ exchange. To begin to examine this possibility further, I enquired whether VAPB and VAPBP56S were MAM proteins.

To do so, I first monitored the presence of VAPB in a biochemical fraction that contains both mitochondria and MAM but not ER from HEK293 cells that were transfected with empty vector, myc-VAPB or myc-VAPBP56S. Both myc-VAPB and myc-VAPBP56S were present in mitochondria plus MAM fraction but compared to myc-VAPB, myc-VAPBP56S levels were increased almost twofold (Figure 4.11). To investigate this further, I purified MAM, mitochondria free of MAM and the remaining non-MAM ER from HEK293 cells transfected with empty vector, myc-VAPB or myc-VAPBP56S, and compared the levels of myc-VAPB and myc-VAPBP56S in these fractions. Compared to myc-VAPB, myc-VAPBP56S levels were elevated in MAM and correspondingly decreased in non-MAM ER; myc-VAPB and myc-VAPBP56S were not detected in pure mitochondria fraction (Figure 4.12). These changes were not due to altered fractionation properties of ER since the levels of protein disulphide isomerase (PDI), a general ER marker, were not altered in the MAM or non-MAM ER fractions (Figure 4.12). Thus, mutant VAPBP56S is enriched in MAM.

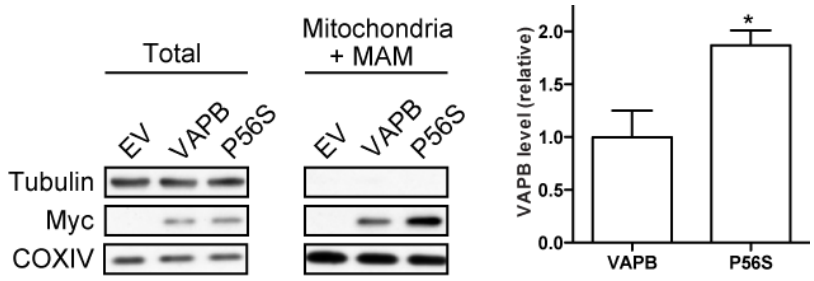


***Figure 4.11. VAPB and VAPBP56S are present in a mitochondrial fraction associated with MAM, and VAPBP56S levels are elevated in this fraction.***

(A) HEK293 cells were transfected with empty vector (EV), myc-VAPB (VAPB) or myc-VAPBP56S (P56S) and mitochondria with associated MAM were isolated. The samples of total cell lysate (Total) and mitochondria with associated MAM (Mitochondria + MAM) were separated by SDS-PAGE, and probed for tubulin (cytosolic marker), COXIV (mitochondrial marker) and myc-VAPB/VAPBP56S using anti-myc antibody. (B) Bar graph shows relative amounts of myc-VAPB (VAPB) and myc-VAPBP56S (P56S) following densitometric quantification of signals. Statistical significance was determined by t-test. N=3 independent experiments; error bars are SEM; * $p<0.05$.

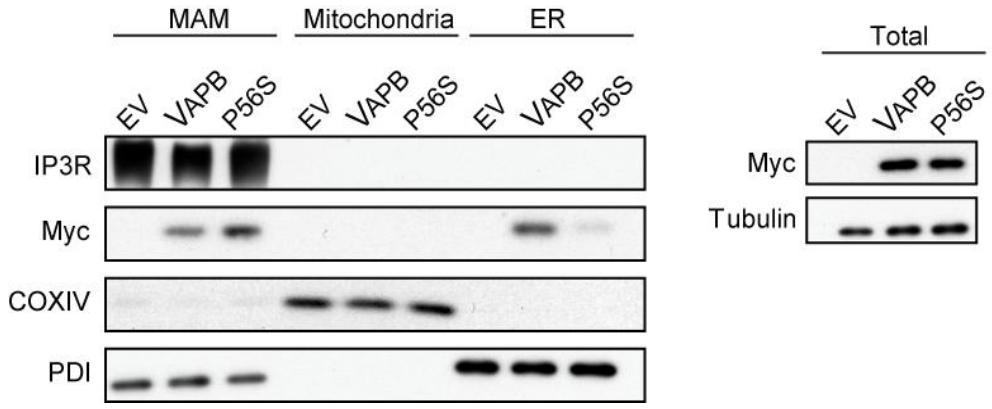


***Figure 4.12. VAPBP56S is present at higher levels in MAM and lower level in non-MAM ER fractions than VAPB.***

MAM, pure mitochondria (Mitochondria) and non-MAM ER (ER) were isolated from HEK293 cells transfected with empty vector (EV), myc-VAPB (VAPB) or myc-VAPBP56S (P56S) as shown. Equal amounts of protein samples were separated by SDS-PAGE and probed on immunoblots for IP3R (MAM marker), PDI (ER marker), COXIV (mitochondrial marker), and myc-VAPB/VAPBP56S using anti-myc antibody. Samples of the total cell lysates (Total) are also shown with tubulin as a loading control. The immunoblots shown are representative of 3 independent experiments.

## 4.2 Discussion

As described in Chapter 3, VAPBP56S selectively disrupts anterograde but not retrograde axonal transport of mitochondria. In this chapter, I aimed to identify possible mechanisms by which VAPBP56S might induce such disruption. There are a number of routes whereby VAPBP56S might selectively damage mitochondrial axonal transport. VAPBP56S might disrupt kinesin-1 function via some mechanism although this would be predicted to influence axonal transport of all kinesin-1 cargoes, not just mitochondria. More selective routes for damage to mitochondrial transport could involve VAPBP56S-induced disruption to the attachment of kinesin-1 to mitochondria. Alternatively, VAPBP56S might induce release of mitochondria with associated kinesin-1 from microtubule rails.

Kinesin-1 attaches to mitochondria via Miro and TRAK, and Miro is a sensor for intracellular $Ca^{2+}$; elevated $Ca^{2+}$ disrupts mitochondria transport via an effect on Miro (Brickley et al., 2005; Brickley and Stephenson, 2011; Fransson et al., 2006; Glater et al., 2006; Guo et al., 2005; MacAskill et al., 2009a; MacAskill et al., 2009b; Saotome et al., 2008; Smith et al., 2006; Stowers et al., 2002; Wang and Schwarz, 2009). Using HEK293 cells, I investigated whether VAPBP56S influences the amounts of Miro1, TRAK1, kinesin-1 and tubulin that are associated with mitochondria. The Miro/TRAK/kinesin-1 complex is highly conserved and others have successfully utilized HEK293 cells to dissect the molecular mechanisms of mitochondrial transport (Wang and Schwarz, 2009). I obtained results to show that VAPBP56S but not VAPB reduces the amount of tubulin but not kinesin-1, Miro1 or TRAK1 that are associated with mitochondria. These results suggest that VAPBP56S causes release of mitochondria with associated Miro1, TRAK1 and kinesin-1 from microtubules.

As detailed above, tubulin acetylation is one of the known mechanisms for regulating attachment of kinesin-1 to microtubules. However, I detected no changes in tubulin acetylation in the presence of either VAPB or VAPBP56S in transfected cells. Alterations to tubulin acetylation thus appear not to be the cause of VAPBP56S-induced release of mitochondria with associated kinesin-1 from microtubules.

Others have shown that elevated [$Ca^{2+}$]c causes release of mitochondria with associated kinesin-1 from microtubules (Wang and Schwarz, 2009). During the course of this work, VAPB was shown to regulate $Ca^{2+}$ exchange between ER and mitochondria and VAPBP56S was defective in this process (De Vos et al., 2012). To test whether VAPBP56S disrupts $Ca^{2+}$ homeostasis, I measured [$Ca^{2+}$]c by Fura2 ratio imaging. VAPBP56S elevated [$Ca^{2+}$]c and others have obtained similar results (Langou et al., 2010). Furthermore, I was able to rescue the VAPBP56S induced transport defect by transfection of a $Ca^{2+}$-insensitive mutant of Miro1. Together, these results support a scenario in which VAPBP56S elevates [$Ca^{2+}$]c and this causes release of mitochondria-associated kinesin-1 from microtubules via an effect on Miro1.

All of these results were obtained from cell culture studies. *In vivo* data to support these results could involve the generation of Miro1 and $Ca^{2+}$-insensitive mutant Miro1 transgenic mice and crossing of such animals with *MitoMouse* (that expresses CFP labeled mitochondria) and VAPBP56S transgenic mice. This would enable monitoring of mitochondrial transport *in vivo* in the presence or absence of VAPBP56S.

In addition, crossing of these mice with Miro1 or $Ca^{2+}$-insensitive Miro1 transgenics would permit *in vivo* testing of the effect of Miro1 on VAPBP56S-induced damage to mitochondrial transport. This *in vivo* approach could also be utilised to test the effect of Miro1 on mutant SOD1-induced damage to mitochondrial transport.

Neurological and pathological assays of these different transgenics might also reveal whether the $Ca^{2+}$-insensitive Miro1 is protective against disease.

# 5 DISCUSSION

## 5.1 Summary

VAPBP56S causes some dominantly inherited familial forms of motor neuron disease including ALS type-8. In this thesis, I showed that VAPBP56S damages axonal transport of mitochondria in both VAPBP56S transfected rat cortical neurons and VAPBP56S transgenic mouse motor neurons. Disruption of mitochondrial transport was directional and involved perturbation of anterograde but not retrograde movement. VAPBP56S selectively decreased the frequency, velocity and persistence of anterograde mitochondrial movement.

Next, I investigated the molecular mechanism underlying the VAPBP56S-mediated perturbation of mitochondrial transport. VAPBP56S did not influence the interaction of Miro1, TRAK1 and kinesin-1 (the motor complex that drives anterograde mitochondrial transport) with mitochondria. However, I found that VAPBP56S reduced the amount of tubulin but not kinesin-1 that is associated with Miro1. Using Fura2 ratio imaging, I showed that VAPBP56S elevated resting $[Ca^{2+}]c$ in transfected rat cortical neurons. Elevation of $[Ca^{2+}]c$ perturbs kinesin-1-mediated mitochondrial transport via the outer mitochondrial membrane protein Miro1 which acts as a $Ca^{2+}$ sensor (MacAskill et al., 2009b; Saotome et al., 2008; Wang and Schwarz, 2009). I demonstrated, that a $Ca^{2+}$-insensitive mutant of Miro1 rescued defective mitochondrial transport in VAPBP56S expressing neurons. Finally, I showed that VAPB is located in MAM, an ER subdomain involved in $Ca^{2+}$ homeostasis, and that VAPBP56S levels are higher than wild-type VAPB levels in MAM. Moreover, VAPB has recently been shown to interact with the outer mitochondrial membrane protein PTPIP51 and that this complex mediates $Ca^{2+}$ exchange between ER and mitochondria (De Vos et al., 2012).

Damage to anterograde axonal transport of mitochondria by VAPBP56S may therefore involve disruption to MAM and ER-mitochondrial $Ca^{2+}$ exchange and elevation of $[Ca^{2+}]c$ which in turn induces release of Miro1 with associated kinesin-1 from microtubules to halt anterograde mitochondrial transport.

## 5.2 Disruption of mitochondrial transport in ALS

Like VAPBP56S, ALS mutant SOD1 also selectively reduces anterograde but not retrograde mitochondrial transport; this phenotype is seen in rat embryonic cortical neurons transfected with several different ALS mutants of SOD1 and also in embryonic motor neurons from SOD1-G93A transgenic mice (De Vos et al., 2007). Thus, two different ALS-associated genetic insults cause similar mitochondrial transport defects. There is also evidence that anterograde axonal transport of mitochondria is also disrupted in human ALS cases. In particular, mitochondria accumulate in the cell body of anterior horn cells in the spinal cord of ALS patients (Sasaki and Iwata, 1996; Sasaki and Iwata, 2007) which is consistent with damage to anterograde mitochondrial transport. Defective mitochondrial transport may therefore be a common pathological event in both FALS and SALS.

However, other studies have concluded that ALS mutant SOD1-G93A reduces both anterograde and retrograde transport of mitochondria (Bilsland et al., 2010; Marinković et al., 2012) and one study reported that SOD1-G93A impairs retrograde but not anterograde mitochondrial transport of mitochondria (Magrané et al., 2012). The reasons for these contrasting observations are not yet known but it is possible that they are caused, at least in part, by the different models used in these studies. De Vos and co-workers have utilised mutant SOD1 transfected embryonic rat cortical neurons and

SOD1-G93A transgenic embryonic mouse motor neurons (De Vos et al., 2007) whereas Magrané and co-workers have used embryonic motor neurons derived from SOD1-G93A transgenic rats (Magrané et al., 2012). Therefore, it is possible that differences between animal models may cause differences in the directionality of the transport defect.

Bilsland and co-workers have investigated mitochondrial transport *in vivo* in SOD1-G93A mice (Bilsland et al., 2010) and Marinković and co-workers used explanted motor neurons from SOD1-G93A and SOD1-G85R mice (Marinković et al., 2012). In SOD1-G93A mice, both groups described perturbation of both anterograde and retrograde mitochondrial transport before the first clinical signs of the disease at postnatal day 36 (Bilsland et al., 2010) or at postnatal day 40 (Marinković et al., 2012). However, Marinković *et al.* have found that the retrograde mitochondrial transport defect has a later onset compared to the anterograde defect (Marinković et al., 2012). The anterograde transport defect appears at postnatal day 20 whereas the retrograde transport defect is not observable until several days later from postnatal day 40 onward (Marinković et al., 2012). These findings suggest that the mitochondrial transport defect may develop gradually in SOD1-G93A transgenic mice; anterograde transport is perturbed first and can be observed as early as the embryonic stage (De Vos et al., 2007). This is followed by a retrograde transport defect that is observed from postnatal day 36 (Bilsland et al., 2010; Marinković et al., 2012).

It has also been reported that wild-type SOD1 overexpressing transgenic mice but not ALS mutant SOD1-G85R transgenic mice that develop motor neuron disease have a mitochondrial transport defect (Marinković et al., 2012). These findings have queried the role of defective axonal transport in ALS (Marinković et al., 2012). However, several other groups have obtained different results and have shown that wild-type

SOD1 does not affect axonal transport and that SOD1-G85R does perturb transport like SOD1-G93A (De Vos et al., 2007; Williamson and Cleveland, 1999). The onset of the transport defect is remarkably late in wild-type SOD1 overexpressing mice compared to SOD1-G93A mice (postnatal day 60 vs. postnatal day 10) respectively (Marinković et al., 2012). It has been reported that some wild-type SOD1 overexpressing mice exhibit signs of premature aging (Avraham et al., 1988; Avraham et al., 1991; Ceballos-Picot et al., 1991) thus it is possible that the late transport defect in wild-type SOD1 overexpressing mice observed by Marinković and co-workers is linked to ageing (Marinković et al., 2012). To answer this question and to better understand the mutant SOD1 induced mitochondrial transport defect further research is needed.

## 5.3 VAPBP56S induced damage to mitochondrial transport is linked to elevated [$Ca^{2+}$]c and release of mitochondria with associated kinesin-1 from microtubules

It has been demonstrated that mitochondrial movement is arrested following an increase of [$Ca^{2+}$]c in H9c2 cardiac myoblast cells (Saotome et al., 2008; Yi et al., 2004) and in dendrites and axons of cultured cortical and hippocampal neurons (Chang et al., 2006; MacAskill et al., 2009b; Rintoul et al., 2003; Wang and Schwarz, 2009). Mitochondrial halting caused by elevated [$Ca^{2+}$]c is reversible and does not show desensitisation following repeated stimulation in both H9c2 myoblasts and hippocampal neurons (MacAskill et al., 2009b; Yi et al., 2004). I showed in this thesis that VAPBP56S significantly elevates resting [$Ca^{2+}$]c in transfected rat cortical neurons and this was associated with perturbed mitochondrial transport. I also found that the VAPBP56S-induced damage to mitochondrial transport could be rescued with a $Ca^{2+}$-

insensitive mutant of Miro1. These results support the notion that VAPBP56S induced damage to mitochondrial transport involves elevated [$Ca^{2+}$]c. During the course of this work, others also showed that VAPBP56S increases [$Ca^{2+}$]c (Langou et al., 2010).

Three independent studies have shown that the Miro EF-hand domains mediate $Ca^{2+}$ dependent regulation of mitochondrial trafficking (MacAskill et al., 2009b; Saotome et al., 2008; Wang and Schwarz, 2009) and two possible mechanisms have been proposed to explain $Ca^{2+}$ dependent regulation of mitochondrial transport (MacAskill et al., 2009b; Wang and Schwarz, 2009). Wang and Schwarz developed a model in which kinesin-1 binds to TRAK which in turn binds to Miro. Increased [$Ca^{2+}$]c causes a conformational change in Miro that enables the N-terminal motor domain of kinesin-1 to directly interact with Miro. Thus, the kinesin-1 motor domain is prevented from binding to and move along microtubules, effectively halting transport (Figure 5.1) (Wang and Schwarz, 2009). In contrast, MacAskill *et al.* proposed that kinesin-1 directly binds to Miro independently of TRAK and that increased [$Ca^{2+}$]c disrupts this interaction, thus releasing mitochondria from kinesin-1 to inhibit mitochondrial transport (Figure 5.1) (MacAskill et al., 2009b). My findings are in line with the model proposed by Wang and Schwarz (Wang and Schwarz, 2009). I found that elevation of TRAK1 expression levels increased the amount of endogenous kinesin-1 bound to Miro1, suggesting that TRAK1 plays a significant role in this interaction. I also demonstrated that VAPBP56S reduced the amount of tubulin but not kinesin-1 that was associated with Miro1 in HEK293 cells. Moreover, this defect was rescued using a $Ca^{2+}$ insensitive mutant Miro1 construct. My data therefore support a mechanism in which ALS-associated mutant VAPBP56S perturbs anterograde axonal transport of mitochondria by disrupting $Ca^{2+}$ homeostasis and affecting the Miro1/TRAK1/kinesin-1 interaction with tubulin (Figure 5.1).

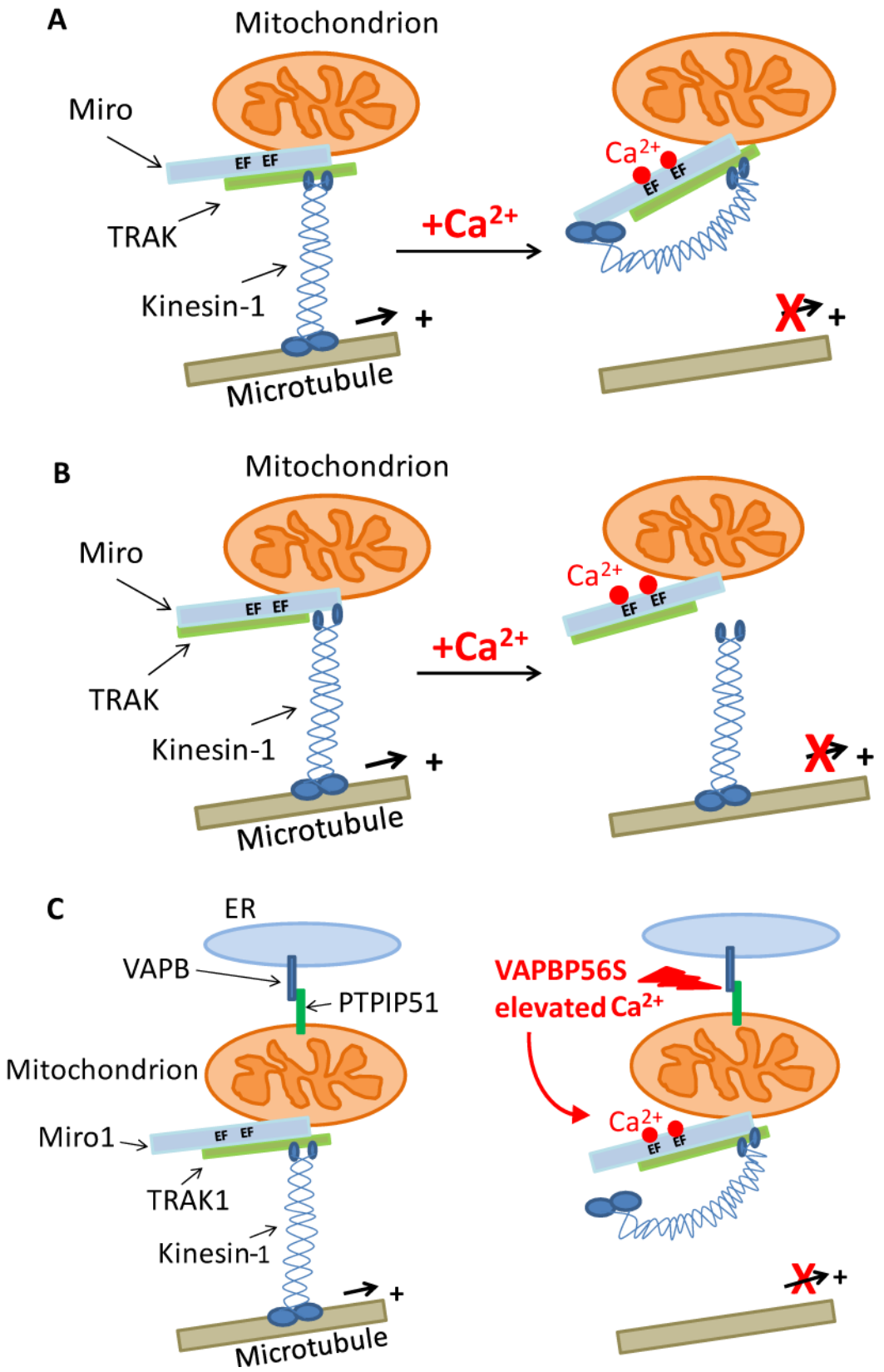


***Figure 5.1 Models of Miro and $Ca^{2+}$dependent regulation of mitochondrial transport, and proposed mechanism for how VAPBP56S disrupts mitochondrial transport.***

(A) $Ca^{2+}$ induced release of kinesin-1 from microtubules. Kinesin-1 is associated with

Miro via interaction with TRAK. Miro is a sensor for intracellular $Ca^{2+}$ via it EF-hands. Increased $Ca^{2+}$ alters the structure of the Miro EF-hands to permit binding of the kinesin-1 motor domain. Since kinesin-1 is no longer attached to microtubule rails, mitochondrial transport is halted (Wang and Schwarz, 2009). (B) Increased $Ca^{2+}$ alters the structure of the Miro EF-hands to induce release of Miro and TRAK from kinesin-1 to halt mitochondrial transport (MacAskill et al., 2009b). (C) Proposed mechanism for how VAPBP56S disrupts mitochondrial transport. VAPB is an ER membrane protein localised to MAM and tethers ER to mitochondria via its interaction with PTPIP51. VAPBP56S disrupts binding to PTPIP51 and perturbs ER-mitochondria $Ca^{2+}$ exchange (De Vos et al., 2012). This perturbation of $Ca^{2+}$ handling leads to increased $[Ca^{2+}]c$ which in turn disrupts the association of mitochondrial kinesin-1 with microtubules and axonal transport via an effect on Miro1.

## 5.4 VAPBP56S and $Ca^{2+}$ mishandling

As described above, the VAPBP56S-induced defect in anterograde transport of mitochondria is $Ca^{2+}$ dependent and correlates with increased [$Ca^{2+}$]c. How VAPBP56S causes this increase in [$Ca^{2+}$]c is not yet clear but may well involve its effect on ER structure (Fasana et al., 2010; Langou et al., 2010; Nishimura et al., 2004; Teuling et al., 2007; Tudor et al., 2010), its interaction with the outer mitochondrial membrane protein PTPIP51 (De Vos et al., 2012) or its role in ER stress and the UPR (Gkogkas et al., 2008; Kanekura et al., 2006; Langou et al., 2010; Suzuki et al., 2009; Tsuda et al., 2008).

### *5.4.1 Perturbation of ER structure*

The ER is a major $Ca^{2+}$ store and overexpression of VAPBP56S induces the formation of large abnormal ER-derived inclusions (Fasana et al., 2010; Langou et al., 2010; Nishimura et al., 2004; Teuling et al., 2007; Tudor et al., 2010). Hence it is possible that this structural effect to ER directly affects $Ca^{2+}$ handing by the ER and leads to a permanent increase in [$Ca^{2+}$]c. However, it has been recently reported that induced pluripotent stem cells derived from VAPBP56S ALS patients do not show large ER aggregates (Mitne-Neto et al., 2011).

### *5.4.2 Perturbation of MAM*

In addition to ER, mitochondria are important $Ca^{2+}$ stores and $Ca^{2+}$ exchange between these organelles impacts upon a number of physiological processes such as

oxidative ATP synthesis, protein folding and apoptotic cell death (Hayashi et al., 2009; Simmen et al., 2010). VAPB interacts with the outer mitochondrial membrane protein PTPIP51 to regulate $Ca^{2+}$ homeostasis (De Vos et al., 2012). Indeed, depleting VAPB or PTPIP51 levels using small interfering RNA caused an increase in peak $[Ca^{2+}]c$ following IP3R-mediated $Ca^{2+}$ release from ER stores that was associated with delayed mitochondrial $Ca^{2+}$ uptake and reduced peak mitochondrial $Ca^{2+}$ levels (De Vos et al., 2012). Moreover, I have shown that a proportion of VAPB is present in MAM and that VAPBP56S is enriched in MAM compared to wild-type VAPB. Furthermore, VAPBP56S aberrantly increases mitochondrial $Ca^{2+}$ uptake upon IP3R-mediated release of $Ca^{2+}$ from ER stores in both HEK293 cells and rat cortical neurons (De Vos et al., 2012). Both the accumulation in MAM and the disruption of $Ca^{2+}$ handling are most likely caused by increased binding of VAPBP56S to PTPIP51 (De Vos et al., 2012). In terms of axonal transport regulation, such an increase in mitochondrial $Ca^{2+}$ uptake could possibly lead to mitochondrial $Ca^{2+}$ overload and saturated mitochondrial $Ca^{2+}$ buffering which can cause a permanently increased $[Ca^{2+}]c$ (Grosskreutz et al., 2007).

### *5.4.3 ER stress*

VAPB is involved in ER stress and the UPR and there is evidence that VAPBP56S is defective in this function (Gkogkas et al., 2008; Kanekura et al., 2006; Langou et al., 2010; Suzuki et al., 2009; Tsuda et al., 2008). It has been shown that under conditions of ER stress CHOP activates ER oxidase 1 α (ERO1-α), which induces IP3R-mediated $Ca^{2+}$ release from the ER (Li et al., 2009; Marciniak et al., 2004). VAPBP56S induced perturbation of the UPR may therefore impact on this process and could induce increased $[Ca^{2+}]c$ and thus defective axonal mitochondrial transport.

## 5.5 Implications for other forms of ALS

I showed in this thesis that VAPBP56S increases $[Ca^{2+}]c$ and selectively disrupts anterograde mitochondrial transport in a $Ca^{2+}$ dependent manner. A very similar defect in anterograde axonal transport of mitochondria has been observed previously in mutant SOD1 models (De Vos et al., 2007). We do not yet know if the same mechanism is causing the inhibition of axonal transport by ALS mutant SOD1, but $[Ca^{2+}]c$ is elevated in mutant SOD1 cellular models (Carrì et al., 1997; Jaiswal et al., 2009; Swerdlow et al., 1998), in motor neurons from mutant SOD1 transgenic ALS models (Kruman et al., 1999; Siklós et al., 2000; Tradewell et al., 2011) and ALS patients (Curti et al., 1996; Siklós et al., 1996).

Although there is no evidence that mutant SOD1 affects ER-mitochondria interactions, mutant SOD1 has been shown to directly bind to VDAC1 (Israelson et al., 2010). VDAC1 is a mitochondrial protein but it is linked to some ER proteins in MAM (Szabadkai et al., 2006). Moreover, mutant SOD1 abnormally localises to mitochondrial intermembrane space and decreases the $Ca^{2+}$ accumulation and retention capacity of mitochondria (Igoudjil et al., 2011). Furthermore, ER stress and activation of the UPR are early phenomenona in mutant SOD1 expressing transgenic mice and cell lines (Atkin et al., 2006; Kikuchi et al., 2006; Nishitoh et al., 2008; Saxena et al., 2009; Tobisawa et al., 2003), and so may also influence $Ca^{2+}$ homeostasis.

Evidence for the involvement of defective axonal transport caused by increased $[Ca^{2+}]c$ in other forms of ALS is less extensive, but mitochondrial clustering has been described in mutant TDP-43 mice (Xu et al., 2011b) and in the spinal cord of ALS patients (Sasaki and Iwata, 1996; Sasaki and Iwata, 2007). Altered $Ca^{2+}$ handling and UPR have been linked to ALS caused by mutations in ubiquilin 2 (Deng et al., 2011),

VCP (Ju et al., 2009; Ju et al., 2008; Ritz et al., 2011; Weihl et al., 2006), and Sigma-1 receptor (Sig-1R) (Al-Saif et al., 2011). Sig-1R is particularly interesting in this context because it is a $Ca^{2+}$ sensitive chaperone of IP3R in the ER that is localised in MAM (Hayashi and Su, 2007). Thus in addition to VAPB, Sig-1R is a second ER-resident MAM protein directly involved in ALS.

## 5.6 Future directions

The results described in this thesis provide novel information on how VAPBP56S may cause ALS. At the same time, the results presented here raise further questions and these, and possible future lines of research are discussed below.

i) An important finding in this thesis is that VAPBP56S increased resting $[Ca^{2+}]c$. However, the source of increased $[Ca^{2+}]c$ and the exact mechanism of this increase are not known. To determine which organelle is the source of the increased $[Ca^{2+}]c$, $Ca^{2+}$ levels could be measured in VAPBP56S and control transfected cells in both the ER and mitochondria using $Ca^{2+}$ indicators targeted to mitochondria or ER (e.g. pericam-mito or aequorin ER).

ii) VAPBT46I shows similar pathological features as VAPBP56S (Chen et al., 2010a). Therefore, it is possible that these two mutants of VAPB cause ALS by similar mechanisms. This could be tested by monitoring axonal transport of mitochondria and $[Ca^{2+}]c$ in VAPBT46I transfected cells.

iii) Mutant SOD1 has been shown to perturb both mitochondrial and vesicle transport (Bilsland et al., 2010; De Vos et al., 2007; Marinković et al., 2012). I

demonstrated in this thesis that VAPBP56S perturbs mitochondrial transport. It would be interesting to investigate if VAPBP56S also affects axonal transport of other non-mitochondrial cargoes similar to mutant SOD1. Since mitochondria provide ATP for molecular motor proteins (kinesins and dynein) and $Ca^{2+}$ can influence the transport of other cargoes, it is possible that axonal transport of other non-mitochondrial cargoes is also affected in VAPBP56S transfected cells. The effect of VAPBP56S on axonal transport of non-mitochondrial cargoes could be investigated by using EGFP-tagged cargoes and time-lapse microscopy.

iv) Elevated $Ca^{2+}$ levels and disrupted mitochondrial transport have also been observed in mutant SOD1 expressing cells (Carrì et al., 1997; De Vos et al., 2007; Jaiswal et al., 2009; Kruman et al., 1999; Siklós et al., 2000; Swerdlow et al., 1998; Tradewell et al., 2011). Thus it would be interesting to investigate whether defective mitochondrial transport caused by mutant SOD1 can also be rescued by expression of the $Ca^{2+}$-insensitive mutant of Miro.

v) Mutant SOD1 has been shown to bind to VDAC1 (Israelson et al., 2010). Thus it is possible that mutant SOD1 is also associated with PTPIP51 and via this interaction perturbs MAM, and disrupts $Ca^{2+}$ homeostasis. To begin to investigate this possibility, immunoprecipitation experiments could be performed to monitor SOD1-PTPIP51 interactions.

vi) Mutations in presenilin-1 and 2 and in α-synuclein cause Alzheimer's disease and Parkinson's disease respectively (Polymeropoulos et al., 1997; Sherrington et al., 1995). It has been shown that presenilin-1 and 2 are enriched in MAM (Area-Gomez et al., 2009). Moreover, overexpression of α-synuclein increases ER-mitochondria interaction (Cali et al., 2012). Damage to mitochondrial axonal transport is seen in both

Alzheimer's and Parkinson's diseases (De Vos et al., 2008). Thus, ER-mitochondria interactions and MAM may be target for damage in other neurodegenerative diseases. Future work in this area is thus warranted.

# REFERENCES


Abe, K., L.H. Pan, M. Watanabe, H. Konno, T. Kato, and Y. Itoyama. 1997. Upregulation of protein-tyrosine nitration in the anterior horn cells of amyotrophic lateral sclerosis. *Neurol. Res.* 19:124-128.

Abel, O., J.F. Powell, P.M. Andersen, and A. Al-Chalabi. 2012. ALSoD: A user-friendly online bioinformatics tool for amyotrophic lateral sclerosis genetics. *Hum. Mutat.* 33:1345-1351.

Abrámoff, M.D., P.J. Magalhaes, and S.J. Ram. 2004. Image processing with ImageJ. *Biophotonics International*. 11:36-42.

Acharya, U., R. Jacobs, J.M. Peters, N. Watson, M.G. Farquhar, and V. Malhotra. 1995. The formation of Golgi stacks from vesiculated Golgi membranes requires two distinct fusion events. *Cell*. 82:895-904.

Ackerley, S., A.J. Grierson, S. Banner, M.S. Perkinton, J. Brownlees, H.L. Byers, M. Ward, P. Thornhill, K. Hussain, J.S. Waby, B.H. Anderton, J.D. Cooper, C. Dingwall, P.N. Leigh, C.E. Shaw, and C.C.J. Miller. 2004. p38α stress-activated protein kinase phosphorylates neurofilaments and is associated with neurofilament pathology in amyotrophic lateral sclerosis. *Mol. Cell. Neurosci.* 26:354-364.

Ackerley, S., A.J. Grierson, J. Brownlees, P. Thornhill, B.H. Anderton, P.N. Leigh, C.E. Shaw, and C.C.J. Miller. 2000. Glutamate slows axonal transport of neurofilaments in transfected neurons. *J. Cell Biol.* 150:165-175.

Ackerley, S., P. Thornhill, A.J. Grierson, J. Brownlees, B.H. Anderton, P.N. Leigh, C.E. Shaw, and C.C.J. Miller. 2003. Neurofilament heavy chain side-arm phosphorylation regulates axonal transport of neurofilaments. *J. Cell Biol.* 161:489-495.

Al-Chalabi, A., P.M. Anderson, P. Nilsson, B. Chioza, J.L. Andersson, C.R. Russ, C.E. Shaw, J.F. Powell, and P.N. Leigh. 1999. Deletions of the heavy neurofilament subunit tail in amyotrophic lateral sclerosis. *Hum. Mol. Genet.* 8:157-164.

al-Chalabi, A., Z.E. Enayat, M.C. Bakker, P.C. Sham, D.M. Ball, C.E. Shaw, C.M. Lloyd, J.F. Powell, and P.N. Leigh. 1996. Association of apolipoprotein E epsilon 4 allele with bulbar-onset motor neuron disease. *Lancet*. 347:159-60.

Al-Saif, A., F. Al-Mohanna, and S. Bohlega. 2011. A mutation in sigma-1 receptor causes juvenile amyotrophic lateral sclerosis. *Ann. Neurol.* 70:913-919.

Albo, F., M. Pieri, and C. Zona. 2004. Modulation of AMPA receptors in spinal motor neurons by the neuroprotective agent riluzole. *J. Neurosci. Res.* 78:200-207.

Alexianu, M.E., B.-K. Ho, A.H. Mohamed, V. La Bella, R.G. Smith, and S.H. Appel. 1994. The role of calcium-binding proteins in selective motoneuron vulnerability in amyotrophic lateral sclerosis. *Ann. Neurol.* 36:846-858.

Amarilio, R., S. Ramachandran, H. Sabanay, and S. Lev. 2005. Differential regulation of endoplasmic reticulum structure through VAP-Nir protein interaction. *J. Biol. Chem.* 280:5934-5944.

Anagnostou, G., M.T. Akbar, P. Paul, C. Angelinetta, T.J. Steiner, and J. de Belleroche. 2010. Vesicle associated membrane protein B (VAPB) is decreased in ALS spinal cord. *Neurobiol. Aging*. 31:969-985.

Andersen, P.M., and A. Al-Chalabi. 2011. Clinical genetics of amyotrophic lateral sclerosis: what do we really know? *Nat. Rev. Neurol.* 7:603-615.

Andressen, C., I. Blumcke, and M.R. Celio. 1993. Calcium-binding proteins: selective markers of nerve cells. *Cell Tissue Res.* 271:181-208.

Aoki, M., C.L.G. Lin, J.D. Rothstein, B.A. Geller, B.A. Hosler, T.L. Munsat, H.R. Horvitz, and R.H. Brown, Jr. 1998. Mutations in the glutamate transporter EAAT2 gene do not cause abnormal EAAT2 transcripts in amyotrophic lateral sclerosis. *Ann.Neurol.* 43:645-653.

Arai, T., M. Hasegawa, H. Akiyama, K. Ikeda, T. Nonaka, H. Mori, D. Mann, K. Tsuchiya, M. Yoshida, Y. Hashizume, and T. Oda. 2006. TDP-43 is a component of ubiquitin-positive tau-negative inclusions in frontotemporal lobar degeneration and amyotrophic lateral sclerosis. *Biochem. Biophys. Res. Commun.* 351:602-611.

Arai, T., M. Hasegawa, T. Nonoka, F. Kametani, M. Yamashita, M. Hosokawa, K. Niizato, K. Tsuchiya, Z. Kobayashi, K. Ikeda, M. Yoshida, M. Onaya, H. Fujishiro, and H. Akiyama. 2010. Phosphorylated and cleaved TDP-43 in ALS, FTLD and other neurodegenerative disorders and in cellular models of TDP-43 proteinopathy. *Neuropathology*. 30:170-181.

Arai, T., T. Nonaka, M. Hasegawa, H. Akiyama, M. Yoshida, Y. Hashizume, K. Tsuchiya, T. Oda, and K. Ikeda. 2003. Neuronal and glial inclusions in frontotemporal dementia with or without motor neuron disease are immunopositive for p62. *Neurosci. Lett.* 342:41-44.

Area-Gomez, E., A.J. de Groof, I. Boldogh, T.D. Bird, G.E. Gibson, C.M. Koehler, W.H. Yu, K.E. Duff, M.P. Yaffe, L.A. Pon, and E.A. Schon. 2009. Presenilins are enriched in endoplasmic reticulum membranes associated with mitochondria. *Am. J. Pathol.* 175:1810-1816.

Armon, C. 2003. An evidence-based medicine approach to the evaluation of the role of exogenous risk factors in sporadic amyotrophic lateral sclerosis. *Neuroepidemiology*. 22:217-228.

Armon, C. 2009. Smoking may be considered an established risk factor for sporadic ALS. *Neurology*. 73:1693-1698.

Atkin, J.D., M.A. Farg, B.J. Turner, D. Tomas, J.A. Lysaght, J. Nunan, A. Rembach, P. Nagley, P.M. Beart, S.S. Cheema, and M.K. Horne. 2006. Induction of the unfolded protein response in familial amyotrophic lateral sclerosis and association of protein-disulfide isomerase with superoxide dismutase 1. *J. Biol. Chem.* 281:30152-30165.

Avraham, K.B., M. Schickler, D. Sapoznikov, R. Yarom, and Y. Groner. 1988. Down's syndrome: abnormal neuromuscular junction in tongue of transgenic mice with elevated levels of human Cu/Zn-superoxide dismutase. *Cell*. 54:823-829.

Avraham, K.B., H. Sugarman, S. Rotshenker, and Y. Groner. 1991. Down's syndrome: morphological remodelling and increased complexity in the neuromuscular junction of transgenic CuZn-superoxide dismutase mice. *J. Neurocytol.* 20:208-215.

Balla, A., and T. Balla. 2006. Phosphatidylinositol 4-kinases: old enzymes with emerging functions. *Trends Cell Biol.* 16:351-361.

Barlowe, C., L. Orci, T. Yeung, M. Hosobuchi, S. Hamamoto, N. Salama, M.F. Rexach, M. Ravazzola, M. Amherdt, and R. Schekman. 1994. COPII: a membrane coat formed by Sec proteins that drive vesicle budding from the endoplasmic reticulum. *Cell*. 77:895-907.

Beal, M.F., R.J. Ferrante, S.E. Browne, R.T. Matthews, N.W. Kowall, and R.H. Brown, Jr. 1997. Increased 3-nitrotyrosine in both sporadic and familial amyotrophic lateral sclerosis. *Ann. Neurol.* 42:644-654.

Beaulieu, J.M., M.D. Nguyen, and J.P. Julien. 1999. Late onset death of motor neurons in mice overexpressing wild-type peripherin. *J. Cell Biol.* 147:531-544.

Beck, M., K. Brickley, H.L. Wilkinson, S. Sharma, M. Smith, P.L. Chazot, S. Pollard, and F.A. Stephenson. 2002. Identification, molecular cloning, and characterization of a novel GABAA receptor-associated protein, GRIF-1. *J. Biol. Chem.* 277:30079-30090.

Bedard, K., and K.-H. Krause. 2007. The NOX family of ROS-generating NADPH oxidases: physiology and pathophysiology. *Physiol. Rev.* 87:245-313.

Beghi, E., G. Logroscino, A. Chio, O. Hardiman, A. Millul, D. Mitchell, R. Swingler, and B.J. Traynor. 2010. Amyotrophic lateral sclerosis, physical exercise, trauma and sports: results of a population-based pilot case-control study. *Amyotroph. Lateral Scler.* 11:289-292.

Benajiba, L., I. Le Ber, A. Camuzat, M. Lacoste, C. Thomas-Anterion, P. Couratier, S. Legallic, F. Salachas, D. Hannequin, M. Decousus, L. Lacomblez, E. Guedj, V. Golfier, W. Camu, B. Dubois, D. Campion, V. Meininger, and A. Brice. 2009. TARDBP mutations in motoneuron disease with frontotemporal lobar degeneration. *Ann. Neurol.* 65:470-473.

Bensimon, G., L. Lacomblez, and V. Meininger. 1994. A controlled trial of riluzole in amyotrophic lateral sclerosis. ALS/Riluzole Study Group. *N. Engl. J. Med.*

330:585-591.

Bernales, S., F.R. Papa, and P. Walter. 2006. Intracellular signaling by the unfolded protein response. *Annu. Rev. Cell Dev. Biol.* 22:487-508.

Bilsland, L.G., E. Sahai, G. Kelly, M. Golding, L. Greensmith, and G. Schiavo. 2010. Deficits in axonal transport precede ALS symptoms in vivo. *Proc. Natl. Acad. Sci. USA.* 107:20523-20528.

BIPM. 2006. The International System of Units. *In* Bureau International des Poids et Mesures. B.I.d.P.e. Mesures, editor.

Birnboim, H.C., and J. Doly. 1979. A rapid alkaline extraction procedure for screening recombinant plasmid DNA. *Nucleic Acids Res.* 7:1513-1523.

Borthwick, G.M., M.A. Johnson, P.G. Ince, P.J. Shaw, and D.M. Turnbull. 1999. Mitochondrial enzyme activity in amyotrophic lateral sclerosis: Implications for the role of mitochondria in neuronal cell death. *Ann. Neurol.* 46:787-790.

Boussif, O., F. Lezoualc'h, M.A. Zanta, M.D. Mergny, D. Scherman, B. Demeneix, and J.P. Behr. 1995. A versatile vector for gene and oligonucleotide transfer into cells in culture and in vivo: polyethylenimine. *Proc. Natl. Acad. Sci. USA.* 92:7297-7301.

Bradford, M.M. 1976. A rapid and sensitive method for the quantitation of microgram quantities of protein utilizing the principle of protein-dye binding. *Anal. Biochem.* 72:248-254.

Brickley, K., M.J. Smith, M. Beck, and F.A. Stephenson. 2005. GRIF-1 and OIP106, members of a novel gene family of coiled-coil domain proteins: association in vivo and in vitro with kinesin. *J. Biol. Chem.* 280:14723-14732.

Brickley, K., and F.A. Stephenson. 2011. Trafficking kinesin protein (TRAK)-mediated transport of mitochondria in axons of hippocampal neurons. *J. Biol. Chem.* 286:18079-18092.

Brickner, J.H., and P. Walter. 2004. Gene recruitment of the activated INO1 locus to the nuclear membrane. *PLoS Biol.* 2:e342.

Brownhill, K., L. Wood, and V. Allan. 2009. Molecular motors and the Golgi complex: staying put and moving through. *Semin. Cell Dev. Biol.* 20:784-792.

Bruijn, L.I., M.W. Becher, M.K. Lee, K.L. Anderson, N.A. Jenkins, N.G. Copeland, S.S. Sisodia, J.D. Rothstein, D.R. Borchelt, D.L. Price, and D.W. Cleveland. 1997. ALS-linked SOD1 mutant G85R mediates damage to astrocytes and promotes rapidly progressive disease with SOD1-containing inclusions. *Neuron.* 18:327-338.

Bruijn, L.I., M.K. Houseweart, S. Kato, K.L. Anderson, S.D. Anderson, E. Ohama, A.G. Reaume, R.W. Scott, and D.L. Cleveland. 1998. Aggregation and motor neuron toxicity of an ALS-linked SOD1 mutant independent from wild-type

SOD1. *Science*. 281:1851-1854.

Bunina, T.L. 1962. On intracellular inclusions in familial amyotrophic lateral sclerosis. *Zh. Nevropatol. Psikhiatr. Im. S S Korsakova.* 62:1293-1299.

Burnashev, N., H. Monyer, P.H. Seeburg, and B. Sakmann. 1992. Divalent ion permeability of AMPA receptor channels is dominated by the edited form of a single subunit. *Neuron*. 8:189-198.

Byrne, S., M. Elamin, P. Bede, A. Shatunov, C. Walsh, B. Corr, M. Heverin, N. Jordan, K. Kenna, C. Lynch, R.L. McLaughlin, P.M. Iyer, C. O'Brien, J. Phukan, B. Wynne, A.L. Bokde, D.G. Bradley, N. Pender, A. Al-Chalabi, and O. Hardiman. 2012. Cognitive and clinical characteristics of patients with amyotrophic lateral sclerosis carrying a C9orf72 repeat expansion: a population-based cohort study. *Lancet Neurol.* 11:232-240.

Byrne, S., C. Walsh, C. Lynch, P. Bede, M. Elamin, K. Kenna, R. McLaughlin, and O. Hardiman. 2011. Rate of familial amyotrophic lateral sclerosis: a systematic review and meta-analysis. *J. Neurol. Neurosurg. Psychiatry*. 82:623-627.

Cai, D., D.P. McEwen, J.R. Martens, E. Meyhofer, and K.J. Verhey. 2009. Single molecule imaging reveals differences in microtubule track selection between Kinesin motors. *PLoS Biol*. 7:e1000216.

Cai, Q., C. Gerwin, and Z.-H. Sheng. 2005. Syntabulin-mediated anterograde transport of mitochondria along neuronal processes. *J. Cell Biol.* 170:959-969.

Cai, Y., B.B. Singh, A. Aslanukov, H. Zhao, and P.A. Ferreira. 2001. The docking of kinesins, KIF5B and KIF5C, to Ran-binding Protein 2 (RanBP2) is mediated via a novel RanBP2 domain. *J. Biol. Chem.* 276:41594-41602.

Cali, T., D. Ottolini, A. Negro, and M. Brini. 2012. Alpha-synuclein controls mitochondrial calcium homeostasis by enhancing endoplasmic reticulum-mitochondria interactions. *J. Biol. Chem.* 287:17914-17929.

Campbell, J.L., and R. Schekman. 1997. Selective packaging of cargo molecules into endoplasmic reticulum-derived COPII vesicles. *Proc. Natl. Acad. Sci. USA*. 94:837-842.

Cao, K., R. Nakajima, H.H. Meyer, and Y. Zheng. 2003. The AAA-ATPase Cdc48/p97 regulates spindle disassembly at the end of mitosis. *Cell*. 115:355-367.

Carpenter, S. 1968. Proximal axonal enlargement in motor neuron disease. *Neurology*. 18:841-851.

Carrì, M.T., A. Ferri, A. Battistoni, L. Famhy, R. Gabbianelli, F. Poccia, and G. Rotilio. 1997. Expression of a Cu,Zn superoxide dismutase typical of familial amyotrophic lateral sclerosis induces mitochondrial alteration and increase of cytosolic $Ca^{2+}$ concentration in transfected neuroblastoma SH-SY5Y cells. *FEBS Lett.* 414:365-368.

Carriedo, S.G., S.L. Sensi, H.Z. Yin, and J.H. Weiss. 2000. AMPA exposures induce mitochondrial Ca(2+) overload and ROS generation in spinal motor neurons in vitro. *J. Neurosci.* 20:240-250.

Carriedo, S.G., H.Z. Yin, and J.H. Weiss. 1996. Motor neurons are selectively vulnerable to AMPA/kainate receptor-mediated injury in vitro. *J. Neurosci.* 16:4069-4079.

Ceballos-Picot, I., A. Nicole, P. Briand, G. Grimber, A. Delacourte, A. Defossez, F. Javoy-Agid, M. Lafon, J.L. Blouin, and P.M. Sinet. 1991. Neuronal-specific expression of human copper-zinc superoxide dismutase gene in transgenic mice: animal model of gene dosage effects in Down's syndrome. *Brain Res*. 552:198-214.

Chang, C., T.W. Yu, C.I. Bargmann, and M. Tessier-Lavigne. 2004. Inhibition of netrin-mediated axon attraction by a receptor protein tyrosine phosphatase. *Science*. 305:103-106.

Chang, D.T.W., A.S. Honick, and I.J. Reynolds. 2006. Mitochondrial trafficking to synapses in cultured primary cortical neurons. *J. Neurosci.* 26:7035-7045.

Chang, K.T., R.F. Niescier, and K.T. Min. 2011. Mitochondrial matrix Ca2+ as an intrinsic signal regulating mitochondrial motility in axons. *Proc. Natl. Acad. Sci. USA*. 108:15465-15461.

Chen, H.J., G. Anagnostou, A. Chai, J. Withers, A. Morris, J. Adhikaree, G. Pennetta, and J.S. de Belleroche. 2010a. Characterisation of the properties of a novel mutation in VAPB in familial ALS. *J. Biol. Chem.* 285:40266-40281.

Chen, S., G.C. Owens, H. Makarenkova, and D.B. Edelman. 2010b. HDAC6 regulates mitochondrial transport in hippocampal neurons. *PLoS One*. 5:e10848.

Chen, X.J., E.N. Levedakou, K.J. Millen, R.L. Wollmann, B. Soliven, and B. Popko. 2007. Proprioceptive sensory neuropathy in mice with a mutation in the cytoplasmic Dynein heavy chain 1 gene. *J. Neurosci.* 27:14515-14524.

Chen, Y.M., C. Gerwin, and Z.H. Sheng. 2009. Dynein light chain LC8 regulates syntaphilin-mediated mitochondrial docking in axons. *J. Neurosci.* 29:9429-9438.

Chen, Y.Z., C.L. Bennett, H.M. Huynh, I.P. Blair, I. Puls, J. Irobi, I. Dierick, A. Abel, M.L. Kennerson, B.A. Rabin, G.A. Nicholson, M. Auer-Grumbach, K. Wagner, P. De Jonghe, J.W. Griffin, K.H. Fischbeck, V. Timmerman, D.R. Cornblath, and P.F. Chance. 2004a. DNA/RNA helicase gene mutations in a form of juvenile amyotrophic lateral sclerosis (ALS4). *Am. J. Hum. Genet.* 74:1128-1135.

Chen, Y.Z., C.L. Bennett, H.M. Huynh, I.P. Blair, I. Puls, J. Irobi, I. Dierick, A. Abel, M.L. Kennerson, B.A. Rabin, G.A. Nicholson, M. Auer-Grumbach, K. Wagner, P. De Jonghe, J.W. Griffin, K.H. Fischbeck, V. Timmerman, D.R. Cornblath, and P.F. Chance. 2004b. DNA/RNA helicase gene mutations in a form of

juvenile amyotrophic lateral sclerosis (ALS4). *Am. J. Hum. Genet.* 74:1128-1135.

Chio, A., G. Benzi, M. Dossena, R. Mutani, and G. Mora. 2005. Severely increased risk of amyotrophic lateral sclerosis among Italian professional football players. *Brain*. 128:472-476.

Cho, K.-i., H. Yi, R. Desai, A.R. Hand, A.L. Haas, and P.A. Ferreira. 2009. RANBP2 is an allosteric activator of the conventional kinesin-1 motor protein, KIF5B, in a minimal cell-free system. *EMBO Rep*. 10:480-486.

Cho, K.I., Y. Cai, H. Yi, A. Yeh, A. Aslanukov, and P.A. Ferreira. 2007. Association of the kinesin-binding domain of RanBP2 to KIF5B and KIF5C determines mitochondria localization and function. *Traffic*. 8:1722-1735.

Choudhary, C., C. Kumar, F. Gnad, M.L. Nielsen, M. Rehman, T.C. Walther, J.V. Olsen, and M. Mann. 2009. Lysine acetylation targets protein complexes and co-regulates major cellular functions. *Science*. 325:834-840.

Chow, C.Y., J.E. Landers, S.K. Bergren, P.C. Sapp, A.E. Grant, J.M. Jones, L. Everett, G.M. Lenk, D.M. McKenna-Yasek, L.S. Weisman, D. Figlewicz, R.H. Brown, and M.H. Meisler. 2009. Deleterious variants of FIG4, a phosphoinositide phosphatase, in patients with ALS. *Am. J. Hum. Genet.* 84:85-88.

Chu, C.-W., F. Hou, J. Zhang, L. Phu, A.V. Loktev, D.S. Kirkpatrick, P.K. Jackson, Y. Zhao, and H. Zou. 2011. A novel acetylation of β-tubulin by San modulates microtubule polymerization via down-regulating tubulin incorporation. *Mol. Biol. Cell*. 22:448-456.

Cohen, T.J., V.M. Lee, and J.Q. Trojanowski. 2011. TDP-43 functions and pathogenic mechanisms implicated in TDP-43 proteinopathies. *Trends. Mol. Med.* 17:659-667.

Collard, J.-F., F. Cote, and J.-P. Julien. 1995. Defective axonal transport in a transgenic mouse model of amyotrophic lateral sclerosis. *Nature*. 375:61-64.

Conde, C., and A. Caceres. 2009. Microtubule assembly, organization and dynamics in axons and dendrites. *Nat. Rev. Neurosci.* 10:319-332.

Cooper-Knock, J., C. Hewitt, J.R. Highley, A. Brockington, A. Milano, S. Man, J. Martindale, J. Hartley, T. Walsh, C. Gelsthorpe, L. Baxter, G. Forster, M. Fox, J. Bury, K. Mok, C.J. McDermott, B.J. Traynor, J. Kirby, S.B. Wharton, P.G. Ince, J. Hardy, and P.J. Shaw. 2012. Clinico-pathological features in amyotrophic lateral sclerosis with expansions in C9ORF72. *Brain*. 135:751-764.

Coppede, F., M. Mancuso, A. Lo Gerfo, C. Carlesi, S. Piazza, A. Rocchi, L. Petrozzi, C. Nesti, D. Micheli, A. Bacci, L. Migliore, L. Murri, and G. Siciliano. 2007. Association of the hOGG1 Ser326Cys polymorphism with sporadic amyotrophic lateral sclerosis. *Neurosci. Lett.* 420:163-168.

Corcia, P., V. Mayeux-Portas, J. Khoris, B. de Toffol, A. Autret, J.-P. Müh, W. Camu,

C. Andres, and A.L.S.R.G. the French. 2002. Abnormal SMN1 gene copy number is a susceptibility factor for amyotrophic lateral sclerosis. *Ann. Neurol.* 51:243-246.

Cote, F., J.-F. Collard, and J.-P. Julien. 1993. Progressive neuronopathy in transgenic mice expressing the human neurofilament heavy gene: a mouse model of amyotrophic lateral sclerosis. *Cell*. 73:35-46.

Cox, P.A., and O.W. Sacks. 2002. Cycad neurotoxins, consumption of flying foxes, and ALS-PDC disease in Guam. *Neurology*. 58:956-959.

Cudkowicz, M.E., J.M. Shefner, D.A. Schoenfeld, R.H. Brown, Jr., H. Johnson, M. Qureshi, M. Jacobs, J.D. Rothstein, S.H. Appel, R.M. Pascuzzi, T.D. Heiman-Patterson, P.D. Donofrio, W.S. David, J.A. Russell, R. Tandan, E.P. Pioro, K.J. Felice, J. Rosenfeld, R.N. Mandler, G.M. Sachs, W.G. Bradley, E.M. Raynor, G.D. Baquis, J.M. Belsh, S. Novella, J. Goldstein, and J. Hulihan. 2003. A randomized, placebo-controlled trial of topiramate in amyotrophic lateral sclerosis. *Neurology*. 61:456-464.

Curti, D., A. Malaspina, G. Facchetti, C. Camana, L. Mazzini, P. Tosca, F. Zerbi, and M. Ceroni. 1996. Amyotrophic lateral sclerosis: oxidative energy metabolism and calcium homeostasis in peripheral blood lymphocytes. *Neurology*. 47:1060-1064.

Csordás, G., C. Renken, P. Várnai, L. Walter, D. Weaver, K.F. Buttle, T. Balla, C.A. Mannella, and G. Hajnóczky. 2006. Structural and functional features and significance of the physical linkage between ER and mitochondria. *J. Cell Biol.* 174:915-921.

Csordás, G., P. Várnai, T. Golenár, S. Roy, G. Purkins, T.G. Schneider, T. Balla, and G. Hajnóczky. 2010. Imaging interorganelle contacts and local calcium dynamics at the ER-mitochondrial interface. *Mol. Cell*. 39:121-132.

D'Amico, A., E. Mercuri, F.D. Tiziano, and E. Bertini. 2011. Spinal muscular atrophy. *Orphanet J. Rare Dis.* 6:71.

Dai, R.M., and C.-C.H. Li. 2001. Valosin-containing protein is a multi-ubiquitin chain-targeting factor required in ubiquitin-proteasome degradation. *Nat. Cell Biol.* 3:740-744.

Dal Canto, M.C., and M.E. Gurney. 1995. Neuropathological changes in two lines of mice carrying a transgene for mutant human Cu,Zn SOD, and in mice overexpressing wild type human SOD: A model of familial amyotrophic lateral sclerosis (FALS). *Brain Res.* 676:25-40.

Damiano, M., A.A. Starkov, S. Petri, K. Kipiani, M. Kiaei, M. Mattiazzi, M. Flint Beal, and G. Manfredi. 2006. Neural mitochondrial Ca2+ capacity impairment precedes the onset of motor symptoms in G93A Cu/Zn-superoxide dismutase mutant mice. *J. Neurochem.* 96:1349-1361.

Danbolt, N.C. 2001. Glutamate uptake. *Prog. Neurobiol.* 65:1-105.

de Brito, O.M., and L. Scorrano. 2008. Mitofusin 2 tethers endoplasmic reticulum to mitochondria. *Nature*. 456:605-610.

De Vos, K., F. Severin, F. Van Herreweghe, K. Vancompernolle, V. Goossens, A. Hyman, and J. Grooten. 2000. Tumor necrosis factor induces hyperphosphorylation of kinesin light chain and inhibits kinesin-mediated transport of mitochondria. *J. Cell Biol.* 149:1207-1214.

De Vos, K.J., A.L. Chapman, M.E. Tennant, C. Manser, E.L. Tudor, K.F. Lau, J. Brownlees, S. Ackerley, P.J. Shaw, D.M. McLoughlin, C.E. Shaw, P.N. Leigh, C.C. Miller, and A.J. Grierson. 2007. Familial amyotrophic lateral sclerosis-linked SOD1 mutants perturb fast axonal transport to reduce axonal mitochondria content. *Hum. Mol. Genet.* 16:2720-2728.

De Vos, K.J., A.J. Grierson, S. Ackerley, and C.C.J. Miller. 2008. Role of axonal transport in neurodegenerative diseases. *Annu. Rev. Neurosci.* 31:151-173.

De Vos, K.J., G.M. Mórotz, R. Stoica, E.L. Tudor, K.-F. Lau, S. Ackerley, A. Warley, C.E. Shaw, and C.C.J. Miller. 2012. VAPB interacts with the mitochondrial protein PTPIP51 to regulate calcium homeostasis. *Hum. Mol. Genet.* 21:1299-1311.

De Vos, K.J., J. Sable, K.E. Miller, and M.P. Sheetz. 2003. Expression of phosphatidylinositol (4,5) bisphosphate-specific pleckstrin homology domains alters direction but not the level of axonal transport of mitochondria. *Mol. Biol. Cell*. 14:3636-3549.

De Vos, K.J., and M.P. Sheetz. 2007. Visualization and quantification of mitochondrial dynamics in living animal cells. *Methods Cell Biol.* 80:627-682.

Debono, M.-W., J.l. Le Guern, T. Canton, A. Doble, and L. Pradier. 1993. Inhibition by riluzole of electrophysiological responses mediated by rat kainate and NMDA receptors expressed in Xenopus oocytes. *Eur. J. Pharmacol.* 235:283-289.

Dehmelt, L., and S. Halpain. 2005. The MAP2/Tau family of microtubule-associated proteins. *Genome Biol*. 6:204.

DeJesus-Hernandez, M., I.R. Mackenzie, B.F. Boeve, A.L. Boxer, M. Baker, N.J. Rutherford, A.M. Nicholson, N.A. Finch, H. Flynn, J. Adamson, N. Kouri, A. Wojtas, P. Sengdy, G.-Y.R. Hsiung, A. Karydas, W.W. Seeley, K.A. Josephs, G. Coppola, D.H. Geschwind, Z.K. Wszolek, H. Feldman, D.S. Knopman, R.C. Petersen, B.L. Miller, D.W. Dickson, K.B. Boylan, N.R. Graff-Radford, and R. Rademakers. 2011. Expanded GGGGCC Hexanucleotide Repeat in Noncoding Region of C9ORF72 Causes Chromosome 9p-Linked FTD and ALS. *Neuron*. 72:245-256.

Deng, H.-X., W. Chen, S.-T. Hong, K.M. Boycott, G.H. Gorrie, N. Siddique, Y. Yang, F. Fecto, Y. Shi, H. Zhai, H. Jiang, M. Hirano, E. Rampersaud, G.H. Jansen, S. Donkervoort, E.H. Bigio, B.R. Brooks, K. Ajroud, R.L. Sufit, J.L. Haines, E. Mugnaini, M.A. Pericak-Vance, and T. Siddique. 2011. Mutations in UBQLN2 cause dominant X-linked juvenile and adult-onset ALS and ALS/dementia.

*Nature*. 477:211-215.

Deng, H.X., A. Hentati, J.A. Tainer, Z. Iqbal, A. Cayabyab, W.Y. Hung, E.D. Getzoff, P. Hu, B. Herzfeldt, R.P. Roos, C. Warner, G. Deng, E. Soriano, C. Smyth, H.E. Parge, A. Ahmed, A.D. Roses, R.A. Hallewell, M.A. Pericakvance, and T. Siddique. 1993. Amyotrophic-lateral-sclerosis and structural defects in Cu,Zn superoxide-dismutase. *Science*. 261:1047-1051.

Dingledine, R., K. Borges, D. Bowie, and S.F. Traynelis. 1999. The glutamate receptor ion channels. *Pharmacol. Rev.* 51:7-62.

Dompierre, J.P., J.D. Godin, B.C. Charrin, F.P. Cordelieres, S.J. King, S. Humbert, and F. Saudou. 2007. Histone deacetylase 6 inhibition compensates for the transport deficit in Huntington's disease by increasing tubulin acetylation. *J. Neurosci.* 27:3571-3583.

Dormann, D., R. Rodde, D. Edbauer, E. Bentmann, I. Fischer, A. Hruscha, M.E. Than, I.R. Mackenzie, A. Capell, B. Schmid, M. Neumann, and C. Haass. 2010. ALS-associated fused in sarcoma (FUS) mutations disrupt Transportin-mediated nuclear import. *EMBO J.* 29:2841-2857.

Duan, W., X. Li, J. Shi, Y. Guo, Z. Li, and C. Li. 2010. Mutant TDP-43 induces oxidative injury in motor neuron-like cell. *Neuroscience*. 169:1621-1629.

Dunckley, T., M.J. Huentelman, D.W. Craig, J.V. Pearson, S. Szelinger, K. Joshipura, R.F. Halperin, C. Stamper, K.R. Jensen, D. Letizia, S.E. Hesterlee, A. Pestronk, T. Levine, T. Bertorini, M.C. Graves, T. Mozaffar, C.E. Jackson, P. Bosch, A. McVey, A. Dick, R. Barohn, C. Lomen-Hoerth, J. Rosenfeld, T. O'Connor D, K. Zhang, R. Crook, H. Ryberg, M. Hutton, J. Katz, E.P. Simpson, H. Mitsumoto, R. Bowser, R.G. Miller, S.H. Appel, and D.A. Stephan. 2007. Whole-genome analysis of sporadic amyotrophic lateral sclerosis. *N. Engl. J. Med.* 357:775-788.

Dunn, S., E.E. Morrison, T.B. Liverpool, C. Molina-Paris, R.A. Cross, M.C. Alonso, and M. Peckham. 2008. Differential trafficking of Kif5c on tyrosinated and detyrosinated microtubules in live cells. *J. Cell Sci.* 121:1085-1095.

Ebneth, A., R. Godemann, K. Stamer, S. Illenberger, B. Trinczek, E.M. Mandelkow, and E. Mandelkow. 1998. Overexpression of tau protein inhibits kinesin-dependent trafficking of vesicles, mitochondria, and endoplasmic reticulum: Implications for Alzheimer's disease. *J.Cell Biol.* 143:777-794.

Elden, A.C., H.J. Kim, M.P. Hart, A.S. Chen-Plotkin, B.S. Johnson, X. Fang, M. Armakola, F. Geser, R. Greene, M.M. Lu, A. Padmanabhan, D. Clay-Falcone, L. McCluskey, L. Elman, D. Juhr, P.J. Gruber, U. Rub, G. Auburger, J.Q. Trojanowski, V.M. Lee, V.M. Van Deerlin, N.M. Bonini, and A.D. Gitler. 2010. Ataxin-2 intermediate-length polyglutamine expansions are associated with increased risk for ALS. *Nature*. 466:1069-1075.

Eymard-Pierre, E., G. Lesca, S. Dollet, F.M. Santorelli, M. di Capua, E. Bertini, and O. Boespflug-Tanguy. 2002. Infantile-onset ascending hereditary spastic paralysis is associated with mutations in the alsin gene. *Am. J. Hum. Genet.* 71:518-527.

Fang, F., P. Quinlan, W. Ye, M.K. Barber, D.M. Umbach, D.P. Sandler, and F. Kamel. 2009. Workplace exposures and the risk of amyotrophic lateral sclerosis. *Environ. Health Perspect.* 117:1387-1392.

Fasana, E., M. Fossati, A. Ruggiano, S. Brambillasca, C.C. Hoogenraad, F. Navone, M. Francolini, and N. Borgese. 2010. A VAPB mutant linked to amyotrophic lateral sclerosis generates a novel form of organized smooth endoplasmic reticulum. *FASEB J.* 24:1419-1430.

Fecto, F., J. Yan, S.P. Vemula, E. Liu, Y. Yang, W. Chen, J.G. Zheng, Y. Shi, N. Siddique, H. Arrat, S. Donkervoort, S. Ajroud-Driss, R.L. Sufit, S.L. Heller, H.-X. Deng, and T. Siddique. 2011. SQSTM1 mutations in familial and sporadic amyotrophic lateral sclerosis. *Arch. Neurol.* 68:1440-1446.

Ferraiuolo, L., J. Kirby, A.J. Grierson, M. Sendtner, and P.J. Shaw. 2011. Molecular pathways of motor neuron injury in amyotrophic lateral sclerosis. *Nat. Rev. Neurol.* 7:616-630.

Ferrante, R.J., S.E. Browne, L.A. Shinobu, A.C. Bowling, M.J. Baik, U. MacGarvey, N.W. Kowall, R.H. Brown, Jr., and M.F. Beal. 1997. Evidence of increased oxidative damage in both sporadic and familial amyotrophic lateral sclerosis. *J. Neurochem.* 69:2064-2074.

Ferri, A., M. Cozzolino, C. Crosio, M. Nencini, A. Casciati, E.B. Gralla, G. Rotilio, J.S. Valentine, and M.T. Carri. 2006. Familial ALS-superoxide dismutases associate with mitochondria and shift their redox potentials. *Proc. Natl. Acad. Sci. USA.* 103:13860-13865.

Figlewicz, D.A., A. Krizus, M.G. Martinoli, V. Meininger, M. Dib, G.A. Rouleau, and J.-P. Julien. 1994. Variants of the heavy neurofilament subunit are associated with the development of amyotrophic lateral sclerosis. *Hum. Mol. Genet.* 3:1757-1761.

Finsterer, J. 2010. Perspectives of Kennedy's disease. *J. Neurol. Sci.* 298:1-10.

Foran, E., and D. Trotti. 2009. Glutamate transporters and the excitotoxic path to motor neuron degeneration in amyotrophic lateral sclerosis. *Antioxid. Redox Signal.* 11:1587-1602.

Fransson, A., A. Ruusala, and P. Aspenström. 2003. Atypical Rho GTPases have roles in mitochondrial homeostasis and apoptosis. *J. Biol. Chem.* 278:6495-6502.

Fransson, S., A. Ruusala, and P. Aspenström. 2006. The atypical Rho GTPases Miro-1 and Miro-2 have essential roles in mitochondrial trafficking. *Biochem. Biophys. Res. Commun.* 344:500-510.

Frederick, R.L., J.M. McCaffery, K.W. Cunningham, K. Okamoto, and J.M. Shaw. 2004. Yeast Miro GTPase, Gem1p, regulates mitochondrial morphology via a novel pathway. *J Cell Biol*. 167:87-98.

Fu, X., C. Ng, D. Feng, and C. Liang. 2003. Cdc48p is required for the cell cycle

commitment point at Start via degradation of the G1-CDK inhibitor Far1p. *J. Cell Biol.* 163:21-26.

Fujita, K., M. Yamauchi, K. Shibayama, M. Ando, M. Honda, and Y. Nagata. 1996. Decreased cytochrome c oxidase activity but unchanged superoxide dismutase and glutathione peroxidase activities in the spinal cords of patients with amyotrophic lateral sclerosis. *J. Neurosci. Res.* 45:276-281.

Fujita, T., A.D. Maturana, J. Ikuta, J. Hamada, S. Walchli, T. Suzuki, H. Sawa, M.W. Wooten, T. Okajima, K. Tatematsu, K. Tanizawa, and S. Kuroda. 2007. Axonal guidance protein FEZ1 associates with tubulin and kinesin motor protein to transport mitochondria in neurites of NGF-stimulated PC12 cells. *Biochem. Biophys. Res. Commun.* 361:605-610.

Funke, A.D., M. Esser, A. Kruttgen, J. Weis, M. Mitne-Neto, M. Lazar, A.L. Nishimura, A.D. Sperfeld, P. Trillenberg, J. Senderek, M. Krasnianski, M. Zatz, S. Zierz, and M. Deschauer. 2010. The p.P56S mutation in the VAPB gene is not due to a single founder: the first European case. *Clin. Genet.* 77:302-303.

Gavin, A.C., M. Bosche, R. Krause, P. Grandi, M. Marzioch, A. Bauer, J. Schultz, J.M. Rick, A.M. Michon, C.M. Cruciat, M. Remor, C. Hofert, M. Schelder, M. Brajenovic, H. Ruffner, A. Merino, K. Klein, M. Hudak, D. Dickson, T. Rudi, V. Gnau, A. Bauch, S. Bastuck, B. Huhse, C. Leutwein, M.A. Heurtier, R.R. Copley, A. Edelmann, E. Querfurth, V. Rybin, G. Drewes, M. Raida, T. Bouwmeester, P. Bork, B. Seraphin, B. Kuster, G. Neubauer, and G. Superti-Furga. 2002. Functional organization of the yeast proteome by systematic analysis of protein complexes. *Nature*. 415:141-147.

Giess, R., M. Beck, R. Goetz, R.M. Nitsch, K.V. Toyka, and M. Sendtner. 2000. Potential role of LIF as a modifier gene in the pathogenesis of amyotrophic lateral sclerosis. *Neurology*. 54:1003-1005.

Giess, R., B. Holtmann, M. Braga, T. Grimm, B. Muller-Myhsok, K.V. Toyka, and M. Sendtner. 2002. Early onset of severe familial amyotrophic lateral sclerosis with a SOD-1 mutation: potential impact of CNTF as a candidate modifier gene. *Am. J. Hum. Genet.* 70:1277-1286.

Gindhart, J.G., J. Chen, M. Faulkner, R. Gandhi, K. Doerner, T. Wisniewski, and A. Nandlestadt. 2003. The kinesin-associated protein UNC-76 is required for axonal transport in the Drosophila nervous system. *Mol. Biol. Cell*. 14:3356-3365.

Gitcho, M.A., R.H. Baloh, S. Chakraverty, K. Mayo, J.B. Norton, D. Levitch, K.J. Hatanpaa, C.L. White, 3rd, E.H. Bigio, R. Caselli, M. Baker, M.T. Al-Lozi, J.C. Morris, A. Pestronk, R. Rademakers, A.M. Goate, and N.J. Cairns. 2008. TDP-43 A315T mutation in familial motor neuron disease. *Ann. Neurol.* 63:535-538.

Gkogkas, C., S. Middleton, A.M. Kremer, C. Wardrope, M. Hannah, T.H. Gillingwater, and P. Skehel. 2008. VAPB interacts with and modulates the activity of ATF6. *Hum. Mol. Genet.* 17:1517-1526.

Gkogkas, C., C. Wardrope, M. Hannah, and P. Skehel. 2011. The ALS8-associated mutant VAPBP56S is resistant to proteolysis in neurons. *J. Neurochem.* 117:286-294.

Glater, E.E., L.J. Megeath, R.S. Stowers, and T.L. Schwarz. 2006. Axonal transport of mitochondria requires milton to recruit kinesin heavy chain and is light chain independent. *J. Cell Biol.* 173:545-557.

Górska-Andrzejak, J., R.S. Stowers, J. Borycz, R. Kostyleva, T.L. Schwarz, and I.A. Meinertzhagen. 2003. Mitochondria are redistributed in Drosophila photoreceptors lacking Milton, a kinesin-associated protein. *J. Comp. Neurol.* 463:372-388.

Greenway, M.J., P.M. Andersen, C. Russ, S. Ennis, S. Cashman, C. Donaghy, V. Patterson, R. Swingler, D. Kieran, J. Prehn, K.E. Morrison, A. Green, K.R. Acharya, R.H. Brown, and O. Hardiman. 2006. ANG mutations segregate with familial and 'sporadic' amyotrophic lateral sclerosis. *Nat. Genet.* 38:411-413.

Grishin, A., H. Li, E.S. Levitan, and E. Zaks-Makhina. 2006. Identification of gamma-aminobutyric acid receptor-interacting factor 1 (TRAK2) as a trafficking factor for the K+ channel Kir2.1. *J. Biol. Chem.* 281:30104-30111.

Gros-Louis, F., R. Lariviere, G. Gowing, S. Laurent, W. Camu, J.P. Bouchard, V. Meininger, G.A. Rouleau, and J.P. Julien. 2004. A frameshift deletion in peripherin gene associated with amyotrophic lateral sclerosis. *J. Biol. Chem.*

Gros-Louis, F., I.A. Meijer, C.K. Hand, M.P. Dube, D.L. MacGregor, M.H. Seni, R.S. Devon, M.R. Hayden, F. Andermann, E. Andermann, and G.A. Rouleau. 2003. An ALS2 gene mutation causes hereditary spastic paraplegia in a Pakistani kindred. *Ann. Neurol.* 53:144-145.

Grosskreutz, J., K. Haastert, M. Dewil, P. Van Damme, G. Callewaert, W. Robberecht, R. Dengler, and L. Van Den Bosch. 2007. Role of mitochondria in kainate-induced fast Ca2+ transients in cultured spinal motor neurons. *Cell Calcium*. 42:59-69.

Grosskreutz, J., L. Van Den Bosch, and B.U. Keller. 2010. Calcium dysregulation in amyotrophic lateral sclerosis. *Cell Calcium*. 47:165-174.

Grynkiewicz, G., M. Poenie, and R.Y. Tsien. 1985. A new generation of Ca2+ indicators with greatly improved fluorescence properties. *J. Biol. Chem.* 260:3440-3450.

Guo, X., G.T. Macleod, A. Wellington, F. Hu, S. Panchumarthi, M. Schoenfield, L. Marin, M.P. Charlton, H.L. Atwood, and K.E. Zinsmaier. 2005. The GTPase dMiro is required for axonal transport of mitochondria to Drosophila synapses. *Neuron*. 47:379-393.

Hadano, S., C.K. Hand, H. Osuga, Y. Yanagisawa, A. Otomo, R.S. Devon, N. Miyamoto, J. Showguchi-Miyata, Y. Okada, R. Singaraja, D.A. Figlewicz, T. Kwiatkowski, B.A. Hosler, T. Sagie, J. Skaug, J. Nasir, R.H. Brown, Jr., S.W.

Scherer, G.A. Rouleau, M.R. Hayden, and J.E. Ikeda. 2001. A gene encoding a putative GTPase regulator is mutated in familial amyotrophic lateral sclerosis 2. *Nat. Genet.* 29:166-173.

Hafezparast, M., R. Klocke, C. Ruhrberg, A. Marquardt, A. Ahmad-Annuar, S. Bowen, G. Lalli, A.S. Witherden, H. Hummerich, S. Nicholson, P.J. Morgan, R. Oozageer, J.V. Priestley, S. Averill, V.R. King, S. Ball, J. Peters, T. Toda, A. Yamamoto, Y. Hiraoka, M. Augustin, D. Korthaus, S. Wattler, P. Wabnitz, C. Dickneite, S. Lampel, F. Boehme, G. Peraus, A. Popp, M. Rudelius, J. Schlegel, H. Fuchs, M.H. de Angelis, G. Schiavo, D.T. Shima, A.P. Russ, G. Stumm, J.E. Martin, and E.M. Fisher. 2003. Mutations in dynein link motor neuron degeneration to defects in retrograde transport. *Science*. 300:808-812.

Hamamoto, I., Y. Nishimura, T. Okamoto, H. Aizaki, M. Liu, Y. Mori, T. Abe, T. Suzuki, M.M.C. Lai, T. Miyamura, K. Moriishi, and Y. Matsuura. 2005. Human VAP-B Is Involved in Hepatitis C Virus Replication through Interaction with NS5A and NS5B. *J. Virol.* 79:13473-13482.

Hammond, J.W., C.F. Huang, S. Kaech, C. Jacobson, G. Banker, and K.J. Verhey. 2010. Posttranslational modifications of tubulin and the polarized transport of kinesin-1 in neurons. *Mol. Biol. Cell*. 21:572-583.

Han, S.M., H. Tsuda, Y. Yang, J. Vibbert, P. Cottee, S.-J. Lee, J. Winek, C. Haueter, H.J. Bellen, and M.A. Miller. 2012. Secreted VAPB/ALS8 major sperm protein domains modulate mitochondrial localization and morphology via growth cone guidance receptors. *Dev. Cell*. 22:348-362.

Hanada, K., K. Kumagai, S. Yasuda, Y. Miura, M. Kawano, M. Fukasawa, and M. Nishijima. 2003. Molecular machinery for non-vesicular trafficking of ceramide. *Nature*. 426:803-809.

Hand, C.K., J. Khoris, F. Salachas, F. Gros-Louis, A.A. Lopes, V. Mayeux-Portas, C.G. Brewer, R.H. Brown, Jr., V. Meininger, W. Camu, and G.A. Rouleau. 2002. A novel locus for familial amyotrophic lateral sclerosis, on chromosome 18q. *Am. J. Hum. Genet.* 70:251-256.

Harraz, M.M., J.J. Marden, W. Zhou, Y. Zhang, A. Williams, V.S. Sharov, K. Nelson, M. Luo, H. Paulson, C. Schoneich, and J.F. Engelhardt. 2008. SOD1 mutations disrupt redox-sensitive Rac regulation of NADPH oxidase in a familial ALS model. *J. Clin. Invest.* 118:659-670.

Hasegawa, M., T. Arai, T. Nonaka, F. Kametani, M. Yoshida, Y. Hashizume, T.G. Beach, E. Buratti, F. Baralle, M. Morita, I. Nakano, T. Oda, K. Tsuchiya, and H. Akiyama. 2008. Phosphorylated TDP-43 in frontotemporal lobar degeneration and amyotrophic lateral sclerosis. *Ann. Neurol.* 64:60-70.

Hayashi, T., R. Rizzuto, G. Hajnóczky, and T.P. Su. 2009. MAM: more than just a housekeeper. *Trends Cell Biol.* 19:81-88.

Hayashi, T., and T.P. Su. 2007. Sigma-1 receptor chaperones at the ER-mitochondrion interface regulate Ca(2+) signaling and cell survival. *Cell*. 131:596-610.

Hayward, C., S. Colville, R.J. Swingler, and D.J. Brock. 1999. Molecular genetic analysis of the APEX nuclease gene in amyotrophic lateral sclerosis. *Neurology*. 52:1899-1901.

He, Y., A. Benz, T. Fu, M. Wang, D.F. Covey, C.F. Zorumski, and S. Mennerick. 2002. Neuroprotective agent riluzole potentiates postsynaptic GABAA receptor function. *Neuropharmacology*. 42:199-209.

Heath, P.R., J. Tomkins, P.G. Ince, and P.J. Shaw. 2002. Quantitative assessment of AMPA receptor mRNA in human spinal motor neurons isolated by laser capture microdissection. *Neuroreport*. 13:1753-1757.

Hentati, A., K. Bejaoui, M.A. Pericak-Vance, F. Hentati, M.C. Speer, W.Y. Hung, D.A. Figlewicz, J. Haines, J. Rimmler, C. Ben Hamida, and et al. 1994. Linkage of recessive familial amyotrophic lateral sclerosis to chromosome 2q33-q35. *Nat. Genet.* 7:425-428.

Hetzer, M., H.H. Meyer, T.C. Walther, D. Bilbao-Cortes, G. Warren, and I.W. Mattaj. 2001. Distinct AAA-ATPase p97 complexes function in discrete steps of nuclear assembly. *Nat. Cell Biol.* 3:1086-1091.

Higgins, C.M.J., C. Jung, H. Ding, and Z. Xu. 2002. Mutant Cu, Zn superoxide dismutase that causes motoneuron degeneration is present in mitochondria in the CNS. *J. Neurosci.* 22:RC215.

Hirano, A., H. Donnenfeld, S. Sasaki, and I. Nakano. 1984a. Fine structural observations of neurofilamentous changes in amyotrophic lateral sclerosis. *J. Neuropathol. Exp. Neurol.* 43:461-470.

Hirano, A., I. Nakano, L.T. Kurland, D.W. Mulder, P.W. Holley, and G. Saccomanno. 1984b. Fine structural study of neurofibrillary changes in a family with amyotrophic lateral sclerosis. *J. Neuropathol. Exp. Neurol.* 43:471-480.

Hirokawa, N., S. Niwa, and Y. Tanaka. 2010. Molecular motors in neurons: transport mechanisms and roles in brain function, development, and disease. *Neuron*. 68:610-638.

Hirokawa, N., and Y. Noda. 2008. Intracellular transport and kinesin superfamily proteins, KIFs: structure, function, and dynamics. *Physiol. Rev.* 88:1089-1118.

Hirokawa, N., Y. Noda, Y. Tanaka, and S. Niwa. 2009. Kinesin superfamily motor proteins and intracellular transport. *Nat. Rev. Mol. Cell Biol.* 10:682-696.

Hirokawa, N., R. Sato-Yoshitake, T. Yoshida, and T. Kawashima. 1990. Brain dynein (MAP1C) localizes on both anterogradely and retrogradely transported membranous organelles in vivo. *J. Cell Biol.* 111:1027-1037.

Holasek, S.S., T.M. Wengenack, K.K. Kandimalla, C. Montano, D.M. Gregor, G.L. Curran, and J.F. Poduslo. 2005. Activation of the stress-activated MAP kinase, p38, but not JNK in cortical motor neurons during early presymptomatic stages of amyotrophic lateral sclerosis in transgenic mice. *Brain Res.* 1045:185-198.

Hollenbeck, P.J., D. Bray, and R.J. Adams. 1985. Effects of the uncoupling agents FCCP and CCCP on the saltatory movements of cytoplasmic organelles. *Cell Biol. Int. Rep.* 9:193-199.

Holthuis, J.C., G. van Meer, and K. Huitema. 2003. Lipid microdomains, lipid translocation and the organization of intracellular membrane transport (Review). *Mol. Membr. Biol.* 20:231-241.

Horner, R.D., K.G. Kamins, J.R. Feussner, S.C. Grambow, J. Hoff-Lindquist, Y. Harati, H. Mitsumoto, R. Pascuzzi, P.S. Spencer, R. Tim, D. Howard, T.C. Smith, M.A. Ryan, C.J. Coffman, and E.J. Kasarskis. 2003. Occurrence of amyotrophic lateral sclerosis among Gulf War veterans. *Neurology*. 61:742-749.

Hosler, B.A., T. Siddique, P.C. Sapp, W. Sailor, M.C. Huang, A. Hossain, J.R. Daube, M. Nance, C. Fan, J. Kaplan, W.Y. Hung, D. McKenna-Yasek, J.L. Haines, M.A. Pericak-Vance, H.R. Horvitz, and R.H. Brown, Jr. 2000. Linkage of familial amyotrophic lateral sclerosis with frontotemporal dementia to chromosome 9q21-q22. *JAMA*. 284:1664-1669.

Huang, H.-M., H.-C. Ou, and S.-J. Hsieh. 2000. Antioxidants prevent amyloid peptide-induced apoptosis and alteration of calcium homeostasis in cultured cortical neurons. *Life Sci.* 66:1879-1892.

Hurd, D.D., and W.M. Saxton. 1996. Kinesin mutations cause motor neuron disease phenotypes by disrupting fast axonal transport in Drosophila. *Genetics*. 144:1075-1085.

Ichimura, T., A. Wakamiya-Tsuruta, C. Itagaki, M. Taoka, T. Hayano, T. Natsume, and T. Isobe. 2002. Phosphorylation-dependent interaction of kinesin light chain 2 and the 14-3-3 protein. *Biochemistry*. 41:5566-5572.

Igaz, L.M., L.K. Kwong, A. Chen-Plotkin, M.J. Winton, T.L. Unger, Y. Xu, M. Neumann, J.Q. Trojanowski, and V.M. Lee. 2009. Expression Of TDP-43 C-terminal fragments in vitro recapitulates pathological features of TDP-43 proteinopathies. *J. Biol. Chem.* 284:8516-8524.

Igaz, L.M., L.K. Kwong, Y. Xu, A.C. Truax, K. Uryu, M. Neumann, C.M. Clark, L.B. Elman, B.L. Miller, M. Grossman, L.F. McCluskey, J.Q. Trojanowski, and V.M. Lee. 2008. Enrichment of C-terminal fragments in TAR DNA-binding protein-43 cytoplasmic inclusions in brain but not in spinal cord of frontotemporal lobar degeneration and amyotrophic lateral sclerosis. *Am. J. Pathol.* 173:182-194.

Igoudjil, A., J. Magrané, L.R. Fischer, H.J. Kim, I. Hervias, M. Dumont, C. Cortez, J.D. Glass, A.A. Starkov, and G. Manfredi. 2011. In vivo pathogenic role of mutant SOD1 localized in the mitochondrial intermembrane space. *J. Neurosci.* 31:15826-15837.

Iida, A., A. Takahashi, M. Kubo, S. Saito, N. Hosono, Y. Ohnishi, K. Kiyotani, T. Mushiroda, M. Nakajima, K. Ozaki, T. Tanaka, T. Tsunoda, S. Oshima, M. Sano, T. Kamei, T. Tokuda, M. Aoki, K. Hasegawa, K. Mizoguchi, M. Morita, Y. Takahashi, M. Katsuno, N. Atsuta, H. Watanabe, F. Tanaka, R. Kaji, I.

Nakano, N. Kamatani, S. Tsuji, G. Sobue, Y. Nakamura, and S. Ikegawa. 2011. A functional variant in ZNF512B is associated with susceptibility to amyotrophic lateral sclerosis in Japanese. *Hum. Mol. Genet.* 20:3684-3692.

Ikegami, K., R.L. Heier, M. Taruishi, H. Takagi, M. Mukai, S. Shimma, S. Taira, K. Hatanaka, N. Morone, I. Yao, P.K. Campbell, S. Yuasa, C. Janke, G.R. MacGregor, and M. Setou. 2007. Loss of α-tubulin polyglutamylation in ROSA22 mice is associated with abnormal targeting of KIF1A and modulated synaptic function. *Proc. Natl. Acad. Sci. USA.* 104:3213-3218.

Ikuta, J., A.s. Maturana, T. Fujita, T. Okajima, K. Tatematsu, K. Tanizawa, and S.i. Kuroda. 2007. Fasciculation and elongation protein zeta-1 (FEZ1) participates in the polarization of hippocampal neuron by controlling the mitochondrial motility. *Biochem. Biophys. Res. Commun.* 353:127-132.

Ince, P., J. Highley, J. Kirby, S. Wharton, H. Takahashi, M. Strong, and P. Shaw. 2011. Molecular pathology and genetic advances in amyotrophic lateral sclerosis: an emerging molecular pathway and the significance of glial pathology. *Acta Neuropathol.* 122:657-671.

Ince, P., N. Stout, P. Shaw, J. Slade, W. Hunziker, C.W. Heizmann, and K.G. Baimbridge. 1993. Parvalbumin and calbindin D-28k in the human motor system and in motor neuron disease. *Neuropathol. Appl. Neurobiol.* 19:291-299.

Ince, P.G., J. Tomkins, J.Y. Slade, N.M. Thatcher, and P.J. Shaw. 1998. Amyotrophic lateral sclerosis associated with genetic abnormalities in the gene encoding Cu/Zn superoxide dismutase: molecular pathology of five new cases, and comparison with previous reports and 73 sporadic cases of ALS. *J. Neuropath. Exp. Neurol.* 57:895-904.

Israelson, A., N. Arbel, S. Da Cruz, H. Ilieva, K. Yamanaka, V. Shoshan-Barmatz, and D.W. Cleveland. 2010. Misfolded mutant SOD1 directly inhibits VDAC1 conductance in a mouse model of inherited ALS. *Neuron*. 67:575-587.

Ito, D., M. Seki, Y. Tsunoda, H. Uchiyama, and N. Suzuki. 2011. Nuclear transport impairment of amyotrophic lateral sclerosis-linked mutations in FUS/TLS. *Ann. Neurol.* 69:152-162.

Itoh, T., G. Sobue, E. Ken, T. Mitsuma, A. Takahashi, and J.Q. Trojanowski. 1992. Phosphorylated high molecular weight neurofilament protein in the peripheral motor, sensory and sympathetic neuronal perikarya: system- dependent normal variations and changes in amyotrophic lateral sclerosis and multiple system atrophy. *Acta. Neuropathol.* 83:240-245.

Iyer, S.P.N., Y. Akimoto, and G.W. Hart. 2003. Identification and cloning of a novel family of coiled-coil domain proteins that interact with O-GlcNAc transferase. *J. Biol. Chem.* 278:5399-5409.

Jacobsson, J., P.A. Jonsson, P.M. Andersen, L. Forsgren, and S.L. Marklund. 2001. Superoxide dismutase in CSF from amyotrophic lateral sclerosis patients with and without CuZn-superoxide dismutase mutations. *Brain*. 124:1461-1466.

Jaiswal, M.K., W.D. Zech, M. Goos, C. Leutbecher, A. Ferri, A. Zippelius, M.T. Carri, R. Nau, and B.U. Keller. 2009. Impairment of mitochondrial calcium handling in a mtSOD1 cell culture model of motoneuron disease. *BMC Neurosci.* 10:64.

Johnson, J.O., J. Mandrioli, M. Benatar, Y. Abramzon, V.M. Van Deerlin, J.Q. Trojanowski, J.R. Gibbs, M. Brunetti, S. Gronka, J. Wuu, J. Ding, L. McCluskey, M. Martinez-Lage, D. Falcone, D.G. Hernandez, S. Arepalli, S. Chong, J.C. Schymick, J. Rothstein, F. Landi, Y.D. Wang, A. Calvo, G. Mora, M. Sabatelli, M.R. Monsurro, S. Battistini, F. Salvi, R. Spataro, P. Sola, G. Borghero, G. Galassi, S.W. Scholz, J.P. Taylor, G. Restagno, A. Chio, and B.J. Traynor. 2010. Exome sequencing reveals VCP mutations as a cause of familial ALS. *Neuron*. 68:857-864.

Johnston, J.A., M.J. Dalton, M.E. Gurney, and R.R. Kopito. 2000. Formation of high molecular weight complexes of mutant Cu,Zn-superoxide dismutase in a mouse model for familial amyotrophic lateral sclerosis. *Proc. Natl. Acad. Sci. USA*. 97:12571-12576.

Ju, J.S., R.A. Fuentealba, S.E. Miller, E. Jackson, D. Piwnica-Worms, R.H. Baloh, and C.C. Weihl. 2009. Valosin-containing protein (VCP) is required for autophagy and is disrupted in VCP disease. *J. Cell Biol.* 187:875-888.

Ju, J.S., S.E. Miller, P.I. Hanson, and C.C. Weihl. 2008. Impaired protein aggregate handling and clearance underlie the pathogenesis of p97/VCP-associated disease. *J. Biol. Chem.* 283:30289-30299.

Kabashi, E., P.N. Valdmanis, P. Dion, D. Spiegelman, B.J. McConkey, C. Vande Velde, J.P. Bouchard, L. Lacomblez, K. Pochigaeva, F. Salachas, P.F. Pradat, W. Camu, V. Meininger, N. Dupre, and G.A. Rouleau. 2008. TARDBP mutations in individuals with sporadic and familial amyotrophic lateral sclerosis. *Nat. Genet.* 40:572-574.

Kagiwada, S., K. Hosaka, M. Murata, J. Nikawa, and A. Takatsuki. 1998. The Saccharomyces cerevisiae SCS2 gene product, a homolog of a synaptobrevin-associated protein, is an integral membrane protein of the endoplasmic reticulum and is required for inositol metabolism. *J. Bacteriol.* 180:1700-1708.

Kaiser, S.E., J.H. Brickner, A.R. Reilein, T.D. Fenn, P. Walter, and A.T. Brunger. 2005. Structural basis of FFAT motif-mediated ER targeting. *Structure*. 13:1035-1045.

Kamel, F., D.M. Umbach, T.A. Lehman, L.P. Park, T.L. Munsat, J.M. Shefner, D.P. Sandler, H. Hu, and J.A. Taylor. 2003. Amyotrophic lateral sclerosis, lead, and genetic susceptibility: polymorphisms in the delta-aminolevulinic acid dehydratase and vitamin D receptor genes. *Environ. Health Perspect.* 111:1335-1339.

Kamel, F., D.M. Umbach, T.L. Munsat, J.M. Shefner, H. Hu, and D.P. Sandler. 2002. Lead exposure and amyotrophic lateral sclerosis. *Epidemiology*. 13:311-319.

Kanai, Y., N. Dohmae, and N. Hirokawa. 2004. Kinesin transports RNA: isolation and characterization of an RNA-transporting granule. *Neuron*. 43:513-525.

Kanai, Y., and M. Hediger. 2004. The glutamate/neutral amino acid transporter family SLC1: molecular, physiological and pharmacological aspects. *Pflügers Arch.* 447:469-479.

Kanai, Y., Y. Okada, Y. Tanaka, A. Harada, S. Terada, and N. Hirokawa. 2000. KIF5C, a novel neuronal kinesin enriched in motor neurons. *J. Neurosci.* 20:6374-6384.

Kanekura, K., I. Nishimoto, S. Aiso, and M. Matsuoka. 2006. Characterization of amyotrophic lateral sclerosis-linked P56S mutation of vesicle-associated membrane protein-associated protein B (VAPB/ALS8). *J. Biol. Chem.* 28:30223-30232.

Kang, J.S., J.H. Tian, P.Y. Pan, P. Zald, C. Li, C. Deng, and Z.H. Sheng. 2008. Docking of axonal mitochondria by syntaphilin controls their mobility and affects short-term facilitation. *Cell*. 132:137-148.

Kapitein, L.C., and C.C. Hoogenraad. 2011. Which way to go? Cytoskeletal organization and polarized transport in neurons. *Mol. Cell. Neurosci.* 46:9-20.

Kasarskis, E.J., J.H. Lindquist, C.J. Coffman, S.C. Grambow, J.R. Feussner, K.D. Allen, E.Z. Oddone, K.A. Kamins, R.D. Horner, and A.G.W.C.R. Team. 2009. Clinical aspects of ALS in Gulf War Veterans. *Amyotroph. Lateral Scler.* 10:35-41.

Kato, T., T. Katagiri, A. Hirano, T. Kawanami, and H. Sasaki. 1989. Lewy body-like hyaline inclusions in sporadic motor neuron disease are ubiquitinated. *Acta Neuropathol*. 77:391-396.

Kawahara, Y., K. Ito, H. Sun, H. Aizawa, I. Kanazawa, and S. Kwak. 2004. Glutamate receptors: RNA editing and death of motor neurons. *Nature*. 427:801.

Kawahara, Y., S. Kwak, H. Sun, K. Ito, H. Hashida, H. Aizawa, S.Y. Jeong, and I. Kanazawa. 2003. Human spinal motoneurons express low relative abundance of GluR2 mRNA: an implication for excitotoxicity in ALS. *J. Neurochem.* 85:680-689.

Kawamata, H., and G. Manfredi. 2008. Different regulation of wild-type and mutant Cu,Zn superoxide dismutase localization in mammalian mitochondria. *Hum. Mol. Genet.* 17:3303-3317.

Kawano, M., K. Kumagai, M. Nishijima, and K. Hanada. 2006. Efficient trafficking of ceramide from the endoplasmic reticulum to the Golgi apparatus requires a VAMP-associated protein-interacting FFAT motif of CERT. *J. Biol. Chem.* 281:30279-30288.

Kieran, D., M. Hafezparast, S. Bohnert, J.R. Dick, J. Martin, G. Schiavo, E.M. Fisher, and L. Greensmith. 2005. A mutation in dynein rescues axonal transport defects and extends the life span of ALS mice. *J. Cell Biol.* 169:561-567.

Kiernan, M.C., S. Vucic, B.C. Cheah, M.R. Turner, A. Eisen, O. Hardiman, J.R. Burrell, and M.C. Zoing. 2011. Amyotrophic lateral sclerosis. *Lancet*. 377:942-

955.

Kikuchi, H., G. Almer, S. Yamashita, C. Guegan, M. Nagai, Z. Xu, A.A. Sosunov, G.M. McKhann, 2nd, and S. Przedborski. 2006. Spinal cord endoplasmic reticulum stress associated with a microsomal accumulation of mutant superoxide dismutase-1 in an ALS model. *Proc. Natl. Acad. Sci. USA.* 103:6025-6030.

Kim, S., S.S. Leal, D. Ben Halevy, C.M. Gomes, and S. Lev. 2010. Structural requirements for VAP-B oligomerization and their implication in amyotrophic lateral sclerosis-associated VAP-B(P56S) neurotoxicity. *J. Biol. Chem.* 285:13839-13849.

Kirk, E., L.S. Chin, and L. Li. 2006. GRIF1 binds Hrs and is a new regulator of endosomal trafficking. *J. Cell Sci.* 119:4689-4701.

Kirkinezos, I.G., S.R. Bacman, D. Hernandez, J. Oca-Cossio, L.J. Arias, M.A. Perez-Pinzon, W.G. Bradley, and C.T. Moraes. 2005. Cytochrome c association with the inner mitochondrial membrane is impaired in the CNS of G93A-SOD1 mice. *J. Neurosci.* 25:164-172.

Kocsis, E., B.L. Trus, C.J. Steer, M.E. Bisher, and A.C. Steven. 1991. Image averaging of flexible fibrous macromolecules: the clathrin triskelion has an elastic proximal segment. *J. Struct. Biol.* 107:6-14.

Kong, J., and Z. Xu. 1998. Massive mitochondrial degeneration in motor neurons triggers the onset of amyotrophic lateral sclerosis in mice expressing a mutant SOD1. *J. Neurosci.* 18:3241-3250.

Konishi, Y., and M. Setou. 2009. Tubulin tyrosination navigates the kinesin-1 motor domain to axons. *Nat. Neurosci.* 12:559-567.

Koutsopoulos, O.S., D. Laine, L. Osellame, D.M. Chudakov, R.G. Parton, A.E. Frazier, and M.T. Ryan. 2010. Human Miltons associate with mitochondria and induce microtubule-dependent remodeling of mitochondrial networks. *Biochim. Biophys. Acta*. 1803:564-574.

Kovacs, G.G., J.R. Murrell, S. Horvath, L. Haraszti, K. Majtenyi, M.J. Molnar, H. Budka, B. Ghetti, and S. Spina. 2009. TARDBP variation associated with frontotemporal dementia, supranuclear gaze palsy, and chorea. *Mov. Disord.* 24:1843-1847.

Kovtun, A., R. Heumann, and M. Epple. 2009. Calcium phosphate nanoparticles for the transfection of cells. *Biomed. Mater. Eng.* 19:241-247.

Kruman, I.I., W.A. Pedersen, J.E. Springer, and M.P. Mattson. 1999. ALS-linked Cu/Zn-SOD mutation increases vulnerability of motor neurons to excitotoxicity by a mechanism involving increased oxidative stress and perturbed calcium homeostasis. *Exp. Neurol.* 160:28-39.

Kusaka, H., and A. Hirano. 1985. Fine structure of anterior horns in patients without

amyotrophic lateral sclerosis. *J. Neuropathol. Exp. Neurol.* 44:430-438.

Kuusisto, E., A. Salminen, and I. Alafuzoff. 2001. Ubiquitin-binding protein p62 is present in neuronal and glial inclusions in human tauopathies and synucleinopathies. *Neuroreport*. 12:2085-2090.

Kwiatkowski, T.J., Jr., D.A. Bosco, A.L. LeClerc, E. Tamrazian, C.R. Vanderburg, C. Russ, A. Davis, J. Gilchrist, E.J. Kasarskis, T. Munsat, P. Valdmanis, G.A. Rouleau, B.A. Hosler, P. Cortelli, P.J. de Jong, Y. Yoshinaga, J.L. Haines, M.A. Pericak-Vance, J. Yan, N. Ticozzi, T. Siddique, D. McKenna-Yasek, P.C. Sapp, H.R. Horvitz, J.E. Landers, and R.H. Brown, Jr. 2009. Mutations in the FUS/TLS gene on chromosome 16 cause familial amyotrophic lateral sclerosis. *Science*. 323:1205-1208.

Lacomblez, L., G. Bensimon, P.N. Leigh, P. Guillet, and V. Meininger. 1996. Dose-ranging study of riluzole in amyotrophic lateral sclerosis. Amyotrophic Lateral Sclerosis/Riluzole Study Group II. *Lancet*. 347:1425-1431.

Lai, C., C. Xie, S.G. McCormack, H.C. Chiang, M.K. Michalak, X. Lin, J. Chandran, H. Shim, M. Shimoji, M.R. Cookson, R.L. Huganir, J.D. Rothstein, D.L. Price, P.C. Wong, L.J. Martin, J.J. Zhu, and H. Cai. 2006. Amyotrophic lateral sclerosis 2-deficiency leads to neuronal degeneration in amyotrophic lateral sclerosis through altered AMPA receptor trafficking. *J. Neurosci.* 26:11798-11806.

Lambrechts, D., E. Storkebaum, M. Morimoto, J. Del-Favero, F. Desmet, S.L. Marklund, S. Wyns, V. Thijs, J. Andersson, I. van Marion, A. Al-Chalabi, S. Bornes, R. Musson, V. Hansen, L. Beckman, R. Adolfsson, H.S. Pall, H. Prats, S. Vermeire, P. Rutgeerts, S. Katayama, T. Awata, N. Leigh, L. Lang-Lazdunski, M. Dewerchin, C. Shaw, L. Moons, R. Vlietinck, K.E. Morrison, W. Robberecht, C. Van Broeckhoven, D. Collen, P.M. Andersen, and P. Carmeliet. 2003. VEGF is a modifier of amyotrophic lateral sclerosis in mice and humans and protects motoneurons against ischemic death. *Nat. Genet.* 34:383-394.

LaMonte, B.H., K.E. Wallace, B.A. Holloway, S.S. Shelly, J. Ascano, M. Tokito, T. Van Winkle, D.S. Howland, and E.L. Holzbaur. 2002. Disruption of dynein/dynactin inhibits axonal transport in motor neurons causing late-onset progressive degeneration. *Neuron*. 34:715-727.

Landers, J.E., A.L. Leclerc, L. Shi, A. Virkud, T. Cho, M.M. Maxwell, A.F. Henry, M. Polak, J.D. Glass, T.J. Kwiatkowski, A. Al-Chalabi, C.E. Shaw, P.N. Leigh, I. Rodriguez-Leyza, D. McKenna-Yasek, P.C. Sapp, and R.H. Brown, Jr. 2008. New VAPB deletion variant and exclusion of VAPB mutations in familial ALS. *Neurology*. 70:1179-1185.

Landers, J.E., J. Melki, V. Meininger, J.D. Glass, L.H. van den Berg, M.A. van Es, P.C. Sapp, P.W. van Vught, D.M. McKenna-Yasek, H.M. Blauw, T.J. Cho, M. Polak, L. Shi, A.M. Wills, W.J. Broom, N. Ticozzi, V. Silani, A. Ozoguz, I. Rodriguez-Leyva, J.H. Veldink, A.J. Ivinson, C.G. Saris, B.A. Hosler, A. Barnes-Nessa, N. Couture, J.H. Wokke, T.J. Kwiatkowski, Jr., R.A. Ophoff, S. Cronin, O. Hardiman, F.P. Diekstra, P.N. Leigh, C.E. Shaw, C.L. Simpson, V.K. Hansen, J.F. Powell, P. Corcia, F. Salachas, S. Heath, P. Galan, F. Georges, H.R.

Horvitz, M. Lathrop, S. Purcell, A. Al-Chalabi, and R.H. Brown, Jr. 2009. Reduced expression of the Kinesin-Associated Protein 3 (KIFAP3) gene increases survival in sporadic amyotrophic lateral sclerosis. *Proc. Natl. Acad. Sci. USA.* 106:9004-9009.

Langou, K., A. Moumen, C. Pellegrino, J. Aebischer, I. Medina, P. Aebischer, and C. Raoul. 2010. AAV-mediated expression of wildtype and ALS-linked mutant VAPB selectively triggers death of motoneurons through a Ca-dependent ER-associated pathway. *J. Neurochem.* 114:795-809.

Larcher, J.C., D. Boucher, S. Lazereg, F. Gros, and P. Denoulet. 1996. Interaction of kinesin motor domains with α- and β-tubulin subunits at a tau-independent binding site - Regulation by polyglutamylation. *J.Biol.Chem.* 271:22117-22124.

Latterich, M., K.-U. Fröhlich, and R. Schekman. 1995. Membrane fusion and the cell cycle: Cdc48p participates in the fusion of ER membranes. *Cell*. 82:885-893.

Laurent, F., G. Labesse, and P. de Wit. 2000. Molecular cloning and partial characterization of a plant VAP33 homologue with a major sperm protein domain. *Biochem. Biophys. Res. Commun.* 270:286-292.

Lawrence, C.J., R.K. Dawe, K.R. Christie, D.W. Cleveland, S.C. Dawson, S.A. Endow, L.S. Goldstein, H.V. Goodson, N. Hirokawa, J. Howard, R.L. Malmberg, J.R. McIntosh, H. Miki, T.J. Mitchison, Y. Okada, A.S. Reddy, W.M. Saxton, M. Schliwa, J.M. Scholey, R.D. Vale, C.E. Walczak, and L. Wordeman. 2004. A standardized kinesin nomenclature. *J. Cell Biol.* 167:19-22.

LeDizet, M., and G. Piperno. 1987. Identification of an acetylation site of Chlamydomonas alpha-tubulin. *Proc. Natl. Acad. Sci. USA*. 84:5720-5724.

Lee, M.K., J.R. Marszalek, and D.W. Cleveland. 1994. A mutant neurofilament subunit causes massive, selective motor neuron death: Implications for the pathogenesis of human motor neuron disease. *Neuron*. 13:975-988.

Leigh, P.N., B.H. Anderton, A. Dodson, J.M. Gallo, M. Swash, and D.M. Power. 1988. Ubiquitin deposits in anterior horn cells in motor neurone disease. *Neurosci. Lett.* 93:197-203.

Leterrier, J.F., D.A. Rusakov, B.D. Nelson, and M. Linden. 1994. Interactions between brain mitochondria and cytoskeleton: Evidence for specialized outer membrane domains involved in the association of cytoskeleton-associated proteins to mitochondria in situ and in vitro. *Micros. Res. Tech.* 27:233-261.

Letourneur, F., E.C. Gaynor, S. Hennecke, C. Demolliere, R. Duden, S.D. Emr, H. Riezman, and P. Cosson. 1994. Coatomer is essential for retrieval of dilysine-tagged proteins to the endoplasmic reticulum. *Cell*. 79:1199-1207.

Leung, C.L., C.Z. He, P. Kaufmann, S.S. Chin, A. Naini, R.K. Liem, H. Mitsumoto, and A.R. Hays. 2004. A pathogenic peripherin gene mutation in a patient with amyotrophic lateral sclerosis. *Brain. Pathol.* 14:290-296.

Lev, S. 2010. Non-vesicular lipid transport by lipid-transfer proteins and beyond. *Nat. Rev. Mol. Cell Biol.* 11:739-750.

Levy, J.R., C.J. Sumner, J.P. Caviston, M.K. Tokito, S. Ranganathan, L.A. Ligon, K.E. Wallace, B.H. LaMonte, G.G. Harmison, I. Puls, K.H. Fischbeck, and E.L. Holzbaur. 2006. A motor neuron disease-associated mutation in p150Glued perturbs dynactin function and induces protein aggregation. *J. Cell Biol.* 172:733-745.

Li, G., M. Mongillo, K.T. Chin, H. Harding, D. Ron, A.R. Marks, and I. Tabas. 2009. Role of ERO1-alpha-mediated stimulation of inositol 1,4,5-triphosphate receptor activity in endoplasmic reticulum stress-induced apoptosis. *J. Cell Biol.* 186:783-792.

Liao, G., and G.G. Gundersen. 1998. Kinesin is a candidate for cross-bridging microtubules and intermediate filaments. *J. Biol. Chem.* 273:9797-9803.

Lill, C.M., O. Abel, L. Bertram, and A. Al-Chalabi. 2011. Keeping up with genetic discoveries in amyotrophic lateral sclerosis: The ALSoD and ALSGene databases. *Amyotroph. Lateral Scler.* 12:238-249.

Lin, C.-L.G., L.A. Bristol, L. Jin, M. Dykes-Hoberg, T. Crawford, L. Clawson, and J.D. Rothstein. 1998. Aberrant RNA processing in a neurodegenerative disease: the cause of absent EAAT2, a glutamate transporter, in Amyotrophic Lateral Sclerosis. *Neuron*. 20:589-602.

Lin, J.H., P. Walter, and T.S. Yen. 2008. Endoplasmic reticulum stress in disease pathogenesis. *Annu. Rev. Pathol.* 3:399-425.

Lipscombe, D., D.V. Madison, M. Poenie, H. Reuter, R.W. Tsien, and R.Y. Tsien. 1988. Imaging of cytosolic Ca2+ transients arising from Ca2+ stores and Ca2+ channels in sympathetic neurons. *Neuron*. 1:355-365.

Litvak, V., Y.D. Shaul, M. Shulewitz, R. Amarilio, S. Carmon, and S. Lev. 2002. Targeting of Nir2 to lipid droplets is regulated by a specific threonine residue within its PI-transfer domain. *Curr. Biol.* 12:1513-1518.

Liu-Yesucevitz, L., A. Bilgutay, Y.J. Zhang, T. Vanderweyde, A. Citro, T. Mehta, N. Zaarur, A. McKee, R. Bowser, M. Sherman, L. Petrucelli, and B. Wolozin. 2010. Tar DNA binding protein-43 (TDP-43) associates with stress granules: analysis of cultured cells and pathological brain tissue. *PLoS One*. 5:e13250.

Liu, J., C. Lillo, P.A. Jonsson, C.V. Velde, C.M. Ward, T.M. Miller, J.R. Subramaniam, J.D. Rothstein, S. Marklund, P.M. Andersen, T. Brannstrom, O. Gredal, P.C. Wong, D.S. Williams, and D.W. Cleveland. 2004. Toxicity of familial ALS-linked SOD1 mutants from selective recruitment to spinal mitochondria. *Neuron*. 43:5-17.

Loewen, C.J., A. Roy, and T.P. Levine. 2003. A conserved ER targeting motif in three families of lipid binding proteins and in Opi1p binds VAP. *EMBO J.* 22:2025-2035.

Logroscino, G., B.J. Traynor, O. Hardiman, A. Chio, D. Mitchell, R.J. Swingler, A. Millul, E. Benn, and E. Beghi. 2010. Incidence of amyotrophic lateral sclerosis in Europe. *J. Neurol. Neurosurg. Psychiatry*. 81:385-390.

Lowe, J., G. Lennox, D. Jefferson, K. Morrell, D. McQuire, T. Gray, M. Landon, F.J. Doherty, and R.J. Mayer. 1988. A filamentous inclusion body within anterior horn neurones in motor neurone disease defined by immunocytochemical localisation of ubiquitin. *Neurosci. Lett.* 94:203-210.

Luty, A.A., J.B. Kwok, C. Dobson-Stone, C.T. Loy, K.G. Coupland, H. Karlstrom, T. Sobow, J. Tchorzewska, A. Maruszak, M. Barcikowska, P.K. Panegyres, C. Zekanowski, W.S. Brooks, K.L. Williams, I.P. Blair, K.A. Mather, P.S. Sachdev, G.M. Halliday, and P.R. Schofield. 2010. Sigma nonopioid intracellular receptor 1 mutations cause frontotemporal lobar degeneration-motor neuron disease. *Ann. Neurol.* 68:639-649.

Ma, H., Q. Cai, W. Lu, Z.H. Sheng, and S. Mochida. 2009. KIF5B motor adaptor syntabulin maintains synaptic transmission in sympathetic neurons. *J. Neurosci.* 29:13019-13029.

MacAskill, A.F., K. Brickley, F.A. Stephenson, and J.T. Kittler. 2009a. GTPase dependent recruitment of Grif-1 by Miro1 regulates mitochondrial trafficking in hippocampal neurons. *Mol. Cell Neurosci.* 40:301-312.

MacAskill, A.F., J.E. Rinholm, A.E. Twelvetrees, I.L. Arancibia-Carcamo, J. Muir, A. Fransson, P. Aspenstrom, D. Attwell, and J.T. Kittler. 2009b. Miro1 is a calcium sensor for glutamate receptor-dependent localization of mitochondria at synapses. *Neuron*. 61:541-555.

Mackenzie, I.R., E.H. Bigio, P.G. Ince, F. Geser, M. Neumann, N.J. Cairns, L.K. Kwong, M.S. Forman, J. Ravits, H. Stewart, A. Eisen, L. McClusky, H.A. Kretzschmar, C.M. Monoranu, J.R. Highley, J. Kirby, T. Siddique, P.J. Shaw, V.M. Lee, and J.Q. Trojanowski. 2007. Pathological TDP-43 distinguishes sporadic amyotrophic lateral sclerosis from amyotrophic lateral sclerosis with SOD1 mutations. *Ann. Neurol.* 61:427-434.

Magrané, J., M.A. Sahawneh, S. Przedborski, Á.l.G. Estévez, and G. Manfredi. 2012. Mitochondrial dynamics and bioenergetic dysfunction is associated with synaptic alterations in mutant SOD1 motor neurons. *J. Neurosci.* 32:229-242.

Majounie, E., A.E. Renton, K. Mok, E.G. Dopper, A. Waite, S. Rollinson, A. Chio, G. Restagno, N. Nicolaou, J. Simon-Sanchez, J.C. van Swieten, Y. Abramzon, J.O. Johnson, M. Sendtner, R. Pamphlett, R.W. Orrell, S. Mead, K.C. Sidle, H. Houlden, J.D. Rohrer, K.E. Morrison, H. Pall, K. Talbot, O. Ansorge, D.G. Hernandez, S. Arepalli, M. Sabatelli, G. Mora, M. Corbo, F. Giannini, A. Calvo, E. Englund, G. Borghero, G.L. Floris, A.M. Remes, H. Laaksovirta, L. McCluskey, J.Q. Trojanowski, V.M. Van Deerlin, G.D. Schellenberg, M.A. Nalls, V.E. Drory, C.S. Lu, T.H. Yeh, H. Ishiura, Y. Takahashi, S. Tsuji, I. Le Ber, A. Brice, C. Drepper, N. Williams, J. Kirby, P. Shaw, J. Hardy, P.J. Tienari, P. Heutink, H.R. Morris, S. Pickering-Brown, and B.J. Traynor. 2012. Frequency of the C9orf72 hexanucleotide repeat expansion in patients with

amyotrophic lateral sclerosis and frontotemporal dementia: a cross-sectional study. *Lancet Neurol*. 11:323-330.

Manfredi, G., and Z. Xu. 2005. Mitochondrial dysfunction and its role in motor neuron degeneration in ALS. *Mitochondrion*. 5:77-87.

Manser, C., F. Guillot, A. Vagnoni, J. Davies, K.F. Lau, D.M. McLoughlin, K.J. De Vos, and C.C.J. Miller. 2011. Lemur tyrosine kinase-2 signalling regulates kinesin-1 light chain-2 phosphorylation and binding of Smad2 cargo. *Oncogene*. 31:2773-2782.

Marciniak, S.J., C.Y. Yun, S. Oyadomari, I. Novoa, Y. Zhang, R. Jungreis, K. Nagata, H.P. Harding, and D. Ron. 2004. CHOP induces death by promoting protein synthesis and oxidation in the stressed endoplasmic reticulum. *Genes Dev.* 18:3066-3077.

Marden, J.J., M.M. Harraz, A.J. Williams, K. Nelson, M. Luo, H. Paulson, and J.F. Engelhardt. 2007. Redox modifier genes in amyotrophic lateral sclerosis in mice. *J. Clin. Invest.* 117:2913-2919.

Marinković, P., M.S. Reuter, M.S. Brill, L. Godinho, M. Kerschensteiner, and T. Misgeld. 2012. Axonal transport deficits and degeneration can evolve independently in mouse models of amyotrophic lateral sclerosis. *Proc. Natl. Acad. Sci. USA*. 109:4296-4301.

Maruyama, H., H. Morino, H. Ito, Y. Izumi, H. Kato, Y. Watanabe, Y. Kinoshita, M. Kamada, H. Nodera, H. Suzuki, O. Komure, S. Matsuura, K. Kobatake, N. Morimoto, K. Abe, N. Suzuki, M. Aoki, A. Kawata, T. Hirai, T. Kato, K. Ogasawara, A. Hirano, T. Takumi, H. Kusaka, K. Hagiwara, R. Kaji, and H. Kawakami. 2010. Mutations of optineurin in amyotrophic lateral sclerosis. *Nature*. 465:223-226.

Mattiazzi, M., M. D'Aurelio, C.D. Gajewski, K. Martushova, M. Kiaei, M.F. Beal, and G. Manfredi. 2002. Mutated human SOD1 causes dysfunction of oxidative phosphorylation in mitochondria of transgenic mice. *J. Biol. Chem.* 277:29626-29633.

Maturana, A.D., T. Fujita, and S.i. Kuroda. 2010. Functions of fasciculation and elongation protein zeta-1 (FEZ1) in the brain. *ScientificWorldJournal*. 10:1646-1654.

Matz, M.V., A.F. Fradkov, Y.A. Labas, A.P. Savitsky, A.G. Zaraisky, M.L. Markelov, and S.A. Lukyanov. 1999. Fluorescent proteins from nonbioluminescent Anthozoa species. *Nat. Biotech.* 17:969-973.

McCommis, K.S., and C.P. Baines. 2011. The role of VDAC in cell death: Friend or foe? *Biochim. Biophys. Acta*. 1818:1444-1450.

Melchior, F., T. Guan, N. Yokoyama, T. Nishimoto, and L. Gerace. 1995. GTP hydrolysis by Ran occurs at the nuclear pore complex in an early step of protein import. *J. Cell Biol.* 131:571-581.

Menzies, F.M., M.R. Cookson, R.W. Taylor, D.M. Turnbull, Z.M.A. Chrzanowska-Lightowlers, L. Dong, D.A. Figlewicz, and P.J. Shaw. 2002. Mitochondrial dysfunction in a cell culture model of familial amyotrophic lateral sclerosis. *Brain*. 125:1522-1533.

Mikoshiba, K. 2006. Inositol 1,4,5-trisphosphate (IP3) receptors and their role in neuronal cell function. *J. Neurochem.* 97:1627-1633.

Millecamps, S., J. Robertson, R. Lariviere, J. Mallet, and J.P. Julien. 2006. Defective axonal transport of neurofilament proteins in neurons overexpressing peripherin. *J. Neurochem.* 98:926-938.

Millecamps, S., F. Salachas, C. Cazeneuve, P. Gordon, B. Bricka, A. Camuzat, L. Guillot-Noel, O. Russaouen, G. Bruneteau, P.F. Pradat, N. Le Forestier, N. Vandenberghe, V. Danel-Brunaud, N. Guy, C. Thauvin-Robinet, L. Lacomblez, P. Couratier, D. Hannequin, D. Seilhean, I. Le Ber, P. Corcia, W. Camu, A. Brice, G. Rouleau, E. Leguern, and V. Meininger. 2010. SOD1, ANG, VAPB, TARDBP, and FUS mutations in familial amyotrophic lateral sclerosis: genotype-phenotype correlations. *J. Med. Genet.* 47:554-560.

Miller, K.E., and M.P. Sheetz. 2004. Axonal mitochondrial transport and potential are correlated. *J. Cell Sci.* 117:2791-2804.

Miller, R.G., D.H. Moore, 2nd, D.F. Gelinas, V. Dronsky, M. Mendoza, R.J. Barohn, W. Bryan, J. Ravits, E. Yuen, H. Neville, S. Ringel, M. Bromberg, J. Petajan, A.A. Amato, C. Jackson, W. Johnson, R. Mandler, P. Bosch, B. Smith, M. Graves, M. Ross, E.J. Sorenson, P. Kelkar, G. Parry, and R. Olney. 2001. Phase III randomized trial of gabapentin in patients with amyotrophic lateral sclerosis. *Neurology*. 56:843-848.

Mironov, S.L. 2007. ADP Regulates Movements of Mitochondria in Neurons. *Biophys. J.* 92:2944-2952.

Mironov, S.L. 2009. Complexity of mitochondrial dynamics in neurons and its control by ADP produced during synaptic activity. *Int. J. Biochem. Cell Biol.* 41:2005-2014.

Mironov, S.L., and N. Symonchuk. 2006. ER vesicles and mitochondria move and communicate at synapses. *J. Cell Sci.* 119:4926-4934.

Misgeld, T., M. Kerschensteiner, F.M. Bareyre, R.W. Burgess, and J.W. Lichtman. 2007. Imaging axonal transport of mitochondria in vivo. *Nat. Methods*.

Mitchell, J., P. Paul, H.J. Chen, A. Morris, M. Payling, M. Falchi, J. Habgood, S. Panoutsou, S. Winkler, V. Tisato, A. Hajitou, B. Smith, C. Vance, C. Shaw, N.D. Mazarakis, and J. de Belleroche. 2010. Familial amyotrophic lateral sclerosis is associated with a mutation in D-amino acid oxidase. *Proc. Natl. Acad. Sci. USA*. 107:7556-7561.

Mitne-Neto, M., M. Machado-Costa, M.C. Marchetto, M.H. Bengtson, C.A. Joazeiro, H. Tsuda, H.J. Bellen, H.C. Silva, A.S. Oliveira, M. Lazar, A.R. Muotri, and M.

Zatz. 2011. Downregulation of VAPB expression in motor neurons derived from induced pluripotent stem cells of ALS8 patients. *Hum. Mol. Genet.* 20:3642-3652.

Mitne-Neto, M., C.R. Ramos, D.C. Pimenta, J.S. Luz, A.L. Nishimura, F.A. Gonzales, C.C. Oliveira, and M. Zatz. 2007. A mutation in human VAP-B-MSP domain, present in ALS patients, affects the interaction with other cellular proteins. *Protein Expr. Purif.* 55:139-146.

Mizuno, Y., M. Amari, M. Takatama, H. Aizawa, B. Mihara, and K. Okamoto. 2006a. Immunoreactivities of p62, an ubiqutin-binding protein, in the spinal anterior horn cells of patients with amyotrophic lateral sclerosis. *J. Neurol. Sci.* 249:13-18.

Mizuno, Y., M. Amari, M. Takatama, H. Aizawa, B. Mihara, and K. Okamoto. 2006b. Transferrin localizes in Bunina bodies in amyotrophic lateral sclerosis. *Acta Neuropathol*. 112:597-603.

Mizuno, Y., Y. Fujita, M. Takatama, and K. Okamoto. 2011. Peripherin partially localizes in Bunina bodies in amyotrophic lateral sclerosis. *J. Neurol. Sci.* 302:14-18.

Morfini, G., G. Pigino, G. Szebenyi, Y. You, S. Pollema, and S.T. Brady. 2006. JNK mediates pathogenic effects of polyglutamine-expanded androgen receptor on fast axonal transport. *Nat. Neurosci.* 9:906-916.

Morfini, G.A., Y.M. You, S.L. Pollema, A. Kaminska, K. Liu, K. Yoshioka, B. Bjorkblom, E.T. Coffey, C. Bagnato, D. Han, C.F. Huang, G. Banker, G. Pigino, and S.T. Brady. 2009. Pathogenic huntingtin inhibits fast axonal transport by activating JNK3 and phosphorylating kinesin. *Nat. Neurosci.* 12:864-871.

Morris, R.L., and P.J. Hollenbeck. 1993. The regulation of bidirectional mitochondrial transport is coordinated with axonal outgrowth. *J. Cell Sci.* 104:917-927.

Morris, R.L., and P.J. Hollenbeck. 1995. Axonal transport of mitochondria along microtubules and F-actin in living vertebrate neurons. *J. Cell Biol.* 131:1315-1326.

Moscat, J., M.T. Diaz-Meco, and M.W. Wooten. 2007. Signal integration and diversification through the p62 scaffold protein. *Trends Biochem. Sci.* 32:95-100.

Moulard, B., A. Sefiani, A. Laamri, A. Malafosse, and W. Camu. 1996. Apolipoprotein E genotyping in sporadic amyotrophic lateral sclerosis: evidence for a major influence on the clinical presentation and prognosis. *J. Neurol. Sci.* 139, Supplement:34-37.

Moumen, A., I. Virard, and C. Raoul. 2011. Accumulation of wildtype and ALS-linked mutated VAPB impairs activity of the proteasome. *PLoS One*. 6:e26066.

Munoz, D.G., C. Greene, D.P. Perl, and D.J. Selkoe. 1988. Accumulation of

phosphorylated neurofilaments in anterior horn motoneurons of amyotrophic lateral sclerosis patients. *J. Neuropathol. Exp. Neurol.* 47:9-18.

Münch, C., R. Sedlmeier, T. Meyer, V. Homberg, A.D. Sperfeld, A. Kurt, J. Prudlo, G. Peraus, C.O. Hanemann, G. Stumm, and A.C. Ludolph. 2004. Point mutations of the p150 subunit of dynactin (DCTN1) gene in ALS. *Neurology*. 63:724-726.

Nakagawa, T., H. Zhu, N. Morishima, E. Li, J. Xu, B.A. Yankner, and J.Y. Yuan. 2000. Caspase-12 mediates endoplasmic-reticulum-specific apoptosis and cytotoxicity by amyloid-β. *Nature*. 403:98-103.

Nakano, T., K. Nakaso, K. Nakashima, and E. Ohama. 2004. Expression of ubiquitin-binding protein p62 in ubiquitin-immunoreactive intraneuronal inclusions in amyotrophic lateral sclerosis with dementia: analysis of five autopsy cases with broad clinicopathological spectrum. *Acta Neuropathol.* 107:359-364.

Nangaku, M., R. Sato-Yoshitake, Y. Okada, Y. Noda, R. Takemura, H. Yamazaki, and N. Hirokawa. 1994. KIF1B, a novel microtubule plus end-directed monomeric motor protein for transport of mitochondria. *Cell*. 79:1209-1220.

Neumann, M., D.M. Sampathu, L.K. Kwong, A.C. Truax, M.C. Micsenyi, T.T. Chou, J. Bruce, T. Schuck, M. Grossman, C.M. Clark, L.F. McCluskey, B.L. Miller, E. Masliah, I.R. Mackenzie, H. Feldman, W. Feiden, H.A. Kretzschmar, J.Q. Trojanowski, and V.M. Lee. 2006. Ubiquitinated TDP-43 in frontotemporal lobar degeneration and amyotrophic lateral sclerosis. *Science*. 314:130-113.

Nguyen, M.D., R.C. Lariviere, and J.P. Julien. 2001. Deregulation of Cdk5 in a mouse model of ALS: Toxicity alleviated by perikaryal neurofilament inclusions. *Neuron*. 30:135-147.

Nicholls, D.G., and S.L. Budd. 2000. Mitochondria and neuronal survival. *Physiol. Rev.* 80:315-360.

Niclas, J., F. Navone, N. Hom-Booher, and R.D. Vale. 1994. Cloning and localization of a conventional kinesin motor expressed exclusively in neurons. *Neuron*. 12:1059-1072.

Nicoletti, F., J. Bockaert, G.L. Collingridge, P.J. Conn, F. Ferraguti, D.D. Schoepp, J.T. Wroblewski, and J.P. Pin. 2011. Metabotropic glutamate receptors: From the workbench to the bedside. *Neuropharmacology*. 60:1017-1041.

Nikawa, J., A. Murakami, E. Esumi, and K. Hosaka. 1995. Cloning and sequence of the SCS2 gene, which can suppress the defect of INO1 expression in an inositol auxotrophic mutant of Saccharomyces cerevisiae. *J. Biochem.* 118:39-45.

Nikolic, M., H. Dudek, Y.T. Kwon, Y.F.M. Ramos, and L.H. Tsai. 1996. The cdk5/p35 kinase is essential for neurite outgrowth during neuronal differentiation. *Genes Dev.* 10:816-825.

Nishimura, A.L., A. Al-Chalabi, and M. Zatz. 2005. A common founder for amyotrophic lateral sclerosis type 8 (ALS8) in the Brazilian population. *Hum.*

*Genet.* 118:499-500.

Nishimura, A.L., M. Mitne-Neto, H.C. Silva, A. Richieri-Costa, S. Middleton, D. Cascio, F. Kok, J.R. Oliveira, T. Gillingwater, J. Webb, P. Skehel, and M. Zatz. 2004. A mutation in the vesicle-trafficking protein VAPB causes late-onset spinal muscular atrophy and amyotrophic lateral sclerosis. *Am. J. Hum. Genet.* 75:822-831.

Nishimura, Y., M. Hayashi, H. Inada, and T. Tanaka. 1999. Molecular cloning and characterization of mammalian homologues of vesicle-associated membrane protein-associated (VAMP-associated) proteins. *Biochem. Biophys. Res. Commun.* 254:21-26.

Nishitoh, H., H. Kadowaki, A. Nagai, T. Maruyama, T. Yokota, H. Fukutomi, T. Noguchi, A. Matsuzawa, K. Takeda, and H. Ichijo. 2008. ALS-linked mutant SOD1 induces ER stress- and ASK1-dependent motor neuron death by targeting Derlin-1. *Genes Dev.* 22:1451-1464.

Nishitoh, H., A. Matsuzawa, K. Tobiume, K. Saegusa, K. Takeda, K. Inoue, S. Hori, A. Kakizuka, and H. Ichijo. 2002. ASK1 is essential for endoplasmic reticulum stress-induced neuronal cell death triggered by expanded polyglutamine repeats. *Genes Dev.* 16:1345-1355.

Ohno, N., G.J. Kidd, D. Mahad, S. Kiryu-Seo, A. Avishai, H. Komuro, and B.D. Trapp. 2011. Myelination and axonal electrical activity modulate the distribution and motility of mitochondria at CNS nodes of ranvier. *J. Neurosci.* 31:7249-7258.

Okamoto, K., S. Hirai, M. Amari, M. Watanabe, and A. Sakurai. 1993. Bunina bodies in amyotrophic lateral sclerosis immunostained with rabbit anti-cystatin C serum. *Neurosci. Lett.* 162:125-128.

Okamoto, K., Y. Mizuno, and Y. Fujita. 2008. Bunina bodies in amyotrophic lateral sclerosis. *Neuropathology*. 28:109-115.

Olkowski, Z.L. 1998. Mutant AP endonuclease in patients with amyotrophic lateral sclerosis. *Neuroreport*. 9:239-242.

Orci, L., M. Stamnes, M. Ravazzola, M. Amherdt, A. Perrelet, T.H. Sollner, and J.E. Rothman. 1997. Bidirectional transport by distinct populations of COPI-coated vesicles. *Cell*. 90:335-349.

Orlacchio, A., C. Babalini, A. Borreca, C. Patrono, R. Massa, S. Basaran, R.P. Munhoz, E.A. Rogaeva, P.H. St George-Hyslop, G. Bernardi, and T. Kawarai. 2010. SPATACSIN mutations cause autosomal recessive juvenile amyotrophic lateral sclerosis. *Brain*. 133:591-598.

Orru, S., V. Mascia, M. Casula, E. Giuressi, A. Loizedda, C. Carcassi, M. Giagheddu, and L. Contu. 1999. Association of monoamine oxidase B alleles with age at onset in amyotrophic lateral sclerosis. *Neuromuscul. Disord.* 9:593-597.

Otomo, A., S. Hadano, T. Okada, H. Mizumura, R. Kunita, H. Nishijima, J. Showguchi-

Miyata, Y. Yanagisawa, E. Kohiki, E. Suga, M. Yasuda, H. Osuga, T. Nishimoto, S. Narumiya, and J.E. Ikeda. 2003. ALS2, a novel guanine nucleotide exchange factor for the small GTPase Rab5, is implicated in endosomal dynamics. *Hum. Mol. Genet.* 12:1671-1687.

Panas, M., G. Karadima, N. Kalfakis, O. Psarrou, P. Floroskoufi, A. Kladi, M.B. Petersen, and D. Vassilopoulos. 2000. Genotyping of presenilin-1 polymorphism in amyotrophic lateral sclerosis. *J. Neurol.* 247:940-942.

Panico, R., W.H. Powell, and J.-C. Richer. 1993. A Guide to IUPAC Nomenclature of Organic Compounds, Recommendations 1993. Blackwell Scientific Publications, Oxford.

Parkinson, N., P.G. Ince, M.O. Smith, R. Highley, G. Skibinski, P.M. Andersen, K.E. Morrison, H.S. Pall, O. Hardiman, J. Collinge, P.J. Shaw, and E.M. Fisher. 2006. ALS phenotypes with mutations in CHMP2B (charged multivesicular body protein 2B). *Neurology*. 67:1074-1077.

Pasinelli, P., M.E. Belford, N. Lennon, B.J. Bacskai, B.T. Hyman, D. Trotti, and R.H. Brown, Jr. 2004. Amyotrophic lateral sclerosis-associated SOD1 mutant proteins bind and aggregate with Bcl-2 in spinal cord mitochondria. *Neuron*. 43:19-30.

Pennetta, G., P. Hiesinger, R. Fabian-Fine, I. Meinertzhagen, and H. Bellen. 2002. Drosophila VAP-33A directs bouton formation at neuromuscular junctions in a dosage-dependent manner. *Neuron*. 35:291-306.

Peretti, D., N. Dahan, E. Shimoni, K. Hirschberg, and S. Lev. 2008. Coordinated lipid transfer between the endoplasmic reticulum and the Golgi complex requires the VAP Proteins and is essential for Golgi-mediated transport. *Mol. Biol. Cell*. 19:3871-3884.

Perry, J.J.P., D.S. Shin, E.D. Getzoff, and J.A. Tainer. 2010. The structural biochemistry of the superoxide dismutases. *Biochim. Biophys. Acta*. 1804:245-262.

Piao, Y.S., K. Wakabayashi, A. Kakita, M. Yamada, S. Hayashi, T. Morita, F. Ikuta, K. Oyanagi, and H. Takahashi. 2003. Neuropathology with clinical correlations of sporadic amyotrophic lateral sclerosis: 102 autopsy cases examined between 1962 and 2000. *Brain Pathol*. 13:10-22.

Pilling, A.D., D. Horiuchi, C.M. Lively, and W.M. Saxton. 2006. Kinesin-1 and Dynein are the primary motors for fast transport of mitochondria in Drosophila motor axons. *Mol. Biol. Cell*. 17:2057-2068.

Polymenidou, M., C. Lagier-Tourenne, K.R. Hutt, S.C. Huelga, J. Moran, T.Y. Liang, S.-C. Ling, E. Sun, E. Wancewicz, C. Mazur, H. Kordasiewicz, Y. Sedaghat, J.P. Donohue, L. Shiue, C.F. Bennett, G.W. Yeo, and D.W. Cleveland. 2011. Long pre-mRNA depletion and RNA missplicing contribute to neuronal vulnerability from loss of TDP-43. *Nat. Neurosci.* 14:459-468.

Polymeropoulos, M.H., C. Lavedan, E. Leroy, S.E. Ide, A. Dehejia, A. Dutra, B. Pike,

H. Root, J. Rubenstein, R. Boyer, E.S. Stenroos, S. Chandrasekharappa, A. Athanassiadou, T. Papapetropoulos, W.G. Johnson, A.M. Lazzarini, R.G. Duvoisin, G. Di Iorio, L.I. Golbe, and R.L. Nussbaum. 1997. Mutation in the α-synuclein gene identified in families with Parkinson's disease. *Science.* 276:2045-2047.

Poorkaj, P., D. Tsuang, E. Wijsman, E. Steinbart, R.M. Garruto, U.K. Craig, N.H. Chapman, L. Anderson, T.D. Bird, C.C. Plato, D.P. Perl, W. Weiderholt, D. Galasko, and G.D. Schellenberg. 2001. TAU as a susceptibility gene for amyotropic lateral sclerosis-parkinsonism dementia complex of Guam. *Arch. Neurol.* 58:1871-1878.

Poot, M., Y.Z. Zhang, J.A. Kramer, K.S. Wells, L.J. Jones, D.K. Hanzel, A.G. Lugade, V.L. Singer, and R.P. Haugland. 1996. Analysis of mitochondrial morphology and function with novel fixable fluorescent stains. *J. Histochem. Cytochem.* 44:1363-1372.

Poulain, F.E., and A. Sobel. 2010. The microtubule network and neuronal morphogenesis: Dynamic and coordinated orchestration through multiple players. *Mol. Cell. Neurosci.* 43:15-32.

Pozo, K., and F.A. Stephenson. 2006. GRIF-1-kinesin-1 interactions: a confocal microscopy study. *Biochem. Soc. Trans.* 34:48-50.

Puls, I., C. Jonnakuty, B.H. LaMonte, E.L. Holzbaur, M. Tokito, E. Mann, M.K. Floeter, K. Bidus, D. Drayna, S.J. Oh, R.H. Brown, C.L. Ludlow, and K.H. Fischbeck. 2003. Mutant dynactin in motor neuron disease. *Nat. Genet.* 33:455-456.

Rabouille, C., T.P. Levine, J.-M. Peters, and G. Warren. 1995. An NSF-like ATPase, p97, and NSF mediate cisternal regrowth from mitotic golgi fragments. *Cell.* 82:905-914.

Raimondi, A., A. Mangolini, M. Rizzardini, S. Tartari, S. Massari, C. Bendotti, M. Francolini, N. Borgese, L. Cantoni, and G. Pietrini. 2006. Cell culture models to investigate the selective vulnerability of motoneuronal mitochondria to familial ALS-linked G93ASOD1. *Eur. J. Neurosci.* 24:387-399.

Rakhit, R., J. Robertson, C.V. Velde, P. Horne, D.M. Ruth, J. Griffin, D.W. Cleveland, N.R. Cashman, and A. Chakrabartty. 2007. An immunological epitope selective for pathological monomer-misfolded SOD1 in ALS. *Nat. Med.* 13:754-759.

Rapizzi, E., P. Pinton, G. Szabadkai, M.R. Wieckowski, G. Vandecasteele, G. Baird, R.A. Tuft, K.E. Fogarty, and R. Rizzuto. 2002. Recombinant expression of the voltage-dependent anion channel enhances the transfer of Ca2+ microdomains to mitochondria. *J. Cell Biol.* 159:613-624.

Ratnaparkhi, A., G.M. Lawless, F.E. Schweizer, P. Golshani, and G.R. Jackson. 2008. A Drosophila model of ALS: human ALS-associated mutation in VAP33A suggests a dominant negative mechanism. *PLoS ONE.* 3:e2334.

Reed, N.A., D. Cai, T.L. Blasius, G.T. Jih, E. Meyhofer, J. Gaertig, and K.J. Verhey. 2006. Microtubule acetylation promotes kinesin-1 binding and transport. *Curr. Biol.* 16:2166-2172.

Reipert, S., F. Steinböck, I. Fischer, R.E. Bittner, A. Zeöld, and G. Wiche. 1999. Association of mitochondria with plectin and desmin intermediate filaments in striated muscle. *Exp. Cell Res.* 252:479-491.

Renton, A.E., E. Majounie, A. Waite, J. Simón-Sánchez, S. Rollinson, J.R. Gibbs, J.C. Schymick, H. Laaksovirta, J.C. van Swieten, L. Myllykangas, H. Kalimo, A. Paetau, Y. Abramzon, A.M. Remes, A. Kaganovich, S.W. Scholz, J. Duckworth, J. Ding, D.W. Harmer, D.G. Hernandez, J.O. Johnson, K. Mok, M. Ryten, D. Trabzuni, R.J. Guerreiro, R.W. Orrell, J. Neal, A. Murray, J. Pearson, I.E. Jansen, D. Sondervan, H. Seelaar, D. Blake, K. Young, N. Halliwell, J.B. Callister, G. Toulson, A. Richardson, A. Gerhard, J. Snowden, D. Mann, D. Neary, M.A. Nalls, T. Peuralinna, L. Jansson, V.-M. Isoviita, A.-L. Kaivorinne, M. Hölttä-Vuori, E. Ikonen, R. Sulkava, M. Benatar, J. Wuu, A. Chió, G. Restagno, G. Borghero, M. Sabatelli, T.I. Consortium, D. Heckerman, E. Rogaeva, L. Zinman, J.D. Rothstein, M. Sendtner, C. Drepper, E.E. Eichler, C. Alkan, Z. Abdullaev, S.D. Pack, A. Dutra, E. Pak, J. Hardy, A. Singleton, N.M. Williams, P. Heutink, S. Pickering-Brown, H.R. Morris, P.J. Tienari, and B.J. Traynor. 2011. A hexanucleotide repeat expansion in *C9ORF72* is the cause of chromosome 9p21-linked ALS-FTD. *Neuron*. 72:257-268.

Rintoul, G.L., A.J. Filiano, J.B. Brocard, G.J. Kress, and I.J. Reynolds. 2003. Glutamate decreases mitochondrial size and movement in primary forebrain neurons. *J Neurosci*. 23:7881-7888.

Ritz, D., M. Vuk, P. Kirchner, M. Bug, S. Schutz, A. Hayer, S. Bremer, C. Lusk, R.H. Baloh, H. Lee, T. Glatter, M. Gstaiger, R. Aebersold, C.C. Weihl, and H. Meyer. 2011. Endolysosomal sorting of ubiquitylated caveolin-1 is regulated by VCP and UBXD1 and impaired by VCP disease mutations. *Nat. Cell Biol.* 13:1116-1123.

Rizzuto, R., P. Pinton, W. Carrington, F.S. Fay, K.E. Fogarty, L.M. Lifshitz, R.A. Tuft, and T. Pozzan. 1998. Close contacts with the endoplasmic reticulum as determinants of mitochondrial Ca2+ responses. *Science*. 280:1763-1766.

Rosen, D.R., T. Siddique, D. Patterson, D.A. Figlewicz, P. Sapp, A. Hentati, D. Donaldson, J. Goto, J.P. O'Regan, H.X. Deng, and R. Brown. 1993. Mutations in the Cu/Zn superoxide dismutase gene are associated with familial amyotrophic lateral sclerosis. *Nature*. 362:59-62.

Rothstein, J.D., L.J. Martin, and R.W. Kuncl. 1992. Decreased glutamate transport in the brain and spinal cord in amyotrophic lateral sclerosis. *New England J. Med.* 326:1464-1468.

Rothstein, J.D., G. Tsai, R.W. Kuncl, L. Clawson, D.R. Cornblath, D.B. Drachman, A. Pestronk, B.L. Stauch, and J.T. Coyle. 1990. Abnormal excitatory amino acid metabolism in amyotrophic lateral sclerosis. *Ann. Neurol.* 28:18-25.

Rothstein, J.G., M. Van Kammen, A.I. Levey, L.J. Martin, and R.W. Kuncl. 1995. Selective loss of glial glutamate transporter GLT-1 in amyotrophic laterlal sclerosis. *Ann. Neurol.* 38:73-84.

Roy, J., S. Minotti, L.C. Dong, D.A. Figlewicz, and H.D. Durham. 1998. Glutamate potentiates the toxicity of mutant Cu/Zn-superoxide dismutase in motor neurons by postsynaptic calcium-dependent mechanisms. *J. Neurosci.* 18:9673-9684.

Rusinol, A.E., Z. Cui, M.H. Chen, and J.E. Vance. 1994. A unique mitochondria-associated membrane fraction from rat liver has a high capacity for lipid synthesis and contains pre-Golgi secretory proteins including nascent lipoproteins. *J. Biol. Chem.* 269:27494-27502.

Russo, G.J., K. Louie, A. Wellington, G.T. Macleod, F. Hu, S. Panchumarthi, and K.E. Zinsmaier. 2009. Drosophila Miro is required for both anterograde and retrograde axonal mitochondrial transport. *J. Neurosci.* 29:5443-5455.

Sabatelli, M., F.L. Conforti, M. Zollino, G. Mora, M.R. Monsurro, P. Volanti, K. Marinou, F. Salvi, M. Corbo, F. Giannini, S. Battistini, S. Penco, C. Lunetta, A. Quattrone, A. Gambardella, G. Logroscino, I. Simone, I. Bartolomei, F. Pisano, G. Tedeschi, A. Conte, R. Spataro, V. La Bella, C. Caponnetto, G. Mancardi, P. Mandich, P. Sola, J. Mandrioli, A.E. Renton, E. Majounie, Y. Abramzon, F. Marrosu, M.G. Marrosu, M.R. Murru, M.A. Sotgiu, M. Pugliatti, C. Rodolico, C. Moglia, A. Calvo, I. Ossola, M. Brunetti, B.J. Traynor, G. Borghero, G. Restagno, and A. Chio. 2012. C9ORF72 hexanucleotide repeat expansions in the Italian sporadic ALS population. *Neurobiol. Aging*. 33:1848:e15-20.

Saeed, M., N. Siddique, W.Y. Hung, E. Usacheva, E. Liu, R.L. Sufit, S.L. Heller, J.L. Haines, M. Pericak-Vance, and T. Siddique. 2006. Paraoxonase cluster polymorphisms are associated with sporadic ALS. *Neurology*. 67:771-776.

Sambrook, J., E.F. Fritsch, and T. Maniatis. 1989. Molecular cloning. A laboratory Manual. Cold Spring Harbor Laboratory Press, Cold Spring Harbor.

Sanelli, T.R., M.M. Sopper, and M.J. Strong. 2004. Sequestration of nNOS in neurofilamentous aggregate bearing neurons in vitro leads to enhanced NMDA-mediated calcium influx. *Brain Res.* 1004:8-17.

Saotome, M., D. Safiulina, G. Szabadkai, S. Das, A. Fransson, P. Aspenstrom, R. Rizzuto, and G. Hajnóczky. 2008. Bidirectional Ca2+-dependent control of mitochondrial dynamics by the Miro GTPase. *Proc. Natl. Acad. Sci. USA*. 105:20728-20733.

Sapp, P.C., B.A. Hosler, D. McKenna-Yasek, W. Chin, A. Gann, H. Genise, J. Gorenstein, M. Huang, W. Sailer, M. Scheffler, M. Valesky, J.L. Haines, M. Pericak-Vance, T. Siddique, H.R. Horvitz, and R.H. Brown, Jr. 2003. Identification of two novel loci for dominantly inherited familial amyotrophic lateral sclerosis. *Am. J. Hum. Genet.* 73:397-403.

Sasaki, S., and M. Iwata. 1996. Impairment of fast axonal transport in the proximal axons of anterior horn neurons in amyotrophic lateral sclerosis. *Neurology*.

47:535-540.

Sasaki, S., and M. Iwata. 2007. Mitochondrial alterations in the spinal cord of patients with sporadic amyotrophic lateral sclerosis. *J. Neuropathol. Exp. Neurol.* 66:10-16.

Saxena, S., E. Cabuy, and P. Caroni. 2009. A role for motoneuron subtype-selective ER stress in disease manifestations of FALS mice. *Nat. Neurosci.* 12:627-636.

Saxton, W.M., and P.J. Hollenbeck. 2012. The axonal transport of mitochondria. *J. Cell Sci.* 125:2095-2104.

Schulte, P.A., C.A. Burnett, M.F. Boeniger, and J. Johnson. 1996. Neurodegenerative diseases: occupational occurrence and potential risk factors, 1982 through 1991. *Am. J. Public Health*. 86:1281-1288.

Schwarzer, C., S. Barnikol-Watanabe, F.P. Thinnes, and N. Hilschmann. 2002. Voltage-dependent anion-selective channel (VDAC) interacts with the dynein light chain Tctex1 and the heat-shock protein PBP74. *Int. J. Biochem. Cell Biol.* 34:1059-1070.

Seibenhener, M.L., T. Geetha, and M.W. Wooten. 2007. Sequestosome 1/p62 - More than just a scaffold. *FEBS Lett.* 581:175-179.

Seitz, A., H. Kojima, K. Oiwa, E.M. Mandelkow, Y.H. Song, and E. Mandelkow. 2002. Single-molecule investigation of the interference between kinesin, tau and MAP2c. *EMBO J.* 21:4896-4905.

Seok Ko, H., T. Uehara, K. Tsuruma, and Y. Nomura. 2004. Ubiquilin interacts with ubiquitylated proteins and proteasome through its ubiquitin-associated and ubiquitin-like domains. *FEBS Lett.* 566:110-114.

Sephton, C.F., C. Cenik, A. Kucukural, E.B. Dammer, B. Cenik, Y. Han, C.M. Dewey, F.P. Roth, J. Herz, J. Peng, M.J. Moore, and G. Yu. 2011. Identification of neuronal RNA targets of TDP-43-containing ribonucleoprotein complexes. *J. Biol. Chem.* 286:1204-1215.

Shaner, N.C., R.E. Campbell, P.A. Steinbach, B.N.G. Giepmans, A.E. Palmer, and R.Y. Tsien. 2004. Improved monomeric red, orange and yellow fluorescent proteins derived from Discosoma sp. red fluorescent protein. *Nat. Biotech.* 22:1567-1572.

Shaw, P.J., V. Forrest, P.G. Ince, J.P. Richardson, and H.J. Wastell. 1995a. CSF and plasma amino acid levels in motor neuron disease: elevation of CSF glutamate in a subset of patients. *Neurodegeneration*. 4:209-216.

Shaw, P.J., P.G. Ince, G. Falkous, and D. Mantle. 1995b. Oxidative damage to protein in sporadic motor neuron disease spinal cord. *Ann. Neurol.* 38:691-695.

Shea, T.B., J.T. Yabe, D. Ortiz, A. Pimenta, P. Loomis, R.D. Goldman, N. Amin, and H.C. Pant. 2004. Cdk5 regulates axonal transport and phosphorylation of neurofilaments in cultured neurons. *J. Cell Sci.* 117:933-941.

Sherrington, R., E.I. Rogaev, Y. Liang, E.A. Rogaeva, G. Levesque, M. Ikeda, H. Chi, C. Lin, G. Li, K. Holman, T. Tsuda, L. Mar, J.-F. Foncin, A.C. Bruni, M.P. Montesi, S. Sorbi, I. Rainero, L. Pinessi, L. Nee, I. Chumakov, D. Pollen, A. Brookes, P. Sanseau, and P.H. St George-Hyslop. 1995. Cloning of a gene bearing missense mutations in early-onset familial Alzheimer's disease. *Nature*. 375:754-760.

Shi, J., S. Lua, J.S. Tong, and J. Song. 2010. Elimination of the native structure and solubility of the hVAPB MSP domain by the Pro56Ser mutation that causes amyotrophic lateral sclerosis. *Biochemistry*. 49:3887-3897.

Shibata, N., A. Hirano, M. Kobayashi, S. Sasaki, K. Takeo, S. Matsumoto, Z. Shiozawa, T. Komori, A. Ikemoto, T. Umahara, and K. Asayama. 1994. Cu/Zn superoxide dismutase-like immunoreactivity in Lewy body-like inclusions of sporadic amyotrophic lateral sclerosis. *Neurosci. Lett.* 179:149-152.

Shibata, N., A. Hirano, M. Kobayashi, T. Siddique, H.X. Deng, W.Y. Hung, T. Kato, and K. Asayama. 1996. Intense superoxide dismutase-1 immunoreactivity in intracytoplasmic hyaline inclusions of familial amyotrophic lateral sclerosis with posterior column involvement. *J. Neuropathol. Exp. Neurol.* 55:481-490.

Siddons, M.A., S.M. Pickering-Brown, D.M. Mann, F. Owen, and P.N. Cooper. 1996. Debrisoquine hydroxylase gene polymorphism frequencies in patients with amyotrophic lateral sclerosis. *Neurosci. Lett.* 208:65-68.

Siklós, L., J. Engelhardt, Y. Harati, R.G. Smith, F. Joó, and S.H. Appel. 1996. Ultrastructural evidence for altered calcium in motor nerve terminals in amyotrophc lateral sclerosis. *Ann. Neurol.* 39:203-216.

Siklós, L., J.I. Engelhardt, M.E. Alexianu, M.E. Gurney, T. Siddique, and S.H. Appel. 1998. Intracellular calcium parallels motoneuron degeneration in SOD-1 mutant mice. *J. Neuropathol. Exp. Neurol.* 57:571-587.

Siklós, L., J.I. Engelhardt, A.G. Reaume, R.W. Scott, R. Adalbert, I. Obál, and S.H. Appel. 2000. Altered calcium homeostasis in spinal motoneurons but not in oculomotor neurons of SOD-1 knockout mice. *Acta Neuropathol.* 99:517-524.

Simmen, T., E.M. Lynes, K. Gesson, and G. Thomas. 2010. Oxidative protein folding in the endoplasmic reticulum: Tight links to the mitochondria-associated membrane (MAM). *Biochim. Biophys. Acta*. 1798:1465-1473.

Simpson, C.L., R. Lemmens, K. Miskiewicz, W.J. Broom, V.K. Hansen, P.W. van Vught, J.E. Landers, P. Sapp, L. Van Den Bosch, J. Knight, B.M. Neale, M.R. Turner, J.H. Veldink, R.A. Ophoff, V.B. Tripathi, A. Beleza, M.N. Shah, P. Proitsi, A. Van Hoecke, P. Carmeliet, H.R. Horvitz, P.N. Leigh, C.E. Shaw, L.H. van den Berg, P.C. Sham, J.F. Powell, P. Verstreken, R.H. Brown, Jr., W. Robberecht, and A. Al-Chalabi. 2009. Variants of the elongator protein 3 (ELP3) gene are associated with motor neuron degeneration. *Hum. Mol. Genet.* 18:472-481.

Simpson, E.P., Y.K. Henry, J.S. Henkel, R.G. Smith, and S.H. Appel. 2004. Increased

lipid peroxidation in sera of ALS patients: a potential biomarker of disease burden. *Neurology*. 62:1758-1765.

Skehel, P.A., R. Fabian-Fine, and E.R. Kandel. 2000. Mouse VAP33 is associated with the endoplasmic reticulum and microtubules. *Proc. Natl. Acad. Sci. USA*. 97:1101-1106.

Skehel, P.A., K.C. Martin, E.R. Kandel, and D. Bartsch. 1995. A VAMP-binding protein from Aplysia required for neurotransmitter release. *Science*. 269:1580-1583.

Skvortsova, V., M. Shadrina, P. Slominsky, G. Levitsky, E. Kondratieva, A. Zherebtsova, N. Levitskaya, A. Alekhin, A. Serdyuk, and S. Limborska. 2004. Analysis of heavy neurofilament subunit gene polymorphism in Russian patients with sporadic motor neuron disease (MND). *Eur. J. Hum. Genet.* 12:241-244.

Sleegers, K., N. Brouwers, S. Maurer-Stroh, M.A. van Es, P. Van Damme, P.W. van Vught, J. van der Zee, S. Serneels, T. De Pooter, M. Van den Broeck, M. Cruts, J. Schymkowitz, P. De Jonghe, F. Rousseau, L.H. van den Berg, W. Robberecht, and C. Van Broeckhoven. 2008. Progranulin genetic variability contributes to amyotrophic lateral sclerosis. *Neurology*. 71:253-259.

Slowik, A., B. Tomik, P.P. Wolkow, D. Partyka, W. Turaj, M.T. Malecki, J. Pera, T. Dziedzic, A. Szczudlik, and D.A. Figlewicz. 2006. Paraoxonase gene polymorphisms and sporadic ALS. *Neurology*. 67:766-770.

Smith, M.J., K. Pozo, K. Brickley, and F.A. Stephenson. 2006. Mapping the GRIF-1 binding domain of the kinesin, KIF5C, substantiates a role for GRIF-1 as an adaptor protein in the anterograde trafficking of cargoes. *J. Biol. Chem.* 281:27216-27228.

Sobue, G., Y. Hashizume, T. Yasuda, E. Mukai, T. Kumagai, T. Mitsuma, and J.Q. Trojanowski. 1990. Phosphorylated high molecular weight neurofilament protein in lower motor neurons in amyotrophic lateral sclerosis and other neurodegenerative diseases involving ventral horn cells. *Acta Neuropathol*. 79:402-408.

Sonawane, N.D., F.C. Szoka, and A.S. Verkman. 2003. Chloride accumulation and swelling in endosomes enhances DNA transfer by polyamine-DNA polyplexes. *J. Biol. Chem.* 278:44826-44831.

Sotelo-Silveira, J.R., P. Lepanto, V. Elizondo, S. Horjales, F. Palacios, L. Martinez-Palma, M. Marin, J.S. Beckman, and L. Barbeito. 2009. Axonal mitochondrial clusters containing mutant SOD1 in transgenic models of ALS. *Antioxid. Redox Signal.* 11:1535-1545.

Soussan, L., D. Burakov, M.P. Daniels, M. Toister-Achituv, A. Porat, Y. Yarden, and Z. Elazar. 1999. ERG30, a VAP-33-related protein, functions in protein transport mediated by COPI vesicles. *J. Cell Biol.* 146:301-311.

Söllner, T., S.W. Whiteheart, M. Brunner, H. Erdjument-Bromage, S. Geromanos, P.

Tempst, and J.E. Rothman. 1993. SNAP receptors implicated in vesicle targeting and fusion. *Nature*. 362:318-324.

Spang, A. 2008. Membrane traffic in the secretory pathway. *Cell. Mol. Life Sci.* 65:2781-2789.

Sprong, H., P. van der Sluijs, and G. van Meer. 2001. How proteins move lipids and lipids move proteins. *Nat. Rev. Mol. Cell Biol.* 2:504-513.

Sreedharan, J., I.P. Blair, V.B. Tripathi, X. Hu, C. Vance, B. Rogelj, S. Ackerley, J.C. Durnall, K.L. Williams, E. Buratti, F. Baralle, J. de Belleroche, J.D. Mitchell, P.N. Leigh, A. Al-Chalabi, C.C. Miller, G. Nicholson, and C.E. Shaw. 2008. TDP-43 mutations in familial and sporadic amyotrophic lateral sclerosis. *Science*. 319:1688-1672.

Stagi, M., P. Gorlovoy, S. Larionov, K. Takahashi, and H. Neumann. 2006. Unloading kinesin transported cargoes from the tubulin track via the inflammatory c-Jun N-terminal kinase pathway. *FASEB J.* 20:2573-2575.

Stamer, K., R. Vogel, E. Thies, E. Mandelkow, and E.-M. Mandelkow. 2002. Tau blocks traffic of organelles, neurofilaments, and APP vesicles in neurons and enhances oxidative stress. *J. Cell Biol.* 156:1051-1063.

Stevenson, A., D.M. Yates, C. Manser, K.J. De Vos, A. Vagnoni, P.N. Leigh, D.M. McLoughlin, and C.C. Miller. 2009. Riluzole protects against glutamate-induced slowing of neurofilament axonal transport. *Neurosci. Lett.* 454:161-164.

Stoothoff, W., P.B. Jones, T.L. Spires-Jones, D. Joyner, E. Chhabra, K. Bercury, Z. Fan, H. Xie, B. Bacskai, J. Edd, D. Irimia, and B.T. Hyman. 2009. Differential effect of three-repeat and four-repeat tau on mitochondrial axonal transport. *J. Neurochem.* 111:417-427.

Stowers, R.S., L.J. Megeath, J. Gorska-Andrzejak, I.A. Meinertzhagen, and T.L. Schwarz. 2002. Axonal transport of mitochondria to synapses depends on milton, a novel Drosophila protein. *Neuron*. 36:1063-1077.

Strong, M., and J. Rosenfeld. 2003. Amyotrophic lateral sclerosis: a review of current concepts. *Amyotroph. Lateral Scler. Other Motor Neuron Disord.* 4:136-143.

Strong, M.J., and P.H. Gordon. 2005. Primary lateral sclerosis, hereditary spastic paraplegia and amyotrophic lateral sclerosis: Discrete entities or spectrum? *Amyotroph. Lateral Scler. Other Motor Neuron Disord.* 6:8-16.

Strong, M.J., S. Kesavapany, and H.C. Pant. 2005. The pathobiology of amyotrophic lateral sclerosis: a proteinopathy? *J. Neuropathol. Exp. Neurol.* 64:649-664.

Su, Q., Q. Cai, C. Gerwin, C.L. Smith, and Z.-H. Sheng. 2004. Syntabulin is a microtubule-associated protein implicated in syntaxin transport in neurons. *Nat. Cell Biol.* 6:941-953.

Sun, Q., S. Bahri, A. Schmid, W. Chia, and K. Zinn. 2000. Receptor tyrosine

phosphatases regulate axon guidance across the midline of the Drosophila embryo. *Development*. 127:801-812.

Suzuki, H., K. Kanekura, T.P. Levine, K. Kohno, V.M. Olkkonen, S. Aiso, and M. Matsuoka. 2009. ALS-linked P56S-VAPB, an aggregated loss-of-function mutant of VAPB, predisposes motor neurons to ER stress-related death by inducing aggregation of co-expressed wild-type VAPB. *J. Neurochem.* 108:973-985.

Suzuki, H., K. Lee, and M. Matsuoka. 2011. TDP-43-induced death is associated with altered regulation of BIM and Bcl-xL and attenuated by caspase-mediated TDP-43 cleavage. *J. Biol. Chem.* 286:13171-13183.

Suzuki, H., and M. Matsuoka. 2011. ALS-linked mutant VAPB enhances TDP-43-induced motor neuronal toxicity. *J. Neurochem.* 119:1099-1107.

Swerdlow, R.H., J.K. Parks, D.S. Cassarino, P.A. Trimmer, S.W. Miller, D.J. Maguire, J.P. Sheehan, R.S. Maguire, G. Pattee, V.C. Juel, L.H. Phillips, J.B. Tuttle, J.P. Bennett, Jr., R.E. Davis, and W.D. Parker, Jr. 1998. Mitochondria in sporadic amyotrophic lateral sclerosis. *Exp. Neurol.* 153:135-142.

Szabadkai, G., K. Bianchi, P. Várnai, D. De Stefani, M.R. Wieckowski, D. Cavagna, A.I. Nagy, T. Balla, and R. Rizzuto. 2006. Chaperone-mediated coupling of endoplasmic reticulum and mitochondrial Ca2+ channels. *J. Cell Biol.* 175:901-911.

Takeuchi, H., Y. Kobayashi, S. Ishigaki, M. Doyu, and G. Sobue. 2002. Mitochondrial localization of mutant SOD1 triggers caspase-dependent cell death in a cellular model of familial amyotrophic lateral sclerosis. *J. Biol. Chem.* 277:50966-50972.

Takuma, H., S. Kwak, T. Yoshizawa, and I. Kanazawa. 1999. Reduction of GluR2 RNA editing, a molecular change that increases calcium influx through AMPA receptors, selective in the spinal ventral gray of patients with amyotrophic lateral sclerosis. *Ann. Neurol.* 46:806-815.

Tanaka, K., Y. Sugiura, R. Ichishita, K. Mihara, and T. Oka. 2011. KLP6: a newly identified kinesin that regulates the morphology and transport of mitochondria in neuronal cells. *J. Cell Sci.* 124:2457-2465.

Tanaka, Y., Y. Kanai, Y. Okada, S. Nonaka, S. Takeda, A. Harada, and N. Hirokawa. 1998. Targeted disruption of mouse conventional kinesin heavy chain, kif5B, results in abnormal perinuclear clustering of mitochondria. *Cell*. 93:1147-1158.

Teuling, E., S. Ahmed, E. Haasdijk, J. Demmers, M.O. Steinmetz, A. Akhmanova, D. Jaarsma, and C.C. Hoogenraad. 2007. Motor neuron disease-associated mutant vesicle-associated membrane protein-associated protein (VAP) B recruits wild-type VAPs into endoplasmic reticulum-derived tubular aggregates. *J. Neurosci.* 27:9801-9815.

Thomas, B., and M.F. Beal. 2007. Parkinson's disease. *Hum. Mol. Genet.* 16 Spec No.

2:R183-194.

Thomas, M.G., M. Loschi, M.A. Desbats, and G.L. Boccaccio. 2011. RNA granules: the good, the bad and the ugly. *Cell Signal*. 23:324-334.

Tiago, T., D. Marques-da-Silva, A.K. Samhan-Arias, M. Aureliano, and C. Gutierrez-Merino. 2011. Early disruption of the actin cytoskeleton in cultured cerebellar granule neurons exposed to 3-morpholinosydnonimine-oxidative stress is linked to alterations of the cytosolic calcium concentration. *Cell Calcium*. 49:174-183.

Ticozzi, N., C. Vance, A.L. LeClerc, P. Keagle, J.D. Glass, D. McKenna-Yasek, P.C. Sapp, V. Silani, D.A. Bosco, C.E. Shaw, R.H. Brown, and J.E. Landers. 2011. Mutational analysis reveals the FUS homolog TAF15 as a candidate gene for familial amyotrophic lateral sclerosis. *Am. J. Med. Genet. B Neuropsychiatr. Genet.* 156:285-290.

Tobisawa, S., Y. Hozumi, S. Arawaka, S. Koyama, M. Wada, M. Nagai, M. Aoki, Y. Itoyama, K. Goto, and T. Kato. 2003. Mutant SOD1 linked to familial amyotrophic lateral sclerosis, but not wild-type SOD1, induces ER stress in COS7 cells and transgenic mice. *Biochem. Biophys. Res. Commun.* 303:496-503.

Todd, P.K., and H.L. Paulson. 2010. RNA-mediated neurodegeneration in repeat expansion disorders. *Ann. Neurol.* 67:291-300.

Toh, B.H., S.J. Lolait, J.P. Mathy, and R. Baum. 1980. Association of mitochondria with intermediate filaments and of polyribosomes with cytoplasmic actin. *Cell Tissue Res*. 211:163-169.

Tollervey, J.R., T. Curk, B. Rogelj, M. Briese, M. Cereda, M. Kayikci, J. Konig, T. Hortobagyi, A.L. Nishimura, V. Zupunski, R. Patani, S. Chandran, G. Rot, B. Zupan, C.E. Shaw, and J. Ule. 2011. Characterizing the RNA targets and position-dependent splicing regulation by TDP-43. *Nat. Neurosci.* 14:452-458.

Topp, J.D., N.W. Gray, R.D. Gerard, and B.F. Horazdovsky. 2004. Alsin is a Rab5 and Rac1 guanine nucleotide exchange factor. *J. Biol. Chem.* 279:24612-24623.

Tradewell, M.L., L.A. Cooper, S. Minotti, and H.D. Durham. 2011. Calcium dysregulation, mitochondrial pathology and protein aggregation in a culture model of amyotrophic lateral sclerosis: Mechanistic relationship and differential sensitivity to intervention. *Neurobiol. Dis.* 42:265-275.

Tran, D., A. Chalhoub, A. Schooley, W. Zhang, and J.K. Ngsee. 2012. Amyotrophic Lateral Sclerosis Mutant VAPB Causes a Nuclear Envelope Defect. *J. Cell Sci.* 125:2831-2836.

Traynelis, S.F., L.P. Wollmuth, C.J. McBain, F.S. Menniti, K.M. Vance, K.K. Ogden, K.B. Hansen, H. Yuan, S.J. Myers, and R. Dingledine. 2010. Glutamate receptor ion channels: structure, regulation, and function. *Pharmacol. Rev.* 62:405-496.

Tsuda, H., S.M. Han, Y. Yang, C. Tong, Y.Q. Lin, K. Mohan, C. Haueter, A. Zoghbi, Y. Harati, J. Kwan, M.A. Miller, and H.J. Bellen. 2008. The amyotrophic lateral

sclerosis 8 protein VAPB is cleaved, secreted, and acts as a ligand for Eph receptors. *Cell*. 133:963-977.

Tu, P.H., P. Raju, K.A. Robinson, M.E. Gurney, J.Q. Trojanowski, and V.M.Y. Lee. 1996. Transgenic mice carrying a human mutant superoxide dismutase transgene develop neuronal cytoskeletal pathology resembling human amyotrophic lateral sclerosis lesions. *Proc. Natl. Acad. Sci. USA*. 93:3155-3160.

Tudor, E.L., C.M. Galtrey, M.S. Perkinton, K.F. Lau, K.J. De Vos, J.C. Mitchell, S. Ackerley, T. Hortobagyi, E. Vamos, P.N. Leigh, C. Klasen, D.M. McLoughlin, C.E. Shaw, and C.C. Miller. 2010. Amyotrophic lateral sclerosis mutant VAPB transgenic mice develop TDP-43 pathology. *Neuroscience*. 167:774-785.

Turabelidze, G., B.P. Zhu, M. Schootman, J.L. Malone, S. Horowitz, J. Weidinger, D. Williamson, and E. Simoes. 2008. An epidemiologic investigation of amyotrophic lateral sclerosis in Jefferson County, Missouri, 1998-2002. *Neurotoxicology*. 29:81-86.

Turner, B.J., J.D. Atkin, M.A. Farg, D.W. Zang, A. Rembach, E.C. Lopes, J.D. Patch, A.F. Hill, and S.S. Cheema. 2005. Impaired extracellular secretion of mutant superoxide dismutase 1 associates with neurotoxicity in familial amyotrophic lateral sclerosis. *J. Neurosci.* 25:108-117.

Urushitani, M., A. Sik, T. Sakurai, N. Nukina, R. Takahashi, and J.P. Julien. 2006. Chromogranin-mediated secretion of mutant superoxide dismutase proteins linked to amyotrophic lateral sclerosis. *Nat. Neurosci.* 9:108-118.

Vagnoni, A., L. Rodriguez, C. Manser, K.J. De Vos, and C.C. Miller. 2011. Phosphorylation of kinesin light chain 1 at serine 460 modulates binding and trafficking of calsyntenin-1. *J. Cell Sci.* 124:1032-1042.

Van Damme, P., D. Braeken, G. Callewaert, W. Robberecht, and L. Van Den Bosch. 2005. GluR2 deficiency accelerates motor neuron degeneration in a mouse model of amyotrophic lateral sclerosis. *J. Neuropathol. Exp. Neurol.* 64:605-612.

Van Damme, P.M.D.P., J.H.M.D.P. Veldink, M.M. van Blitterswijk, A.P. Corveleyn, P.W.J.P. van Vught, V.M.D.P. Thijs, B.M.D.P. Dubois, G.P. Matthijs, L.H.M.D.P. van den Berg, and W.M.D.P. Robberecht. 2011. Expanded ATXN2 CAG repeat size in ALS identifies genetic overlap between ALS and SCA2. *Neurology*. 76:2066-2072.

Van Deerlin, V.M., J.B. Leverenz, L.M. Bekris, T.D. Bird, W. Yuan, L.B. Elman, D. Clay, E.M. Wood, A.S. Chen-Plotkin, M. Martinez-Lage, E. Steinbart, L. McCluskey, M. Grossman, M. Neumann, I.L. Wu, W.S. Yang, R. Kalb, D.R. Galasko, T.J. Montine, J.Q. Trojanowski, V.M. Lee, G.D. Schellenberg, and C.E. Yu. 2008. TARDBP mutations in amyotrophic lateral sclerosis with TDP-43 neuropathology: a genetic and histopathological analysis. *Lancet Neurol.* 7:409-416.

Van Den Bosch, L., W. Vandenberghe, H. Klaassen, E. Van Houtte, and W.

Robberecht. 2000. Ca2+-permeable AMPA receptors and selective vulnerability of motor neurons. *J. Neurol. Sci.* 180:29-34.

van Es, M.A., F.P. Diekstra, J.H. Veldink, F. Baas, P.R. Bourque, H.J. Schelhaas, E. Strengman, E.A. Hennekam, D. Lindhout, R.A. Ophoff, and L.H. van den Berg. 2009a. A case of ALS-FTD in a large FALS pedigree with a K17I ANG mutation. *Neurology*. 72:287-288.

van Es, M.A., P.W. Van Vught, H.M. Blauw, L. Franke, C.G. Saris, P.M. Andersen, L. Van Den Bosch, S.W. de Jong, R. van 't Slot, A. Birve, R. Lemmens, V. de Jong, F. Baas, H.J. Schelhaas, K. Sleegers, C. Van Broeckhoven, J.H.J. Wokke, C. Wijmenga, W. Robberecht, J.H. Veldink, R.A. Ophoff, and L.H. van den Berg. 2007. ITPR2 as a susceptibility gene in sporadic amyotrophic lateral sclerosis: a genome-wide association study. *Lancet Neurol.* 6:869-877.

van Es, M.A., P.W.J. van Vught, H.M. Blauw, L. Franke, C.G.J. Saris, L. Van Den Bosch, S.W. de Jong, V. de Jong, F. Baas, R. van't Slot, R. Lemmens, H.J. Schelhaas, A. Birve, K. Sleegers, C. Van Broeckhoven, J.C. Schymick, B.J. Traynor, J.H.J. Wokke, C. Wijmenga, W. Robberecht, P.M. Andersen, J.H. Veldink, R.A. Ophoff, and L.H. van den Berg. 2008. Genetic variation in DPP6 is associated with susceptibility to amyotrophic lateral sclerosis. *Nat Genet*. 40:29-31.

van Es, M.A., J.H. Veldink, C.G. Saris, H.M. Blauw, P.W. van Vught, A. Birve, R. Lemmens, H.J. Schelhaas, E.J. Groen, M.H. Huisman, A.J. van der Kooi, M. de Visser, C. Dahlberg, K. Estrada, F. Rivadeneira, A. Hofman, M.J. Zwarts, P.T. van Doormaal, D. Rujescu, E. Strengman, I. Giegling, P. Muglia, B. Tomik, A. Slowik, A.G. Uitterlinden, C. Hendrich, S. Waibel, T. Meyer, A.C. Ludolph, J.D. Glass, S. Purcell, S. Cichon, M.M. Nothen, H.E. Wichmann, S. Schreiber, S.H. Vermeulen, L.A. Kiemeney, J.H. Wokke, S. Cronin, R.L. McLaughlin, O. Hardiman, K. Fumoto, R.J. Pasterkamp, V. Meininger, J. Melki, P.N. Leigh, C.E. Shaw, J.E. Landers, A. Al-Chalabi, R.H. Brown, Jr., W. Robberecht, P.M. Andersen, R.A. Ophoff, and L.H. van den Berg. 2009b. Genome-wide association study identifies 19p13.3 (UNC13A) and 9p21.2 as susceptibility loci for sporadic amyotrophic lateral sclerosis. *Nat. Genet.* 41:1083-1087.

Van Hoecke, A., L. Schoonaert, R. Lemmens, M. Timmers, K.A. Staats, A.S. Laird, E. Peeters, T. Philips, A. Goris, B. Dubois, P.M. Andersen, A. Al-Chalabi, V. Thijs, A.M. Turnley, P.W. van Vught, J.H. Veldink, O. Hardiman, L. Van Den Bosch, P. Gonzalez-Perez, P. Van Damme, R.H. Brown, Jr., L.H. van den Berg, and W. Robberecht. 2012. EPHA4 is a disease modifier of amyotrophic lateral sclerosis in animal models and in humans. *Nat. Med.* 18:1418-1422.

Van Landeghem, G.F., P. Tabatabaie, G. Beckman, L. Beckman, and P.M. Andersen. 1999. Manganese-containing superoxide dismutase signal sequence polymorphism associated with sporadic motor neuron disease. *Eur. J. Neurol.* 6:639-644.

Vance, C., B. Rogelj, T. Hortobagyi, K.J. De Vos, A.L. Nishimura, J. Sreedharan, X. Hu, B. Smith, D. Ruddy, P. Wright, J. Ganesalingam, K.L. Williams, V. Tripathi, S. Al-Saraj, A. Al-Chalabi, P.N. Leigh, I.P. Blair, G. Nicholson, J. de

Belleroche, J.M. Gallo, C.C. Miller, and C.E. Shaw. 2009. Mutations in FUS, an RNA processing protein, cause familial amyotrophic lateral sclerosis type 6. *Science*. 323:1208-1211.

Vance, J.E. 1990. Phospholipid synthesis in a membrane fraction associated with mitochondria. *J. Biol. Chem.* 265:7248-7256.

Vande Velde, C., K.K. McDonald, Y. Boukhedimi, M. McAlonis-Downes, C.S. Lobsiger, S. Bel Hadj, A. Zandona, J.-P. Julien, S.B. Shah, and D.W. Cleveland. 2011. Misfolded SOD1 associated with motor neuron mitochondria alters mitochondrial shape and distribution prior to clinical onset. *PLoS One*. 6:e22031.

Vande Velde, C., T.M. Miller, N.R. Cashman, and D.W. Cleveland. 2008. Selective association of misfolded ALS-linked mutant SOD1 with the cytoplasmic face of mitochondria. *Proc. Natl. Acad. Sci. USA*. 105:4022-4027.

Varoqueaux, F., A. Sigler, J.S. Rhee, N. Brose, C. Enk, K. Reim, and C. Rosenmund. 2002. Total arrest of spontaneous and evoked synaptic transmission but normal synaptogenesis in the absence of Munc13-mediated vesicle priming. *Proc. Natl. Acad. Sci. USA*. 99:9037-9042.

Vedrenne, C., and H.P. Hauri. 2006. Morphogenesis of the endoplasmic reticulum: beyond active membrane expansion. *Traffic*. 7:639-646.

Veldink, J.H., L.H. van den Berg, J.M. Cobben, R.P. Stulp, J.M. De Jong, O.J. Vogels, F. Baas, J.H. Wokke, and H. Scheffer. 2001. Homozygous deletion of the survival motor neuron 2 gene is a prognostic factor in sporadic ALS. *Neurology*. 56:749-752.

Verhage, M., and J.B. Sørensen. 2008. Vesicle docking in regulated exocytosis. *Traffic*. 9:1414-1424.

Vijayvergiya, C., M.F. Beal, J. Buck, and G. Manfredi. 2005. Mutant superoxide dismutase 1 forms aggregates in the brain mitochondrial matrix of amyotrophic lateral sclerosis mice. *J. Neurosci.* 25:2463-2470.

Villa Braslavsky, C.I., C. Nowak, D. Gorlich, A. Wittinghofer, and J. Kuhlmann. 2000. Different structural and kinetic requirements for the interaction of Ran with the Ran-binding domains from RanBP2 and importin-beta. *Biochemistry*. 39:11629-11639.

Wagner, O.I., J. Lifshitz, P.A. Janmey, M. Linden, T.K. McIntosh, and J.-F. Leterrier. 2003. Mechanisms of mitochondria-neurofilament interactions. *J. Neurosci.* 23:9046-9058.

Wang, H.U., and D.J. Anderson. 1997. Eph family transmembrane ligands can mediate repulsive guidance of trunk neural crest migration and motor axon outgrowth. *Neuron*. 18:383-396.

Wang, X., and T.L. Schwarz. 2009. The mechanism of Ca2+ -dependent regulation of

kinesin-mediated mitochondrial motility. *Cell*. 136:163-174.

Wang, X., D. Winter, G. Ashrafi, J. Schlehe, Y.L. Wong, D. Selkoe, S. Rice, J. Steen, M.J. LaVoie, and T.L. Schwarz. 2011. PINK1 and Parkin target Miro for phosphorylation and degradation to arrest mitochondrial motility. *Cell*. 147:893-906.

Wang, X.S., S. Lee, Z. Simmons, P. Boyer, K. Scott, W. Liu, and J. Connor. 2004. Increased incidence of the Hfe mutation in amyotrophic lateral sclerosis and related cellular consequences. *J. Neurol. Sci.* 227:27-33.

Watts, G.D., J. Wymer, M.J. Kovach, S.G. Mehta, S. Mumm, D. Darvish, A. Pestronk, M.P. Whyte, and V.E. Kimonis. 2004. Inclusion body myopathy associated with Paget disease of bone and frontotemporal dementia is caused by mutant valosin-containing protein. *Nat. Genet.* 36:377-381.

Webber, E., L. Li, and L.S. Chin. 2008. Hypertonia-associated protein Trak1 is a novel regulator of endosome-to-lysosome trafficking. *J. Mol. Biol.* 382:638-651.

Weihl, C.C., S. Dalal, A. Pestronk, and P.I. Hanson. 2006. Inclusion body myopathy-associated mutations in p97/VCP impair endoplasmic reticulum-associated degradation. *Hum. Mol. Genet.* 15:189-199.

Weihofen, A., K.J. Thomas, B. Ostaszewski, M. Cookson, and D.J. Selkoe. 2009. Pink1 forms a multi-protein complex with Miro and Milton, linking Pink1 function to mitochondrial trafficking. *Biochemistry*. 48:2045-2052.

Weir, M.L., A. Klip, and W.S. Trimble. 1998. Identification of a human homologue of the vesicle-associated membrane protein (VAMP)-associated protein of 33 kDa (VAP-33): a broadly expressed protein that binds to VAMP. *Biochem. J.* 333:247-251.

Wengenack, T.M., S.S. Holasek, C.M. Montano, D. Gregor, G.L. Curran, and J.F. Poduslo. 2004. Activation of programmed cell death markers in ventral horn motor neurons during early presymptomatic stages of amyotrophic lateral sclerosis in a transgenic mouse model. *Brain Res.* 1027:73-86.

Whitehead, T.P., L.J. Kricka, T.J. Carter, and G.H. Thorpe. 1979. Analytical luminescence: its potential in the clinical laboratory. *Clin. Chem.* 25:1531-1546.

Wickner, W. 2010. Membrane fusion: five lipids, four SNAREs, three chaperones, two nucleotides, and a Rab, all dancing in a ring on yeast vacuoles. *Annu. Rev. Cell Dev. Biol.* 26:115-136.

Wiedemann, F.R., G. Manfredi, C. Mawrin, M.F. Beal, and E.A. Schon. 2002. Mitochondrial DNA and respiratory chain function in spinal cords of ALS patients. *J. Neurochem.* 80:616-625.

Williamson, T.L., and D.W. Cleveland. 1999. Slowing of axonal transport is a very early event in the toxicity of ALS-linked SOD1 mutants to motor neurons. *Nat. Neurosci.* 2:50-56.

Winter, L., C. Abrahamsberg, and G. Wiche. 2008. Plectin isoform 1b mediates mitochondrion-intermediate filament network linkage and controls organelle shape. *J. Cell Biol.* 181:903-911.

Wolff, A.M., J.G. Litske Petersen, T. Nilsson-Tillgren, and N. Din. 1999. The open reading frame YAL048c affects the secretion of proteinase A in S. cerevisiae. *Yeast*. 15:427-434.

Wolfson, C., S. Kilborn, M. Oskoui, and A. Genge. 2009. Incidence and prevalence of amyotrophic lateral sclerosis in Canada: a systematic review of the literature. *Neuroepidemiology*. 33:79-88.

Wong, E., and A.M. Cuervo. 2010. Integration of Clearance Mechanisms: The Proteasome and Autophagy. *Cold Spring Harb. Perspect. Biol.* 2:a006734.

Wong, P.C., C. Pardo, D.R. Borchelt, M.K. Lee, N.G. Copeland, N.A. Jenkins, S.S. Sisodia, D.W. Cleveland, and D.L. Price. 1995. An adverse property of a familial ALS-linked SOD1 mutation causes motor neuron disease characterised by vacuolar degeneration of mitochondria. *Neuron*. 14:1105-1116.

Wood, J.D., T.P. Beaujeux, and P.J. Shaw. 2003. Protein aggregation in motor neurone disorders. *Neuropathol. Appl. Neurobiol.* 29:529-545.

Wootz, H., I. Hansson, L. Korhonen, U. Napankangas, and D. Lindholm. 2004. Caspase-12 cleavage and increased oxidative stress during motoneuron degeneration in transgenic mouse model of ALS. *Biochem. Biophys. Res. Commun.* 322:281-286.

Worms, P.M. 2001. The epidemiology of motor neuron diseases: a review of recent studies. *J. Neurol. Sci.* 191:3-9.

Wozniak, M.J., M. Melzer, C. Dorner, H.U. Haring, and R. Lammers. 2005. The novel protein KBP regulates mitochondria localization by interaction with a kinesin-like protein. *BMC Cell Biol.* 6:35.

Wu, C.H., C. Fallini, N. Ticozzi, P.J. Keagle, P.C. Sapp, K. Piotrowska, P. Lowe, M. Koppers, D. McKenna-Yasek, D.M. Baron, J.E. Kost, P. Gonzalez-Perez, A.D. Fox, J. Adams, F. Taroni, C. Tiloca, A.L. Leclerc, S.C. Chafe, D. Mangroo, M.J. Moore, J.A. Zitzewitz, Z.S. Xu, L.H. van den Berg, J.D. Glass, G. Siciliano, E.T. Cirulli, D.B. Goldstein, F. Salachas, V. Meininger, W. Rossoll, A. Ratti, C. Gellera, D.A. Bosco, G.J. Bassell, V. Silani, V.E. Drory, R.H. Brown, Jr., and J.E. Landers. 2012. Mutations in the profilin 1 gene cause familial amyotrophic lateral sclerosis. *Nature*. 488:499-503.

Wu, D.C., D.B. Ré, M. Nagai, H. Ischiropoulos, and S. Przedborski. 2006. The inflammatory NADPH oxidase enzyme modulates motor neuron degeneration in amyotrophic lateral sclerosis mice. *Proc. Natl. Acad. Sci. USA*. 103:12132-12137.

Xia, Z.G., H. Dudek, C.K. Miranti, and M.E. Greenberg. 1996. Calcium influx via the NMDA receptor induces immediate-early gene-transcription by a MAP

kinase/ERK-dependent mechanism. *J. Neurosci.* 16:5425-5436.

Xu, S., G. Peng, Y. Wang, S. Fang, and M. Karbowski. 2011a. The AAA-ATPase p97 is essential for outer mitochondrial membrane protein turnover. *Mol. Biol. Cell*. 22:291-300.

Xu, Y.F., Y.J. Zhang, W.L. Lin, X. Cao, C. Stetler, D.W. Dickson, J. Lewis, and L. Petrucelli. 2011b. Expression of mutant TDP-43 induces neuronal dysfunction in transgenic mice. *Mol. Neurodegener.* 6:73.

Xu, Z., L.C. Cork, J.W. Griffin, and D.W. Cleveland. 1993. Increased expression of neurofilament subunit NF-L produces morphological alterations that resemble the pathology of human motor neuron disease. *Cell*. 73:23-33.

Yamaoka, S., M. Miyaji, T. Kitano, H. Umehara, and T. Okazaki. 2004. Expression cloning of a human cDNA restoring sphingomyelin synthesis and cell growth in sphingomyelin synthase-defective lymphoid cells. *J. Biol. Chem.* 279:18688-18693.

Yang, Y., A. Hentati, H.X. Deng, O. Dabbagh, T. Sasaki, M. Hirano, W.Y. Hung, K. Ouahchi, J. Yan, A.C. Azim, N. Cole, G. Gascon, A. Yagmour, M. Ben-Hamida, M. Pericak-Vance, F. Hentati, and T. Siddique. 2001. The gene encoding alsin, a protein with three guanine-nucleotide exchange factor domains, is mutated in a form of recessive amyotrophic lateral sclerosis. *Nat. Genet.* 29:160-165.

Ye, Y., H.H. Meyer, and T.A. Rapoport. 2001. The AAA ATPase Cdc48/p97 and its partners transport proteins from the ER into the cytosol. *Nature*. 414:652-656.

Ye, Y., Y. Shibata, M. Kikkert, S. van Voorden, E. Wiertz, and T.A. Rapoport. 2005. Recruitment of the p97 ATPase and ubiquitin ligases to the site of retrotranslocation at the endoplasmic reticulum membrane. *Proc. Natl. Acad. Sci. USA*. 102:14132-14138.

Ye, Y., Y. Shibata, C. Yun, D. Ron, and T.A. Rapoport. 2004. A membrane protein complex mediates retro-translocation from the ER lumen into the cytosol. *Nature*. 429:841-847.

Yi, M., D. Weaver, and G. Hajnóczky. 2004. Control of mitochondrial motility and distribution by the calcium signal: a homeostatic circuit. *J. Cell Biol.* 167:661-672.

Yokoseki, A., A. Shiga, C.F. Tan, A. Tagawa, H. Kaneko, A. Koyama, H. Eguchi, A. Tsujino, T. Ikeuchi, A. Kakita, K. Okamoto, M. Nishizawa, H. Takahashi, and O. Onodera. 2008. TDP-43 mutation in familial amyotrophic lateral sclerosis. *Ann. Neurol.* 63:538-542.

Zhang, B., P. Tu, F. Abtahian, J.Q. Trojanowski, and V.M. Lee. 1997. Neurofilaments and orthograde transport are reduced in ventral root axons of transgenic mice that express human SOD1 with a G93A mutation. *J. Cell Biol.* 139:1307-1315.

Zhang, Y.J., Y.F. Xu, C. Cook, T.F. Gendron, P. Roettges, C.D. Link, W.L. Lin, J.

Tong, M. Castanedes-Casey, P. Ash, J. Gass, V. Rangachari, E. Buratti, F. Baralle, T.E. Golde, D.W. Dickson, and L. Petrucelli. 2009. Aberrant cleavage of TDP-43 enhances aggregation and cellular toxicity. *Proc. Natl. Acad. Sci. USA*. 106:7607-7612.

Zhao, W., D.R. Beers, J.S. Henkel, W. Zhang, M. Urushitani, J.-P. Julien, and S.H. Appel. 2010. Extracellular mutant SOD1 induces microglial-mediated motoneuron injury. *Glia*. 58:231-243.

Zhu, Y.B., and Z.H. Sheng. 2011. Increased axonal mitochondrial mobility does not slow amyotrophic lateral sclerosis (ALS)-like disease in mutant SOD1 mice. *J. Biol. Chem.* 286:23432-23440.